Analytical Approaches for Offline/Online Assessment of Protection System Behavior and Identification of Critical Protection System in Transient Stability Studies

by

Ramin Vakili

A Dissertation Presented in Partial Fulfillment
of the Requirements for the Degree
Doctor of Philosophy

Approved July 2022 by the
Graduate Supervisory Committee:

Mojdeh Hedman, Chair
Vijay Vittal
Raja Ayyanar
Meng Wu

ARIZONA STATE UNIVERSITY

August 2022

ABSTRACT

Modeling protection devices is essential for performing accurate stability studies. Modeling all the protection devices in a bulk power system is an intractable task due to the limitations of current stability software, and the difficulty in updating the setting data for thousands of protection devices. One of the critical protection schemes that is not adequately modeled in stability studies is distance relaying. Therefore, this dissertation proposes two different methods for identifying the critical distance relays for any contingency, which are required to be modeled in stability studies. The first method is an iterative analytical algorithm and the second method is an ML-based method. The performances of both the methods are evaluated on the Western Electricity Coordinating Council (WECC) system and the results show that to have an accurate assessment of system behavior, modeling the critical distance suffices, and modeling all the distance relays in not necessary. Furthermore, modeling various generator protective relays in stability studies is also crucial. However, no comprehensive framework has been developed that provides guidelines on proper representation of generator protective relays in stability studies and evaluate their impact on the dynamic response of a system. To fill this gap, this dissertation proposes a comprehensive systematic framework which enables proper representation of generator protective relays in stability studies, thereby increasing the accuracy of these studies. The framework is tested on a particular area of the WECC system and the behaviors of different generator protective relays is evaluated.

Finally, this dissertation proposes a comprehensive machine-learning (ML)-based online dynamic security assessment (DSA) method that broaden the concept of online DSA

by predicting loss of synchronism (LOS) in generators, and the operation of critical protective relays in a power system. The performance of the method is tested on the WECC system in the presence of different noise levels and missing phasor measurement unit (PMU) data. The results reveal that the method can provide precise and fast predictions and is robust to noise and missing PMU data. Therefore, the method can be reliably used in power systems to enhance situational awareness by providing early warnings of impending problems in the system.

Dedicated to

the yakamoz[1] in my dark nights, Maede

And to the angles with whose support and love I was blessed,

my parent and my lovely sister, Aylin

[1] Yakamoz is a Turkish word that has no direct translation in English. It means “The shimmering beautiful moonlight as it reflects on the ocean/sea at night”. It was voted the most beautiful word in the world in 2007.

ACKNOWLEDGMENTS

First and foremost, I would like to wholeheartedly thank my supervisor, Dr. Mojdeh Khorsand Hedman, for supporting my Ph.D. research, training me to be a researcher, and her confidence in my work. This dissertation would not be possible without her ideas, knowledge, and support.

I would also like to thank Professor Vijay Vittal, who has been closely involved in most of my Ph.D. research and I learnt a lot by working with him. His experience and knowledge were always a key to solve many problems.

I would like to express my gratitude to Professor Raja Ayyanar and Professor Meng Wu for being on my dissertation committee and helping me improve this work with their insightful comments and encouragements.

Last but not the least, I would like to thank my wife, Maede, who made my life more beautiful than I ever thought. Without her warm support and patience this dissertation was not possible. I would also like to thank my parents and sister for the sacrifices they made for me, so I could pursue my dreams. No matter how far I am from them, my heart always beats for them.

Some parts of this work were supported by Salt River Project (SRP) company.

TABLE OF CONTENTS

CHAPTER Page

CHAPTER Page

CHAPTER Page

APPENDIX Page

LIST OF TABLES

Table Page

Table Page

LIST OF FIGURES

Figure Page

Figure Page

Figure Page

Figure Page

Figure Page

Figure Page

Figure Page

NOMENCLATURE

Abbreviations

ANN	Artificial Neural Networks
AVR	Automatic Voltage Regulator
CAPE	Computer-Aided Protection Engineering
CAPE-TS	CAPE-Transient Stability
COI	California-Oregon Intertie
CVM	Core Vector Machine
DSA	Dynamic Security Assessment
DT	Decision Tree
EIPP	Eastern Interconnection Phasor Project
ELM	Extreme Learning Machine
EMS	Energy Management System
GCC	Generator Capability Curve
HV	High Voltage
ISO	Independent System Operator
LOS	Loss of Field
LOS	Loss of Synchronism
MEL	Minimum Excitation Limiter
MILP	Mixed-Integer Linear Programming
ML	Machine Learning
MSS	Minimum Sample Split

MSL	Minimum Sample Leaf
MVE	Minimum Voltage Evaluation
NERC	North American Electric Reliability Corporation
NPV	Negative Predictive Value
OC	Overcurrent
OEL	Overexcitation Limiter
OF	Overfrequency
OOS	Out-Of-Step
OV	Overvoltage
PDC	Phasor Data Concentrator
PMU	Phasor Measurement Units
PSLF	Positive Sequence Load Flow
PSS/E	Power System Simulator for Engineering
RAS	Remedial Action Scheme
RF	Random Forest
ROC	Rate of Change
RTDS	Real-Time Digital Simulator
SCV	Swing Center Voltage
SCADA	Supervisory Control and Data Acquisition
SSSL	Steady-State Stability Limit
SVM	Support Vector Machine
TD	Time Domain

TPR	True-Positive Rate
TRV	Transient Recovery Voltage
TVE	Total Vector Error
UEL	Underexcitation Limiter
UF	Underfrequency
UFLS	Under-Frequency Load Shedding
UV	Undervoltage
UVLS	Under-Voltage Load Shedding
VSC	Voltage Source Converter
WAMS	Wide Area Measurement System
WECC	Western Electricity Coordinating Council

Chapter 1: Introduction

1.1 Overview

Power system dynamic behavior is governed by two main aspects following a major disturbance: *protection scheme behavior* and *the dynamic characteristics of the fundamental assets of the system including generators, loads, and control devices* [1]. Analyzing the historical data of prior outages and blackouts reveals that unforeseen relay mis-operations were one of the main factors in many of these events [2]-[3]. In this regard, the North American Electric Reliability Corporation (NERC) has identified protection systems as critical reliability assets in modern power grids [4] that play a crucial role in defining the system behavior during and after disturbances. Therefore, it is critical to represent protective relays in power system transient stability studies to obtain a realistic assessment of system behavior after a disturbance. Without modeling and assessing the behavior of protection schemes, power system analysis may manifest unrealistic system behavior [5]. For instance, a probable distance relay mis-operation after an initial event, which in turn leads to uncontrolled islanding and cascading outages, might not be captured in offline transient stability studies without including distance relay models [6]. Thus, proper control actions might not be designed to prevent these relay mis-operations. In fact, mis-operation or lack of operation of protection systems exacerbates the condition of a power system which is experiencing a disturbance and leads it toward a major blackout. In this regard, some of the well-known blackouts have been analyzed, and it was shown that the 1996 and 2003 North American blackouts could have been avoided by proper load

shedding before the mis-operation of a single protective relay [7]-[8]. A relay mis-operation on a transmission line connecting Italy to the rest of Europe was a critical factor causing the 2003 Italian blackout [9]. Also, it is discussed in [10] that the lack of proper studies of protection systems and coordination of remedial action schemes (RAS) is known to be one of the main causes of US Southwest blackout in 2011. These studies highlight the fact that modeling protection systems and monitoring their behavior during the propagation of the contingency under study are essential to have an authentic and precise assessment of the system response.

There are different types of protective relays in the system, such as UVLS and UFLS relays, that need to be modeled precisely to perform accurate transient stability studies. These protective relays usually are represented in power system stability studies. However, distance relays, which are among the most common and critical protective relays, are usually not modeled in these studies [5]. References [4], [5], and [11] show that the lack of representation of distance relays in transient stability studies can result in an erroneous analysis of the post-disturbance behavior of power systems. This conclusion is also confirmed in this dissertation via further simulations using the data from the WECC system.

Although, modeling all the distance relays in the system for transient stability studies may result in a better assessment of system behavior [5], modeling thousands of distance relays in a bulk power system, such as the WECC system, is an intractable task due to following reasons: 1) The current limitations of industrial software tools, such as GE positive sequence load flow analysis (PSLF), does not allow adding thousands of distance

relay models to the dynamic data file, and 2) The changes that protection engineers make in the settings of these relays for various purposes make it a challenging task to ensure updated settings in dynamic models. There are two main settings that govern the functionality in distance relays: (i) the reach of the operation zones, and (ii) the time delay for the operation of each zone. Maintaining updated settings information for thousands of distance relays in dynamic models is an intractable task. Hence, the setting information of some of the distance relays in the dynamic file of the system, which is used for transient stability studies, might be outdated and different from the actual relay settings. Performing transient stability studies with outdated settings can lead to inaccurate assessment of system behavior. As an example, if zone 3 reach of a relay in the dynamic data file is smaller than the actual zone 3 reach of that relay, it is possible that an operation of a relay in the real-word system is not observed in transient stability studies. This distance relay operation may, in turn, lead to another chain of subsequent events and thus, the behavior of the system observed in transient stability studies might be completely different from that of the real-world system. This fact is also confirmed in this dissertation by performing a case study with outdated and updated relay settings on the WECC system and analyzing the response of the system in these case studies. Therefore, the need for a method that can identify the critical distance relays to be modeled in transient stability studies is strongly felt by the industry [3],[5], and [9].

Two methods are proposed in this dissertation, i.e., analytical algorithmic method and ML-based method, to address both the challenges by identifying the critical distance relays. As the number of critical distance relays for each type of contingency is far less than the

total number of distance relays in the system, the proposed methods eliminate the challenges associated with modeling all the distance relays in the system. Moreover, it is indeed less challenging to keep the updated setting information for this subset of protective relays in the dynamic files of power systems.

Chapter 3 of this dissertation aims at illustrating the importance of modeling distance relays in the system and proposing the analytic algorithmic approach used to identify the critical distance relays that need to be modeled for performing stability studies on a contingency. The proposed algorithm is based on iteratively monitoring the apparent impedance of the transmission lines and applying minimum voltage evaluation (MVE) method on each transmission line. The algorithm includes the dynamic model of the distance relays identified by either of the methods as critical distance relays in the dynamic file of the system at each iteration.

Chapter 4 presents the ML-based method proposed to identify the critical distance relays. This method works based on training an ML model to learn the latent correlation between the impedance trajectories observed by the distance relays during the early stages of a contingency and the behavior of the distance relays for several seconds later. For any contingency, the method performs an initial run of early-terminated transient stability study and uses the impedance trajectories observed by the distance relays as the features of the trained ML models. Then, the trained ML model predict if any distance relay operates for the duration of the simulation and identifies them as critical distance relays.

The recent trends in increasing the reliance on renewable resources, which are inherently intermittent, for power generation and the increase in the number of man-made

or natural threats have exposed modern power systems to an unprecedented level of uncertainty. Offline stability studies consider a deterministic operation condition and topology of the system. Therefore, due to the high level of uncertainty, assessing a modern power system behavior during severe disturbances using offline stability studies might not correctly capture the system behavior. Inaccurate assessment of system behavior might lead to the failure in initiating proper remedial actions, which in turn might lead to cascading outages and blackouts [12], [7], and [8].

The insufficiency of offline stability studies has created a need for online security assessment of power systems that can provide fast and reliable assessments of the system security considering its current operating condition and topology. In online DSA methods, the security of a power system is evaluated online and as the disturbance proceeds considering the current operating condition and topology of the system [7]. Hence, online DSA methods can eliminate disadvantages of relying only on offline security assessments. Online DSA methods should be fast enough to provide enough time for operators (or automatic control systems) to take proper preventive or remedial actions. Thus, online DSA methods can play a critical role in preventing catastrophic events or reducing the severity of these events by providing early indications of the troubles in the system [7].

In this regard, online DSA methods should be fast enough to provide enough time for automatic control systems to take proper preventive or remedial actions. There are many hurdles for using conventional DSA methods such as time-domain simulations, which consists of solving a set of non-linear differential equations, and transient energy function methods in online applications. The computational complexity of analyzing N-k

contingencies and the massive size of power systems make such methods too slow to be used in online applications. Also, dynamic changes in transmission topology during disturbance propagation in the system due to relay operations add to the challenges of implementing conventional methods in online applications [9]. The recent advancements in power system monitoring have provided an overwhelming amount of synchronous measurement data from different parts of modern power grids. This measurement data can be efficiently used by machine-learning-based methods to predict the security of power systems [9]. Therefore, ML-based online DSA methods have gained a significant interest, recently.

Following severe disturbances, some of the generators in the system might start to lose synchronism with respect to the other generators. If this condition is not promptly detected, the protection system of the generators might trip them, which leads to a further mismatch between generation and load in the system. This mismatch leads to deceleration or acceleration of the rotor of the other generators, which in turn may lead to a local or system-wide LOS condition. Subsequently, cascading outages may occur, which jeopardize system stability and may lead the system toward blackout. Therefore, it is essential for an efficient online DSA method to promptly detect LOS conditions in generators ahead of time, thereby enabling operators to initiate proper corrective actions to avoid cascading outages.

As mentioned earlier, protection systems play a crucial role in defining the response of power systems to disturbances. In this regard, one of the most important features of an online DSA method is the ability to predict critical protection system behavior ahead of time. Distance relays as well as UFLS and UVLS relays are among the most common and

critical protective relays in power systems. Unstable power swings, i.e., LOS condition, may lead to distance relay operation along the electrical center of power swing, which can result in formation of uncontrolled islands. Mismatch of generation and load within these uncontrolled islands can lead to further outages and even blackouts. Therefore, predicting distance relay mis-operation at the early stages of a contingency is crucial for avoiding blackouts.

Moreover, maintaining acceptable voltage and frequency profiles throughout the system and continuous serving of load are critical for secure power system operation. Early prediction of UFLS and UVLS relay operations after a major disturbance provides valuable information, e.g., areas that might experience frequency and voltage drop and the consequent load shedding. This information enables initiation of proper control actions to alleviate the situation.

Therefore, chapter 5 of this dissertation proposes a comprehensive ML-based online DSA method which provides a detailed prediction of impending LOS condition in generators as well as operation of distance relays, UFLS, and UVLS relays in the system, for several seconds later. The method trains different ML models using the results of extensive offline transient stability studies. The trained models use different periods of the voltage angle/magnitude measurements obtained from the electrically closest high-voltage buses (above 345 kV) to the generator/relay locations in the system at the early stage of a disturbance as the input features. The predictions of the trained models are sent to the operators, informing them of the areas of the system which will be impacted by the disturbance. Thus, the operators can initiate proper control actions to alleviate the situation.

Different reasons for mis-operation of protective relays as well as its influence in the dynamic response of the system along with the sequence of events leading to blackout in the system are discussed in the remainder of this chapter.

1.2 Relay mis-operation

Besides human errors, weather-related events, and device failures, mis-operation of protective relays, also known as hidden failures, is one of the most critical factors in leading power systems toward blackout [13]. Relay mis-operation may happen due to excessive loading on the lines or unstable power swings and may result in formation of unintentional islands in the system [13].

When a system is heavily loaded, some of the critical lines in the system may carry a significant amount of power; this may cause the apparent impedance trajectory seen from either side of the line traverse into zone 3 operation zone of the relay. The distance relay might mis-interpret this as a fault and trip the line without any fault. This, in turn, results in overload in other alternative transmission paths, and potentially mis-operation of other distance relays. This will further weaken the system which is already under stress and jeopardize its stability [13].

Another possible cause of hidden failure is unstable power swings due to severe contingencies in the system. The initiating event may result in a power swing, which can cause a voltage drop across some of the lines in the system, also referred to as the electrical center. The distance relays on the line observe this voltage drop, which is also a drop in the impedance trajectory of the line, and mis-interpret this condition as a fault and trip the line. These hidden failures might result in unintentional islanding of part of the system. It is

likely that no generation/load balance exists in these islands, which might cause a frequency drop in these islands and lead the system toward blackout. The impedance trajectory observed by a distance relay during unstable power swing is discussed in depth in [14].

This shows how the behavior of protective relays could affect the whole system behavior during major disturbances. Therefore, modeling protection systems and assessing their behavior is necessary for conducting precise stability studies. Furthermore, for designing a proper out-of-step (OOS) blocking scheme for preventing relay mis-operation during OOS condition detailed stability studies with modeling critical protective relays should be performed.

It can also be concluded that online monitoring of protective relays in a system and predicting their operation several seconds in advance can greatly help operators prevent the mentioned protective relay hidden failures by initiating proper control actions. Therefore, it can be a desirable property for an online DSA method to be able to monitor the system in real-time and predict protective relay behavior several seconds in advance.

1.3 Different stages of a system from normal operation to blackout

The series of events leading to a blackout usually starts with a single line or generator outage which can occur as a result of equipment failure, environmental factors, or human error factor [9]. In this stage, if proper remedial actions are taken (either by the operator or automatic control system) the system will traverse to a new stable state. However, depending on the severity of the event and resiliency of the power system it might still be in an emergency state [9]. In this emergency state, the operator can take system

readjustment actions to bring the system back to the normal operating condition. However, if after the initial event no proper remedial action is taken or while the system is in emergency state, another event happens, cascading outages might start in the system. In this stage, additional equipment failures and protection system mis-operation occur. As a result, overloaded lines will start to trip one after another (cascading outages) and the system might start to split up due to stability problems. In this situation, the proper automatic control such as activation of UFLS and UVLS relays as well as coordinated damping controls should initiate to prevent blackout in the system. If no control action is taken or the control actions are not enough to bring the system back to a stable operating condition, the system will traverse into the point of no return. It means that after this point no remedial action can bring the system back to a stable operating condition and blackout will happen in the system. In this stage due to cascading outages of transmission lines, the system splits into uncontrolled islands where there is a large mismatch between the load and generation. This load/generation mismatch leads to frequency decay in the system, and the large mismatch of reactive power reserve and load lead the system toward voltage collapse. Finally, the blackout occurs in the system. The described sequence of events and the stages of a power system from the normal operating condition to a blackout is depicted in Figure 1.1.

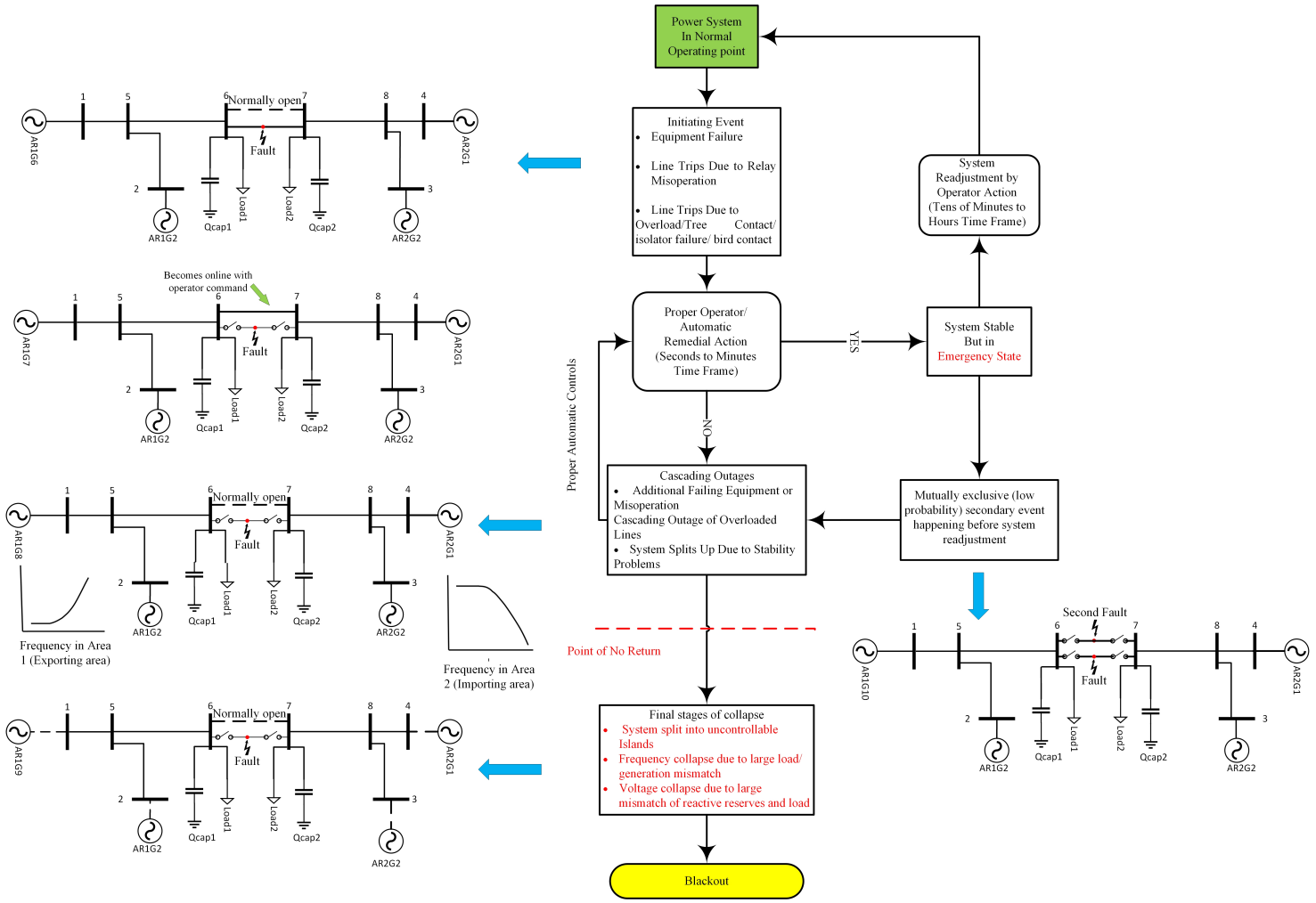

Figure 1.1 General sequence of events leading to a blackout [9].

Chapter 2: Impact of power swing on protection systems and OOS protection

Sudden disturbances in power systems, such as a fault on a transmission line, loss of a generation unit, and a large change in load, can cause changes in electrical power outputs of the generators. Due to the delay in the operation time of the governor and other mechanical parts of the generators, the change in a generator mechanical power input is much slower than the change in its electrical power output. Thus, an imbalance occurs between the electrical power output and mechanical power input of the generators. This imbalance, in turn, causes an acceleration or deceleration of the generators and may lead to a change in their relative rotor angles. These changes in generator rotor angles create stable or unstable power swings on transmission lines. The protective relays might mis-interpret these power swings as three-phase faults and trip the line. Relay mis-operation may cause the forming of unintentional islands in the system. Most likely, there is no balance between generation and load in these islands, which may lead to frequency decay in the system and eventually, a system-wide blackout may happen. This condition, which is called an out-of-step condition, and mis-operation of the relay located in the electrical center of the system should be observed in transient stability studies, thereby, enabling the operators to implement out-of-step blocking schemes. Then, they can separate the system at the desired points to form intentional islands where the load and generation could be balanced by proper load-generation shedding plan.

In this chapter, the impact of power swing on different protective relays is studied. Then, different methods for identifying stable and unstable power swings which can lead to relay mis-operation are introduced and compared, and the MVE method which is used in the research is thoroughly explained.

2.1 Rotor angle stability and loss of synchronism

To study how a generator behaves during and after a disturbance, a simple two-machine system, which is a simplified representation of a power system, is illustrated in Figure 2.1.

If it is assumed that the resistance of the line and machine *A* and *B* are negligible in comparison to their reactance. Figure 2.2 shows the electric power-angle curve of one of these equivalent generators. The mechanical power input of this equivalent machine is considered to be constant and represented in the figure by P_M.

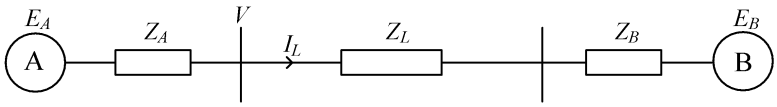

Figure 2.1 One-line diagram of a two-machine system [13]

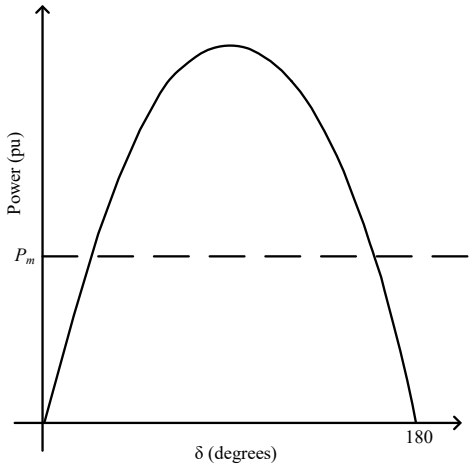

Figure 2.2 Power angle curve [13]

Figure 2.3 illustrates the power angle curve of a generator before, during, and after the occurrence of a contingency. Before the occurrence of the contingency, the generator works in its normal steady-state condition and the rotor angle is δ_1. After the occurrence of the contingency, the transfer capability of the system reduces significantly while the rotor angle remains the same (δ_1) due to inertia. This causes the operating point to traverse from point A and point B in Figure 2.3. At point B, the electric output power is lower than the mechanical input power; thus, the rotor angle begins to accelerate until it reaches δ_2 which is shown in Figure 2.3 by the transition between point B and point C. δ_2 is the angle at which the protection system cleared the fault by removing the faulted line. Area A_1 represents the kinetic energy obtained by the generator during the fault. After the fault is cleared, the transfer capability is improved, which allows the machine to transfer more power at angle δ_2 and the operation point traverse from point C to point D. At this point, the electric power output is higher than the mechanical power input, causing the rotor to decelerate. However, the rotor angle continues to increase due to the rotor inertia. If the excess kinetic energy obtained by the machine (A_1) is not used up before electric power becomes less than the input mechanical power, the rotor angle will keep increasing and the machine will lose synchronism with respect to the rest of the system [13].

The critical clearing angle is defined as the clearing angle that for clearing angles higher than this angle, the machine will lose synchronism with respect to the rest of the system (i.e., area A_1 will not be equal to area A_2). The critical clearing time depends on the system condition and the type of contingency. However, [15] and [16] propose that the likelihood of recovering from swing which has exceeded 120 degrees, is marginal. Therefore, for the

purpose of setting an out-of-step protection system, 120 degrees is usually accepted as a proper value.

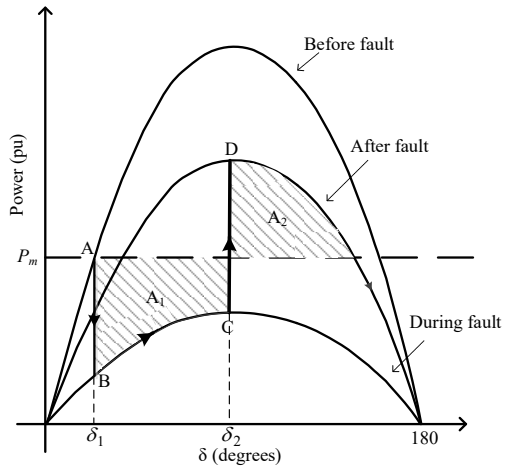

Figure 2.3 Power angle curve for various network conditions [13]

In Figure 2.1, E_A and E_B can represent a group of generators located in areas A and B, respectively. If we assume area A as the exporting area (the area where the generation level is higher than the load level) and area B as the importing area (the area where the generation level is lower than the load level), a fault on the tie-line connecting the two area will cause generators in area B lose synchronism with respect to the generators in area A. In this condition, Figure 2.3 can represent power angle curves of the group of generators in one area.

2.2 Stable and unstable power swings

The difference between a stable and unstable power swing relies on the ability of the system to find a new stable operation condition after the power swing. If the power system finds a new stable operation condition after a power swing, the power swing is considered

as a stable power swing. Whereas, in unstable power swings, the system cannot reach a new stable condition and generators' rotor angles continue to separate.

As a result of an unstable power swing, loss of synchronism between different groups of generators in different areas of the system occurs and a generator or group of generators slip poles. In this condition, which is known as an out-of-step condition, terminal voltage angles of a generator or a group of generators exceed 180 degrees relative to the rest of the interconnected power system. This difference in terminal voltage angles of the generators may lead to severe voltage drop along some of the lines connecting these groups of generators. The protective relays observing this severe voltage drop may mis-interpret the situation as a three-phase fault and trip the line. Although promptly separating the area after loss of synchronism is vital for bringing the system back to a stable operation condition and to avoid a possible blackout, mis-operations of protective relays result in the formation of unintentional islands and exacerbate the power system operating condition [15]. Therefore, in order to avoid the formation of unintentional islands as a result of relay mis-operations, protective relays should be temporarily blocked from unintentional tripping during stable or unstable dynamic conditions. Blocking functionality is usually imbedded in modern distance relays to prevent unintentional distance relay operation in these conditions. A well-designed protective relaying scheme should be able to distinguish between faults and power swings and block the tripping operation of the relays during power swings while being able to identify faults during power swings [17].

During a fault, the voltage, current, and load characteristics start to deviate from its normal value to the value that can trigger the relay instantly. However, during power swing

condition, these values change slowly from their normal value since it takes time for the rotor angles to change due to inertia. Therefore, the rate of change of voltage, current, and the impedance observed by distance relays in power swing condition is less than those in a fault condition. This fact is the basis of most of the methods trying to distinguish between power swings and fault conditions [18].

A well-designed separation (islanding) scheme should precisely distinguish between faults, stable power swings, as well as unstable power swings, and separate the system at predefined locations when the voltage angle difference is suitable for safe separation of the system.

An OOS condition imposes many risks to power systems, the most important of which are as follows [17]:

1. Breaker failure due to transient recovery voltage (TRV): OOS condition may impose a TRV on the circuit breaker and cause its damage. The highest stress on the circuit breaker occurs when the voltage angles across the breaker are 180 degrees apart and it may cause damage to the circuit breaker. The OOS protection scheme should not trip when the angle difference between islands is close to 180 degrees

2. Load-generation imbalance in isolated islands which may result in wide-spread outages in the islands.

3. Slipping pole in synchronous generators, i.e., OOS condition, creates thermal and mechanical stress on the generator, may cause physical damage to the generator, and reduces the life of the machine.

4. Undesired circuit breaker tripping during a stable power swing weakens the already disturbed system and may result in additional line tripping; This may cause cascading outages of lines, which is against the NERC standards [15].

5. Failure to trip a line during an unstable power swing may result in pole slipping of the generator and may cause cascading outages in the system.

Considering the risk imposed on the system by OOS condition, it is necessary that this condition can be detected in comprehensive stability studies, and it is observed that which distance relays will mis-operate due to OOS condition and separate the system. Those relays should be equipped with OOS blocking scheme that enables operators to prevent relay mis-operation in this condition. Then, comprehensive stability studies should be performed with modeling critical protective relays to find the best locations to form intentional islands where generation-load balance could be achieved with proper load-generation shedding plan with the goal of minimizing loss of load and maintaining maximum service continuity. Therefore, besides OOS blocking scheme, the protective relays should be equipped with OOS tripping scheme to enable tripping the relays in the desired locations in order to form intentional islands during the OOS condition. It is also required that the protection scheme prevent line reclosing after the OOS tripping function is invoked [19].

2.3 impact of power swings on protection systems

Power swings are categorized to have a local mode or inter-area mode. In local mode power swings, a generator oscillates with respect to the rest of the system, whereas, in inter-area mode, a group of generators oscillates with respect to the other groups. Inter-area

power swings impose more risks to the power system since as explained earlier, in this type of power swing the protective relays on transmission lines observe the power swing and may mis-interpret it as a fault and trip the line, causing the formation of unintentional islands in the system. In local mode power swings, however, the local protective relays such as the protective relays of the out-of-step generator and its step-up transformer observe the power swing [13].

The protective relays, which are involved in local and inter-area power swings, and the impacts of power swings on these protective relays are reviewed in the remainder of this section.

2.3.1 Impact of inter-area mode power swings on protection systems

Inter-area power swings can cause the relative rotor angles of groups of generators to separate 180 degrees with respect to each other (generator pole slipping). This OOS condition causes a dramatic drop in voltage along the line(s) located in the electrical center of the system. The responses of different protective relays to the OOS condition are different. Some of them, such as distance relays, respond to OOS conditions, while other relays, such as differential relays, do not respond to this condition. Different types of relays and their responses to OOS conditions are described in the following section [13].

2.3.1.1 Effects of power swings on overcurrent relays

Overcurrent relays monitor the flow of the current on the line and operate if the current exceeds a predefined value. Figure 2.4 shows a transmission line equipped with an overcurrent relay. In this figure, for instance, if a fault occurs on point *X*, the current measured by the relay will be $I_L = \frac{V_1}{Z_L}$; However, in OOS condition where $\delta = 180$ with

the assumption that $V_1 = V_2$, the current measured by the relay will be $I_L = 2\frac{V_1}{Z_L}$, which is higher than the fault current and will trigger the relay. Furthermore, these relays may even operate during stable power swing, since the current might be higher than their pickup settings, which is one of the disadvantages of this type of protective relays [20].

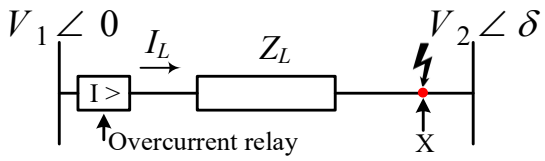

Figure 2.4 Impacts of out-of-step condition on overcurrent relay

2.3.1.2 Effects of power swings on differential relays

Differential relays measure and compare the value of a particular quantity, such as current, at two different points, and they detect a fault condition and send tripping signals if these values are different. Figure 2.5. illustrates a differential relay. As it can be seen in this figure, during a power swing, the current pass through both point A and B and the relay does not observe any difference in the value of the current. Therefore, differential relays do not respond to power swings, and if tripping is desired, this protection device should be accompanied by a backup or supplementary relay.

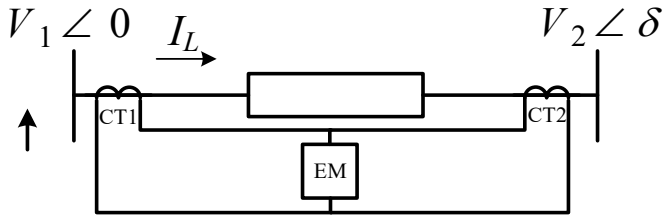

Figure 2.5 Impacts of out-of-step condition on a differential relay

2.3.1.3 Effects of power swings on distance relays

A distance relay measures the voltage, current, and angle between voltage and current seen from the point it is installed and evaluate these parameters in term of impedance, which is proportional to the distance of the relay from the fault. In other words, distance relays measure the electrical distance between the fault location and the relay and operate if this distance is less than a predefined value. This predefined value is usually set as a fraction h of the length of the line from the relay location. This distance is also called the "reach point" of the relay. As it is shown in Figure 2.6, the impedance seen from the relay location can be calculated by (2.1).

$$Z_R = \frac{V_1}{I_L} \tag{2.1}$$

Depending on the location of the fault, the impedance observed by the relay changes. For example, in Figure 2.6, point h is set as the reach point of the relay and Z_L is the impedance of the transmission line per unit of length. Therefore, the criterion for the operation of the distance relay is a comparison between the impedance observed by the relay and the impedance of the reach point, which is equal to hZ_L. When a fault occurs at distance D of the relay, the impedance observed from the relay is equal to DZ_L, which is smaller than hZ_L. Therefore, the relay will respond to the fault without any delay. However, if the fault occurs at distance E of the relay, the impedance observed by the relay is equal to EZ_L, which is higher than hZ_L. Therefore, the distance relay does not respond to the fault without a time delay. The tripping criterion in this type of relays is independent of the operating point and topology of the system.

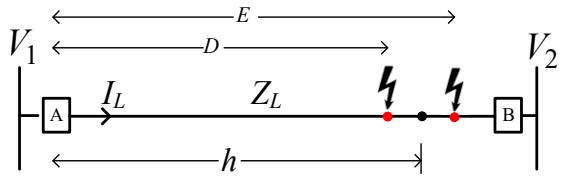

Figure 2.6 Reach point of a distance relay

A common practice in the industry is to set the reach point of the relay at 80 to 90 percent of the length of the line. For the faults occurring beyond this point, relay A responds with a predefined time delay, while relay B responds to the fault immediately. This practice leads to a sequential tripping and helps with relay coordination. Various operational characteristics have been designed for distance relays such as impedance characteristic, reactance characteristic, blinder characteristic, modified impedance characteristic, lens characteristic, and mho characteristic. These characteristics are thoroughly explained in [21]. Mho characteristic with 3 operation zone, shown in Figure 2.7, is the most widely used characteristic in distance relays.

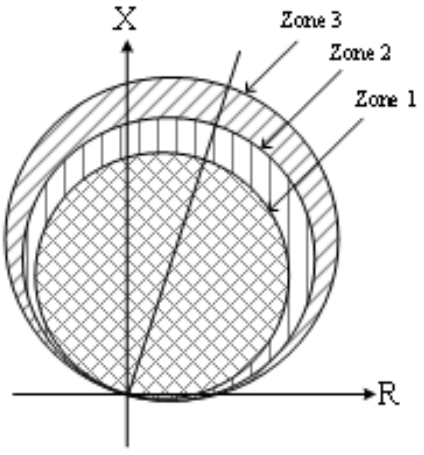

Figure 2.7 Mho characteristic of a distance relay with three operation zones

During a fault or a power swing, If the impedance trajectory observed by a distance relay traverse into one of the operation zones of the relay, shown in Figure 2.7, after a predefined delay, the relay will respond to the fault by tripping the respective line. The mho characteristic is inherently directional and does not respond to the fault occurring behind the relay [21].

For coordinating the reach of different zones of a distance relay a common practice is to set the zone one reach of the relay to cover 80%-90% of the line length. This zone responds to a fault condition instantly, and the time delay for its operation is zero. Zone 2 protection should cover the rest of the line along with a portion of the adjacent line. It is a common practice to set the zone 2 reach to cover 120% of the line length. Zone 2 setting should not overreach the zone 1 of the adjacent downstream line. Therefore, a time delay of 0.25 seconds (without considering the operation time of the adjacent circuit breaker) is suggested for this zone. Finally, zone 3 acts as a backup for the relay on the adjacent line since it covers the adjacent line completely. If the distance relay of the adjacent line fails to operate, zone 3 of the relay responds to the fault with a time delay of 1 to 2 seconds and trip the line. Zone 3 of distance relays can be set to observe faults in the backward direction as well. The coordination of three operation zones of distance relays is depicted in Figure 2.8, considering the zone 1, 2, and 3 reach of 80%, 120%, and 220% of the line length [21].

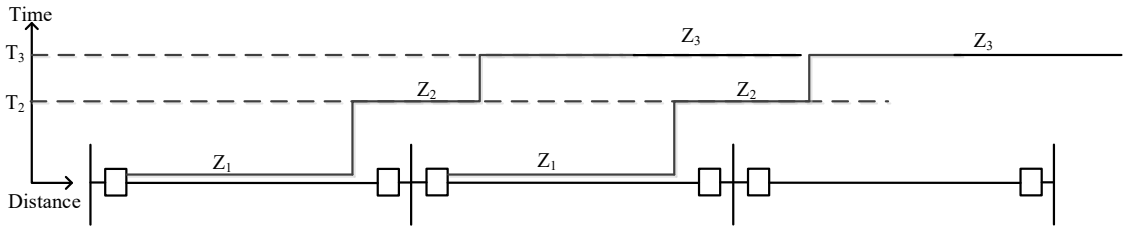

Figure 2.8 Transmission lines protected by distance relays

During power swing, swing impedance may traverse into one of the operation zones of a distance relay. If swing impedance traverse into zone 1, the relay operates instantly and trips the line. Whereas if the swing impedance traverses into zone 2 or 3, the operation of the relay depends on the time it takes for the swing locus to cross zone 2 or 3 boundaries of the relay. For instance, if the power swing is stable, the swing locus may leave zone 2 or 3 of the relay before the breaker or relay characteristic time delay is exhausted.

Furthermore, the impedance of the line, which is proportional to its length, affects the operation of its corresponding distance relays during power swings. To study the impact of line impedance on the operation of the distance relays, the system in Figure 2.9, a two-bus equivalent model of the system, is considered. If the impedance of the line is small in comparison with the system impedance, the relay operation zones and swing locus look like Figure 2.10. In this case, the swing locus enters the relay operation zone when the system angular difference is far bigger than 120 degrees [21], and one of the operation zones of the relay will operate depending on the time delay of the zones and the circuit breaker. In [20], it is discussed that the likelihood of a system to recover from a power swing is almost zero after the angular difference passes 90 degrees. Therefore, in this case, where the angular difference is far bigger than 120 degrees, the likelihood of the system recovering to a stable operating condition is almost zero. In this condition, separation of the system is not desirable, and the OOS protection scheme should block the tripping of this relay.

On the other hand, if the line impedance is large in comparison to the system impedance, the relay operation zones and swing locus look like Figure 2.11. In this case,

the swing locus may enter the relay operation zones when the system angular difference is less than 90 degrees, meaning that in this case, the relay may even trip for any stable power swing. In this case, either the relay should be blocked, or if the tripping of the relay is desired, it should be restricted using a supplementary characteristic such as blinders [16].

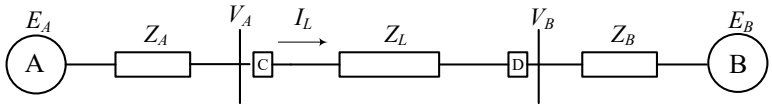

Figure 2.9 Equivalent system used to study loss of synchronism characteristic

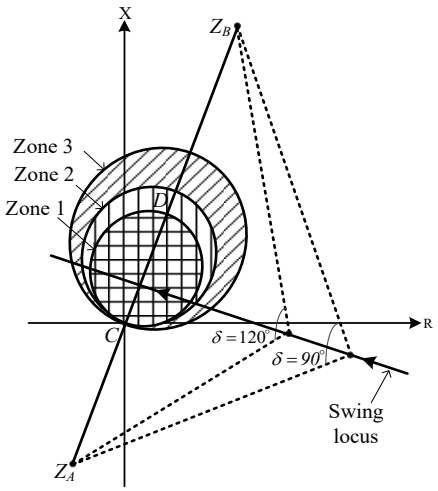

Figure 2.10 Effect of power swing on distance relays: small line impedance in comparison to system impedance [16]

For assessing if a swing locus entering a relay zone will cause relay tripping or not, the time it takes for swing locus to traverse through the relay zone is calculated using (2.2). If this traverse time is greater than the time delay for that zone plus the circuit breaker operation time, the relay will trip the line. δ_2 and δ_1 for zone 3 are shown in Figure 2.11 and S is the slip in degrees per second [16].

$$T = \frac{\delta_2 - \delta_1}{S} \tag{2.2}$$

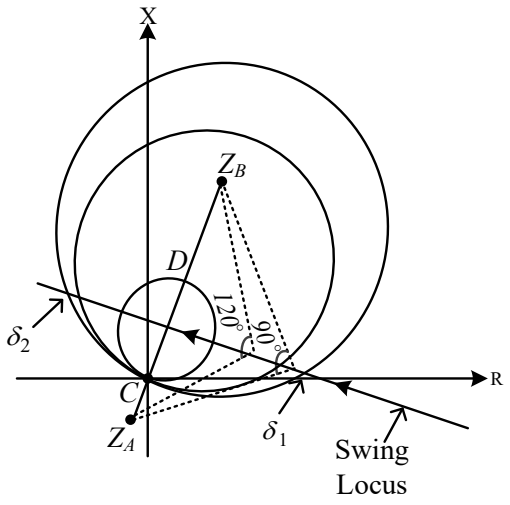

Figure 2.11 Effect of power swing on distance relays: large line impedance in comparison to the system impedance [16]

2.3.1.4 Impacts of power swings on under-frequency and under-voltage load shedding

UFLS and UVLS relays shed pre-defined blocks of loads when the frequency or voltage drops below the set points of these relays, respectively. These relays do not directly get engaged in power swing. However, in the case of distance relay mis-operation which leads to the formation of unintentional islands, the potential load-generation imbalance could cause frequency/voltage drop and consequently, the UFLS and UVLS relay operations in these islands. Although UFLS and UVLS are among the most effective remedial actions to re-establish generation-load balance in intentional islands, in unintentional islands, the block of load shedding may be more than the amount of generation-load imbalance, and the operation of these relays may exacerbate the system condition [13].

2.3.2 Impact of local mode power swings on protection systems

As mentioned before, in local mode power swings a generator loses synchronism with respect to the rest of the system (generator OOS condition). The necessity of protecting generators with an OOS protection scheme was highlighted after the United States 1965 northeastern blackout [22]. Most of the protective schemes of the generators are unable to provide complete OOS protection for the generators. Therefore, for this purpose, the generators should be equipped with protection schemes specifically designed for providing out-of-step relaying for generators [22].

The OOS protective relays designed for generators monitor the generator and its step-up transformer and initiate tripping if the electrical center of a power system disturbance passes through the generator or its step-up transformer [16].

It is recommended in reference [16] that instead of performing out-of-step tripping for generators, it is more desirable to separate the system in appropriate locations to form intentional islands with generation-load balance. The reason is that generators are preferred to remain online and be ready to resynchronize the islands after separation. To identify the appropriate location for separating the system, it is necessary to perform comprehensive stability studies with modeling the critical distance relays. Then, a proper OOS blocking scheme along with the appropriate location for separating the system can be identified.

2.4 Literature review on power swing detection methods

The first critical step during an OOS condition is to detect the power swing promptly and initiate an appropriate OOS blocking scheme to avoid a system-wide blackout [19]. Several power swing detection methods are presented in the literature. These methods can

be categorized into conventional methods and non-conventional methods, each of which has its own advantages and disadvantages. Some of these methods are briefly reviewed in this chapter [19].

Conventional methods for detecting power swings are based on the rate of change (ROC) of the swing impedance. The swing impedance locus travels in the impedance plane slowly. However, in the fault condition, the impedance changes instantly. This feature is used in conventional methods to distinguish between a power swing and a fault condition. Some of the well-known conventional methods are as follows:

Blinder Schemes:

This scheme is based on adding two blinders to the relay impedance characteristic. In this method, the time that it takes for power swing locus to travel between two blinders is recorded and compared to a time setting. If the traverse time of the power swing locus is greater than a predefined time setting, a power swing is detected. Power swing blocking scheme cannot be achieved using this method since the swing locus should completely pass the relay impedance characteristic and reach to the left blinder.

Dual-Blinder Schemes:

To address the shortcoming of the blinder scheme, the dual-blinder scheme can be used. In this scheme, there are two blinders (inner and outer) at each side of the impedance characteristic of the relay, and the traverse time of the swing locus between inner and outer blinders is recorded and compared with a time setting. This method can detect the power swing before its locus enters the impedance characteristics of the relay.

Concentric characteristic scheme:

The Concentric scheme works like the dual-blinder scheme. The traverse time of swing locus between the outer characteristic and the inner characteristic is recorded and is compared with a time setting. If the traverse time is bigger than the time setting, a power swing is detected. Figure 2.14 shows the characteristics of different conventional schemes for power swing detection.

Both dual-blinder and concentric characteristic schemes have the disadvantage of difficulty in defining an appropriate time setting. To ensure the precise OOS blocking scheme operation, a power swing should be detected before the swing locus enters any of the relay impedance characteristics. Therefore, the inner blinder should be located outside the largest relay impedance characteristics, and the outer blinder should be located outside of the load zone to prevent incorrect blocking operation in heavy load conditions. Achieving such a meticulous setting is a challenging task when the line impedance is large in comparison to the network impedance. Therefore, several stability studies should be conducted, and the fastest power swing should be detected to define the time settings of the blinders. Moreover, the slip that is used for calculating the traverse time of the power swing locus usually changes after the first slip cycle. Therefore, setting a fixed impedance separation between the blinders and a fixed time delay might not be so precise for OOS blocking scheme. Furthermore, calculating the source impedance for a bulk power system is a complicated task, since it changes with network topology and commitment of

generators or other network elements. The source impedances can also change during a disturbance, making it very hard to set a fixed setting for the OOS blocking scheme.

To address the shortcomings of conventional methods, several non-conventional methods have been proposed in the literature. Some of these methods are elaborated upon in this chapter.

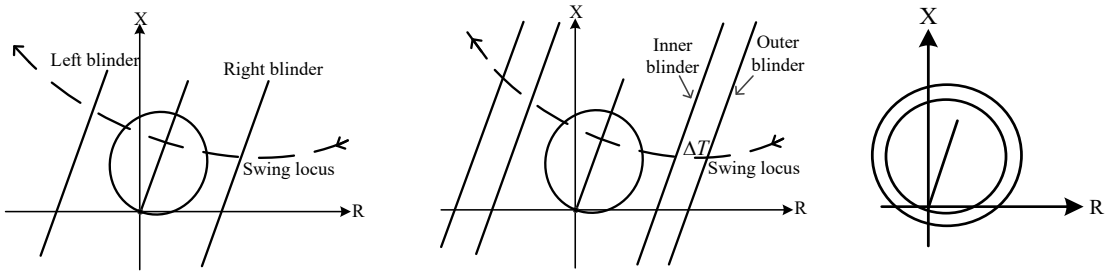

(a) (b) (c)

Figure 2.12 The characteristics of different conventional schemes for power swing detection: (a) Blinder scheme, (b) Dual-blinder scheme, (c) Concentric characteristic scheme (other forms of this scheme are also possible) [13]

Continuous impedance calculation:

This method is presented in reference [23]. The method monitors the swing impedance progression in the impedance plane and detects the impedance trajectory as a power swing trajectory if three criteria of continuity, monotony, and smoothness are met. Continuity means that the change in X and R of the impedance trajectory should be less than a threshold. Monotony indicates that the trajectory does not change direction. Smoothness shows how abruptly the impedance trajectory changes. As mentioned before, unlike a fault condition, the impedance trajectory does not change abruptly during power swings. The

advantage of this method is that it needs no settings, and for covering even the very slow power swings, the method is accompanied by a concentric characteristic [23].

Continuous calculation of incremental current:

During power swings voltage and current change dramatically. Therefore, to detect a power swing, reference [24] proposes a method that measures and monitors the present current value and the previous sampled value to detect power swing condition. If the difference is more than 5 percent of the nominal current and it lasts for 3 cycles, the condition is detected as a power swing. This method is accompanied by an additional delta current detector to detect a new step change in current beyond the power swing. As mentioned before, step changes in voltage or current do not occur during a power swing (smoothness is a characteristic of power swings). Therefore, the step change in current is an indicator of a fault condition. This method can address the shortcoming of traditional methods in detecting very fast power swings, especially in heavy load conditions. However, in a very slow slip (below 0.1 Hz), detecting the power swing is difficult since the change in current value is less than 5% of the nominal value [24].

R-Rdot out-of-step scheme:

This method, which utilizes the ROC of impedance for detecting OOS condition is first devised for the Pacific 500 kV intertie and installed in the early 1980s. References [24]-[25] introduced a new variable *U*, defined by (2.3), which captures the change in impedance observed by the relay and its ROC.

$$U = (Z - Z_1) + T_1 \frac{d_Z}{d_t} \tag{2.3}$$

In this equation, Z is the apparent impedance magnitude observed by the relay. Z_1 is the impedance of the swing that is to be tripped and T_1 is the slope representing *Rdot/R*. $Z_1$and T_1 are calculated from system studies. OOS tripping will start if *U* becomes a negative value. In fact, equation (2.3) is composed of two parts. The first part, that is $(Z - Z_1)$, is similar to the conventional methods. The second part, that is $T_1 \frac{d_Z}{d_t}$, will accelerate the operation of OOS tripping if the impedance changes at a higher rate (when the derivative is negative). In this method, a high $\frac{d_Z}{d_t}$ is used to anticipate instability, and the amount of anticipation depends on T_1. Another modification of this method is to use the resistance and its ROC instead of the impedance values used in (2.3). This modification has the advantage of reducing the method sensitivity to the location of the swing center with respect to the relay location [24].

The drawback of the R-Rdot method is that for setting its parameters properly, extensive simulation studies for various contingencies are needed.

Rate of change of swing center voltage:

This method is based on the monitoring of the voltage and its ROC at the swing center. If the two-machine equivalent system of Figure 2.9 is considered as the system under study, and the voltages of the two machines are considered equal ($E = |E_R| = |E_S|$), the swing center voltage (SCV) can be calculated using (2.4) [26].

$$SCV(t) = \sqrt{2}E\, sin(\omega t + \frac{\theta(t)}{2})\, cos(\frac{\theta(t)}{2}) \tag{2.4}$$

Where θ is the angle difference between the two sources. The magnitude of SCV is between 0 and 1 p.u. Under normal load conditions, SCV stays constant, however, during

an OOS condition, where the angle difference between the two sources is 180 degrees, this value becomes zero. (2.5) can be approximated using the positive-sequence magnitude of the source voltage (E_1):

$$SCV1 \approx E_1 cos\,(\frac{\theta}{2}) \tag{2.5}$$

The ROC of SCV1 can be calculated using (2.6):

$$\frac{d_{SCV1}}{d_t} \approx -\frac{E_1}{2} sin\,(\frac{\theta}{2}) \frac{d_\theta}{d_t} \tag{2.6}$$

In (2.6), if the machines go out of synchronism, the ROC of SCV1 will be minimum (a large negative value). Also, at this condition, the value of SCV1, calculated using (2.5), will be zero. These two facts are used in this method to detects power swings. This method usually detects the power swing when the angle difference is around 180 degrees.

Synchrophasor-based out-of-step relaying:

In this method, system angle separation is approximated by the difference in phase angle measured by synchrophasors at the line ends. If the equivalent two-machine system in Figure 2.9 is considered, and it is assumed that synchrophasors measure the positive-sequence voltages at both ends of the line, the ratio of measured voltages can be represented by (2.7):

$$\frac{V_{1A}}{V_{1B}} = \frac{\frac{Z_S}{Z_T}+(1-\frac{Z_S}{Z_T})K_E\angle\theta}{\frac{Z_S+Z_L}{Z_T}+(1-\frac{Z_S+Z_L}{Z_T})K_E\angle\theta} \tag{2.7}$$

where $Z_T = Z_S + Z_L + Z_R$ and $K_E = \frac{|E_A|}{|E_B|}$. Assuming that the source impedance is negligible with respect to the line impedance and $K_E = 1$, the ratio of the voltages at both ends of the line will be equal to 1 with the angle of θ. This means that the system angle

separation θ (the angle difference between the two sources) can be measured by monitoring the ratio of the voltages at both ends of the line, which can be used for OOS detection [27].

The method proposed in [27], uses the positive-sequence voltage measured by synchrophasors at two locations of the network. It also measures the slip frequency S_R, which is the ROC of the angle difference between the two measurements of the synchrophasors, and the acceleration A_R, which is the ROC of the slip frequency. Then three criteria are checked by the method to detect OOS condition and start the network separation:

1. If S_R is not zero and it keeps increasing (A_R is positive).
2. if (2.8) holds true in the network.

$$A_R > slope \times S_R + A_{Offset} \tag{2.8}$$

Slope and A_{Offset} are the parameters that need to be set in the method.

- If the absolute value of the angle difference between the two synchrophasors becomes greater than a pre-defined threshold.

Using state-plane trajectories analysis for out-of-step detection:

The analysis of the state-plane trajectory is proposed in [27] as a method for detecting the OOS condition. This method is faster, more efficient, and more accurate than the Synchrophasor-based method. This method first, finds a single-machine equivalent of the system. Next, it performs system analysis on this single-machine equivalent network and obtains the state planes (relative rotor speed versus relative voltage angle) during and after the fault. The maximum potential energy of the system is used to calculate the critical clearing angle and time. Then, the stability of a power swing is predicted using the

calculated critical clearing time [27]. However, using the single-machine equivalent of the system might lead to inaccurate analysis of system behavior during and after a fault.

Using decision tree technique for out-of-step condition detection:

References [28]-[29] implemented a machine-learning-based method to distinguish between stable and unstable power swings. The decision tree algorithm is used in these references to train a machine learning algorithm using the results of extensive stability analysis performed offline. The trained algorithm can be used to categorize a power swing in unseen samples into stable or unstable categories.

Frequency deviation of voltage:

Reference [30] has devised a method that uses discrete Fourier transform to calculate the angular velocity of bus voltage and the angular acceleration of the generator rotor angle. These two parameters are shown in the same plane in this reference and the criterion for OOS detection is developed. In this method, the need for measuring the current of the line has been eliminated.

Out-of-step detection using swing impedance trajectory circles:

Power swing impedance trajectory has been used in [31] to detect power swings. The proposed method in this reference describes the impedance locus of a power swing and a fault as a circular characteristic. In both power swing and fault condition, the center of the impedance trajectory is located outside the relay impedance characteristic. However, in a fault condition, the center of the impedance trajectory shifts to a location inside the relay impedance characteristic. This feature is used to distinguish between a fault condition and a power swing [31].

Minimum voltage evaluation method:

This method is based on the fact that during the OOS condition, the voltage at the electrical center substantially decreases [32]. The method uses the bus voltages of the system recorded in each step of transient stability studies for solving a single-variable nonlinear optimization problem for identifying the lines which are located in the electrical center [32]. More details about this method are presented in chapter 3.

Various methods for detecting power swings and distinguishing them from a fault condition are discussed in this section. When using any of these methods, an unstable power swing is detected, proper OOS tripping and blocking actions should be performed to avoid cascading outages in the system and blackout. Therefore, the potential location for relay mis-operation due to OOS conditions should be identified through conducting comprehensive planning studies with modeling critical distance relays, and OOS blocking scheme should be implemented in these locations. In this dissertation, an algorithm is proposed to identify the critical distance relays to be modeled in stability studies in order to precisely access the system behavior during disturbances. By modeling the critical distance relays identified by the proposed method, all local and system-wide impacts of a disturbance can be captured. Therefore, the transmission lines which will experience distance relay mis-operation during OOS condition can also be identified and proper OOS tripping and blocking actions can be implemented.

2.5 Summary

In this chapter rotor angle stability, different types of power swings and out-of-step condition are discussed. The impacts of a local and inter-area power swing on the system

and various protective relays are studied. Various out-of-step detection methods proposed in previous research works are presented and analyzed.

Chapter 3: Minimum Voltage Evaluation method and the proposed iterative algorithm for identifying critical distance relays

As mentioned in Chapter 1, representing protection systems in stability study software can significantly improve the preciseness and authenticity of stability studies. In this regard, the importance of modeling protective relays in transient stability studies has been investigated in some of the previous research works. Reference [33] analyzes the importance of modeling distance relays in planning studies by investigating a real-world case study. In this case study, the series of events leading to a major blackout initiated by a lightning strike and exacerbated by distance relay mis-operations due to overload on lines. To analyze the impact of protection devices on dynamic simulation, reference [1] performs several case studies with modeling distance relays, under/over voltage protective relays, as well as under/over frequency protective relays in the system based on the NERC standards or the best engineering practices. Reference [11] investigates the importance of modeling critical assets of the system including protective relays. The importance of performing transient stability studies with modeling protective relays in analyzing the vulnerability of a system has been demonstrated in this paper which highlights the shortcomings of steady-state analysis in identifying the critical system vulnerabilities.

As mentioned in the references, the behavior of the protection system during and after the occurrence of a contingency significantly affects the performance of the system, and the stability studies conducted without modeling protection systems may not precisely reflect the performance of the system. One of the most important protective relays that can

play a significant role in defining the system response to a disturbance is distance relay. Nevertheless, the current trend in the industry is to conduct transient stability studies without modeling distance relays. Therefore, proper modeling and representation of protection systems in stability software tools, such as GE PSLF, has been a concern in the industry for a long time.

As mentioned in chapter 1, modeling all the distance relays existing in a bulk power system has technical and practical challenges. Therefore, the need for developing an algorithm to identify the critical distance relays to be modeled in transient stability studies for achieving a precise assessment of system behavior is felt for a long time [5]. Such an algorithm will address both the mentioned challenges by significantly reducing the number of relays needed to be modeled in transient stability studies for assessing the system behavior during a disturbance.

In this regard, a link between computer-aided protection engineering (CAPE) software, which is software for analysis of protective relay response, and power system simulator for engineering (PSS/E) software has been developed in [34]. The link enables simultaneous analysis of protection systems response along with the dynamic response of the system in transient stability studies. The internal interface between CAPE and PSS/E is established using the CAPE-Transient Stability (CAPE-TS) module [34]. In every simulation step, the transient stability program (PSS/E) updates the positive-sequence voltage profile of the system and sends it to the CAPE software. Then, the CAPE software evaluates the operation of protective relays and the status of breakers. If any operation is identified by the CAPE, the network topology is simultaneously updated in the dynamic and protection

models. In the next iteration, the voltage profile of the system is calculated by the PSS/E software considering the updated network configuration and is send back to the CAPE [34]. Although the CAPE-PSS/E platform makes it possible to simultaneously analyze the protection system response and the dynamic response of the system, there are some disadvantages associated with this platform. In each iteration of the developed platform, the CAPE software only analyzes the operation of protective relays and the status of breakers which are located in the vicinity of the fault location. As thoroughly explained in Chapter 2, some severe disturbances might cause inter-area power swings and mis-operation of protective relays. These protective relays, which are not necessarily located in the vicinity of the fault location, are required to be analyzed for having a precise assessment of system behavior. Therefore, it is essential that any algorithm developed for identifying the critical distance relays be capable of identifying these distance relay mis-operations occurring at distant locations, as well. Such an algorithm enables a more realistic assessment of power system behavior while using transient stability analysis software, including the CAPE-TS co-simulation platform. Furthermore, the platform developed in [34] imposes a significant computational burden on the system since it needs to analyze numerous protective schemes in the grid at each iteration. Thus, this method requires an extended simulation time [35].

Different methods have also been proposed in the literature for identifying the critical protective relays in order to conduct precise transient stability studies. In reference [6] and [36] after a random fault or abnormal system condition, the vulnerable region is defined as the set of power system circuits which will be disconnected due to hidden failures

(unwanted operation) of distance relays in the system. The size of the vulnerable region is considered to depend on the location and size of initial events and the design of the protection schemes around the area of the initiating event. The general distance relay models with three operation zones are then considered for the transmission lines located in the identified vulnerable zones. The author of [37] has also considered vulnerability regions for the hidden failures of protection systems. The range of the vulnerability region depends on the setting of the related distance relays and the severity of the initiating event. Furthermore, a vulnerability index has been provided to identify the importance of vulnerable regions to model protective relays. The loss of stability of power systems is considered as the criterion for computing the vulnerability index. For modeling the primary protection of the transmission lines pilot relays have been used in this paper. Since pilot relays do not provide back-up protection, zone 2 and 3 protection of distance relays are modeled as the back-up protection. In all these works, the location and size of the initiating event identify the critical protection schemes. However, as stated before, the initial event may lead to several distance relay mis-operations on the lines far from the location of the initial event. Therefore, the approaches used in these papers cannot capture the system-wide effects of a disturbance and may yield an inaccurate assessment of system behavior.

Different methods of power swing detection including the methods based on ROC of the apparent impedance or resistance of relays, continuous calculation of incremental current, synchrophasor measurements, R-Rdot schemes, ROC of the swing center voltage, the behavior of center of circular locus of the impedance trajectory, wavelet transform, and the chaos theory are presented in references [19], [24], [26]-[27], [30]-[31], and [38]-[41].

These methods, if properly implemented in conjunction with stability studies, might be able to detect relay operations due to power swings and OOS conditions. However, they cannot identify all the critical distance relays required for performing accurate stability studies.

The independent system operator (ISO) of New England uses a generic distance relay model that has a zone-3 reach of 300% of line impedances for all the transmission lines. In the planning studies, if the relay trajectories are observed within their zone-3 reach, the actual data of these relays are collected, and the relays are represented in the analysis with accurate settings [42]. The operations of distance relays affect the system response to disturbances. After observing the operation of the first distance relay in a study, the system behavior for the remainder of the simulation time might be different from its behavior without modeling distance relays. Therefore, the set of critical distance relays, i.e., relays with impedance trajectories within their zone-3 reach, might be different from the set identified in the initial study. Therefore, another study should be performed to identify the new set of critical relays. However, this iterative process for identifying the critical distance relays has not been considered in [42].

Reference [43] proposes a random search algorithm based on power system heuristics for fast rare event simulation which are caused by relay mis-operations. Reference [5] proposes a generic strategy for identifying the critical distance relays to be modeled in transient stability studies for all contingencies. The proposed model in [5] utilizes a mixed-integer linear program (MILP) which is based on the prior generator grouping information and the network structure. The algorithm proposed in this paper is able to identify the

critical lines which may experience relay mis-operation due to unstable power swings. However, it does not consider the identification of distance relays which are located in the vicinity of the fault location and may operate due to the initial effects of the fault. Furthermore, the proposed strategy in [5], is a generic strategy which tries to find the critical distance relays for all kind of contingencies. Nevertheless, the type and location of the contingency significantly affect the set of critical distance relays which should be modeled for conducting precise stability studies. Thus, a methodology that identifies contingency-specific critical distance relays is of interest.

An iterative algorithm is proposed in this chapter that uses two methods of apparent impedance monitoring and the MVE to identify the critical distance relays that are required to be modeled in the stability studies of different contingencies. Modeling these critical distance relays enables capturing the local and wide-spread impacts of the contingency on the system and the behavior of distance relays during the contingency without exceeding the capabilities of stability software. Therefore, the proposed algorithm can address the need of the industry for an algorithm to eliminate both the mentioned challenges of modeling distance relays in stability studies.

With the recent trends in increasing penetration levels of renewable resources in power systems, the dynamic characteristics of power systems are impacted by renewable resources and their converters. As shown in [44] and [45], the dynamic control of voltage source converters (VSCs), which are usually used to integrate renewable resources into power systems, can lead the system toward instability under some operating conditions. Also, during some contingencies, the dynamic control of these VSCs might interfere with

the dynamic response of some of the distance relays, leading to mis-operation of these relays. Therefore, these mis-operating distance relays should be modeled in the transient stability studies of the contingencies. The renewable resources existing in a power system with their precise dynamic characteristics along with the dynamic characteristic and control of their converters can be included in the transient stability studies. Since the algorithm monitors all the lines in the system and identifies any probable distance relay operation (or mis-operation), these operations/mis-operations of distance relays due to inference with the dynamic response of renewable resources can be captured by the algorithm as well. Therefore, unlike previous methods, the proposed algorithm can identify these distance relays as critical and model them in transient stability studies, which enables a precise assessment of the dynamic behavior of the systems with a high penetration level of renewable resources.

In this chapter, the two methods used by the proposed iterative algorithm to identify critical distance relays including the apparent impedance monitoring method and the MVE method proposed in [32] are explained. Next, the proposed algorithm is explained in detail. Then, the shortcomings of the existing practices of relay modeling in transient stability studies are explained in detail. Finally, simulation results are presented to assess the performance of the proposed algorithm by analyzing different types of contingencies on the WECC system representing the 2018 summer-peak load case.

3.1 Identification of Critical Distance Relays

In this chapter, first, the two methods used in the proposed algorithm for identifying the critical distance relays are described. Then, the algorithm is explained in detail.

3.1.1 The apparent impedance monitoring method

The apparent impedance monitoring method checks whether the impedance trajectory of any transmission line (seen from both sides of the line) at any time interval of the transient stability study has traversed into any one of the operation zones of its distance relays or not. If that is the case, the distance relays are flagged as critical distance relays.

To shed light on the performance of the method, a three-phase *N-3* bus fault is studied on the WECC system and the impedance trajectories of some of the distance relays identified by the method are shown in Figure 3.1 (a), (b), and (c), respectively. The trajectories from relays at the two ends of a line are shown beneath each other. Figure 3.1 shows the characteristics of these critical relays, i.e., operation zones, as well. Note that in all the sub-figures of Figure 3.1, the y-axis and x-axis are reactance and resistance in p.u., respectively. As seen, the impedance trajectories of the distance relays traverse into their operation zones. Therefore, the method correctly identifies the distance relays as critical.

3.1.2 Minimum voltage evaluation method

The analytical MVE method proposed in [32] is used to detect unstable power swings which may lead to distance relay mis-operations. The method is based on the fact that during an OOS condition, different groups of generators start to form in the grid. The generators in each group may lose synchronism with respect to the generators in other groups. In this condition, the voltage angle differences at the two ends of some of the lines connecting these groups of generators, i.e., the lines located in the electrical center of the power swing, might become close to 180 degrees, which causes a significant voltage dropping along the connecting lines. The distance relays on these lines might misinterpret

the situation as a fault and open the lines [32]. Therefore, these distance relays should be considered in transient stability studies since their operations might lead to unintentional islanding and probable cascading outages in the system. OOS blocking schemes should be included on these lines to block mis-operations of their distance relays and avoid uncontrolled islanding. Furthermore, OOS schemes accompany tripping at appropriate locations to initiate controlled islanding during OOS conditions. However, varying operating conditions and disturbances can result in various relay mis-operations, which may or may not be equipped with OOS schemes.

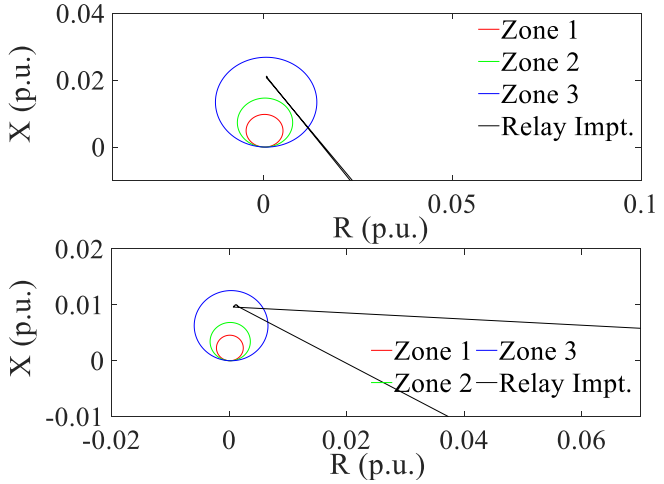

(a)

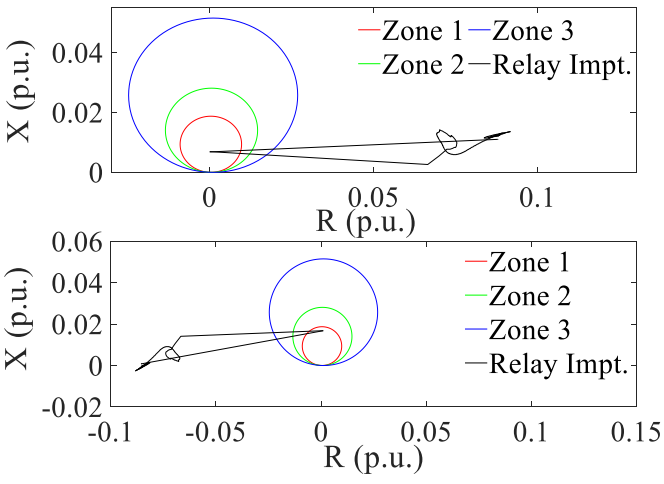

(b)

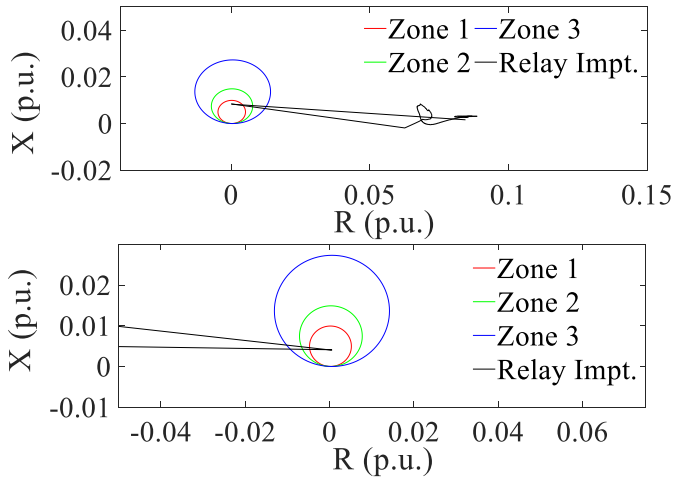

(c)

Figure 3.1 The relay impedances (Impt) of three of the transmission lines identified by the apparent impedance monitoring method and the operation zone of their relays.

The MVE method uses the bus voltages and line currents recorded at each step of the transient stability study and solves a single-variable nonlinear optimization model for each line at each time step. By doing so, the MVE identifies the lines which are located at the electrical center and may experience distance relay mis-operation due to OOS condition. If the shunt admittances of the lines are neglected, and the impedance per unit length of the lines are equal along the line, each transmission line can be represented as Figure 3.2.

Figure 3.2 Voltage along a transmission line

Considering Figure 3. 2, the voltage along each transmission line can be calculated using (3.1).

$$V_a = V_1 - a(R + jX)I_1 = (V_{1r} - aRI_{1r} + aXI_{1i}) + j(V_{1i} - aRI_{1i} - aXI_{1r}) \qquad (3.1)$$

Where V_1 is the voltage at bus 1, I_1 is the flow on the line, and R and X are the resistance and reactance of the line, respectively. a is the fraction of the line length under study. V_{1r} and V_{1i} are the real and imaginary parts of V_1, respectively. Likewise, I_{1r} and I_{1i} are the real and imaginary parts of I_1, respectively. The MVE method solves the optimization problem (3.2) and (3.3) to find the minimum voltage magnitude along each transmission line at each time interval.

Objective: Minimize

$$|V_a| = \sqrt{(V_{1r} - aRI_{1r} + aXI_{1i})^2 + (V_{1i} - aRI_{1i} - aXI_{1r})^2} \quad (3.2)$$

Subject to: $0 \leq a \leq 1$ (3.3)

All the variables in the right-hand side of (3.2) are known from each time step of a transient stability study except for a. Therefore, the optimization problem (3.2) - (3.3) is a single-variable optimization model which can be easily solved for each line at each time interval of the transient stability study.

The optimization problem of (3.2) and (3.3) can have local optimal solutions at the endpoints (i.e. $a = 0$ and $a = 1$), the points where the first derivative of $|V_a|$ with respect to a is zero (i.e. $\frac{d|V_a|}{da} = 0$), and the points where the first derivative of $|V_a|$ with respect to a does not exist. Among these local minima, the smallest value of $|V_a|$ is considered as the global minimum of (3.2) - (3.3). If for any transmission line, this global minimum becomes zero at any time interval of transient stability study, without any fault being applied to the line, it can be concluded that the line is in the electrical center. In this situation, due to the severe voltage dip along the line, the impedance observed by the distance relays installed

on either side of the line may traverse into one of the operating zones of their mho characteristics. The relays mis-interpret the situation as a fault and will operate. Therefore, these distance relays need to be modeled in the transient stability study of the contingency and the algorithm used for the purpose of identifying the critical distance relays should be equipped with such a method as MVE to identify the lines which are in the electrical center.

Note that since the transient stability study is performed at discrete time steps, the zero voltage at the electrical center might happen between two consecutive time steps. Therefore, the zero minimum voltage might not be obtained in the optimization problems solved in discrete time steps. However, because power swing traverses slowly, a small threshold for voltage magnitude can be considered for identifying the electrical center [32]. Therefore, if (3.4) holds, the line is considered to be in the electrical center.

$$\left|V_a^{min}\right| \leq \varepsilon \tag{3.4}$$

In (3.4), $\left|V_a^{min}\right|$ is the minimum voltage magnitude along the transmission line. This voltage occurs at a_{min} fraction of the length of the line and is obtained by solving the optimization problem (3.2) and (3.3). ε is the considered threshold for voltage and is set to 0.05. More details of the MVE method can be obtained from [32].

The contingency of Chapter 3.1.1 is also considered here, and the impedance trajectories seen from both ends of some of the lines identified by the MVE method along with the characteristics of their distance relays are illustrated in Figure 3.3. a, b, and c, respectively. As seen in Figure 3.3, the impedance trajectories of these lines traverse into one of the operation zones of their distance relays. Thus, depending on the location of the

voltage drop along the line, the relay on either end of the line may respond to the condition by opening the line, which shows that the MVE method has correctly identified that the lines are located in the electrical center. Note that, the impedance trajectories shown in Figure 3.1 and Figure 3.3 are obtained using the "zmetr" models invoked in the dynamic file while performing the transient stability analysis for the contingencies. Zmetr is a standard dynamic model in the PSLF library that is modeled on either end of a line to measure the apparent resistance and reactance of the line observed from that end of the line at each step of the simulation [46].

3.1.3 The proposed algorithm for identifying the critical distance relays

Figure 3.4 depicts the flowchart of the proposed algorithm. As shown in this flowchart, in the first step of the algorithm, a transient stability study without modeling any distance relays is performed for the contingency under study for the entire desired study time, e.g., 10 seconds. Then, the algorithm obtains all the information required by the apparent impedance monitoring and the MVE methods to identify critical distance relays from the results of the transient stability study. It is to be noted that all the required data including bus voltages and the apparent impedances of the lines are captured at each time interval of the transient stability study without any change in the existing practice.

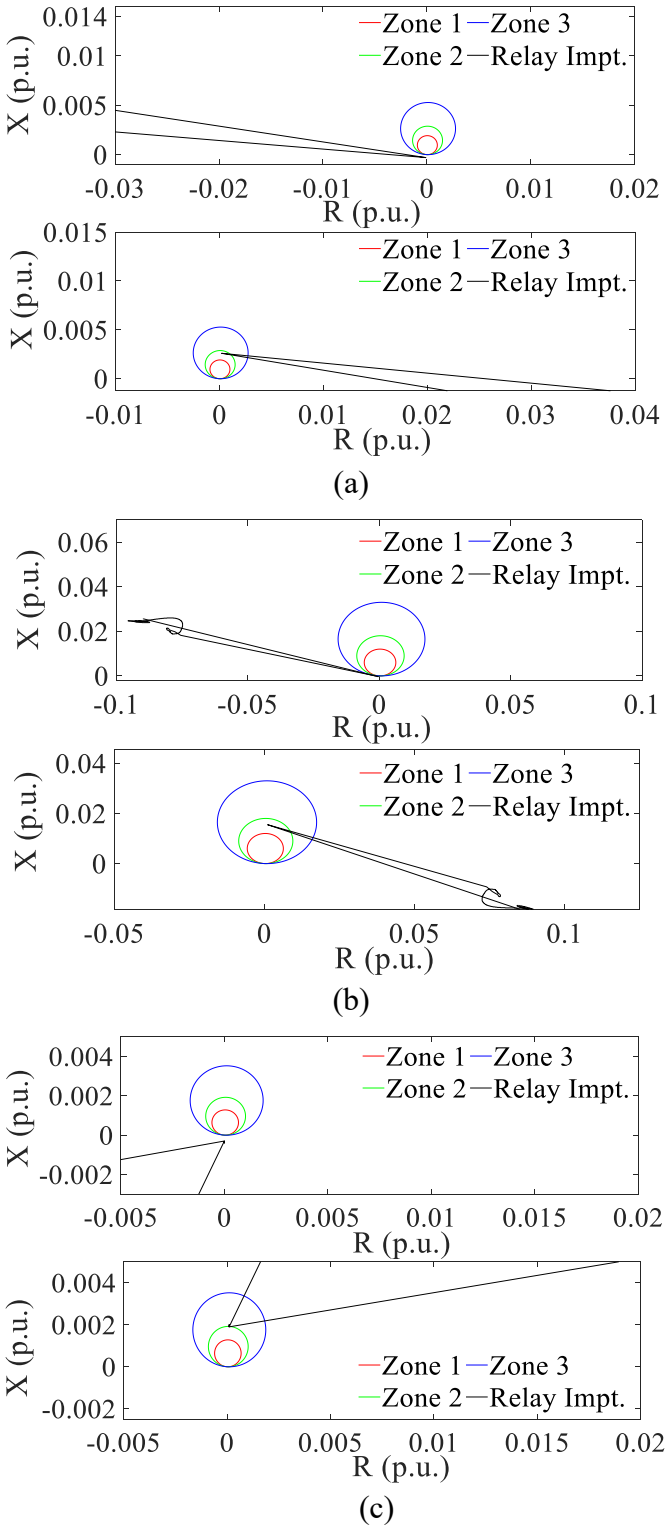

Figure 3.3 The relay impedances of some of the lines identified by the MVE method and operation zones of their relays.

After obtaining the required data from the stability software, the apparent impedance monitoring and the MVE methods identify the lines that are prone to experience distance relay operation. Then, at each iteration (except the first one), the algorithm checks whether any new critical distance relays, which have not been identified in the previous iterations, are identified by either of the two methods. If no new critical distance relay is identified, the algorithm stops; the results of the last iteration of the transient stability study captures the behavior of the system during the contingency. Otherwise, if there exists any new critical distance relay, the algorithm includes their models on both sides of the corresponding transmission lines. Then, the algorithm performs the next iteration of the transient stability study for the entire desired study time while including the distance relays identified by either of the methods. Subsequently, the algorithm utilizes the two methods again and finds new critical distance relays. This iterative process continues until no new critical distance relay is identified by either of the two methods. Since at each iteration, the transient stability study is conducted for the entire simulation time, if no distance relay is identified as a critical distance relay by the algorithm, it is guaranteed that no new critical distance relay will be identified in the next iterations, as well.

Note that OOS schemes implemented in distance relays are not considered in this dissertation. However, if the detailed information about the relays that are equipped with OOS schemes is provided from the protection group, such schemes can be included on the distance relays that are flagged by the algorithm as critical distance relays. Thus, the algorithm can evaluate the effectiveness of the OOS schemes of such relays.

For any type of contingency, this algorithm provides a dynamic data file that includes

all the distance relay models required for analyzing the contingency. It also provides the results of transient stability study performed with modeling all the critical distance relays.

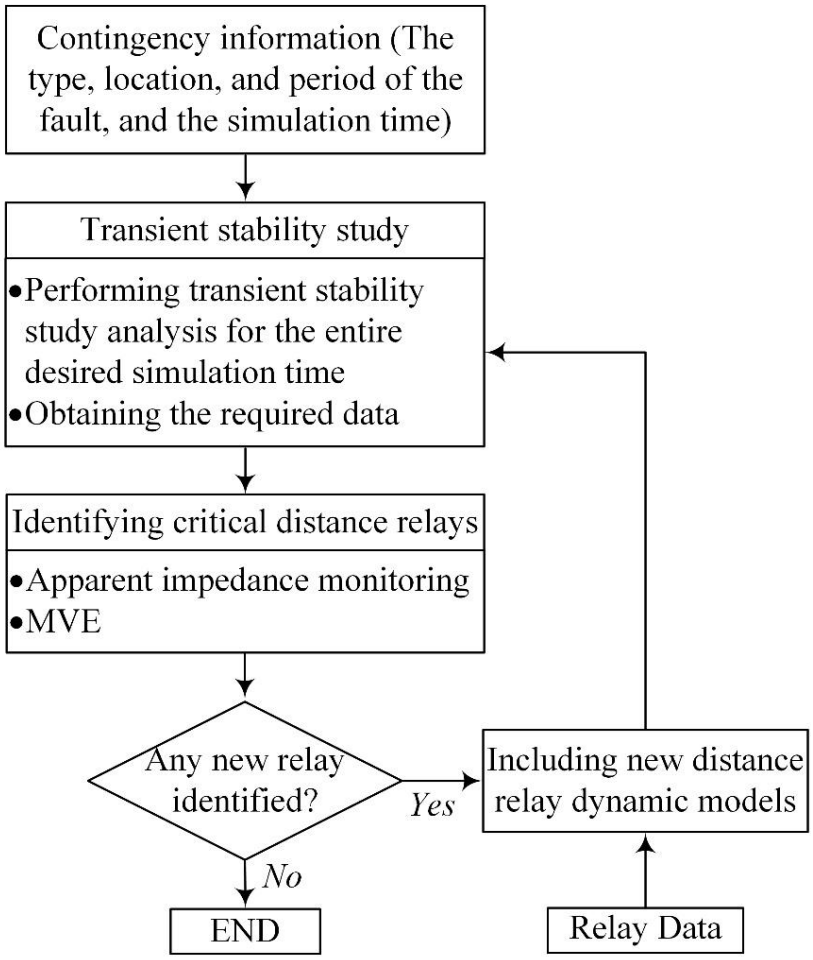

Figure 3.4 The flowchart of the proposed iterative algorithm.

The proposed algorithm addresses the challenges of modeling all the distance relays by significantly reducing the number of distance relays required to be modeled for performing precise transient stability studies. Therefore, the algorithm equips electric utilities with an efficient offline tool for performing precise transient stability studies for different types of contingencies in their planning studies.

The accuracy of the proposed method is tested in chapter 3.3 considering different types

of contingencies, and the results are compared with a reference case which includes distance relay models on all the lines with the voltage level of 345 kV and above. Before evaluating the performance of the proposed method, the most important shortcomings of current practices of existing relay modeling practice are elaborated upon in chapter 3.2.

3.2 Drawbacks of the existing relay modeling practice

Although node-breaker models are gaining more attention in recent years, the common utility practice in transient stability studies is still to represent the system using the bus-branch model. Even though modeling and studying the system using the bus-branch model is easier, it has a drawback associated with simulating bus faults when distance relays are represented. In the bus-branch model shown in Figure 3.5 (a), when a fault occurs on a bus, all the distance relay models placed on the lines connected to the bus observe the fault and react to it by opening the respective lines. However, this is not usually the case in actual systems, where the substation architecture is in a node-breaker structure as shown in Figure 3.5 (b). A bus fault in the node-breaker model is cleared by isolating the faulted bus via breaker opening. Therefore, to obtain a precise characterization of a bus fault, the faulted bus needs to be modeled using a node-breaker model. The closest approximation of an

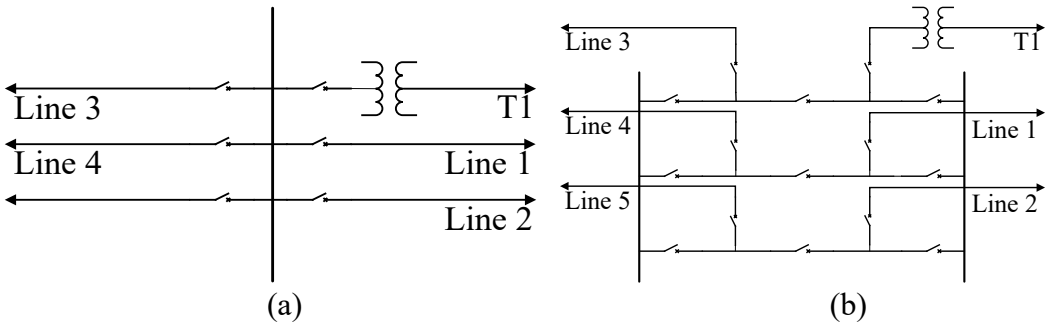

Figure 3.5 The bus-branch (a), and the node-breaker (b) representation of a bus

actual bus fault in the bus-branch model is placing a line fault on a small fraction (e.g., 0.05) of the line length from the intended bus. This will approximately have the same effects of a fault on the bus and only the distance relay of one line will react to it.

To demonstrate this drawback, since we do not have access to the node-breaker representation of the WECC system, a case of bus fault on bus 50 of the small test system shown in Figure 3.6 (a) is studied. For comparison, the same bus fault is studied in the bus-branch representation of the test case, shown in Figure 3.6 (b). Moreover, a 3-phase line fault on the line between bus 50 and 100 in Figure 3.6 (b) is studied in the bus-branch model. The fault is applied at a distance of 5% of the length of the line from bus 50 to approximate the response of the node-breaker model to the bus fault. The faults were cleared after 4 cycles [47].

The relative rotor angles of generators (with respect to generator 1, the slack generator) for each case are illustrated in Figure 3.7. Figure 3.7 (a) and Figure 3.7 (b) show that the relative rotor angle of generator 2 is different in the two cases of simulating the bus fault using the node-breaker model and the bus-branch model. In Figure 3.7 (b), Generator 2 was separated due to multiple relay operations after the initial bus fault. Figure 3.7 (c) shows that the line fault occurring at the close vicinity of the bus can approximately imitate the response of the node-breaker model to the bus fault.

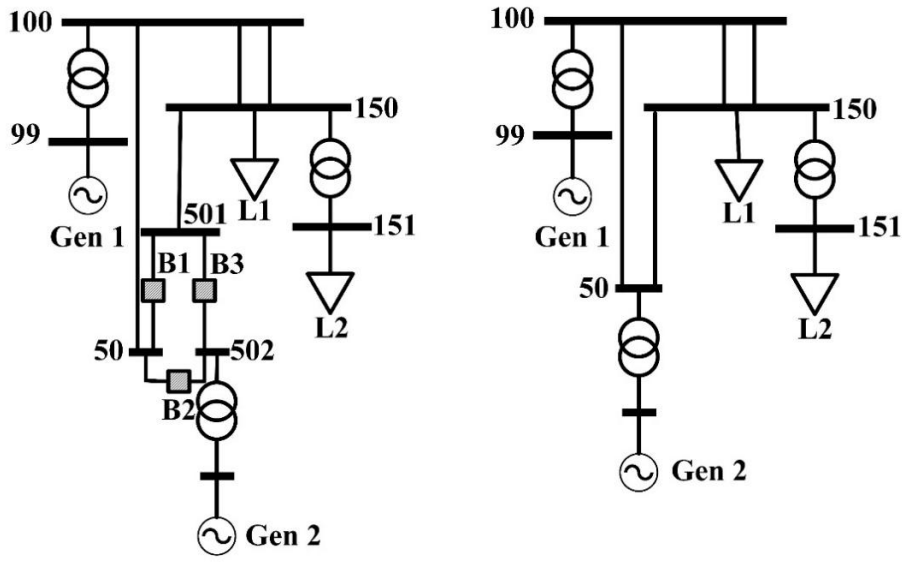

(a) (b)

Figure 3.6 The node-breaker (a), and the bus-branch (b) models of the test case

To also show this point in the WECC system, as we do not have access to the node-breaker representation of the system, a case of bus fault on a 500 kV bus of the system (bus 1) is studied to represent the behavior of the system to a bus fault in the bus-branch model. The result is compared with a case of applying a 3-phase fault on the 500 kV line connecting bus 1 to the bus 2. The fault is applied at 0.05 length of the line from bus 1. Both faults were cleared after 4 cycles. Note that throughout this dissertation, random numbers are used to represent elements, e.g., bus numbers, to protect the proprietary data. The rotor angles of a set of generators are illustrated for both cases in Figure 3.8. As seen in Figure 3.8, the relative rotor angles are different in the two cases, which shows that the bus-branch model cannot precisely represent the response of the system to a bus fault when distance relays are modeled.

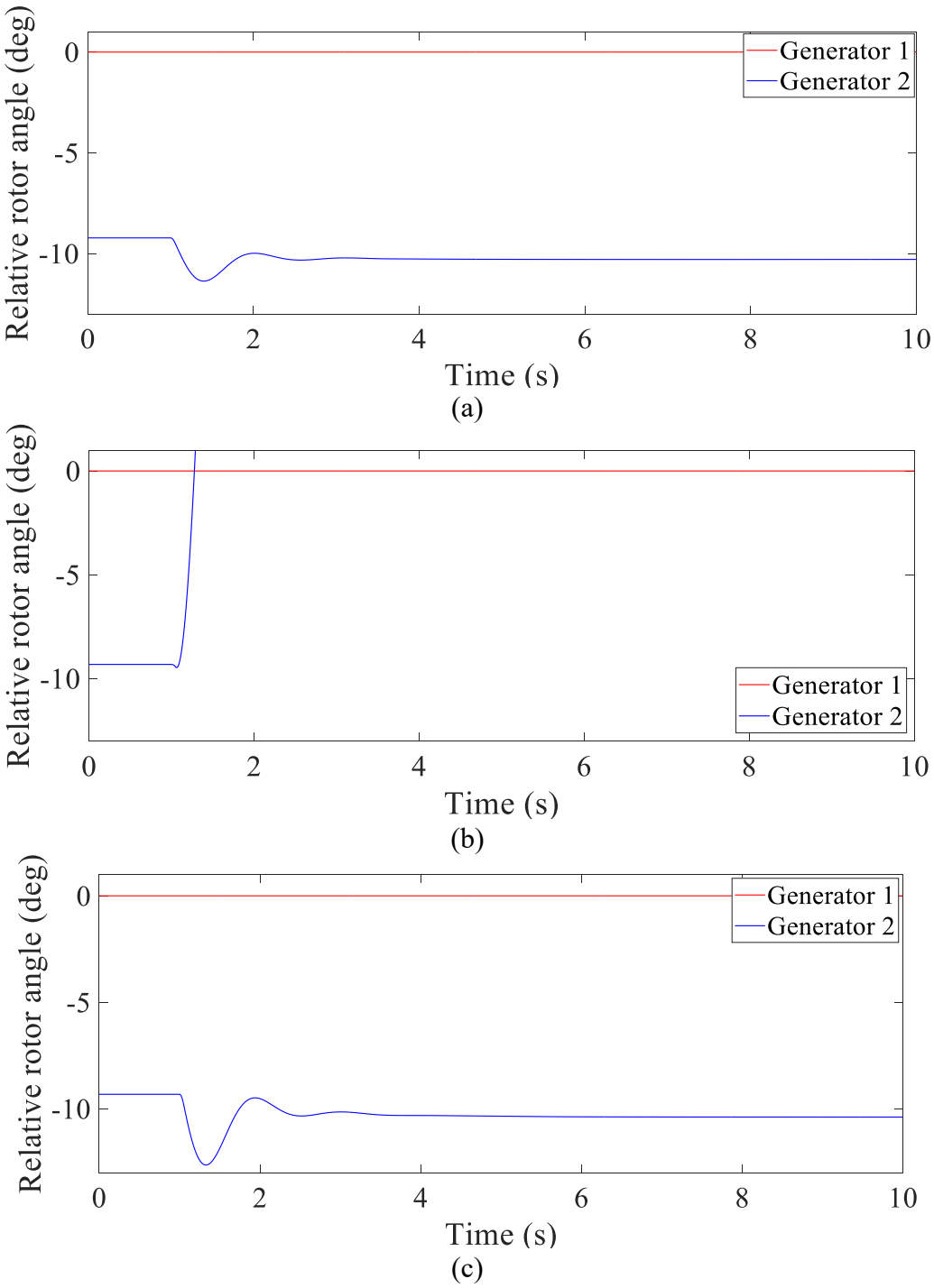

Figure 3.7 Relative rotor angles: (a) a bus fault in node-breaker model, (b) a bus fault in bus-branch model, and (c) line fault near a bus in bus-branch model.

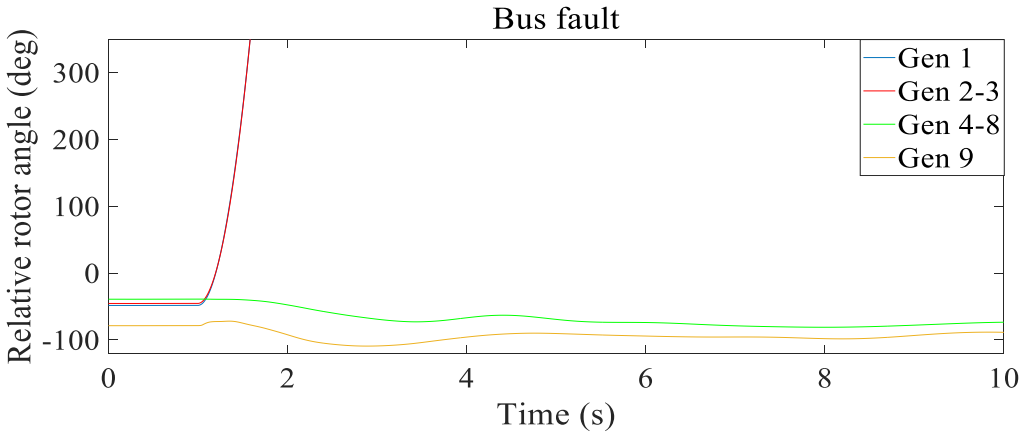

(a)

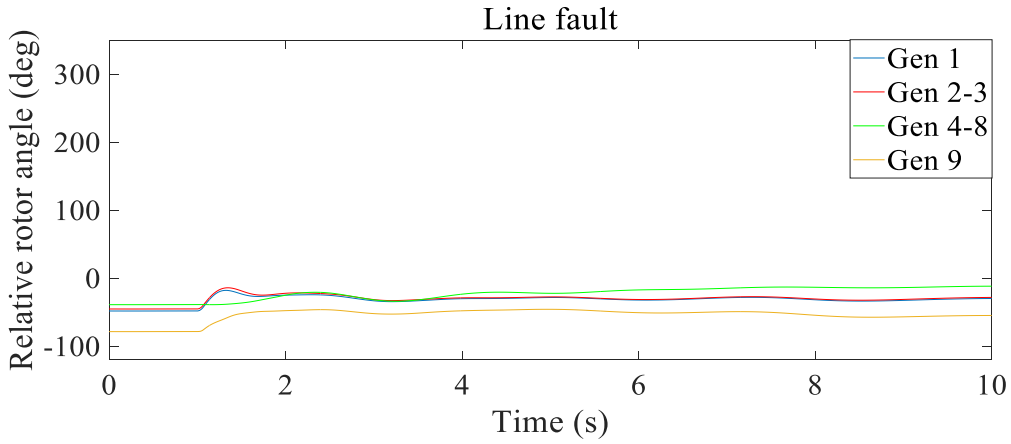

(b)

Figure 3.8 The relative rotor angles of a set of generators after a bus fault in the bus-branch model (a), and a line fault near the bus, an approximation of a bus fault in node-breaker model (b)

Another challenge of relay modeling in stability studies is the nontrivial coordination to maintain and update relay settings for a large number of distance relays. In the current practices of stability studies, for analyzing a disturbance while modeling distance relays, the dynamic models of all the relays are required to be included. This makes it a challenging task to keep the setting information of distance relays updated in the dynamic models. As mentioned earlier, performing stability studies using outdated relay settings might lead to

a completely different assessment of system behavior. To illustrate this point, a line fault is studied on the WECC system. The same line fault is also studied with changes in the zone-2 and -3 reaches of two distance relays from 120 and 220 percent of the related line impedance to 100 and 120 percent of the line impedance, respectively. A 0.05s change in zone-2 and zone-3time delays of the distance relays is also applied.

The rotor angles of a set of generators are shown in Figure 3.9 to show the difference of the system response with the change in the distance relay settings. Figure 3.9 confirms that conducting transient stability studies without updated relay settings might lead to invalid results. Therefore, it is necessary to keep track of the changes that are made in distance relay settings. The proposed algorithm simplifies this task by significantly reducing the number of distance relays that need to be included in transient stability studies while modeling a disturbance.

3.3 Test case

The WECC system data representing the 2018 summer peak load case is used to conduct the simulations and evaluate the performance of the proposed iterative algorithm. The system includes 23297 buses, 18347 lines, 4224 generators, and 9050 transformers. The maximum generation capacity of the system is 281.38 GW, and the load is 174.3 GW.

The proposed algorithm is tested by comparing its performance in identifying critical distance relays with a reference case, where all the distance relays are included on the high voltage transmission lines. Two distance relay models from the PSLF model library [46], namely, “Zlin1” and “Zlinw” models, are used in this study:

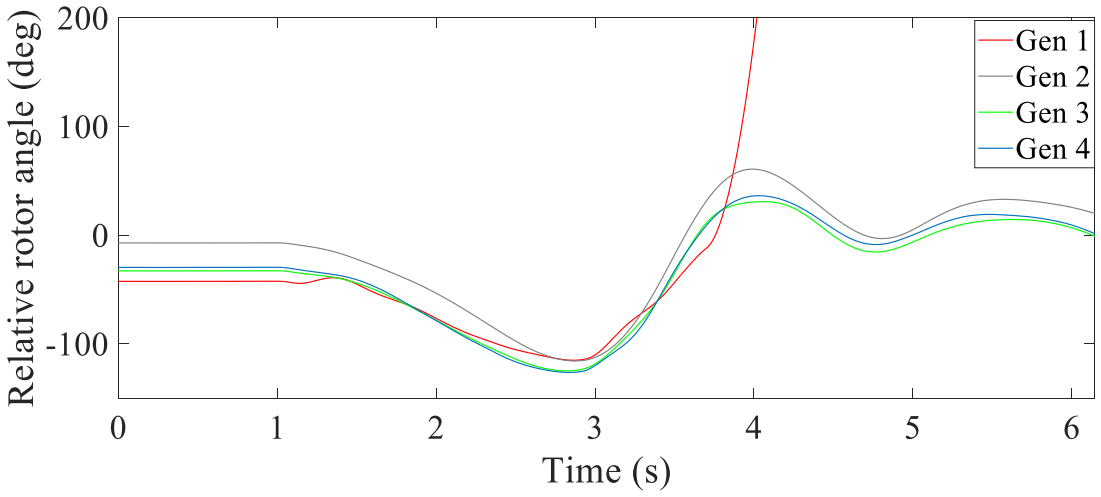

(a)

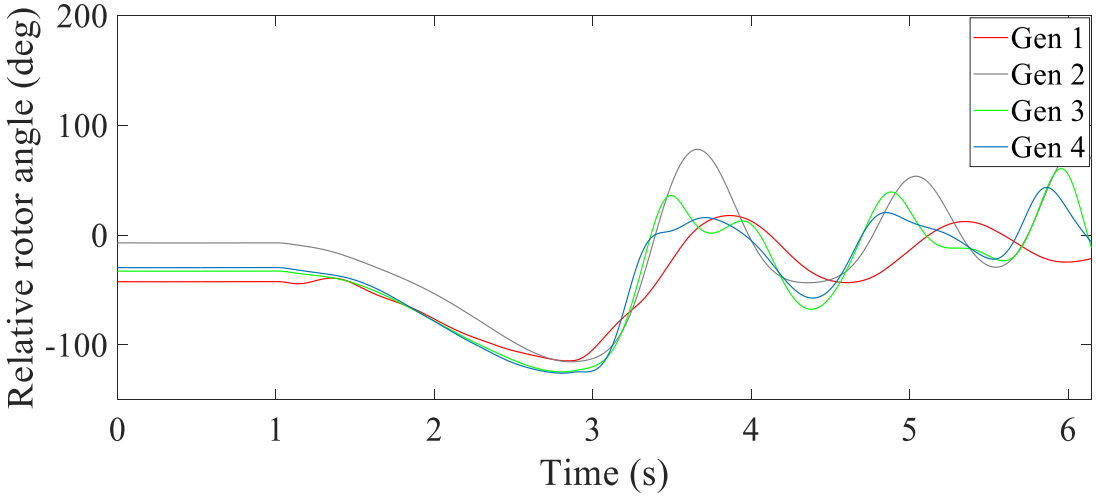

(b)

Figure 3.9 The relative rotor angles of a set of generators in two cases of (a) using the outdated and (b) using the updated distance relay settings

- "Zlinw", which is a generic distance relay model with two operation zones in the PSLF model library [46], is used to monitor all the lines in the system with the voltage level between 100 kV and 345 kV. This model is included in both the test case and the reference case.

- "Zlin1", which is a more accurate distance relay model with three operation zones in the PSLF model library [46], is used to model distance relays on the transmission lines with the voltage level of 345 kV and above in the reference case. The proposed algorithm is used to identify critical distance relays on transmission lines with the voltage levels of 345 kV and above; *Zlin1* models are included on critical distance relay locations during the proposed iterative process. The results of this case with *Zlin1* modeled only on critical lines are compared with the reference case, where *Zlin1* is modeled on all the lines with the voltage level of 345 kV and above.

It is to be noted that the choice of *Zlinw* for the lines with a voltage level less than 345 kV is made based on the software limitation as modeling *Zlin1* on all the transmission lines overwhelms the dynamic file and is beyond the existing capability of the PSLF. The *Zlinw* model does not need to be modeled for every line with their specific settings; rather, it is just one model with two operation zones that monitors all the lines between its minimum and maximum voltage settings.

Although the proposed algorithm can identify all the critical lines at any voltage level, in order to compare the results of the algorithm with the reference case, the settings of the algorithm are modified to only identify the critical lines with voltage levels of 345 kV and above. To illustrate the importance of modeling distance relays on the dynamic response of the system, another case is studied that does not include any distance relay models.

For all the distance relays modeled on the transmission lines at voltage levels of 345 kV and above in the reference case as well as for the critical distance relays identified by

the algorithm (*Zlin1* models), zone-1, -2, and -3 reaches are considered to be 80%, 120%, and 220% of the line impedances, respectively. The time delays of zone-1, -2, and -3 operations of the *Zlin1* models are set to be 0, 0.2, and 0.3 seconds, respectively. Similar settings are used for zone 1 and 2 of the *Zlinw* model. Also, the time delay of circuit breakers, i.e., the delay between the time when a distance relay sends a tripping signal to a circuit breaker and the time when the circuit breaker opens the line, is set to 0.05 (s) in both cases. Note that while generic relay settings are used for simplicity, the algorithm can be used in planning studies with the accurate relay settings from the protection engineering groups of utilities.

3.4 Evaluating the performance of the proposed method

Different types of contingencies including line faults and bus faults followed by removing one or more lines are studied, and the performance of the algorithm is compared with the reference case and the case of not modeling any distance relays. The contingencies selected for the case studies are among the contingencies that have local as well as widespread impacts on the WECC system. These contingencies cause multiple distance relay operations near the fault location and as they are severe disturbances, they cause unstable power swings on some of the transmission lines of the system, which results in multiple distance relay mis-operations in the system due to unstable power swings. Therefore, analyzing the proposed algorithm using these case studies shows whether the algorithm can capture distance relay operations due to the local and widespread impacts of the contingencies.

3.4.1 Case study 1

In this case study, a line fault is modeled on the 500 kV line between bus 3 and bus 4, which is a part of the California-Oregon Intertie (COI) and is cleared 4 cycles later by opening the line. During the contingency, the distance relays of 16 lines operate (before the system becomes unstable and the transient stability study terminates) in both the reference case and the case of using the proposed algorithm. The results of the transient stability studies carried out on the three cases of modeling no distance relays, using the reference dynamic file, and using the proposed algorithm are illustrated in Figure 3.10 (a), (b), and (c), respectively.

As shown in Figure 3.10 (a), without modeling distance relays, only small oscillations are observed in the rotor angles of a set of generators, which are finally damped. However, the same generators start to lose synchronism with respect to each other in Figure 3.10 (b), the reference case. Figure 3.10 (c) shows that the proposed algorithm is able to capture the behavior of the system exactly like the reference case, even for severe disturbances with widespread effects on the system and multiple distance relay operations. Note that while only the relative rotor angles of the selected generators are shown for all the case studies for the sake of clarity, the relative rotor angles of all the generators show the exact same behavior in the reference case and the proposed method.

It needs to be mentioned that in a real-world system, there are remedial actions that start after the occurrence of severe disturbances to alleviate their effects on the system. Controlled islanding and load shedding are among the most important remedial actions which are widely used to suppress the system-wide effects of disturbances and bring the

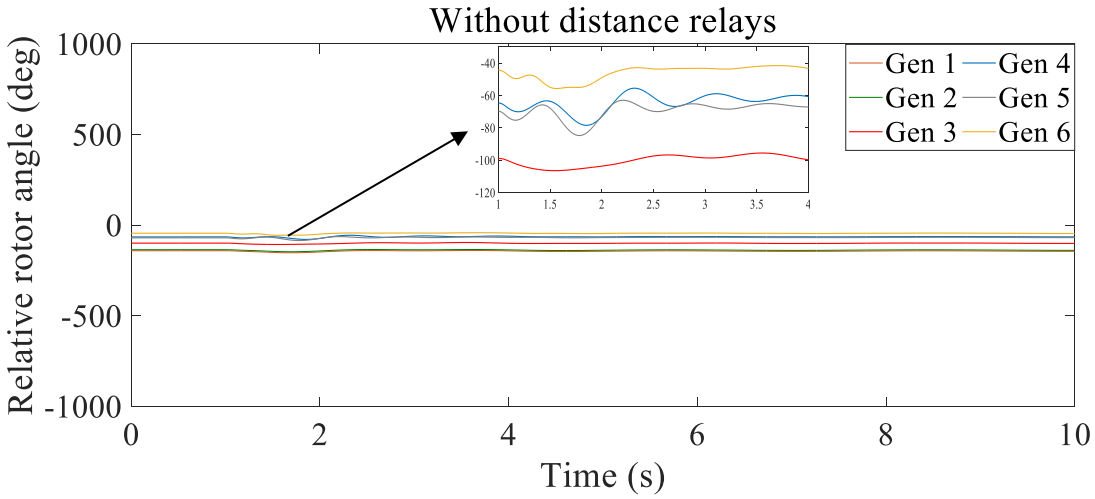

(a)

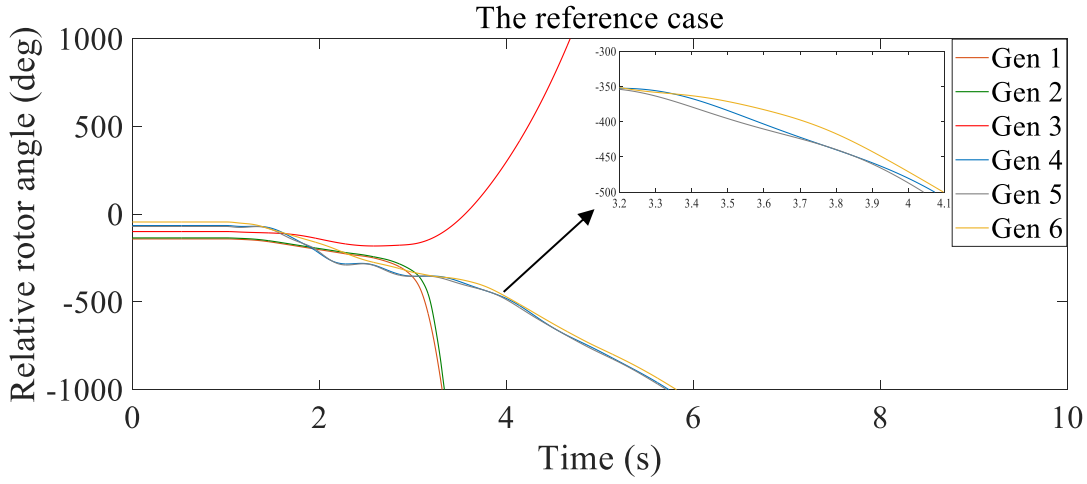

(b)

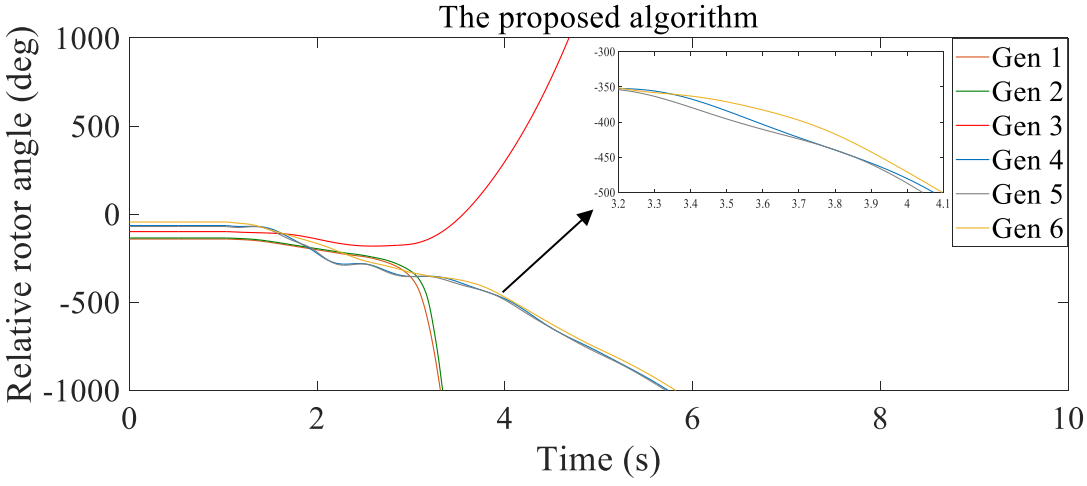

(c)

Figure 3.10 The relative rotor angles of a set of generators in case study 1.

system back to a stable condition. However, in this dissertation, we do not have access to the remedial actions used in the WECC system, and the transient stability studies were conducted without considering remedial actions. Nevertheless, the remedial actions can be included in the proposed algorithm, and it will be able to capture the behavior of the system in this case, as well. Table 3.1 shows the list of the relays which operated in this case study. It needs to be mentioned that the first two columns in all the tables providing the list of relay operations show the relay operations in the reference case along with their time of operation, whereas the third and fourth columns show the relay operations in the proposed algorithm along with their time of operation. As seen in Table 3.1, the same distance relays operate at the same time in both cases, which shows that the algorithm can identify all the critical distance relays in the system.

Table 3.1 The list of all distance relay operations in case study 1

The reference case		The proposed algorithm	
Time (s)	Relay	Time (s)	Relay
1.050	Lines 1, 2, 3	1.050	Lines 1, 2, 3
1.921	Line 4	1.921	Line 4
2.692	Line 5	2.692	Line 5
2.862	Line 6	2.862	Line 6
2.879	Lines 7, 8	2.879	Lines 7, 8
2.900	Line 9	2.900	Line 9
3.054	Line 10	3.054	Line 10
3.079	Line 11	3.079	Line 11
3.108	Line 12	3.108	Line 12
3.296	Line 13	3.296	Line 13
5.954	Line 14	5.954	Line 14
6.291	Line 15	6.291	Line 15
6.300	Line 16	6.300	Line 16

3.4.2 Case study 2

In this case study, a bus fault occurs on bus 3 for 4 cycles and is cleared by removing three COI lines. COI includes three 500 kV transmission lines transferring a total power of around 4113 MW from the north to the south during the summer peak load. These lines are very critical tie lines of the WECC system as they transfer a huge amount of power during the summer peak load. The outage of these lines has always been a critical contingency for the WECC system. Therefore, in this case study, the occurrence of this N-3 outage after a bus fault on bus 3 is studied. During the contingency, the distance relays of 25 lines operate (before the termination of the transient stability study) in both the reference case and the case using the proposed algorithm. The results of transient stability studies performed in the cases of not modeling distance relays, using the reference dynamic file, and using the proposed algorithm are depicted in Figure 3.11 (a), (b), and (c), respectively.

Comparing Figure 3.11 (a) and (b) shows that without modeling distance relays, the response of the system is completely different from that of the reference case. Also, Figure 3.11 (b)-(c) show that the generator rotor angles are similar in both the reference case and the proposed algorithm, which demonstrates the accuracy of the proposed algorithm in capturing the actual response of the system. Note that with distance relays modeled, the network solution in the stability software diverges at 6.283 (s) and the transient stability study terminates after the system becomes unstable in this case. For simulating the bus fault, the bus-branch model is used in this dissertation. However, if the node-breaker model of the system is provided, the algorithm is also expected to be able to identify the critical distance relays in the node-breaker model.

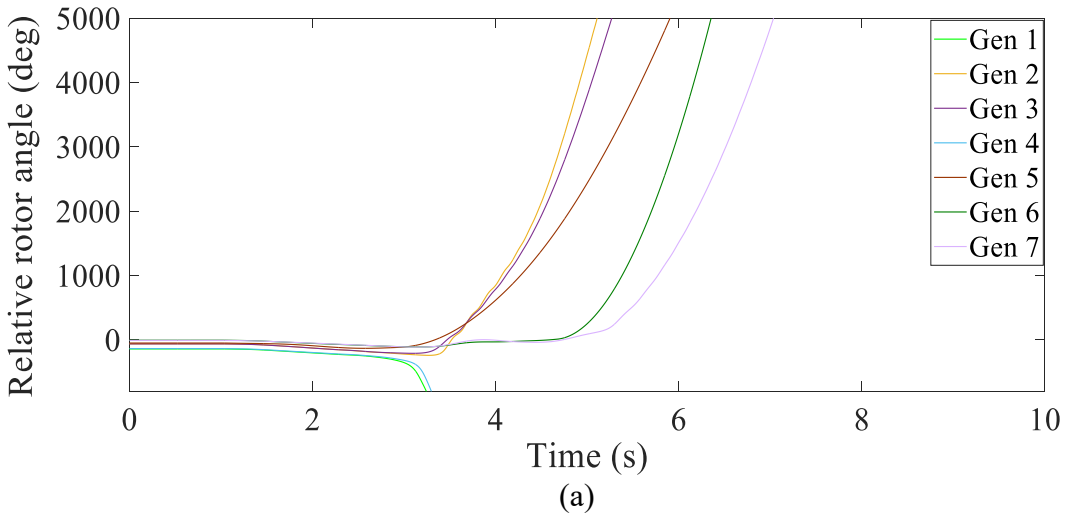

(a)

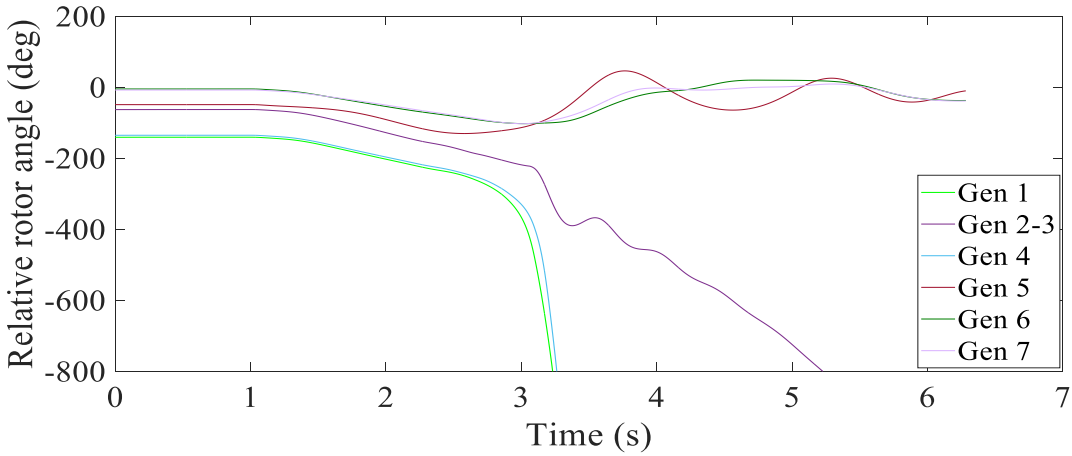

(b)

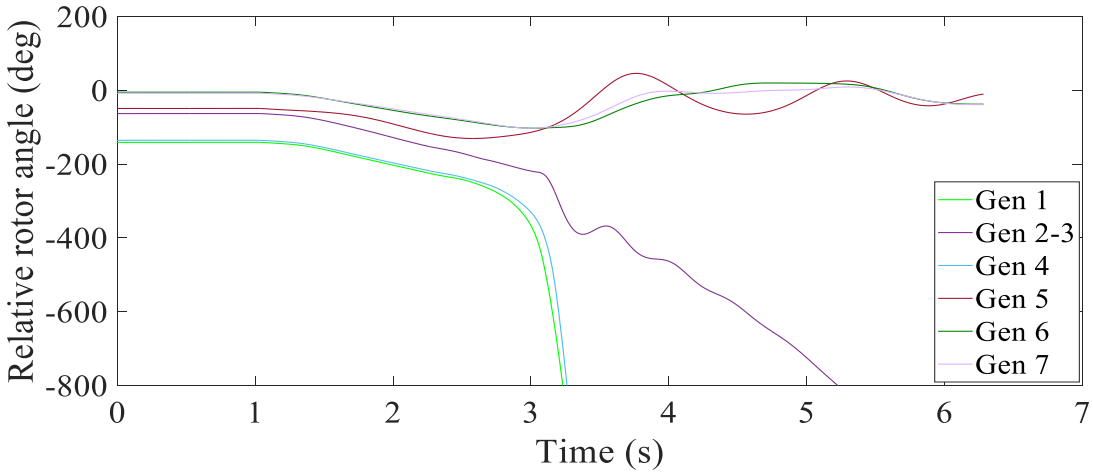

(c)

Figure 3.11 The relative rotor angles of a set of generators in case study 2.

The list of the relays which operated during this case study is provided in Table 3.2. As seen in this table, the same distance relays operate at the same time in both cases. This result shows that the algorithm can identify all the critical distance relays in this case study, too.

Table 3.2 The list of all distance relay operations in case study 2

The reference case		The proposed algorithm	
Time (s)	Relay	Time (s)	Relay
1.050	Lines 1, 2, 3, 17, 18, 19, 20	1.050	Lines 1, 2, 3, 17, 18, 19, 20
1.946	Line 4	1.946	Line 4
2.750	Line 5	2.750	Line 5
2.921	Line 21	2.921	Line 21
2.933	Line 7	2.933	Line 7
3.025	Line 8	3.025	Line 8
3.046	Line 9	3.046	Line 9
3.104	Line 11	3.104	Line 11
3.117	Line 10	3.117	Line 10
3.129	Line 22	3.129	Line 22
3.142	Line 12	3.142	Line 12
3.321	Line 13	3.321	Line 13
5.875	Line 14	5.875	Line 14
6.104	Line 15	6.104	Line 15
7.712	Line 23	7.712	Line 23
8.542	Line 24	8.542	Line 24
8.596	Line 25	8.596	Line 25

3.4.3 Case study 3

To analyze the performance of the proposed algorithm in more common less severe disturbances, a line fault was applied on a 500 kV line for 4 cycles and is cleared by opening the faulted line (*N-1* outage). The results of transient stability studies performed in the cases

of not modeling distance relays, using the reference dynamic file, and using the proposed algorithm are depicted in Figure 3.12 (a), (b), and (c), respectively.

As it is shown in this figure, there is a small yet observable difference between the case of modeling no distance relay and the reference case. The reason for observing a small difference between these two cases is the fact that unlike previous case studies where a severe disturbance was applied to the system, the disturbance is small in this case study, and it does not have wide-spread impacts on the system. It is observed that the algorithm yields the results which are similar to that of the reference case.

Table 3.3 shows the list of relays that operated during this contingency. As can be seen in this table, only one relay reacts to the fault and the algorithm correctly identifies that distance relay as a critical distance relay.

3.4.4 Case study 4

To evaluate the performance of the proposed algorithm in unlikely cases of multiple faults occurring consecutively in the system, a case is studied where a line fault occurs on the 500 kV line between bus 3 and bus 5 and is cleared by removing the faulted line and the 500 kV line between bus 3 and bus 6. The second fault occurs four seconds later, on the 500 kV line connecting bus 4 to bus 6 and is cleared by removing the faulted line. For this contingency, in both the reference case and the proposed algorithm, the distance relays of 16 lines operate. The results of transient stability studies carried out in the cases of modeling no distance relays, the reference case, and the proposed algorithm are shown in Figure 3.13 (a), (b), and (c), respectively.

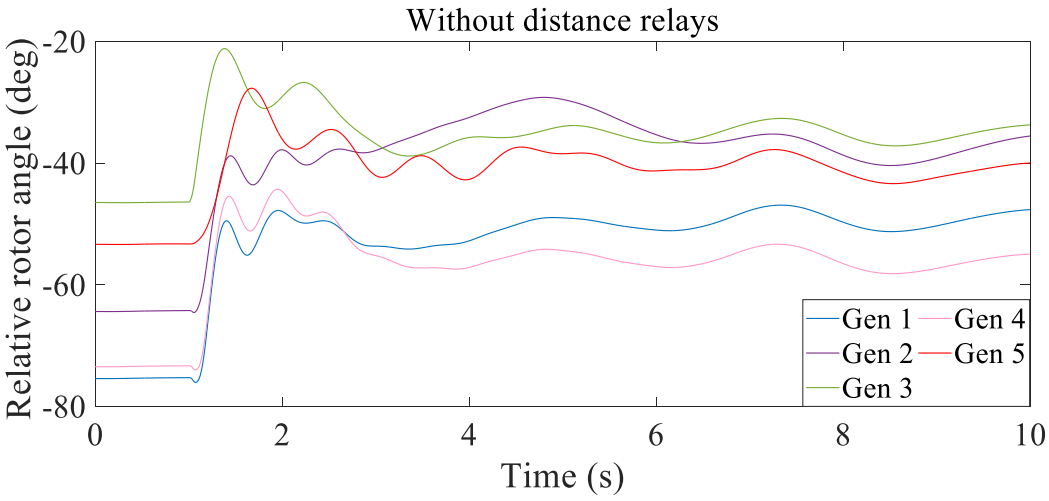

(a)

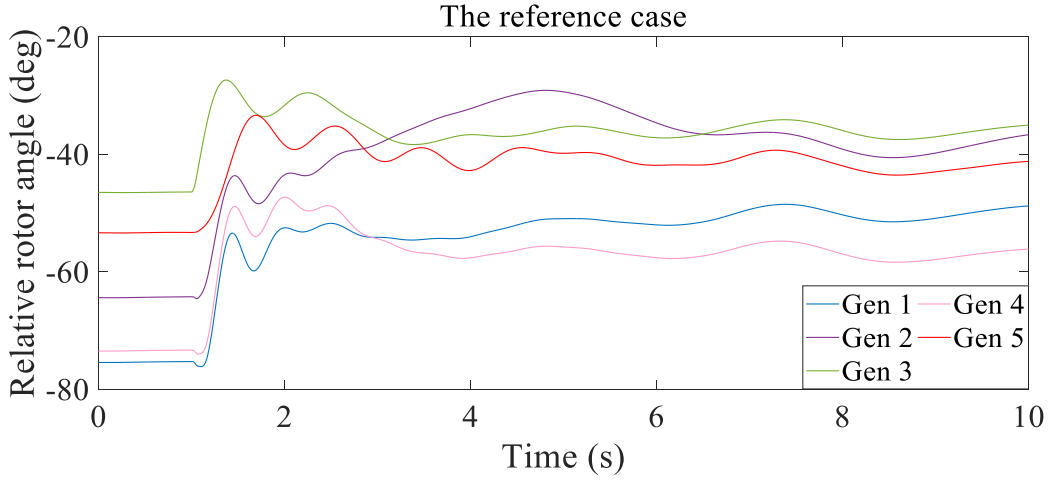

(b)

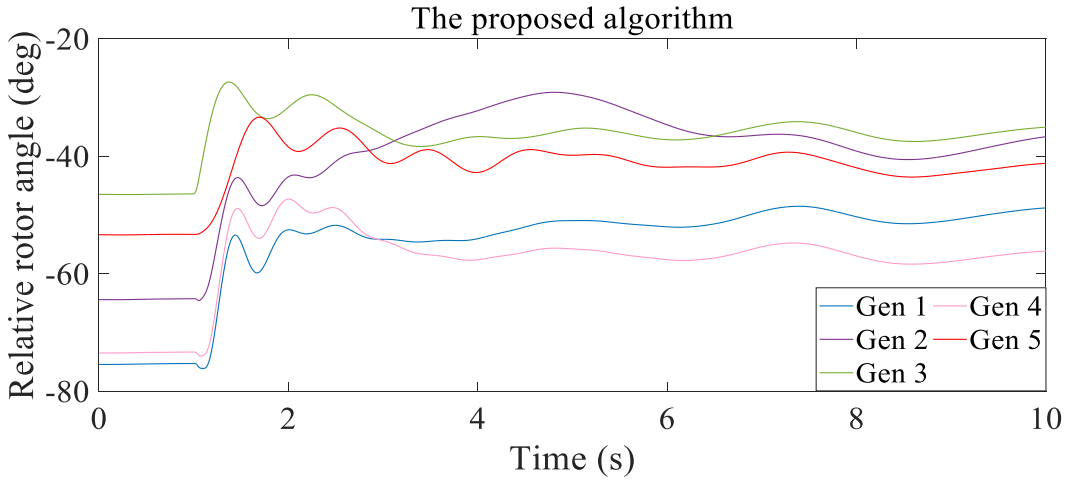

(c)

Figure 3.12 The relative rotor angles of a set of generators in case study 3.

Table 3.3 The list of all distance relays that operated in case study 3.

Reference case		Proposed algorithm	
Time (s)	Relay	Time (s)	Relay
1.050	Line 32	1.050	Line 32

As can be seen in Figure 3.13 (a), the dynamic response of the system without modeling distance relays is significantly different from that of the reference case. Comparing Figure 3.13 (b) and (c) shows that the algorithm can accurately capture the behavior of the system during this disturbance. The list of all relay operations in both cases is provided in Table 3.4. Table 3.4 shows that the same distance relays operate in both the reference case and the proposed algorithm, which demonstrate that the proposed algorithm accurately identifies all the critical relays. In this case study, with modeling distance relays, the network solution diverges at 6.162 (s) and the transient stability study terminates after the system becomes unstable.

3.4.5 Analyzing the results

These case studies show that the proposed algorithm can correctly identify the critical distance relays which are required to be modeled for performing precise transient stability studies on different types of contingencies, even in cases where multiple consecutive faults occur in the system. The results (generator rotor angles) obtained from analyzing the reference case and the proposed algorithm are exactly the same. However, using the algorithm, only the identified critical distance relays are modeled, which noticeably reduces the number of distance relays required to be modeled in comparison with the reference case. Therefore, the proposed algorithm eliminates the problem of modeling all

the distance relays in bulk power systems, i.e., software limitations and keeping the relay settings updated in the dynamic files. To demonstrate how much the proposed algorithm can reduce the number of distance relay models required to be modeled in the dynamic file

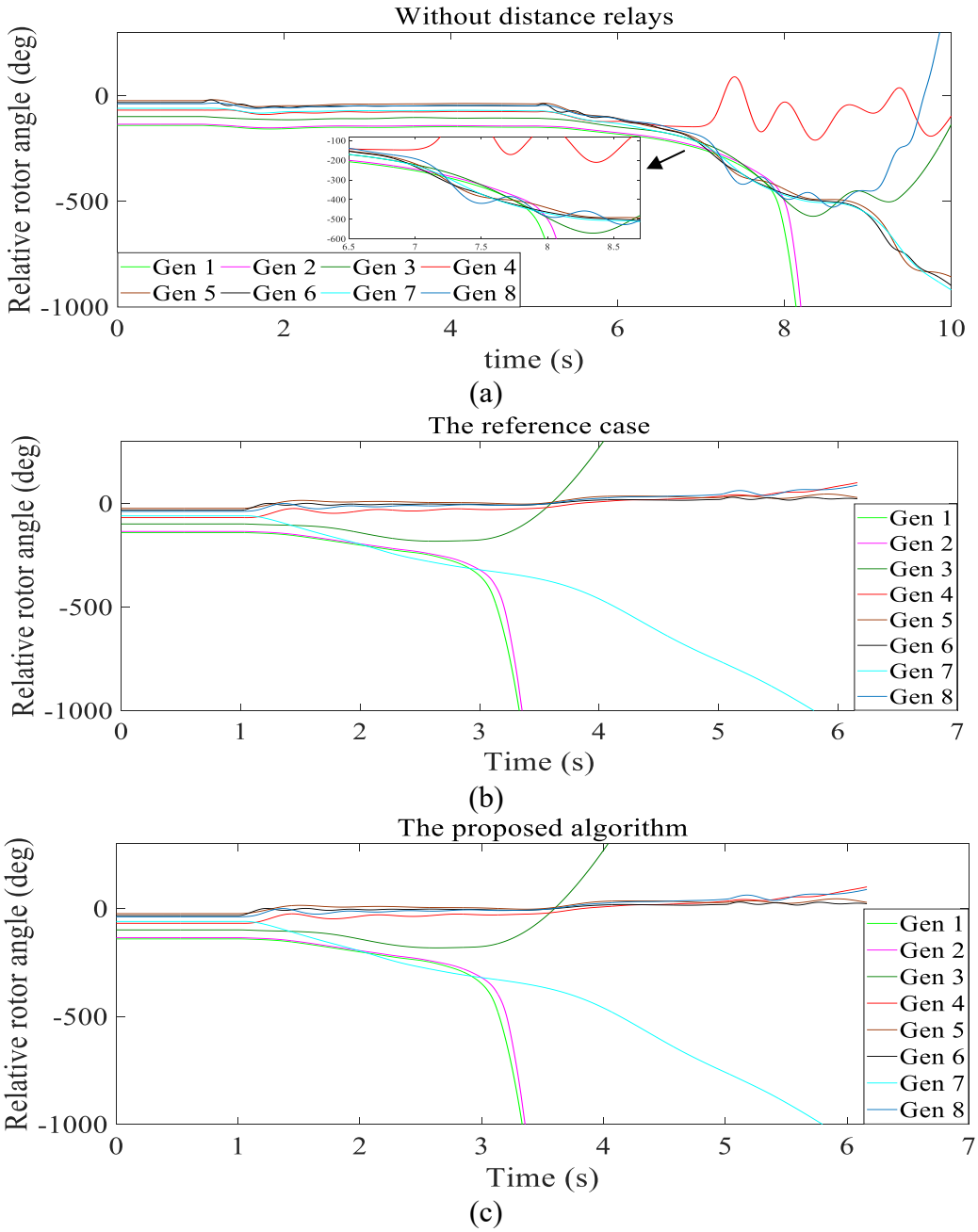

Figure 3.13 The relative rotor angles of the selected generators in case study 4.

of the system, the total number of critical distance relays (identified by the algorithm) is compared with the total number of the distance relay models in the reference dynamic data file, and the results are provided in Table 3.5. This table also shows that what percentage of the distance relays used in the reference case is identified by the algorithm as the critical distance relays in each case study. It needs to be mentioned that the total number of distance relays modeled in the reference case is 1146 relays.

Table 3.4 The list of all distance relays that operated in case study 4.

The reference case		The proposed algorithm	
Time (s)	Relay	Time (s)	Relay
1.050	Lines 1, 2, 3	1.050	Lines 1, 2, 3
1.933	Line 4	1.933	Line 4
2.737	Line 5	2.737	Line 5
2.896	Line 7	2.896	Line 7
2.904	Line 21	2.904	Line 21
2.925	Line 8	2.925	Line 8
2.942	Line 9	2.942	Line 9
3.010	Line 10	3.010	Line 10
3.104	Line 11	3.104	Line 11
3.137	Line 12	3.137	Line 12
3.321	Line 13	3.321	Line 13
5.867	Line 14	5.867	Line 14
6.112	Line 15	6.112	Line 15
6.162	Line 16	6.162	Line 16

Table 3.5 The total number of the identified critical distance relays in each case study

Case study	Total number of identified critical relays	Percentage of the total number of distance relays
1	84	7.33%
2	92	8.03%
3	20	1.74%
4	104	9.07%

As can be seen in Table 3.5, the total number of distance relays required to be modeled for capturing the behavior of the system in each case study is less than 10 percent of the total number of distance relays modeled in the reference case. For smaller disturbances, such as the disturbance in case study 3, which does not have system-wide effects, the total number of critical distance relays required to be modeled is as low as about 2 percent of the total number of distance relays modeled in the reference case.

It is worth emphasizing that by identifying only a fraction of the total number of distance relays as critical, the proposed algorithm can assist engineers to easily obtain and use the updated relay settings in their studies to have a more realistic analysis of system behavior. This critical factor greatly reduces the model maintenance burden and facilitates better coordination between planning and protection groups of electricity companies.

3.5 Summary

In this chapter, first, the importance of modeling distance relays in transient stability studies and the current challenges in performing precise stability studies with modeling all the distance relays in the system are discussed. Then, it is discussed that these challenges in modeling distance relays in transient stability studies have created the need for developing an algorithm that can identify the critical distance relays in the system for each contingency. Different methods proposed in the literature for identifying the critical distance relays are also discussed in depth and their drawbacks are explained in depth. Then, the proposed iterative algorithm is introduced as a novel method for identifying critical distance relays that can address the shortcomings of the previous methods. The

apparent impedance monitoring and MVE methods which are used in the proposed algorithm are thoroughly explained. Then, the proposed algorithm is explained in detail.

In the second part of this chapter, two most important drawbacks of existing relay modeling practice for performing transient stability studies are discussed in depth. These drawbacks include the shortcoming of bus-branch model in analyzing bus faults as well as the challenges of keeping the relay setting updated in the dynamic file and the consequences of performing stability studies with outdated relay settings. In this part, through performing several case studies, it is shown that the widely used bus-branch model cannot accurately capture the response of the system to a bus fault when distance relays are modeled in the studies. It was shown that to approximate the response of a system in node-breaker structure to a bus fault using a bus-branch model, a line fault should be performed at a close vicinity of the faulty bus. Furthermore, it is shown in this part that performing transient stability studies with outdated relay settings can lead to a completely erroneous assessment of system response.

The test case and the reference dynamic data file used in this work are introduced in the third part of this chapter. Also, the dynamic models used for modeling distance relays along with their related settings are described in part three of this chapter.

In the fourth part of this chapter, to evaluate the performance of the proposed algorithm, different case studies are analyzed considering the three cases of using the proposed algorithm, the reference case, and not modeling any distance relays. The results reveal that the transient stability studies carried out without modeling distance relays might not correctly assess the behavior of the system during contingencies. Also, the results

demonstrate that the proposed algorithm can precisely identify the critical distance relays required for performing transient stability studies of each contingency and can capture the actual behavior of the system by modeling these critical distance relays.

The proposed algorithm identifies a far smaller percentage of all the distance relays in the system as critical (less than 10% in all the analyzed case studies in this chapter) and models them in transient stability studies of each contingency. Therefore, in large power systems like the WECC system, this method enables modeling distance relays in transient stability studies and analyzing their behavior without exceeding the current limitations of stability software. Also, the algorithm eases the challenging task of keeping the settings of a large number of distance relays updated in their dynamic models by only including critical distance relays for each contingency. Therefore, only a small number of distance relays need to be accurately tracked for changes. Finally, selecting a considerably smaller percentage of distance relays to be modeled in a transient stability study reduces the computational burden of the computing system and enables the inclusion of more dynamic models in the analysis of various contingencies.

Chapter 4: Machine learning-based method for identifying critical distance relays

The importance of modeling distance relays in stability studies, the challenges of modeling all the distance relays existing in a bulk power system in stability studies, as well as the drawbacks of current practice of modeling distance relays in stability studies are discussed thoroughly in chapters 1 and 3. Different methods proposed in the literature for identifying the critical distance relays and modeling them in stability studies are also reviewed in chapter 3 and their advantages and disadvantages are discussed. Then, an iterative algorithm is proposed that uses the apparent impedance monitoring and the minimum voltage evaluation methods to identify the critical distance relays for studying any contingency. Although this method can identify all the critical distance relays for each contingency, precisely, it imposes a heavy computational burden to the computer system as several runs of transient stability studies should be performed for identifying all the critical distance relays for each contingency. This, in turn, leads to excessive simulation time.

The recent developments in data-driven methods and computational capability of computer systems on one hand, and the availability of huge amount of data on the other hand, have paved the way for the application of data-driven methods in different engineering problems including various power system problems. Nowadays, the required data for machine learning algorithms can easily be synthesized from performing numerous

simulations or obtained from various wide area measurement devices existing in modern power systems (e.g., PMUs). Using this overwhelming amount of data, the state-of-the-art ML algorithms can extract very sophisticated and nonlinear patterns between various variables and parameters in the system (input features) and the thing to be predicted, e.g., the stability of the system, the failure probability of an asset, the loss of synchronism in generators, and operation of protective relays, to mention but a few. Therefore, ML models, if trained properly, can provide reliable and fast answers to the problems that are very difficult or time-consuming to be solved with analytical methods.

Among research works that focused on solving different power system problems using ML algorithms, only a few works have considered predicting distance relay operations. In this regard, the authors in [48] proposed a method that uses the S-transform signal processing technique and artificial neural networks (ANN) to distinguish between a fault, stable swing, and unstable swing condition in order to avoid unintended operation of protective devices. The S-transform technique is used to extract the proper features required by the ANN to predict if a condition is a fault, stable power swing, or unstable power swing. The extracted features are then fed into the ANN for prediction. A technique is also proposed in [49] to distinguish between three phase faults, power swing and load encroachment conditions. The proposed technique is based on predicting the apparent impedance observed by a distance relay K step ahead and comparing these predicted apparent impedances with their actual values. If these methods are properly implemented in conjunction with stability studies, they might be able to detect distance relay operations

due to power swings and OOS conditions or three phase faults. However, they cannot identify all the critical distance relays required for performing accurate stability studies.

In this regard, a fast ML-based method is proposed in this chapter to reliably identify the critical distance relays required for performing precise transient stability studies of any contingency. The method trains an ML model which promptly identifies all the critical distance relays that need to be modeled in the transient stability study of a contingency. To create the dataset required for training the model, the results of extensive offline transient stability studies of different types of contingencies under various operating conditions and topologies of the WECC system are utilized. After being trained, the model uses the results of an initial early-terminated transient stability study of the contingency under study to identify the critical distance relays for that contingency. The number of critical distance relays identified by the method for any contingency is far less than the total number of distance relays in the system. Therefore, the method eliminates the challenges associated with modeling all the distance relays in the system. The method is also very fast as it only requires one additional transient stability study which is terminated only one cycle after the initiating fault.

In this chapter, the proposed ML-based method for identifying critical distance relays is explained. Next, descriptions of the Random Forest algorithm, the metrics used to evaluate the performance of the trained model, the grid search and the K-fold cross-validation methods, as well as the Shapley additive explanations (SHAP) method are provided. The process of training the RF model is described in detail. Then, the performance of the trained model is evaluated in terms of the metric used and a detailed

description of the importance of each feature and its participation in defining the prediction of the model is provided. To further show the performance of the proposed method in identifying the critical distance relays and capturing the actual behavior of the system during different contingencies, several case studies are performed on the WECC system data representing the 2018 summer peak load and the results are provided.

4.1 ML-based method for identification of critical distance relays

The ML-based method developed in this chapter works based on the latent correlation between the impedance trajectories observed by the distance relays during the early stages of a contingency and the behavior of the distance relays for several seconds later. Figure 4.1 shows the flowchart of the proposed method. During the training stage, extensive transient stability studies are performed on different types of contingencies under different operating conditions and topologies of the system. The contingencies studied at this stage include bus faults and line faults followed by removing one or more transmission lines, as well as generator outage contingencies. The impedance trajectories of distance relays and their operations are recorded in these studies to build a comprehensive dataset for training the ML model. Then, if available, the results of the offline studies can be mixed with the historical records of the impedance trajectories observed by distance relays in the system during different contingencies along with the record of their operations.

The real and imaginary parts of the impedance trajectories observed by distance relays at the time of the fault and 1 cycle after the fault are used as the features of the ML model. The operations of distance relays during each contingency are used to label the data set (1 for operation and 0 for not operation). Note that after the model is trained using the

comprehensive dataset, it is used to identify critical distance relays for any contingency. Hence, the process of building a comprehensive dataset through conducting extensive transient stability studies is only performed once at the training stage.

The problem of predicting distance relay operations is a binary classification problem (with two classes of 0 and 1). Throughout this chapter, the following definitions for class 0 and class 1 of the classification problem hold:

- Class 0: This class represents the samples of no-operation of distance relays, i.e., the samples where a distance relay does not operate for the entire simulation time, in the dataset.
- Class 1: This class represents the samples of distance relay operations in the dataset.

Different types of ML algorithms can be used for this problem. As it can train robust models with high accuracy and prediction/training speed, an RF classifier is used in this chapter to train the ML model for identifying the critical distance relays. To achieve the best performance, a two-stage grid search method is used to tune the hyperparameters of the RF model. During the grid search method, to realistically evaluate the performances of the RF models trained with different combinations of hyperparameter values, the K-fold cross-validation method is utilized. The grid search and the K-fold cross-validation methods are explained in chapter 4.2.

In the application stage, the trained model is used to identify the critical distance relays for any contingency under study. Note that this contingency might be a new contingency that has not been studied during building the dataset for training/testing the model; as the

results confirm, the proposed approach performs well for such out-of-sample scenarios. First, the proposed method performs an initial transient stability study without modeling distance relays. Since the trained model only needs the impedance trajectories observed by distance relays at the time of fault and 1 cycle after that, the initial transient stability study can be terminated 1 cycle after the fault, which can considerably reduce the simulation time. Note that the impedance trajectories observed by distance relays can be easily captured at each time interval of the transient stability study without any change in the existing practice of performing these studies and without any need to model the distance relays. Then, the method extracts the input features of the trained model (the impedance trajectories observed by the distance relays) from the results of the initial transient stability study.

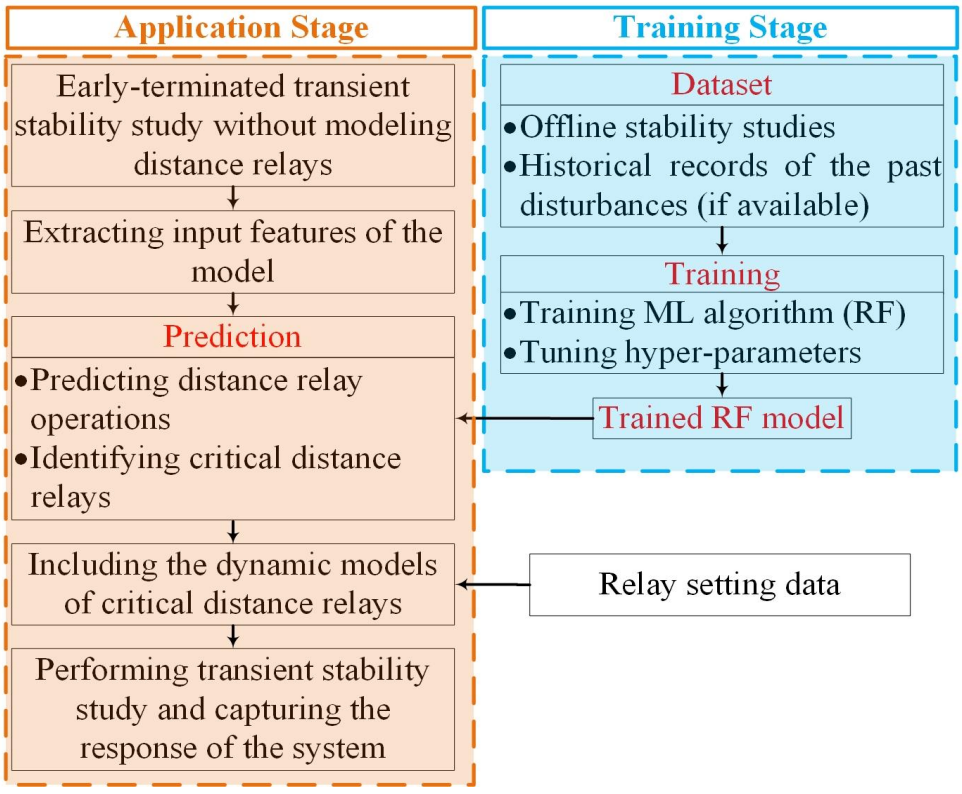

Figure 4.1 The flowchart of the proposed method.

Subsequently, the trained RF model predicts whether the distance relays in the system operate for the entire simulation time or not. The distance relays that are identified by the trained RF model are the critical distance relays for the contingency under study. Thus, at the next stage, their dynamic models are included in the dynamic file of the system. In this stage, the updated relay settings for the identified critical distance relays can be obtained (from the protection groups of utilities) and included in the dynamic models of the distance relays to achieve a more precise assessment of system behavior.

Finally, using the stability software, the method performs a transient stability study with modeling all the critical distance relays to captures the actual response of the system to the contingency. It is to be noted that unlike the case of modeling all the distance relays, the small number of the critical distance relays identified by the proposed method can easily be included in stability studies without violating the current limitations of stability software. Also, keeping track of the changes that are made in the settings of this small number of critical distance relays is much easier. Therefore, the proposed method addresses the challenges of modeling all the distance relays in a bulk power system.

Before providing a detailed explanations of the test case and the process of training and testing the RF model, a brief explanation of the RF algorithm, the metrics used to evaluate the performance of the trained model, the grid search and K-fold cross-validation methods used in the training and testing process of the model, as well as the SHAP feature importance method used to evaluate the importance of each feature in defining the prediction of the trained model is provided in the following chapter.

4.2 The Random Forest algorithm, the metrics and methods used to train and test the model, and the SHAP feature importance evaluation method

A brief explanation of the RF algorithm along with its advantages, which make it suitable for predicting distance relay operations, are provided in this section. Also, the metrics, the grid search method, and the K-fold cross-validation method used in the process of training and testing the RF model are explained. Finally, the SHAP method used to evaluate the importance of each feature in defining the prediction of the proposed model along with its advantages are explained.

4.2.1 Random Forest

The RF algorithm is a well-known and successful ML algorithm for classification problems, such as the problem of predicting distance relay operations, as well as regression problems. Random Forest consists of a large number of individual decision trees (DTs) that operates as an ensemble. In the regression problems, the output of the RF is the average of the predictions of the individual DTs of the RF. On the other hand, in classification problems, the output of RF is selected based on the most votes from the individual DTs of the RF [50].

Figure 4.2 shows a conceptual RF that is composed of *N* decision trees. As illustrated in this figure each DT of the RF is trained using a subset of the input features and independently make its own prediction. The final decision of the RF is made by taking all the predictions of the individual DTs into account. More details about the building blocks of the RF algorithm, i.e., decision trees, are provided in Appendix A.

Numerous advantages of the RF algorithm have made it a popular ML algorithm to be widely deployed in many classification and regression problems [51]. Some of the most important advantages of the RF algorithm that make it suitable for the application of predicting distance relay operation are as follows:

- One of the widely known problems of an individual DT is overfitting. This causes DT to have a poor performance on new datasets. To overcome this problem, the RF algorithm trains multiple DTs on different parts of the training set using bootstrap aggregating or bagging techniques. This eliminates the overfitting problem of a single DT. Therefore, RF can have high accuracy on new datasets [52].

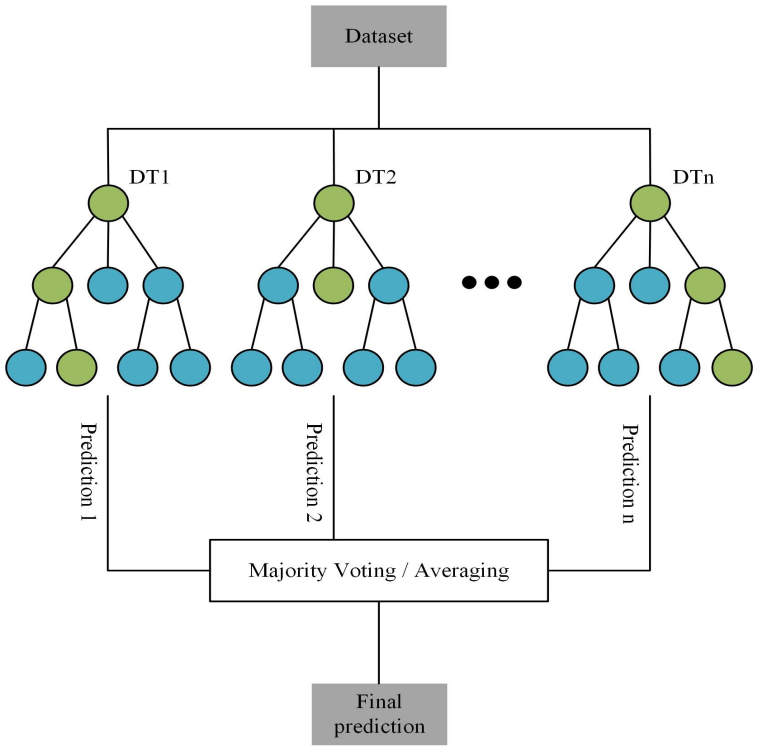

Figure 4.2 Conceptual representation of the Random Forest algorithm

- The performance of the RF in handling unbalanced and non-linear datasets is outstanding [52]. For the application of predicting distance relay operation, as the dataset is unbalanced and has more "no-operation" cases, i.e., the cases where a distance relay does not operate during the simulation time, than the operation cases, this feature of the RF is of great importance.

- The RF has a high training and prediction speed, and it can easily handle high dimensional data, as it only uses a subset of features to train each individual DT. Furthermore, since the RF algorithm is parallelizable, the process can be divided between multiple computers, which can significantly increase the speed of the algorithm. The high speed of the RF algorithm is favorable for the application of predicting distance relay operation since the algorithm can predict the operation of all the distance relays in bulk power systems and identify critical distance relays in a short time [51]-[52].

4.2.2 Metrics

Recall or true-positive rate (TPR) is the fraction of all the positive cases, i.e., distance relay operation cases in this chapter, that the trained model correctly predicts as positive cases. Recall can be formulated using (4.1) [53].

$$Recall = \frac{TP}{TP+FN} \tag{4.1}$$

In this equation, *TP* and *FN* are the numbers of true-positive cases, i.e., the cases of distance relay operations (class 1) that the trained model correctly predicted as operation cases, and false-negative cases, i.e., the distance relay operation cases that the trained model erroneously predicted as no-operation cases (class 0), respectively.

In the application of identifying the critical distance relays, it is of the highest importance that the trained model does not miss any distance relay operation. In other words, ideally, the trained model should predict all the distance relay operations. Hence, the number of false-negative cases should be very low, and the Recall value should be very high to guarantee that all the distance relay operations are correctly captured by the trained model. Therefore, in this chapter, maximizing the Recall value is considered as the objective of the grid search on the hyperparameters of the RF classifier.

Another metric that is used in this chapter for evaluating the performance of the trained model is the Precision metric. Precision is defined as the fraction of all the positive predictions of the trained model that are correct positive predictions. Precision can be formulated using (4.2) [53].

$$Precision = \frac{TP}{TP+FP} \tag{4.2}$$

In (4.2), FP is the number of false-positive cases, i.e., the no-operation cases of distance relays that the trained model erroneously predicted as operation cases. For the application of identifying the critical distance relays, a high number of false-positive cases show that the trained model is prone to misclassify many of the no-operation cases of distance relays as operation cases and identify those distance relays as critical. Therefore, a large number of distance relays might be included in the dynamic file of the system, which is undesirable; modeling a large number of distance relay might cause the same challenges of modeling all the distance relays in the system. However, modeling additional distance relays in the final stability analysis will not impact the accuracy of analysis as long as the number of these relays does not exceed the limitation of stability analysis software tools and the relay

settings are accurate. Thus, although maximizing the Precision value is not considered the main objective in this chapter, it is tried to achieve a suitable value for the Precision that does not result in the modeling of many distance relays in transient stability studies.

In order to visualize the definition of the Recall and Precision, Figure 4.3 is provided. In this figure, positive cases (relay operation cases) are shown with filled circles and negative cases (no operation cases) are shown with hallow circles. Therefore, all the cases in the left rectangle are positive cases and all the cases in the right rectangle are negative cases. The circle shown in the middle of the figure is the hypothesis learned by the trained model, in a way that the model predicts all the cases that fall within the circle as positive cases and all other cases as negative cases. In this condition, the cases that fall within the left semi-circle are true-positive prediction (as the trained model correctly predicts them as positive cases) and all the cases that fall within the right semi-circle are the false-positive cases (as the trained model erroneously predict them as positive cases). Therefore, in this case, the Recall is the number of the cases that fall within the left semi-circle divided by the total number of the cases that fall within the left rectangle (all positive cases). On the other hand, the precision is the number of cases that fall within the left semi-circle divided by the total number of cases that fall within the middle circle (all positive predictions of the trained model).

4.2.3 Grid search method

The grid search, also known as parameter sweep, is a traditional method to optimize the hyperparameters of an ML algorithm. In grid search, an exhaustive search is performed through a specified range of the hyperparameter space of the ML algorithm. Because the

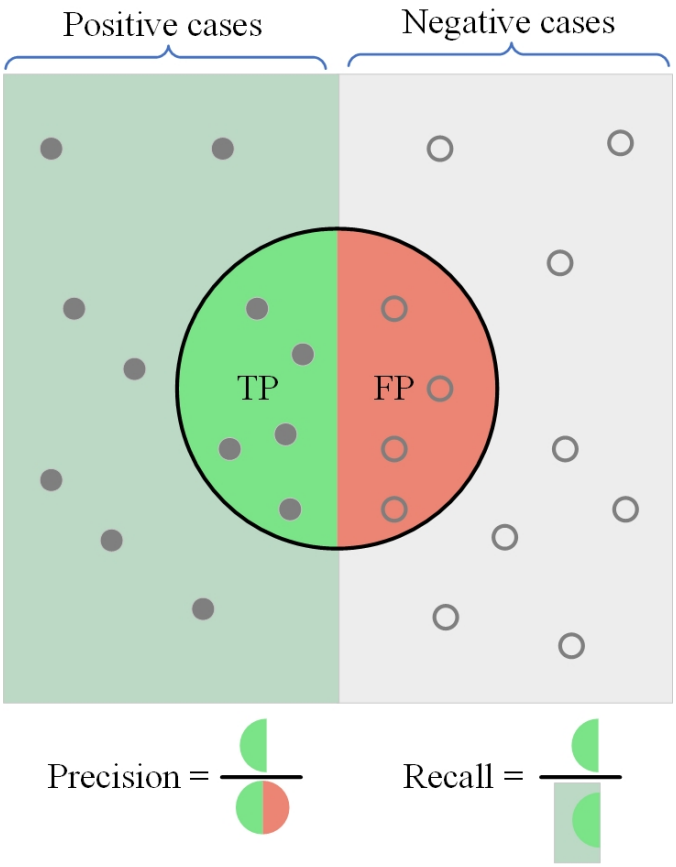

Figure 4.3 Visualization of the definition of the Precision and Recall

parameter space of an ML algorithm for some of the hyperparameters may include spaces with real or unbounded values, it is necessary to set proper bounds for these hyperparameters before using the grid search method. A performance measure should also be considered to direct the grid search in optimizing the hyperparameters. In this chapter, as mentioned earlier, maximizing Recall value is considered as the performance measure. The performance metric should be measured by the cross-validation method during the grid search method [54]-[56].

The grid search method can be easily used to optimize the hyperparameters of an ML model. Its biggest disadvantage is that when the number of hyperparameters to be tuned

increases, this method can be computationally heavy and time-consuming. However, because the hyperparameters to be tuned are usually independent of each other, the processing task of the grid search can be divided into several parallel tasks with little or no effort, and each task can be performed with a separate computer [57].

4.2.4 K-fold cross-validation

The K-fold cross-validation method is a resampling procedure used to evaluate the performances of the trained models on new and out-of-sample cases. The method has a single parameter called *K* that refer to the number of groups that a given dataset is to be split into. The flowchart of the K-fold cross-validation method is shown in Figure 4.4. As seen in this flowchart, first, the method randomly shuffles the dataset. Then, it splits the dataset into *K* parts (called folds). Subsequently, within an iterative process, each fold is selected as a test data set (hold out), and the remaining *K-1* folds serve as the training set. A model is trained on the training set and is tested on the test set. The score/error of the trained model is recorded, and the trained model is discarded. The iterations stop when all the folds are used as a test set. The average of the recorded scores/errors (the Recall value in this chapter) in all the iterations is the performance metric used to compare the performances of the models trained in each iteration of the grid search method [58]-[59].

4.2.5 Shapley Additive Explanations method

The SHAP method proposed by Lundberg and Lee [60] is a method that explains individual predictions by computing the contribution of each feature to the prediction (measured by Shapley values). The method uses coalitional game theory to compute Shapley values. The values of the features of a data instance are the players in this game.

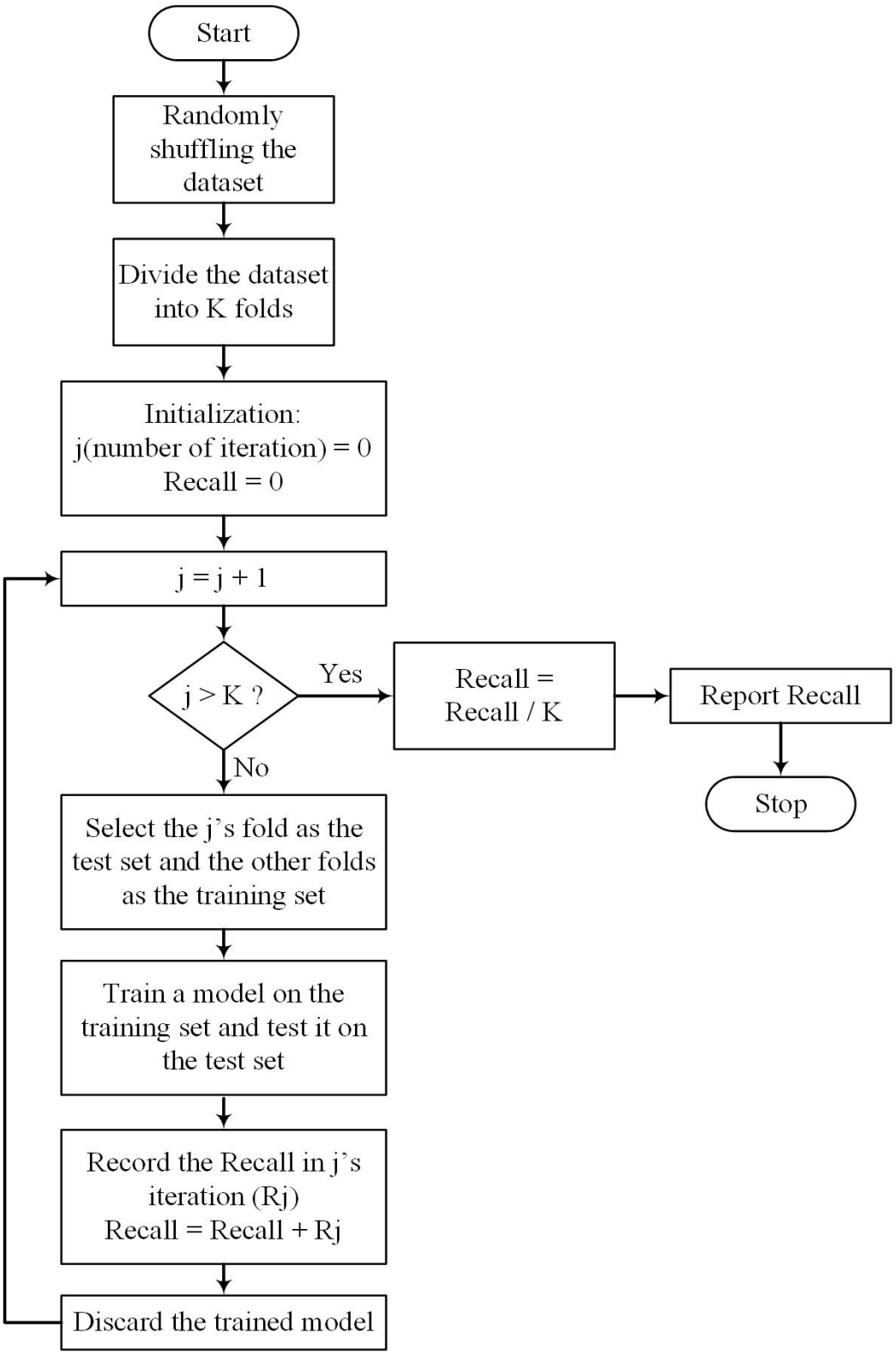

Figure 4.4 The flowchart of the K-fold cross-validation method.

Shapley values shows how the prediction of a model can be fairly distributed among the features. SHAP is represented as an additive feature attribution model, a linear model. This can connect LIME and Shapley values. The explanations are specified in SHAP as (4.3) [61].

$$g(z') = \emptyset_0 + \sum_{j=1}^{M} \emptyset_j z'_j \quad (4.3)$$

Where g is the explanation model, $z' \in \{0,1\}^M$ is the coalition vector, M is the maximum coalition size and $\emptyset_j \in \mathbb{R}$ is the feature attribution (Shapley value) for a feature j. In the coalition vector, an entry of "1" means that the related feature value is present, i.e., contributes to the prediction of the model, and the entry of "0" means that the related feature is absent, i.e., does not contribute to the prediction of the model.

The representation of coalitions as linear models is a trick for computing the $\emptyset$'s. For the instance of interest x, the coalition vector x' is a vector of all 1's (all feature values are present). Thus, (4.3) can be simplified to:

$$g(x') = \emptyset_0 + \sum_{j=1}^{M} \emptyset_j \quad (4.4)$$

Shapley values, $\emptyset_j$'s, are the only solution that satisfies the properties of efficiency, symmetry, dummy, and additivity. More details about the properties of Shapley values can be found in [61].

For an instance x, the contribution of each feature value to the prediction is estimated by KernelSHAP, which is consist of the following 5 steps:

1. Creating sample coalitions $z'_k \in \{0,1\}^M,\ k \in \{1, \dots, K\}$
2. Getting prediction for each z'_k by converting z'_k to the original feature space and then applying model $\hat{f}$: $\hat{f}(h_x(z'_k))$

3. Computing the weight for each z_k' with the SHAP kernel

4. Fitting weighted linear model

5. Returning Shapley values $\emptyset_k$ (the coefficients of the linear model)

Coalitions z_k' are created randomly with the chain of 0's and 1's. For converting the coalition of feature values to valid data instances, a function $h_x(z') = z$ is needed, where $h_x : \{0,1\}^M \rightarrow \mathbb{R}^p$ The function h_x maps 1's to the related value from the instance *x* that needs to be explained. It also maps 0's to the other values of other instances sampled from the dataset. More details about calculating Shapley values can be obtained from [61].

values per feature is summed across the entire data using (4.5) [61].

$$I_j = \sum_{i=1}^{n} \left| \emptyset_j^{(i)} \right| \tag{4.5}$$

Random Forest built-in feature importance, i.e., Gini feature importance, has the disadvantage of being biased toward the numerical features with high cardinality – the number of possible values that a feature can have. Also, in the case of having correlated features, the Gini importance might select one of the features and ignore the importance of the other one, which can lead to a wrong assessment of feature importance. However, the SHAP method does not have these problems. Also, it has an easy and fast implementation for tree-based models [61]. Therefore, it is used in this chapter to evaluate the importance of the features used to predict distance relay operations.

4.3 Test case

The performance of the proposed method is evaluated on the WECC system data representing the 2018 summer peak load case. The specification of this system is

mentioned in Chapter 3.3. To create the dataset for training the RF model, extensive offline transient stability studies are performed using PSLF software. To be able to observe the behavior of distance relays in the offline transient stability studies, the same reference dynamic file of Chapter 3 is used, which includes "Zlin1" distance relay models on the transmission lines with a voltage level of 345 kV and above and a "Zlinw" distance relay model that monitors all the transmission lines in the system with the voltage level between 100 kV and 345 kV.

It is to be noted that, as mentioned in Chapter 3, since the *Zlin1* model needs to be included on each transmission line, it is only modeled on the lines with a voltage level equal to or higher than 345 kV since these lines are the most critical lines of the system. Modeling *Zlin1* on every transmission line overwhelms the dynamic file of the system and exceeds the current limitation of the PSLF software tool. Therefore, for the lines with a lower voltage level, the *Zlinw* model is used, as this model does not need to be included on each transmission line.

4.4 Training and testing the RF model

As mentioned in Chapter 4.1, to build a comprehensive dataset for training the RF model, numerous transient stability studies are performed on the WECC system. Various operating points and topologies of the system are also considered in these studies to include cases in the dataset that also captures the behavior of the system when the pre-fault operating condition or topology of the system is different. This guarantees the accuracy of the model trained using this dataset even when the operating condition or the topology of the system is different.

The well-known “scikit-learn” library [62] in Python is used to train the RF model. In order to achieve a better performance, the two-stage grid search method is used to tune the hyperparameters of the RF model. The objective is to maximize the Recall metric while keeping the Precision value at an acceptable range. Furthermore, the K-fold cross-validation method with 5 folds is used to assess the performance of the trained models.

The most important hyperparameters of the RF classifier are *class weights*, *the number of trees in the forest*, *the maximum depth of the trees*, *the minimum sample split (MSS)*, *the minimum sample leaf (MSL)*, *the number of features considered when looking for the best split*, and *whether bootstrap samples are used when building trees*. Precise tuning of the hyperparameters is critical for enhancing the performance of the trained model. Explaining the role of each of these hyperparameters in the performance of the RF model is out of the scope of this dissertation, and more details in this regard can be found on the “scikit-learn” library [62].

To precisely tune the hyperparameters of the model, the grid search method with two stages is used. These hyperparameters can take a wide range of values. Hence, at the first stage of the grid search, an approximation of the best value for each hyperparameter is obtained. Then, at the second stage, the grid search method searches around the approximate value obtained from the first stage to find the exact value for each hyperparameter that yields the best performance. For instance, for the *class weights* of each class (class 0 for no-operation and class 1 for operation), the best value is found to be the weight of 1 for class 0 and the weight of 10 for class 1, at the first stage. Then, at the second stage, 6 candidate values of weight 5, 10, 15, 20, 25, and 30 are considered for class 1 and

the weight of 1 is considered for class 0 to tune the hyperparameter more precisely. At this stage, the best values for the weights of class 1 and class 0 are found to be 20 and 1, respectively. Likewise, the grid search method searches for the best values of all the mentioned hyperparameters at two stages.

To show the impact of changing each hyperparameter on the performances of the trained models, the change in Recall value for the various *number of trees in the forest* and the *depth of trees* is provided in Figure 4.5 (a). Also, the change in the Recall value for the various number of the *class weights* and the *number of trees in the forest* is provided in Figure 4.5 (b). Note that, in Figure 4.5 (b), the set of the numbers on the X-axis (the *class weight* axis) shows the weight of each class. For example, "0:1, 1:10" means the weight of 1 for class 0 and the weight of 10 for class 1. The other sets of numbers are interpreted, likewise. The "balanced" weight on this axis means a weight for a class that is inversely proportional to the class frequency in the input dataset [62]. For example, if the "balanced" option is used for the *class weight* and the number of samples in the dataset belonging to class 1 is 3 times that belonging to class 0, the weight of class 1 will be 1/3 of the weight of class 0.

Figure 4.5 (a) shows that in comparison to the *number of trees in the forest*, the *maximum depth of trees* has slightly more impact on the performance of the trained model. It also shows that the trained model has a better performance when the *maximum depth of trees* is set to 10. On the other hand, Figure 4.5 (b) shows that the *class weights* have the highest impact on the performance of the trained model, and as the weight of class 1 (operation cases) increases, the Recall value increases, as well. Note that, this increase

comes at the price of deteriorating the Precision value of the trained model. Therefore, although the weight of 100 for class 1 gives the highest Recall value in the first stage of the grid search method (above 0.99), the performance of the trained model in terms of the Precision value is very poor for this weight of class 1 (below 0.5). Thus, for the first stage, the weight of 10 is selected for class 1, which has a high Recall value (around 0.979), while it keeps the Precision at a reasonable value (above 0.7).

Table 4.1 shows the best values obtained for each hyperparameter from the grid search method. Using the values provided in Table 4.1 for training the RF model yields the best results in terms of the Recall value (while maintaining a high Precision value). The performance of the trained model is evaluated on the entire dataset, including over 900 contingencies, using the K-fold cross-validation method. The results reveal that the trained model has Recall and Precision values of 0.981 and 0.737, respectively. The high Recall value of the trained model can ensure that it can correctly identify all the critical distance relays for a contingency and does not miss any distance relay operation, even under different operating points and topologies of the system. On the other hand, the reasonably high value of Precision shows that the model does not identify many distance relays in the system as critical distance relays. Using the hyperparameters obtained from the grid search, the final RF model is trained on the whole dataset and implemented in the proposed method to identify the critical distance relays for any contingency in the application stage.

Table 4.1 The selected hyperparameters of the RF model

Hyperparameter	Tuned Value
Class weights	1 for class “0” and 20 for class “1”
Number of trees in the forest	15
Maximum depth of trees	15
MSS	2
MSL	2
The number of features	“auto”—equal to the square root of the number of all the features
Bootstrap	“False”—meaning the whole dataset is used to build each tree

4.5 Analyzing feature importance using the SHAP method

To evaluate the importance of each input feature of the trained model, i.e., different samples of the relay impedance trajectories, in defining the predictions of the trained model, the SHAP feature importance method is utilized. The mean absolute SHAP values obtained for each feature of the trained model are provided in Figure 4.6. The Y-axis of Figure 4.6 shows different features of the trained model, and the X-axis shows the corresponding mean absolute SHAP value, i.e., the average impact that each feature has on the output (prediction) magnitude of the trained model. The blue and red bars in Figure 4.6 show the impact of each feature in predicting class 1 (operation cases) and class 0 (no-operation cases), respectively, and the most important feature appears at the top. Note that, in this figure, *S1R, S2R, S3R, S4R, S5R,* and *S6R* are the real parts of the impedance trajectory observed by a distance relay one time-step (one-fourth of a cycle) before the fault, at the

time of fault, one time-step after the fault, 2 time-steps after the fault, 3 time-steps after the fault, and 4 time-steps (1 cycle) after the fault, respectively. Likewise, *S1X, S2X, S3X, S4X, S5X,* and *S6X* are the imaginary parts of the impedance trajectory observed by a distance relay at the mentioned time steps.

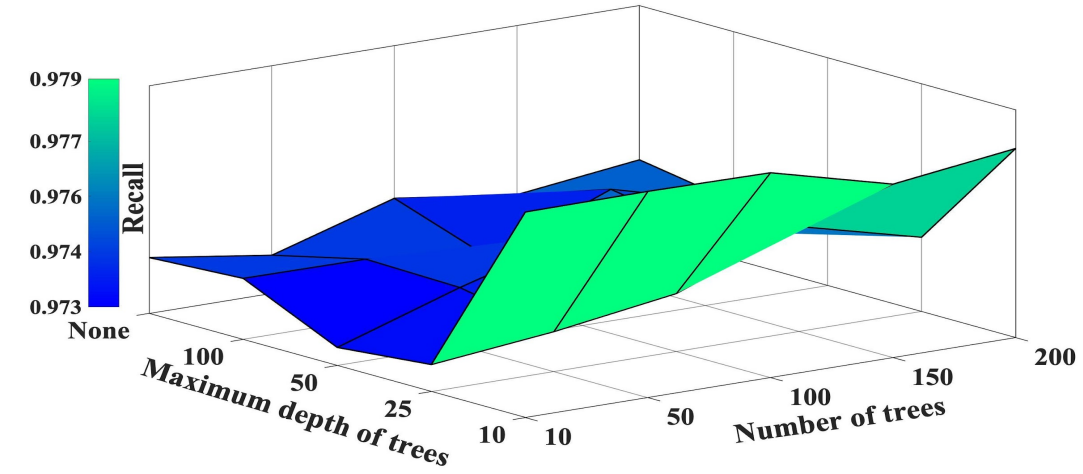

(a)

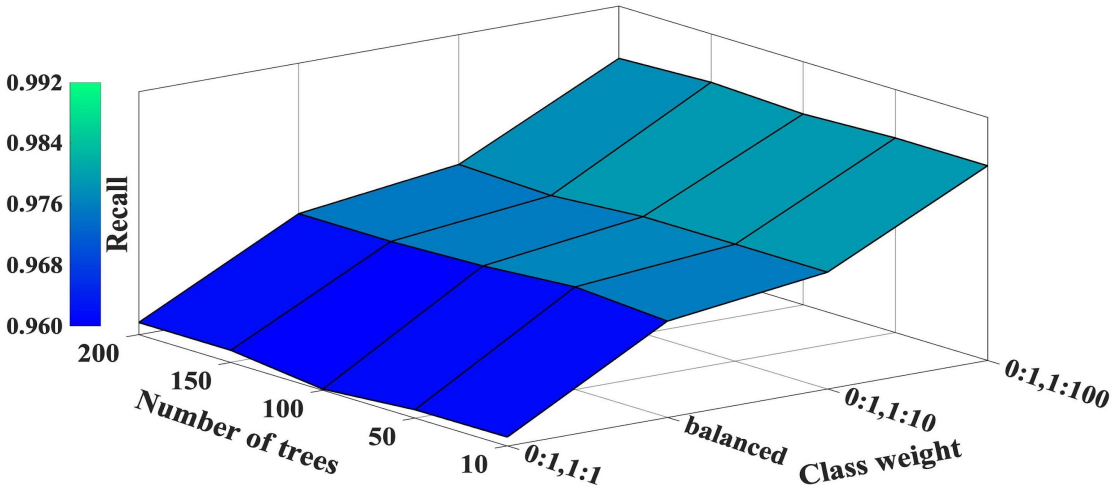

(b)

Figure 4.5 The change in Recall value for different values of the *maximum depth of trees* and the *number of trees in the forest* (a), different values of *class weights* and the *number of trees in the forest* (b).

As can be seen in Figure 4.6, the real part of the impedance trajectory observed at 4 time-steps after the fault (the last sample) and the imaginary part of the impedance trajectory observed at the time of fault have the highest impact on defining the predictions of the trained model, both for the operation and no-operation cases.

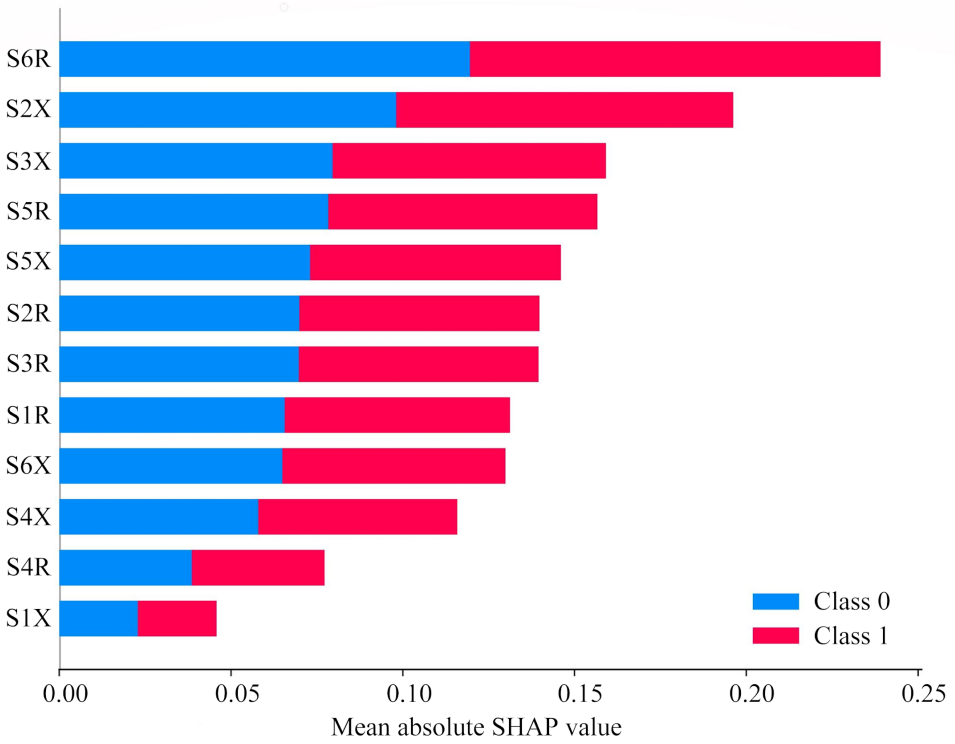

Figure 4.6 The SHAP feature importance of the trained model

To further analyze the importance of each feature along with its impact on the prediction of the model, a SHAP summary plot of the trained model is provided in Figure 4.7. The summary plot not only shows the importance of each feature, but also shows the relationship between the value of a feature and its impact on the prediction of the trained model. Each point in the summary plot represents a SHAP value for a feature and an instance (a single case in the training set). Similar to the SHAP feature importance figure (Figure 4.6), the Y-axis shows the different features of the model and the feature at the top

is the most important feature. The X-axis shows the SHAP value for each feature and each instance. The color of each point shows the value of the related feature in that instance (blue color represents a low value and red represent a high value).

As also can be seen in Figure 4.7, *S6R* is the most important feature of the trained model. Furthermore, Figure 4.7 shows that the low value of *S6R* has a negative impact on the magnitude of the predictions of the trained model (reduces the magnitude of the predictions), which means that a low value of this feature increases the probability of the predictions to be 0 (no-operation). A high value of *S2X* (the second most important feature) and *S3X* (the third most important feature) has a negative impact on the magnitude of the predictions of the trained model and increases the probability of the predictions to be 0. No linear relationship exists between the value of the other features and the magnitude of the predictions of the trained model. In other words, it is not clear if an increase or decrease in the value of the other features direct the prediction toward "1" or "0".

This detailed analysis of the importance of each feature and its impact on the prediction of the trained model provides insight into how the trained model predicts the operations of distance relays and considerably enhances the interpretability of the trained model.

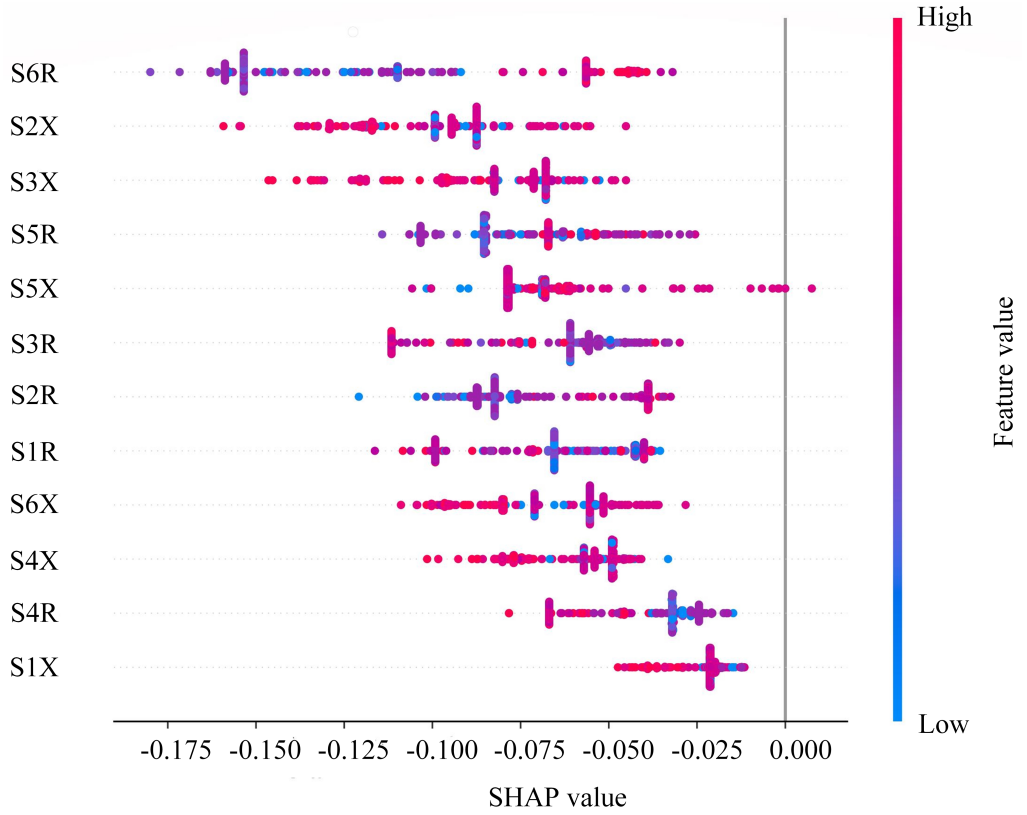

Figure 4.7 The summary plot of the trained model.

4.6 Case studies

To further illustrate the performance of the proposed method in identifying the critical distance relays and capturing the precise response of the system during various contingencies three different case studies are considered for more detailed studies. Different operating conditions and topologies of the system are considered in these studies. Similar to chapter 3, for each contingency, three different cases are analyzed:

- Case 1: To show the impact of modeling distance relays on the response of the system, the first case considered in studying each contingency performs the transient stability studies without modeling distance relays.

- Case 2: In this case, the reference dynamic file, which was used for performing transient stability studies during creating the dataset stage, is used for performing transient stability studies of each contingency. Note that, as mentioned earlier, this dynamic file includes *Zlin1* models for the lines with a voltage level equal to or higher than 345 kV and a *Zlinw* model for the lines with a voltage level between 100 kV and 345 kV. This case is referred to as the reference case throughout this chapter.

- Case 3: In this case, the proposed method is used to identify the critical distance relays for the contingencies under study. Then, the transient stability studies are performed with only including *Zlin1* models for the identified critical distance relays. Similar to the second case, the *Zlinw* model is used in the third case to monitor the lines with a voltage level between 100 and 345 kV. Note that, the proposed method can identify all the critical distance relays on the lines at any voltage level. However, to be able to compare the results of the method with the second case (the reference case), the settings of the method are modified to only identify the critical distance relays on the lines with voltage levels of 345 kV and above.

In both the second and the third cases, zone-1, -2, and -3 reaches of *Zlin1* models are considered to be 80%, 120%, and 220% of the line impedances, respectively. Time delays of 0, 0.2, and 0.3 seconds are considered for zone 1, 2, and 3 operations of *Zlin1* models, respectively. The same zone 1 and 2 reaches and time delays are also used for the *Zlinw* model. In both cases, circuit breaker delay time is set to 0.05 seconds. Note that, similar to

Chapter 3, generic relay settings used to model the distance relays and similar to the current practice of the industry, the bus-branch representation of the WECC system is used for performing transient stability studies in all the case studies.

4.6.1 Case study 1

In this case study, a bus fault occurs on Bus 3 of the system and is cleared after 4 cycles by removing the three 500 kV transmission lines that comprise COI. As mentioned in Chapter 3, these three lines are very critical tie lines of the WECC system, and their outage is a critical emergency for the WECC system, which has the potential to jeopardize the system stability. Therefore, this critical N-3 outage has been considered in this case study. To evaluate the performance of the proposed method under new and unseen pre-fault operating conditions, a new pre-fault operation condition of the WECC system is considered in this case study. In the new operating condition, a uniform increase of 2 percent in the large loads (above 100 MW) of the areas that import power through the COI, which leads to a 55.71 MW increase in the net load of these areas, is considered. This increase in the load is compensated by three of the largest generators existing in the areas that send power through COI, without violating the limitations of any generation unit in the system.

The results of transient stability studies performed for Case 1 (modeling no distance relay), Case 2 (the reference case), and Case 3 (the proposed method) of this contingency are illustrated in Figure 4.8 (a), (b), and (c), respectively. Comparing Figure 4.8 (a) and (b) shows that without modeling distance relays the dynamic response of the system in terms of the relative rotor angles of a set of generators is completely different from that of the

reference case. Also, comparing Figure 4.8 (b) and (c) illustrate that the proposed method can capture the behavior of the system exactly as the reference case, even for severe disturbances such as the disturbance of this case study and a new pre-fault operating condition of the system. For the sake of clarity, only the rotor angles of a set of selected generators are shown for all the case studies. However, the relative rotor angles of all the generators show exactly the same response in the reference case and the proposed method.

In this case study, with the distance relays modeled in the system, the network solution diverges at 6.321 (s) and the transient stability study terminates. Similar to case studies analyzed in Chapter 3, transient stability studies are performed without considering remedial actions. However, if the remedial actions are included, the proposed method is expected to be able to capture the behavior of the system.

Table 4. 2 shows the list of the relays that operate in the reference case and the method. Lines 1,2, and 3 are in the area that imports power through COI, and line 4 is in the area that exports power through COI (Lines 1-4 are in the vicinity of the fault location). Therefore, the distance relays of these lines operate due to the initial impacts of the disturbance. The ability to predict the operations of these distance relays shows that the method can correctly capture the distance relay operations due to the initial impacts of disturbances. All other lines listed in Table 4.2 are in the areas far from the fault location. Lines 8, 10, 15, and 17 are the tie-lines that connect two areas far from the fault location. The ability to correctly predict the operations of the distance relays of these lines and identify them as critical shows that the method can correctly capture the distance relay operations that occur due to the system-wide impacts of disturbances. Hence, it is observed

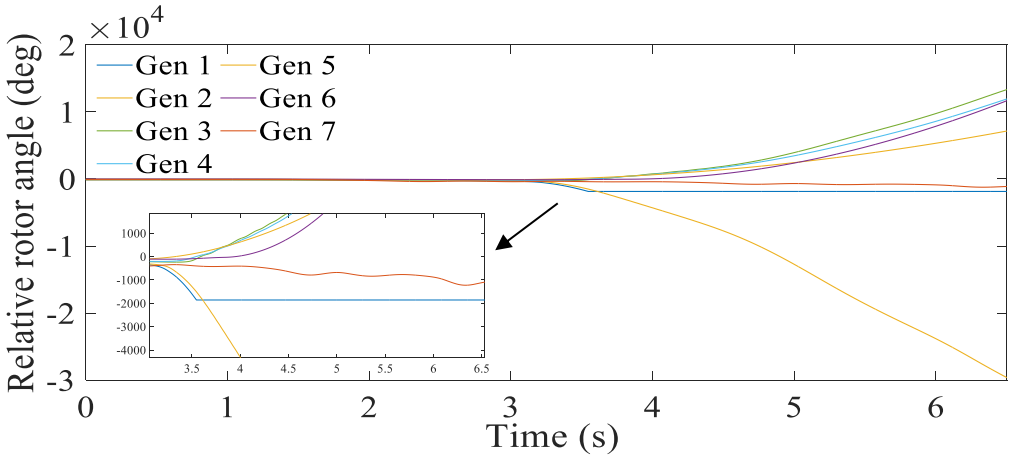

(a)

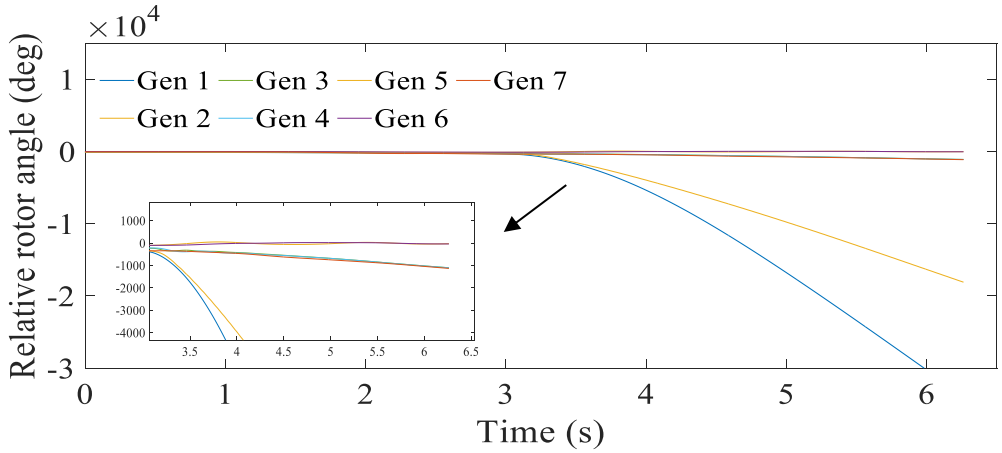

(b)

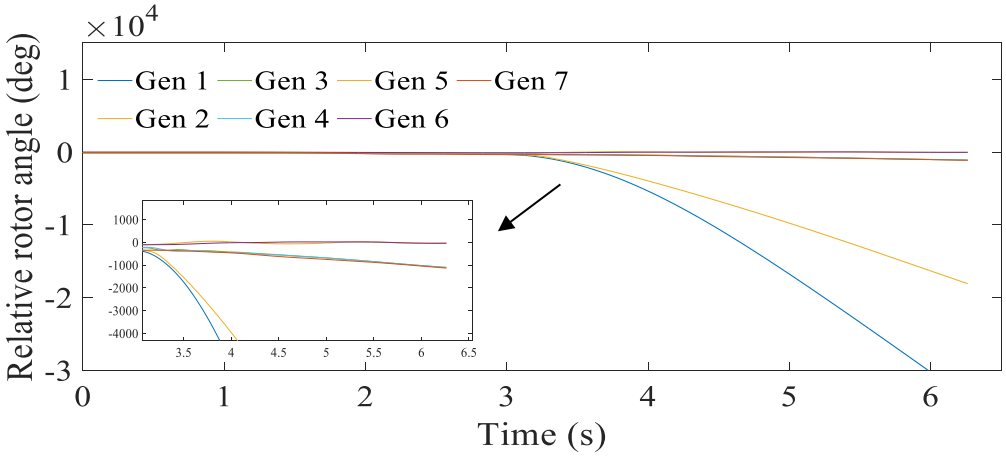

(c)

Figure 4.8 The relative rotor angles of a set of generators in case study 1: (a) Case 1, (b) Case 2, and (c) Case 3.

that the method can identify all the critical distance relays for this severe contingency under the new pre-fault operating condition of the system.

Table 4.2 The list of all distance relay operations in case study 1.

The reference case		The proposed method	
Time (s)	Relay	Time (s)	Relay
1.050	Lines 1, 2, 3	1.050	Lines 1, 2, 3
1.888	Line 4	1.888	Line 4
2.629	Line 5	2.629	Line 5
2.671	Line 6	2.671	Line 6
2.683	Lines 7	2.683	Lines 7
2.767	Line 8	2.767	Line 8
2.771	Line 9	2.771	Line 9
2.950	Line 10	2.950	Line 10
2.979	Line 11	2.979	Line 11
3.009	Line 12	3.009	Line 12
3.025	Line 13	3.025	Line 13
3.179	Line 14	3.179	Line 14
5.921	Line 15	5.921	Line 15
6.321	Line 16, 17	6.321	Line 16, 17

4.6.2 Case study 2

To evaluate the performance of the method in the case of a different pre-fault topology of the system, the N-3 COI outage is considered. However, in this case study, the pre-fault topology of the system is modified by taking two critical 500 kV transmission lines of the system out of service. Each of these lines approximately carries 384 MW of power.

The results of transient stability studies performed for Case1 (modeling no distance relay), Case 2 (the reference case), and Case 3 (the proposed method) of this contingency are illustrated in Figure 4.9 (a), (b), and (c), respectively. As shown in Figure 4.9 (a), without modeling distance relays the response of the system is different from the reference case. Also, comparing Figure 4.9 (b) and (c) shows that the system response is similar in

both the reference case and the proposed method, showing the accuracy of the method in capturing the response of the system. Similar to case study 1, in this case study, with modeling distance relays, the network solution in the stability software diverges at 6.259 (s) and the transient stability study terminates.

Table 4.3 provides the list of all distance relay operations in the reference case (Case 2) and the proposed method (Case3). Similar to Case study 1, distance relay operations occur both on the lines close to the fault location and the lines far from it. As seen in Table 4.3, the method can correctly predict all the distance relay operations in this contingency, which shows the ability of the method to identify distance relay operations due to the initial and system-wide impacts of this severe contingency under the new pre-fault topology of the system.

4.6.3 Case study 3

To evaluate the performance of the proposed method in other types of disturbances, a case of *N-3* generator outage is considered in this case study. The selected three generators are among the generators with the highest active power generation in the WECC system. These generators produce a total active power of around 1,268 MW. Furthermore, the pre-fault operating point of case study 1 is considered in this case study, as well. This *N-3* generator outage has widespread impacts throughout the system, causing several distance relay mis-operations due to unstable power swings. Thus, identifying the critical distance relays for this contingency by the proposed method further highlights the ability of the method to identify the distance relays that might misoperate due to unstable power swings at locations far from the location of the initial event.

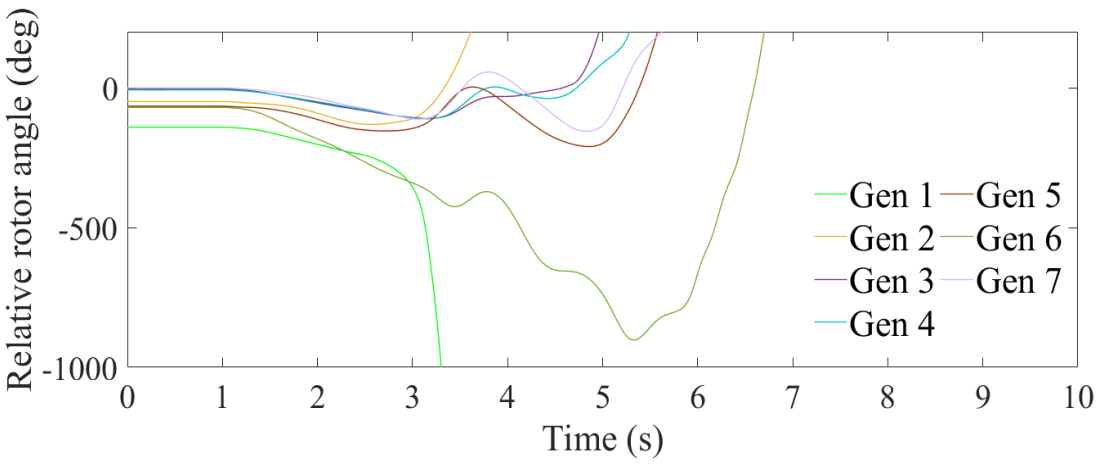

(a)

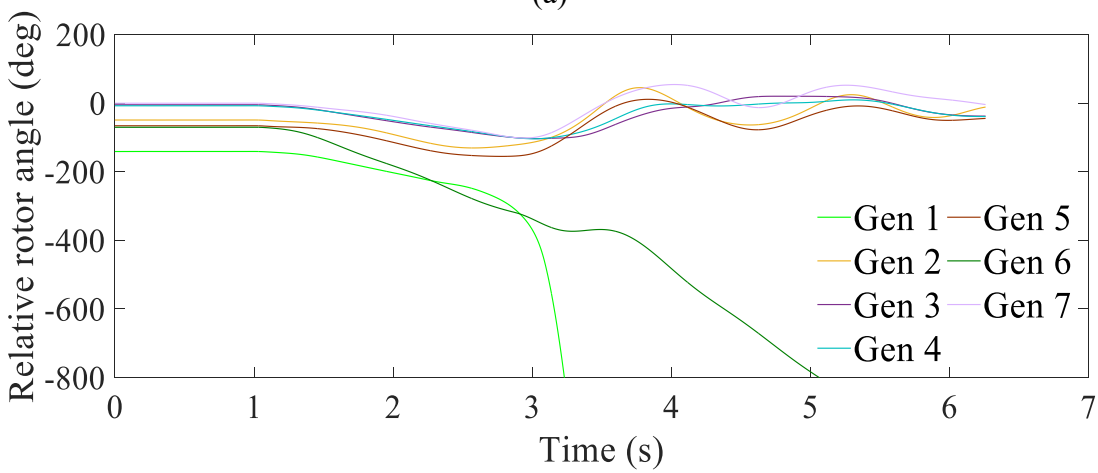

(b)

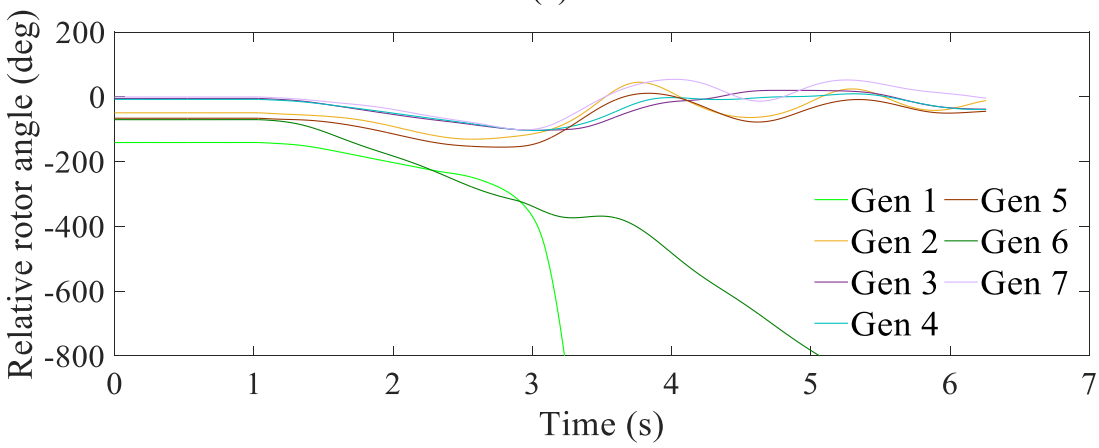

(c)

Figure 4.9 The relative rotor angles of a set of generators in case study 2: (a) Case 1, (b) Case 2, and (c) Case 3.

Table 4.3 The list of all distance relay operations in case study 2.

The reference case		The proposed method	
Time (s)	Relay	Time (s)	Relay
1.050	Lines 1, 2, 3	1.050	Lines 1, 2, 3
1.917	Line 4	1.917	Line 4
2.692	Line 5	2.692	Line 5
2.854	Line 9	2.854	Line 9
2.863	Lines 6, 8	2.863	Lines 6, 8
2.884	Line 7	2.884	Line 7
3.046	Line 10	3.046	Line 10
3.063	Line 11	3.063	Line 11
3.092	Line 12	3.092	Line 12
3.096	Line 13	3.096	Line 13
3.275	Line 14	3.275	Line 14
5.925	Line 15	5.925	Line 15
6.242	Line 17	6.242	Line 17
6.259	Line 16	6.259	Line 16

The results of transient stability studies performed for Case 1 (modeling no distance relay), Case 2 (the reference case), and Case 3 (the proposed method) are shown in Figure 4.10 (a), (b), and (c), respectively. By comparing Figure 4.10 (a) and (b), it is revealed that without modeling distance relays, transient stability studies cannot capture the actual response of the system. Also, as can be seen in Figure 4.10 (c), the dynamic response of the system in the case of using the proposed method is the same as that in the reference case shown in Figure 4.10 (b). Table 4.4 provides the list of distance relay operations in both the reference case and the proposed method. As seen in this table, the method can correctly identify all the distance relays that operate in the reference case as critical. This further shows the capability of the method in predicting distance relay operation due to the system-wide impacts of a disturbance.

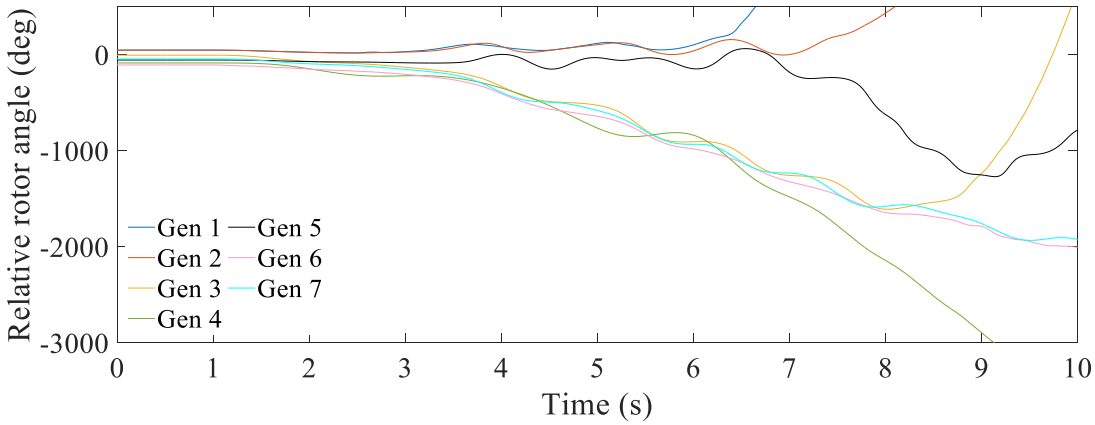

(a)

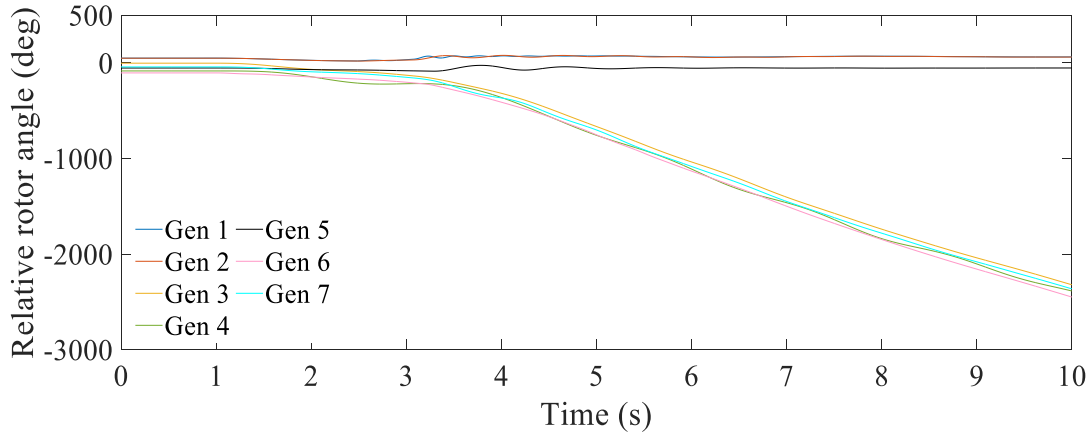

(b)

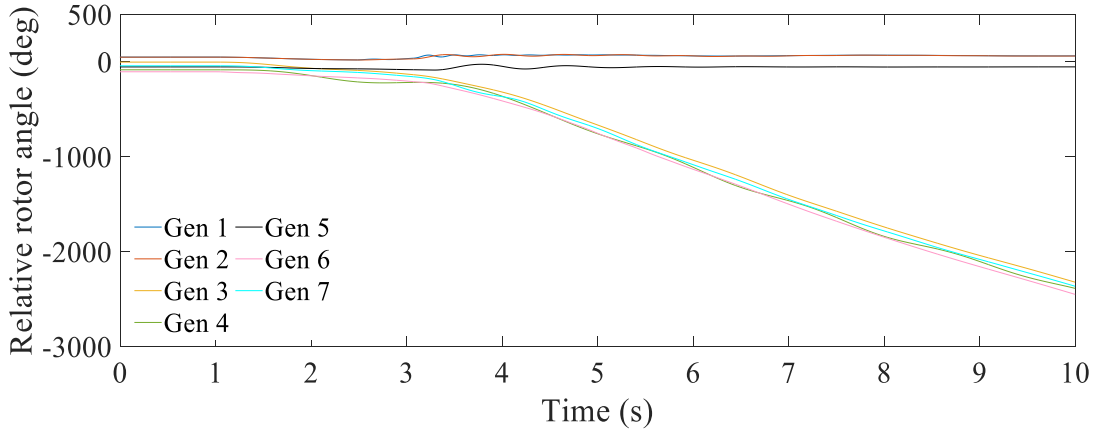

(c)

Figure 4.10 The relative rotor angles of a set of generators in case study 3: (a) Case 1, (b) Case 2, and (c) Case 3.

Table 4.4 The list of all distance relay operations in case study 3.

The reference case		The proposed method	
Time (s)	Relay	Time (s)	Relay
3.075	Line 15	3.075	Line 15
3.283	Line 17	3.283	Line 17

4.6.4 Analyzing the results

The results show that the proposed ML-based method have the high Recall value of 0.981 on new and out-of-sample cases, which illustrate its great performance in identifying all the critical distance relay. The method also has a reasonably high Precision value (above 0.7) on new and out-of-sample cases, which indicates that the method does not mis-identify many distance relays as critical. To further show that to what extent the proposed method reduces the number of distance relays models included in transient stability studies, Table 4.5 shows the number of distance relays identified as critical in each case study. It also shows that what percentage of the total number of distance relays in the reference case are identified as critical distance relays in each case study. As seen in Table 4.5, the total number of critical distance relays in each case study is less than 3.23% of the total number of distance relays in the reference case.The analyzed case studies further show that the proposed ML-based method can correctly identify the critical distance relays in any type of contingency under different pre- fault operating conditions and topologies of the system and can precisely capture the actual response of the system to the contingency. However, using the method, only critical distance relays are modeled in the system, which, as seen in Table 4.5, drastically reduces the number of distance relays required to be modeled for performing precise transient stability studies. Therefore, the dynamic models of this small

number of critical distance relays with their updated settings can easily be obtained and included in the dynamic file of the system without violating the current limitation of stability software tools. This also significantly decreases the maintenance burden of keeping the distance relay setting information updated in the dynamic file of the system and the computational burden of the computing system.

Table 4.5 The total number of the identified critical distance relays.

Case study	Total number of the identified critical distance relays	Percentage of the total number of distance relays
1	37	3.23%
2	35	3.05%
3	26	2.27%

For the contingencies studied in this section, the processing time of the three major processes performed in the proposed method to identify the critical distance relays is provided in Table 4.6. These three major processes are as follows:

- Process 1: Performing the initial early-terminated transient stability analysis of the contingency under study.
- Process 2: Extracting the required features of the ML model from the results of the transient stability study and pre-processing them to be fed into the trained ML model.
- Process 3: Predicting the operation of all the distance relays in the system.

The processing time of performing transient stability studies depends on the type of the disturbance being studied as well as the operating condition and topology of the system. Therefore, as seen in Table 4.6, the processing time for performing the initial transient

stability study is different for each case study, whereas the processing time for extracting the features and the prediction time of the ML model are the same for all the case studies. The total processing time for any contingency studied is less than 111 seconds. The three contingencies studied in this section are among the most severe disturbances of the WECC system. Hence, solving transient stability studies of these contingencies requires more processing time than other contingencies. The fact that the processing time of the method for these contingencies is less than 111 seconds guarantees that the processing time for any other contingency is also very small. This shows that the method can be used in planning studies to promptly identify the critical distance relays for a large number of the contingencies that are required to be studied.

Table 4.6 The processing time of the proposed method.

Case study	Process 1 (s)	Process 2 (s)	Process 3 (s)	Process 4 (s)
1	108.95	1.2	0.008	110.16
2	108.70	1.2	0.008	109.91
3	22.46	1.2	0.008	23.67

4.7 Summary

In this chapter, after recapping the discussion made in Chapter 3 on the importance of modeling distance relays in transient stability studies and the current challenges of modeling all the distance relays existing in bulk power systems in stability studies, a machine learning-based method is proposed to identify the critical distance relays for performing transient stability studies of any contingency. The proposed method is based on training an ML algorithm to learn the latent pattern between the impedance trajectories

observed by distance relays during the early stages of a contingency and their operations for several seconds later.

Then, the proposed method is explained in depth and the RF algorithm that is used to train the ML model for predicting distance relay operations is introduced. The metrics and methods used in the training and testing process of the RF model, including the grid search and the K-fold cross-validation methods, along with the SHAP feature importance method are briefly explained, in this chapter.

Subsequently, the process of training and testing the RF models is elaborated upon. In this section, tuning the hyperparameters of the RF model using the two-stage grid search method, the importance of each hyperparameter in improving the performance of the trained model, and using K-fold cross-validation method to evaluate the performance of the methods trained at each iteration of the grid search method are explained, in depth.

In order to enhance the interpretability of the trained RF model, the SHAP method is used to evaluate the importance of each feature of the trained RF model in defining the prediction of the model. It is shown that how low or high values of each feature of the trained model can lead the prediction of the model toward 0 (no-operation) or 1 (operation).

Finally, several case studies are considered in this chapter to assess the performance of the method on severe contingencies under new topologies and operating points of the WECC system. The results show that the transient stability studies performed without modeling distance relays can manifest an inaccurate system behavior. Also, the results show the great performance of the proposed method in identifying the critical distance relays and capturing the actual behavior of the system. It is observed that in comparison to

the reference case, the proposed method models a far smaller number of distance relays in transient stability studies (less than 3.23% of all the distance relays in all the case studies). It can be concluded that the small number of critical distance relays identified by the proposed ML-based method can be easily modeled in stability studies without exceeding the limitations of stability software. Also, using this method, only critical distance relays are required to be accurately tracked for changes in their settings, which considerably reduces the maintenance burden. Finally, by reducing the number of distance relays modeled in the studies, the method significantly reduces the computational burden of the computing system. Thus, more dynamic models can be included in the analysis of various contingencies.

Also, it is observed that the total processing time for any of the studied contingencies is below 111 seconds, which illustrates the high speed of the method in identifying the critical distance relays in the system.

Chapter 5: Comprehensive Online Dynamic Security Assessment: Prediction of Loss of Synchronism in Generators and Behavior of Protection Systems

Power systems are the backbone of any modern society, and their reliable and uninterrupted operation is of paramount importance. The recent trends in increasing the reliance on renewable resources, which are inherently intermittent, for power generation and the increase in the number of man-made or natural threats have exposed modern power systems to an unprecedented level of uncertainty. Offline stability studies consider a deterministic operation condition and topology of the system. Considering increasing levels of uncertainty in power systems, reliance on offline deterministic analyses may result in inaccurate assessment of system stability and security. Inaccurate assessment of system behavior might lead to the failure in designing proper remedial actions, which in turn might lead to cascading outages and blackouts [63]-[65].

As mentioned in Chapter 1, the insufficiency of offline stability studies has created an urgent need for a fast and reliable online security assessment of modern power systems. Online DSA methods can address the shortcomings of offline stability studies by considering the operating condition and topology of the system at each moment and as the contingency proceeds. Therefore, the online DSA methods should be fast enough to provide enough time for automatic control systems to take proper control actions. However, the hurdles mentioned in Chapter 1 for using the conventional DSA methods in online applications have made these methods too slow to be used as online DSA methods.

Wide Area Measurements (WAMS) using PMUs are being widely used in the WECC system to provide a wide range of applications such as situational awareness for operational decision making. Eastern Interconnection Phasor Project (EIPP) provides new opportunities to deploy the measurements from PMUs in real-time analysis to evaluate the system dynamic performance [66]. Using this online information provided by PMUs, many research papers have developed different ML-based online DSA methods which can provide predictions of system security following various contingencies.

In this chapter, different online DSA methods developed in the literature along with their shortcomings are discussed. A new comprehensive ML-based method is presented that equips the control system with an online tool which provides a detailed assessment of system security by predicting the behavior of the generators as well as different protective relays in the system. By predicting loss-of-synchronism in the generators and the operation of distance relays as well as UFLS and UVLS relays using the online measurements provided by the PMUs installed throughout the system, the method can provide a much broader concept of DSA. This detailed information provides an insight into how the disturbance spread in the grid, which generators of the system will experience LOS condition, and which areas of the system will experience voltage/frequency drop and consequent load shedding. It can also trigger automatic control system to initiate the proper control actions to alleviate the condition of the system and prevent cascading outages and blackouts.

The developed DSA method is tested on the WECC system data representing the 2018 summer peak load case considering different types of contingencies under different

operating points and topologies of the system. The performance of the method is evaluated using 5 distinct metrics under 3 different noise levels and 4 different scenarios of missing PMU data. Finally, several case studies are performed to show how the trained models can capture the relay operations and the occurrence of LOS condition in generators during these case studies.

5.1 Online Dynamic Security Assessment

In online DSA methods, the stability of the system is evaluated for the current operating condition and as it occurs [64]. The uncertainties associated with offline security assessment methods are eliminated in online DSA methods as they analyze a snapshot of the current operating condition of the system. Their analysis of the system security can provide valuable information about how a disturbance impacts the system and can be used to initiate proper control actions.

There need to be further studies on whether online DSA could have prevented recent major events such as the 2003 North America blackout. However, it is expected that online DSA methods can play a significant role in preventing such events because these methods can provide early indications of the pending troubles in the system. Thus, they can provide enough time for taking proper remedial actions [64]. Online DSA methods can also provide accurate security classification decisions following various possible contingencies. In other words, they can analyze if the system is going toward instability by assessing the current situation of the gird. If the situation is found to be insecure, they provide an early warning of impending instability in the system. In this regard, the U.S.-Canada Power System Outage Task Force's final report on 2003 North America blackout recommends conducting

research on the evaluation and adaptation of tools and technologies which are related to reliability assessment, aiming at developing guidelines for real-time operating reliability assessment tools [3].

The main components of online DSA systems are illustrated in Figure 5.1. As seen in this figure, system measurements can be obtained from supervisory control and data acquisition (SCADA), PMUs, and disturbance recorders. These online measurements are passed into the DSA system and the state estimator. Finding the current state and dynamic model of the network is very important for online DSA systems, especially if the method used for DSA requires a fully defined system state and dynamic model [64]. The results of online DSA can be directly sent to real-time control to start control actions or can be sent to the operator through energy management system (EMS) local display or web, and then the operator can decide on implementing control actions.

The advancements made in power system monitoring provide an overwhelming amount of data, which can be efficiently used for operational decision-making. Utilizing this data and its underlying patterns, machine learning algorithms have proven to be an effective tool for real-time analysis of modern power systems stability and are widely used as online DSA methods. In this regard, a literature review on the application of ML algorithms for developing online DSA methods is provided in the following chapter.

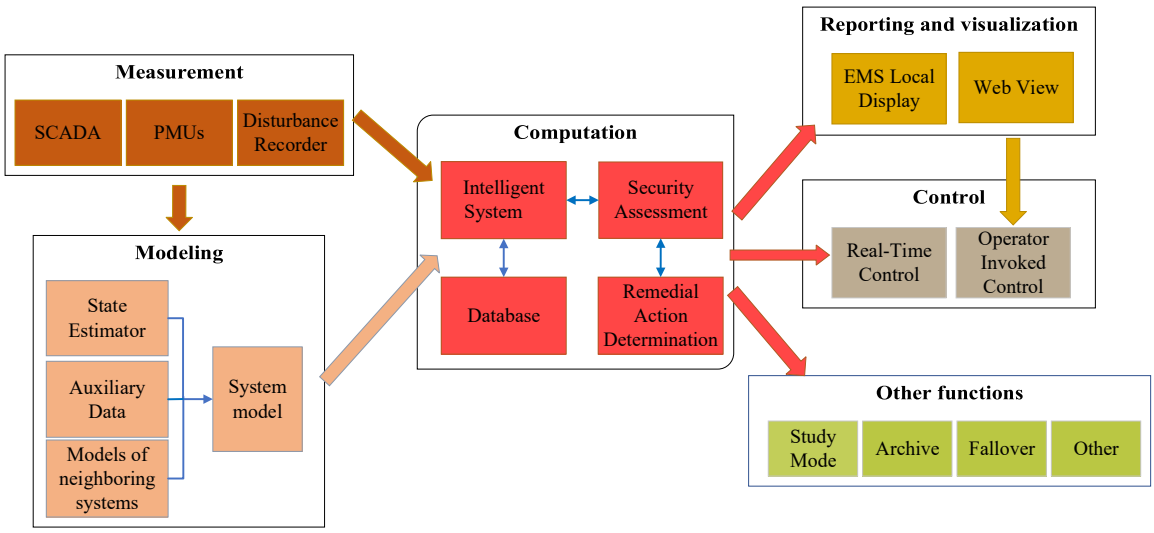

Figure 5.1 The components of an online DSA system [64].

5.1.1 Literature Review on ML-based online DSA methods

Many research papers developed ML-based online DSA methods to evaluate the transient stability of power systems. The authors in [66], and [67]–[68] devised DT models to predict transient stability of power systems in online applications. The authors in [69]–[71] used different neural network-based algorithms to predict the transient stability of power systems. Support vector machine (SVM) classifiers were developed in [72]-[73] to predict the transient stability of power systems. Also, a comparison between the performance of the proposed SVM in three cases of considering generator voltages, frequencies, and rotor angles as the input features of the algorithm were conducted in [71]. For predicting transient stability of power systems, the authors in [73] developed a core vector machine (CVM), a variant of SVM, model to eliminate the curse of dimensionality of SVM as the size of data sets increases. Furthermore, different online DSA methods based on ensemble learning algorithms are developed in [74]–[76] to predict the transient stability of power systems.

Many research papers also focused on predicting the voltage stability of power systems using different ML algorithms. In this regard, [77]-[78] developed DT models to provide online voltage stability assessment. Predicting voltage magnitude violation, thermal limit violation, as well as transient stability of power system is also considered in [77]. The authors in [79] introduced a power flow margin index, voltage margin index, disconnected generator index, and other indices to be used as input features to train an online ANN model for predicting voltage security of power systems. The authors in [80] used an ANN to predict the dynamic voltage security margin to measure the maximum load increase that may occur before a specific contingency causes instability in the system. In [80], a systematic imbalance learning machine model was trained for online short-term voltage stability assessment. Also, the authors in [81]- [82] developed ANN and extreme learning machine (ELM) models for predicting the steady-state stability of power systems, respectively. For predicting LOS condition in generators, ANN and DT models are developed in [29] and [83]-[84]. However, the features used in these references—including pre-fault mechanical input power, generators kinetic energy deviation, average acceleration during the fault, initial rotor angle, and type of contingency—are not easily measurable in the real-time operation of power systems.

As discussed in Chapter 1, if the occurrence of LOS condition in generators are not promptly detected and proper control actions are not initiated, the stability of the system might be jeopardized, and system-wide cascading outages might happen in the system. Therefore, it is essential for an efficient online DSA method to promptly detect LOS condition in generators. Also, it is discussed in Chapter 1 that the behavior of protection

systems during a disturbance play a critical role in defining the response of the system to the disturbance. In this regard, one of the most important features of an online DSA method is the ability to predict critical protection system behavior ahead of time. Distance relays as well as UFLS and UVLS relays are among the most critical protective relays that can significantly impact the response of a system to a disturbance. To the best of our knowledge, no work in the literature completely incorporates predicting the LOS condition in generators and the behavior of critical protective relays in online DSA methods. To fill this gap, this chapter presents a comprehensive ML-based online DSA method that provides a detailed prediction of impending LOS condition in generators as well as any impending operation of distance relays, UFLS, and UVLS relays, for up to 10 seconds later. The proposed method uses the voltage angle/magnitude measurements obtained from the electrically closest high-voltage buses (above 345 kV) to the generator/relay locations in the system as the input features of the ML models. The proposed method can provide a valuable tool for utilities which can have the following benefits:

- The method can provide a fast and precise tool for online monitoring of the system and predicting the behavior of the generators and protection systems under different operating points and topologies of the system.
- The method can be used to trigger automatic control actions if it predicts impending troubles in the system (such as occurring multiple LOS condition in generators)
- The method provides valuable information about the distance relays that are likely to mis-operate during an OOS condition. Therefore, OOS blocking

signals can be sent to those relays to prevent formation of uncontrolled islanding in the system, which is a necessary action in preventing cascading outages.

- The method also provides valuable information about the potential UFLS and UVLS relay operations after a disturbance. This identifies the areas in the system that will experience frequency/voltage drop. Proper remedial actions then can be initiated to recover the frequency/voltage in those areas.
- PMU measurements have inherent errors, and they can also be polluted with external noises. Furthermore, PMU measurements can be missed due to several reasons such as PMU or phasor data concentrator (PDC) malfunctions, communication failure or congestion, and cyber-attack. The proposed method is robust against external noises and measurement errors, as well as missing PMU measurements. This guarantees a reliable operation of the proposed method in real-time applications.

5.2 The proposed comprehensive ML-based online DSA method

As mentioned in Chapter 5.1, the ML-based online DSA methods presented in the literature try to train an ML model to extract the underlying pattern between specific features, such as generator voltage or frequency measured by PMUs, and stability of the system. A new ML-based online DSA method is presented in this chapter which broadens the concept of dynamic security assessment and significantly increase situational awareness in the system by predicting protective relay operations and occurrence of LOS condition in generators for several seconds after a disturbance.

For predicting LOS condition in generators, the proposed method relies on the latent correlation between the voltage angles of the electrically closest high-voltage (HV) buses to the generator locations and the occurrence of LOS condition in generators. Likewise, for predicting protective relay operations, the method relies on the latent correlation between the voltage angles/magnitudes of the closest HV buses to the relay locations and the operation of the relays.

The conceptual representation of the method is provided in Figure 5. 2. It is assumed that the HV buses with a voltage level of 345 kV and above are equipped with PMUs. These PMUs transmit synchronous measurements of the voltage angles and magnitudes of the related buses to the control center. In the proposed scheme, the received data needs to be pre-processed in the control center, and the proper input features for each of the ML models trained in advance to predict UFLS, UVLS, and distance relay operations, as well as LOS condition in generators should be extracted. The measurement data used as input features of each of the ML models are summarized in Table 5.1. This measurement data is obtained from the 5 electrically closest HV buses to the generator/relay buses.

Note that, only the buses a with voltage level of 345 kV and above are assumed to be equipped with PMUs. Hence, the measurement data from the buses with lower voltage levels are not used, even if they are the closest buses to the relay/generator locations. Also, note that, there are two reasons for choosing voltage angles/magnitudes of the electrically closest buses to the relay/generator locations as the features of the RF models. First, these variables have a higher correlation with relay operations or occurrence of LOS conditions

in generators. Second, bus voltage angles and magnitudes can be synchronously measured and transmitted to the control center by PMUs, easily.

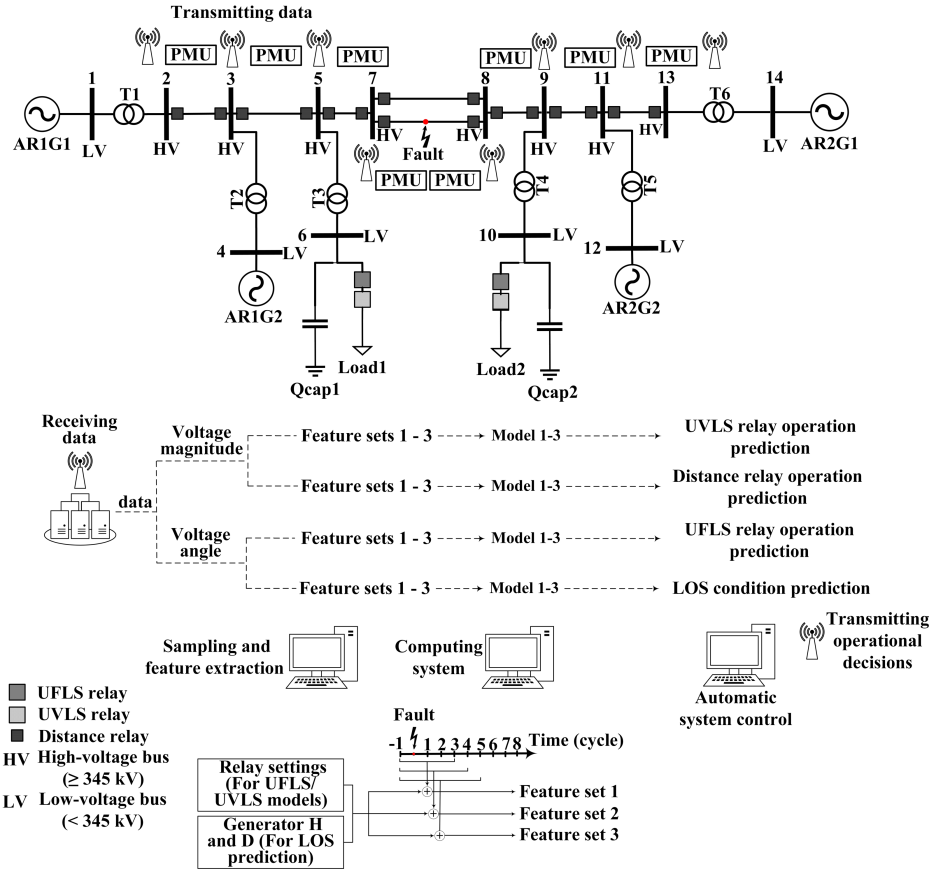

Figure 5.2 Conceptual representation of the proposed method

Table 5.1 Measurement data used by each ML model as input features

ML model	Measured variable
Predicting LOS condition	Voltage angle
Predicting distance relay operation	Voltage magnitude
Predicting UFLS relay operation	Voltage angle
Predicting UVLS relay operation	Voltage magnitude

The related relay settings, such as the pickup frequency or voltage of different stages and their time delays, are also included as the input features of the models that predict UFLS and UVLS relay operations. Also, the inertia (H) and damping factor (D) of the

generators are added to the input features of the models that predict LOS conditions in generators. Distance relay settings can be similarly considered as input features. However, as a generic relay setting is considered for all the distance relays in the test system, the zonal reaches and time delays of distance relays are not considered as input features. Nevertheless, the concept of the proposed approach can be used with the distance relay settings as features where the actual relay settings are available.

To provide different trust levels and prediction speeds, for each application of predicting UFLS, UVLS, and distance relay operation as well as LOS condition in generators, three different ML models are trained in advance. Each model uses different periods of the measurement data as its features. The periods of measurement data used by each of the ML models are illustrated in Table 5.2. Note that in Table 5.2, the measurement samples before and after the time of fault are shown by negative and positive signs, respectively.

Table 5.2 Periods of measurement data used by each of the ML models

ML model	Measured period (cycles)						
	-1	Fault	+1	+2	+3	+4	+5
1							
2							
3							

In this approach, as the contingency proceeds and more updated measurement data is received from PMUs, the models that need longer periods of measurement data can make their predictions. The predictions from these models guarantee the accuracy of the predictions of the other models that need a shorter periods of measurement data. Note that while using a longer period of measurement data as the features of the trained models might yield more reliable predictions, this reliability comes at the price of delayed predictions,

which in turn leads to a delay in initiating control actions. Thus, there is a trade-off between the speed and reliability of the predictions. The proposed method includes both types of models: the ones that need shorter periods of measurement data (hence can provide fast predictions) and the ones that need a longer period of measurement data (hence can provide more reliable predictions). Therefore, the method can provide different levels of reliability and speed of predictions.

After feeding the features to the trained models, the models make their predictions of the relay operations or occurrence of LOS conditions in the generators for several seconds later. The predictions are then sent to the automatic control system. Using the valuable information obtained from these predictions the automatic control system initiates proper control actions to alleviate the situation and avoid cascading outages and blackout.

5.3 Training the RF models

A comprehensive dataset created by performing different types of contingencies under various operating conditions and topologies of the system is required for training and testing the ML models. In this regard, using GE PSLF software, multiple offline transient stability studies including bus faults and line faults followed by tripping one or more transmission line(s) as well as generator outage contingencies are conducted. In some of these studies, different operating conditions and topologies of the WECC system are considered. Overall, 929 contingencies are studied.

During these transient stability studies, the operations of relays as well as generator rotor angles are captured to label the dataset. For any generator, if the rotor angle deviates more than 180 degrees from its initial value, that generator is considered to experience LOS

condition [21], [15]. However, [15] and [16] propose that recovering from a swing that has exceeded 120 degrees is very unlikely. Hence, 120 degrees is usually accepted as a proper value for setting an out-of-step protection system. Therefore, in this dissertation, to have a higher security margin, the generators whose relative rotor angles deviate more than 120 degrees are labeled as being in a LOS condition. Also, the features of the ML models, mentioned in Table 5.1, are captured during these studies.

To make the dataset more comprehensive, historical records of bus voltage data obtained from PMUs during different contingencies along with the record of relay operations and the occurrence of LOS condition in generators during these contingencies can also be added to the results of offline transient stability studies. However, in this dissertation, we do not have access to such historical records. Therefore, only the results of extensive offline transient stability studies are used to build the dataset.

The problems of predicting protective relay operations and LOS conditions in generators are binary classification problems (having two classes of 0 and 1). The following definitions for classes 0 and 1 hold throughout this chapter:

- Class 0: For the application of predicting protective relay operations, class 0 represents the samples of no-operation of protective relays, i.e., the samples where protective relays do not operate for the entire simulation time, in the dataset. Whereas for the application of predicting LOS conditions in generators, class 0 shows the samples where LOS conditions do not occur in generators, i.e., generators maintain their stable operation conditions.

- Class 1: For the application of predicting protective relay operations, class 1 shows the samples of relay operations in the dataset. For the application of predicting LOS conditions in generators, on the other hand, this class represents the samples of the occurrence of LOS conditions in generators.

Different ML algorithms can be used for classification problems. Because of its high accuracy and prediction speed, the RF algorithm is used to train the ML models. For training the RF models, the "scikit-learn", which is a well-known Python library, is used [62]. As mentioned in Chapter 4.4, the most important hyperparameters of the RF classifier are *class weights*, *the number of trees in the forest*, the *maximum depth of the trees*, the *MSS*, the *MSL*, the *number of features considered when looking for the best split*, and *whether bootstrap samples are used when building trees*. Precise tuning of these hyperparameters significantly improves the performance of the trained model. Therefore, in order to achieve the best performance, a two-stage grid search method is utilized to fine-tune the hyperparameters of the RF models. During each iteration of the grid search method, the K-fold cross-validation method with 5 folds is used to provide a realistic assessment of the performances of the trained models. The F1 score is considered the main metric for evaluating the performances of the models. Accuracy, recall, precision, and negative predictive value (NPV) metrics are also used to provide a more detailed evaluation. Brief explanations of the RF algorithm, the grid search method, and the K-fold cross-validation method is provided in Chapter 4.2. The metrics used in this chapter for evaluating the performances of the trained models are explained in the next chapters.

To show the impact of changing each hyperparameter on the performances of the trained models Figures 5.3 – 5.6 are provided. The change in the F1 score for the various *number of trees in the forest* and the *maximum depth of the trees* for the models trained to predict LOS condition in generators and the models trained to predict the operations of UFLS, UVLS, as well as distance relays are shown in Figures 5.3 (a), 5.4 (a), 5.5 (a), and 5.6 (a), respectively. Note that these figures illustrate the impact of changing the hyperparameters on the performance of the models that use 7 cycles of measurement data. However, the impact of changing the hyperparameters on the other models can be shown, likewise. Also, the change in the F1 score for the various number of the *class weights* hyperparameter and the *number of trees in the forest* for the models trained to predict LOS condition in generators and the models trained to predict the operations of UFLS, UVLS, as well as distance relays are shown in Figures 5.3 (b), 5.4 (b), 5.5 (b), and 5.6 (b), respectively. Note that the figures show the F1 score of the models trained with different combination of the hyperparameters at the first stage of the grid search method. Similar figures can be obtained for the second stage of the grid search method, where the method searches to find the best values for each hyperparameter around the values obtained at the first stage. The best value for each hyperparameter along with its corresponding F1 score is also shown as a data tip on each figure.

For the models trained to predict LOS condition in generators and operation of distance relays, as seen in Figures 5.3 and 5.6, in comparison to the *number of trees in the forest*, the *maximum depth of trees* and the *class weight* hyperparameters have more impact on the

performance of the trained models. The *maximum depth of trees* has the highest impact on the performance of these models, especially when the values of this hyperparameter is low.

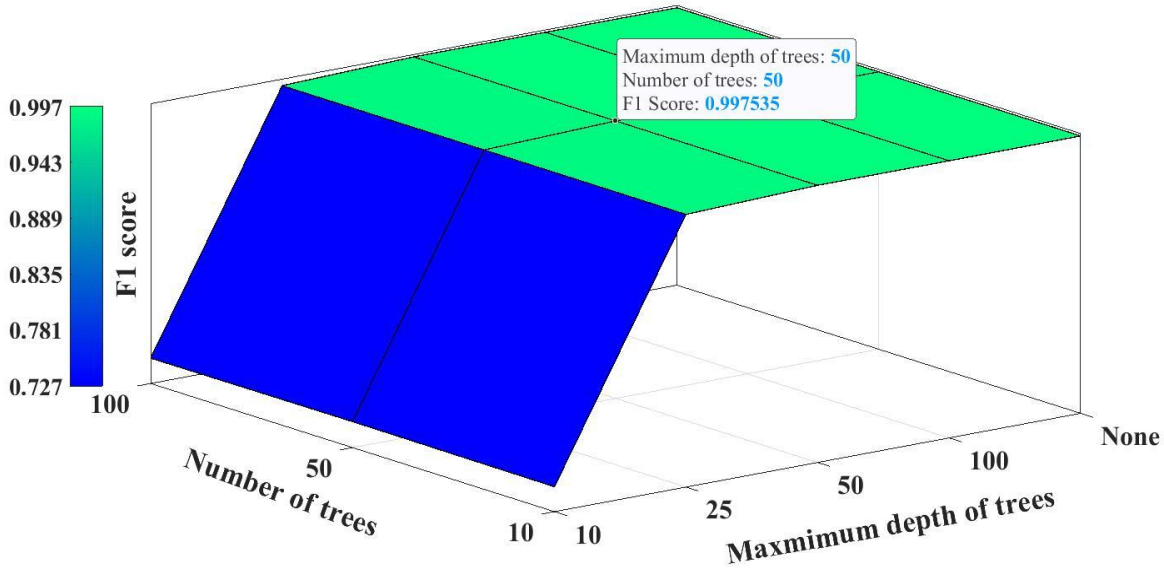

(a)

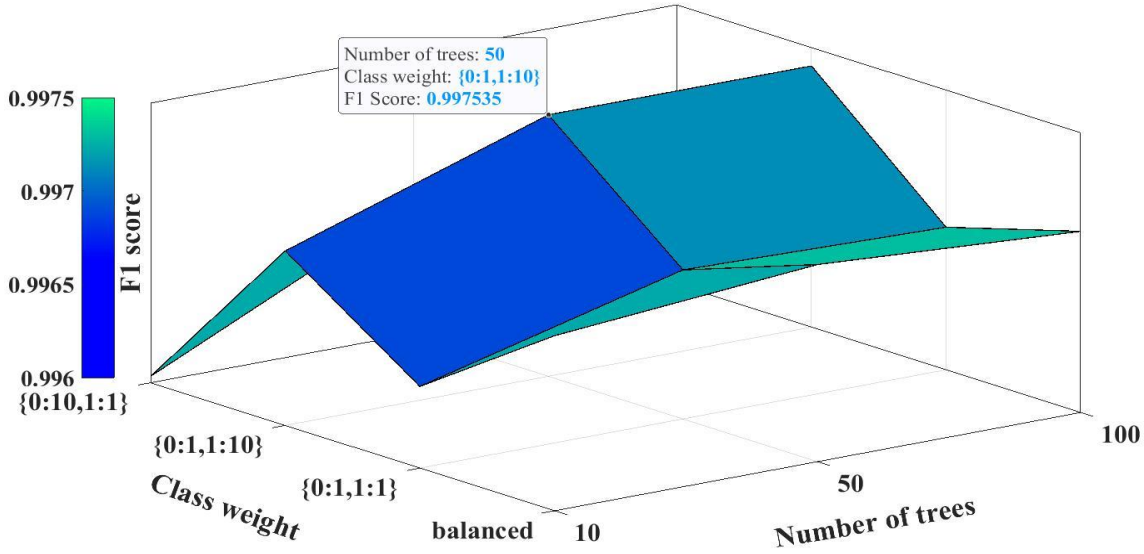

(b)

Figure 5.3 The change in the F1 score of the model trained to predict LOS condition in generators for the different values of the *maximum depth of trees* and the *number of trees in the forest* (a), different values of *class weights* and the *number of trees in the forest* (b).

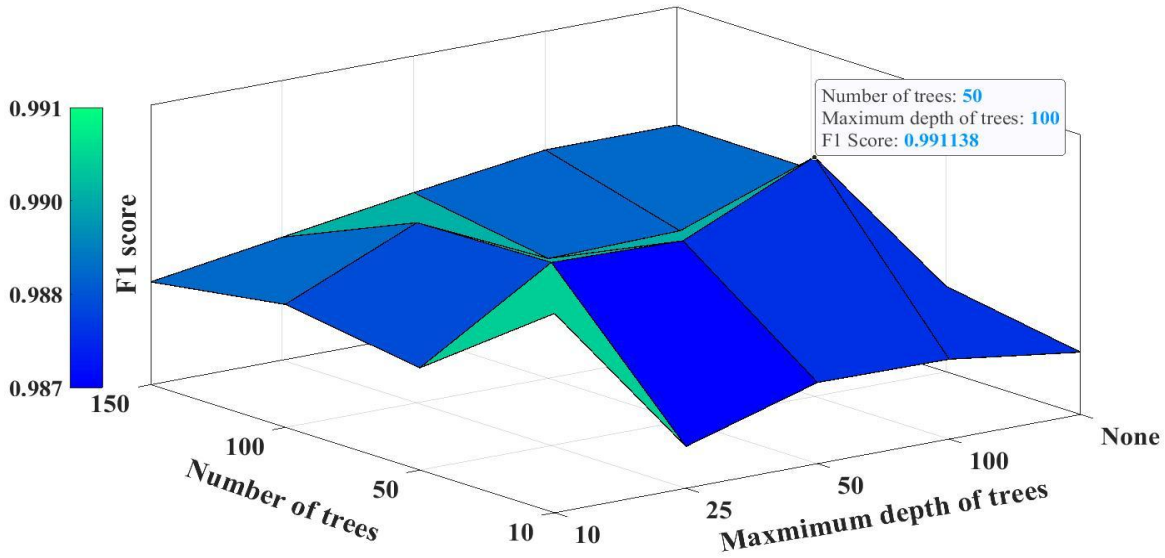

(a)

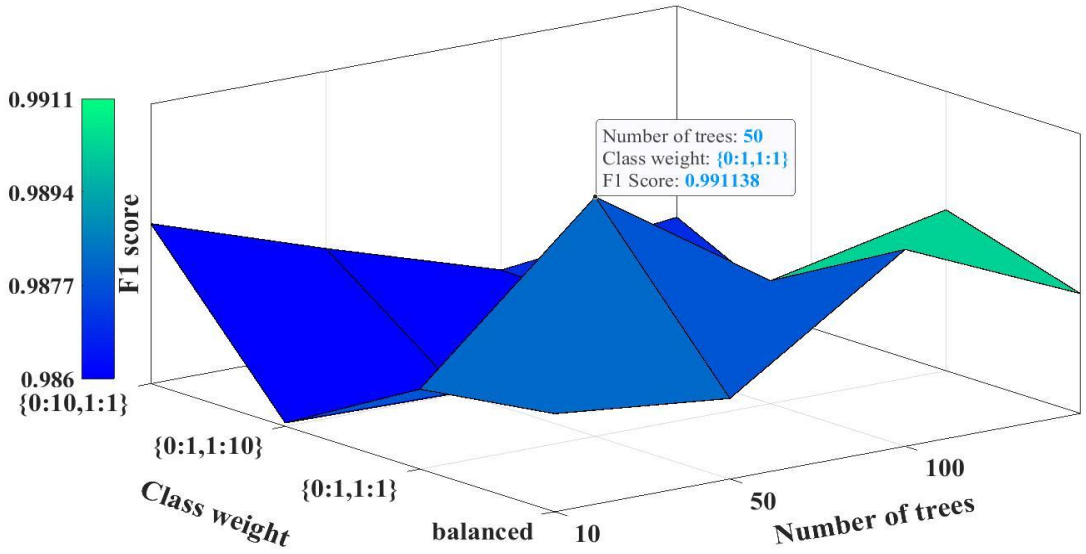

(b)

Figure 5.4 The change in the F1 score of the model trained to predict UFLS relay operations for different values of the *maximum depth of trees* and the *number of trees in the forest* (a), the different values of *class weights* and the *number of trees in the forest* (b).

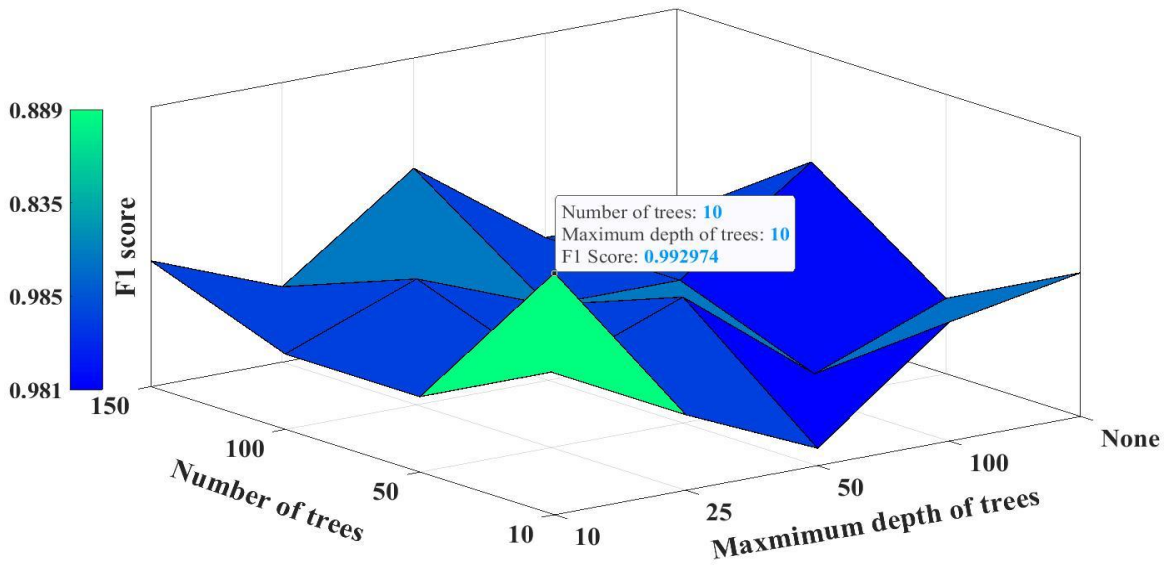

(a)

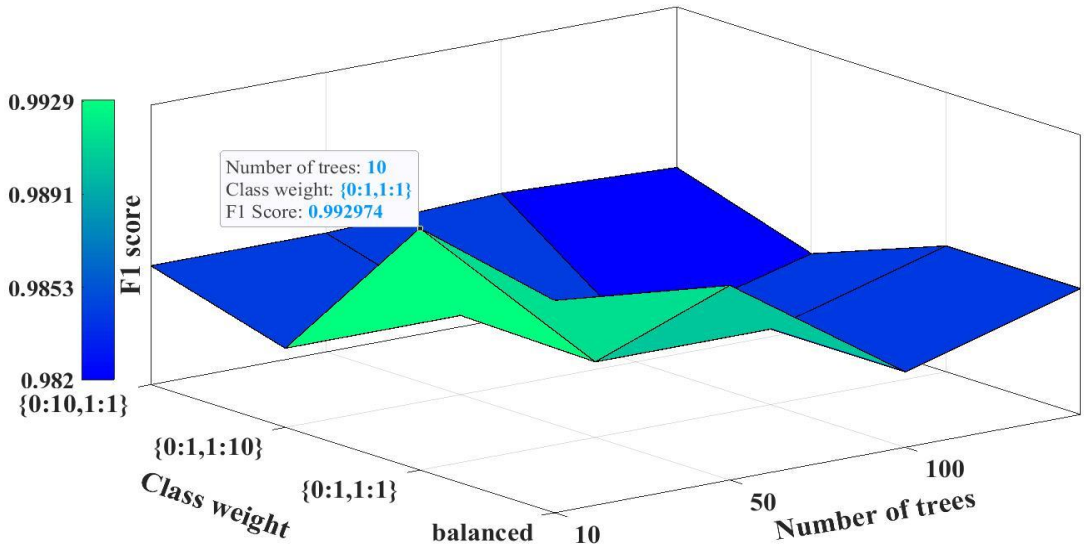

(b)

Figure 5.5 The change in the F1 score of the model trained to predict UVLS relay operations for different values of the *maximum depth of trees* and the *number of trees in the forest* (a), the different values of *class weights* and the *number of trees in the forest* (b).

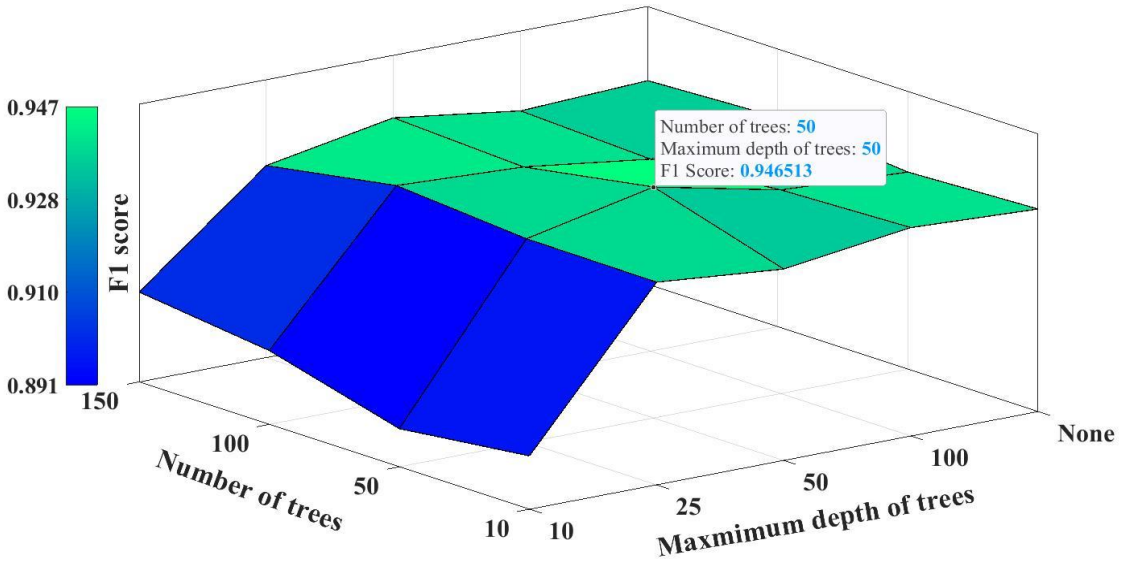

(a)

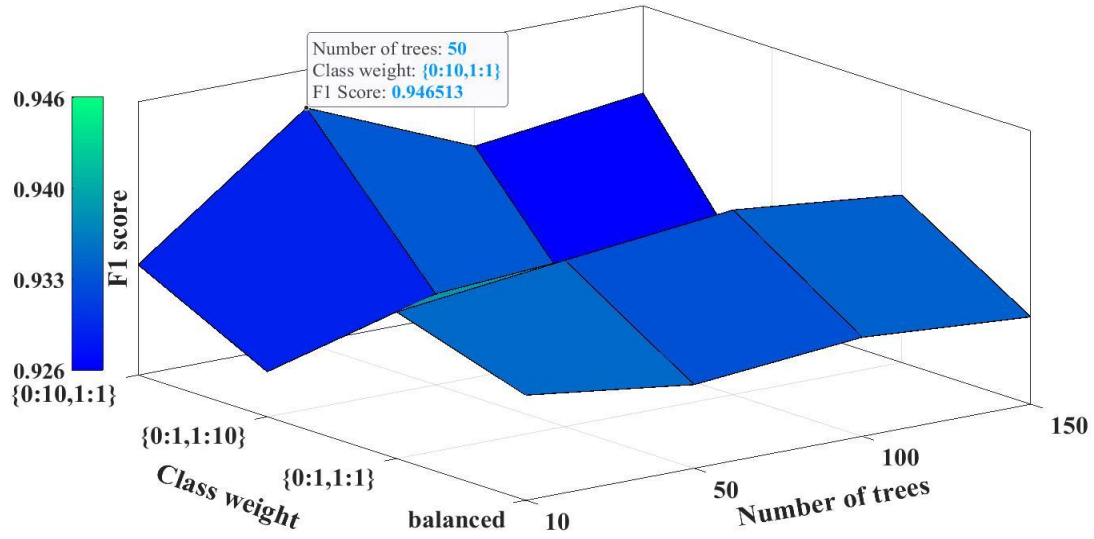

(b)

Figure 5.6 The change in the F1 score of the model trained to predict distance relay operations for different values of the *maximum depth of trees* and the *number of trees in the forest* (a), the different values of *class weights* and the *number of trees in the forest* (b).

For the models trained to predict UFLS and UVLS relay operations, as seen in Figures 5.4 and 5.5, in comparison to the *number of trees in the forest* and the *maximum depth of trees*, the *class weight* hyperparameter has more impact on the performances of these models.

5.4 The metrics used to evaluate the performances of the trained models

In order to meticulously evaluate the performances of the trained models, 5 metrics of accuracy, recall, precision, F1 score, and NPV, defined in (5.1)-(5.5), are utilized.

$$Accuracy = \frac{TP+TN}{TP+TN+FP+FN} \tag{5.1}$$

$$Recall = \frac{TP}{TP+FN} \tag{5.2}$$

$$Precision = \frac{TP}{TP+FP} \tag{5.3}$$

$$F1\ score = 2 \times \frac{(precision \times recall)}{(precision+recall)} \tag{5.4}$$

$$NPV = \frac{TN}{TN+FN} \tag{5.5}$$

In these equations, TP is the number of true-positive predictions. True-positive predictions are the cases that belong to class 1 and the trained model correctly predicts these cases to belong to class 1. TN is the number of true-negative predictions. True-negative predictions are the cases that belong to class 0 and the model correctly predicts these cases to belong to class 0. FP is the number of false-positive predictions. False-positive predictions are the cases that belong to class 0 and the. model falsely predicts them to belong to class 1. Finally, FN is the number of false-negative predictions. False-negative predictions are the cases that belong to class 1 and the model falsely predicts them to belong to class 0.

Accuracy shows that overall, what portion of the predictions of the trained models are correct predictions. In unbalanced datasets, where the number of the samples of one class dominated the other, the accuracy metric might not yield a good evaluation of the performance of the trained models. For instance, if there are 99 cases of class 0 in the dataset and 1 case of class 1 (e.g., the case of predicting if a patient has a rare disease), and we train an ML model that just return prediction of 0 for any case, regardless of the input features, the trained model will still have 99% accuracy on the dataset. This is not a valid assessment of the performance of the trained model. Since our dataset is also unbalanced and there are more no-operation cases of relays than the operation cases and there are more stable operation condition cases in generators than the LOS condition cases, other metrics are required for having a better assessment of the performances of the trained models.

As mentioned in Chapter 4.2.2, the Recall shows that what portion of all the relay operation cases or LOS condition cases in generators (cases belonging to class 1) are correctly predicted by the trained model. A high Recall value (a value close to 1) can ensure that nearly all the relay operations and LOS conditions in generators are correctly identified by the models, and no impending relay operation or LOS condition in generators is missed.

On the other hand, the Precision shows that what portion of the predictions of the trained model that a protective relay operates or a generator experiences LOS during a contingency (predictions that a case belongs to class 1) are correct predictions. Likewise, NPV shows that what portion of the predictions that a relay does not operate, or a generator does not experience LOS during a contingency (predictions that a case belongs to class 0)

of the trained model are correct predictions. High precision and NPV values (values close to 1) can guarantee the accuracy of nearly all the predictions of the models.

Finally, the F1 score creates a compromise between the Recall and the Precision. A high value of the F1 score guarantees the capability of the trained models in distinguishing between different classes. For unbalanced datasets, where the number of samples of one class dominates the other, the F1 score yield a better assessment of the performances of the trained models. Therefore, in this chapter, the F1 score is used as the main metric for evaluating the performances of the models.

In order to visualize the definition of the Accuracy, Recall, Precision, and NPV metrics, a visualization similar to Figure 4.3 is provided in Figure 5.7. In this figure, positive and negative cases are shown with filled and hallow circles, respectively. Therefore, all the cases in the left rectangle are positive cases and all the cases in the right rectangle are negative cases. The hypothesis learnt by the trained model is shown with the black circle in the middle of the figure. The model predicts all the cases that fall within the circle as positive cases and all other cases as negative cases. In this condition, true-positive predictions are the ones that fall within the left semi-circle and all the cases that fall within the right semi-circle are the false-positive predictions. False-negative predictions are all the cases that fall within the left rectangle but do not fall within the middle circle, whereas the true-negative cases are the cases that fall within the right rectangle but do not fall within the middle circle. Therefore, the Accuracy, Recall, Precision, and NPV can be visualized as Figure 5.7.

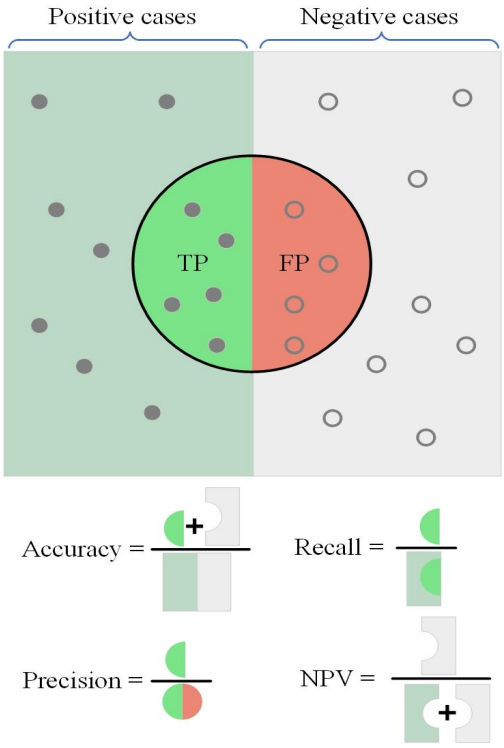

Figure 5.7 Visualization of the definition of the Accuracy, Precision, Recall, and NPV

5.5 Test system and dynamic model description

In order to implement the proposed online DSA method and evaluate its performance, the WECC system data representing the 2018 summer peak load case is utilized. There are 3399 UFLS relays and 470 UVLS relays throughout the WECC system (based on the models included in the dynamic file of the system). Similar to previous chapters, in order to capture the responses of distance relays in transient stability studies, two dynamic models of distance relays from the PSLF model library [46] are used:

- For modeling distance relays on the lines with the voltage level of 345 kV and above, the "Zlin1" models are used. The responses of the *Zlin1* relays are recorded during offline transient stability studies and are used to create the dataset needed to train the models that predict distance relay operations.

- For protecting the lines with a voltage level between 100 kV and 345 kV, a *Zlinw* model is used.

  As mentioned, due to the limitations of stability software tools in the number of dynamic models that can be included in stability studies, only the lines with the voltage level of 345 kV and above are modeled with *Zlin1*. The lines with lower voltage levels are modeled with *Zlinw*, as *Zlinw* does not need to be specifically modeled for each transmission line and it can monitor all the lines within its minimum and maximum voltage settings.

5.6 Numerical results and analysis

Using the metrics described in Chapter 5.4, the performances of the RF models trained using the best values of the hyperparameters obtained from the grid search method are evaluated. The results for predicting the operations of distance relays, UFLS relays, and UVLS relays as well as LOS condition in generators are provided in Table 5.3 (a), (b), (c), and (d), respectively. As seen in these tables, all the trained models yield high values of F1 score, which guarantee the great performances of the trained models in distinguishing between operation (class 1) and no-operation cases (class 0) of the relays as well as between the LOS condition (class 1) and stable operation condition (class 0) in generators. Analyzing the Recall and Precision metrics of each model shows that a very low number of false-negative and false-positive predictions are observed in the predictions of the trained models. This can guarantee that the trained models can correctly capture all the impending distance relay, UFLS relay, and UVLS relay operations as well as LOS condition in any generator.

The prediction time of each model is provided in Table 5.4. As seen in Table 5.4, the prediction time of the trained models is very low, and it can be ignored in comparison with the period of measurement data required for prediction. If we take the period of data required for the prediction of each model into account, the first models—the models that use 5 cycles of data—can provide their predictions approximately 66.7 ms after the fault. The second and the third models—the models that use 6 and 7 cycles of data, respectively—can provide their predictions approximately 83.4 and 100 ms after the fault, respectively. This shows that all the trained models are fast enough to be used as online DSA method.

Table 5.3 The performances of the models trained for predicting: (a) distance relay, (b) UFLS relay, (c) UVLS relay, and (d) LOS condition in generators

(a)

Model	Accuracy	Recall	Precision	NPV	F1score
1	0.990	0.906	0.898	0.995	0.902
2	0.995	0.922	0.968	0.996	0.945
3	0.995	0.928	0.966	0.996	0.947

(b)

Model	Accuracy	Recall	Precision	NPV	F1score
1	0.995	0.987	0.994	0.995	0.991
2	0.995	0.987	0.996	0.994	0.991
3	0.995	0.987	0.996	0.994	0.991

(c)

Model	Accuracy	Recall	Precision	NPV	F1score

1	0.995	0.991	0.995	0.995	0.993
2	0.997	0.995	0.995	0.998	0.995
3	0.997	0.995	0.995	0.998	0.995

(d)

Model	Accuracy	Recall	Precision	NPV	F1score
1	0.998	0.997	0.997	0.998	0.997
2	0.998	0.997	0.998	0.998	0.998
3	0.998	0.998	0.998	0.998	0.998

Table 5.4 Prediction time of the trained models

Model	Distance relay (μs)	UFLS relay (μs)	UVLS relay (μs)	LOS (μs)
1	23.4	35.1	258	25.2
2	28	26.6	203	19.6
3	15.7	19.5	145	15.6

By comparing the performances of the models that use different periods of measurement data, it is observed that using a longer period of measurement data for prediction generally enhances the performances of the trained models. However, as observed, this enhancement in the performance comes at the price of a longer delay in predictions of the models. As mentioned earlier, the method provides the opportunity to compromise the reliability and the speed of predictions by providing both types of models that use a shorter period of measurement data and the models that use a longer period of measurement data.

5.6.1 Evaluating the impact of external noise and measurement error on the performance of the trained models

PMU measurement data are usually accompanied by measurement errors and external noises. If the trained models are not robust against noise, their performances can be adversely impacted. Therefore, the performances of the trained models need to be evaluated in the presence of measurement errors and noises. In this regard, different levels of noise are added to the voltage magnitude/angle data used for testing the performances of the trained models. IEEE Standard C37.118.1-2011 [85] requires PMUs to provide measurements with less than 0.01 total vector error (TVE), which implies a voltage magnitude measurement error of less than 1 percent of the voltage magnitude and voltage angle measurement error of less than 0.573 degrees. Industrial PMUs far exceed the IEEE standard requirement. For instance, industrial PMUs with accuracies of ± 0.03% in phasor magnitude and ± 0.01 degrees in phasor angle have been manufactured [86]-[88]. In this regard, the performances of the trained models are evaluated in the presence of noise levels equal to 0.03, 0.1, and 0.25 of the IEEE standard TVE. The performances of the models trained to predict distance relay, UFLS relay, and UVLS relay operations as well as LOS condition in generators in terms of the F1 score are provided in Table 5.5 (a), (b), (c), and (d). As seen in these tables, all the trained models are robust against the noise levels of industrial PMUs and can provide reliable predictions.

5.6.2 Evaluating the impact of missing PMU measurements on the performance of the trained models

PMU measurements might not always be synchronously available due to practical issues, including but not limited to PMU or PDC malfunctions, communication failures or congestions, and cyber-attacks [89]. This missing data can adversely affect the performances of the trained models and lead to inaccurate predictions. Hence, it is urgent that the trained models be robust against possible missing data.

Table 5.5 The performances of the models trained for predicting: (a) distance relay, (b) UFLS relay, (c) UVLS relay, and (d) LOS condition in generators in the presence of different noise levels

(a)

Model	0.03 IEEE standard TVE	0.1 IEEE standard TVE	0.25 IEEE standard TVE
1	0.901	0.890	0.807
2	0.943	0.941	0.889
3	0.945	0.947	0.922

(b)

Model	0.03 IEEE standard TVE	0.1 IEEE standard TVE	0.25 IEEE standard TVE
1	0.989	0.988	0.978
2	0.990	0.985	0.982
3	0.991	0.987	0.978

(c)

Model	0.03 IEEE standard TVE	0.1 IEEE standard TVE	0.25 IEEE standard TVE
1	0.993	0.989	0.975
2	0.993	0.995	0.981
3	0.995	0.995	0.973

(d)

Model	0.03 IEEE standard TVE	0.1 IEEE standard TVE	0.25 IEEE standard TVE
1	0.938	0.903	0.874
2	0.950	0.916	0.887
3	0.958	0.925	0.891

In this regard, the performances of the trained models are evaluated considering the following four scenarios of missing PMU measurement data:

- Scenario 1: Missing one random measurement sample
- Scenario 2: Missing two random measurement samples
- Scenario 3: Missing two consecutive measurement samples
- Scenario 4: Completely missing the measurement samples from one random PMU

The missing sample(s) are randomly selected among the measurement samples used as the features of the trained. Also, the PMU whose measurement data are missed is randomly selected among the PMUs whose measurement data are used as the features of the trained models.

In scenarios 1 and 2, using (5.6), the missing sample(s) are replaced by the average of their preceding and succeeding samples. Note that, $s_{n,m}$ represents sample m from bus n (the missing sample), and $s^*_{n,m}$ represents the value that is replaced with $s_{n,m}$ to be used as the feature(s) of the trained models.

$$s^*_{n,m} = \frac{s_{n,m-1} + s_{n,m+1}}{2} \tag{5.6}$$

In scenario 3, considering $s_{n,m}$ as the first missing sample and $s_{n,m+1}$ as the second one, the missing samples are replaced with the values calculated using (5.7) and (5.8), respectively.

$$s^*_{n,m} = \frac{s_{n,m-1} + s_{n,m+2}}{2} \tag{5.7}$$

$$s^*_{n,m+1} = \frac{s^*_{n,m} + s_{n,m+2}}{2} \tag{5.8}$$

In scenario 4, each measurement sample of the PMU whose data are missed is replaced with the values calculated using (5.9).

$$s^*_{n,m} = \begin{cases} \frac{s_{n-1,m} + s_{n+1,m}}{2} \times \beta_n & ,\forall m \in M_i, i \in \{1,2,3\} \quad if\ n \neq 1 \\ s_{n+1,m} \times \beta_n & ,\forall m \in M_i, i \in \{1,2,3\} \quad if\ n = 1 \end{cases} \tag{5.9}$$

In (5.9), M_i is the set of measurement samples used as the features of model *i*. β_n is a scaling factor and is defined in (5.10). Note that, since the voltage magnitude/angles of different buses are different from each other, this scaling factor is required if the measurement samples of one bus need to be replaced with those of another bus (or with the average of measurement samples of two other buses).

$$\beta_n = \begin{cases} \frac{2 \times s_{n,1}}{s_{n-1,1} + s_{n+1,1}} & if\ n \neq 1 \\ \frac{s_{1,1}}{s_{2,1}} & if\ n = 1 \end{cases} \tag{5.10}$$

In (5.10), $s_{n,1}$ is the first measurement sample from bus *n*, i.e., the voltage magnitude/angle from bus *n* captured one cycle before the fault (steady-state pre-fault condition). Equation (5.10) states that if the samples from one bus are to be replaced with those from another bus (or with the average of measurement samples from two other buses), a scaling factor is required. The factor should be equal to the ratio of the steady-state pre-fault voltage magnitude/angle of the bus whose measurement samples are missed

to that of the bus to be used as a replacement (or to the average steady-state voltage magnitude/angles of the two other buses that are used as replacements).

Using (5.6)-(5.10) for replacing the missing measurement samples, the performances of the trained models are evaluated for new and out-of-sample cases, in the presence of measurement noises equal to 0.03 of standard IEEE TVE and the four scenarios of missing PMU measurement data. The results in terms of the F1 score for the models trained to predict distance relay operations, UFLS and UVLS relay operations, as well as LOS conditions in generators are provided in Table 5.6 (a)-(d), respectively. Each column in these tables represents one of the three different models that are trained for each application, and each row represents different scenarios of missing PMU data. As seen in Table 5.6, all the trained models maintain a great performance in different scenarios of missing PMU data, even for predicting new cases and in the presence of measurement errors and noises. The great performances of the models in the presence of noise and missing PMU data can guarantee the reliability of the models in practical applications, where PMU data are along with measurement errors, might be polluted with external noises, and might be missed during the process of being transmitted to the operation center.

Table 5.6 The performances of the models trained for predicting: (a) distance relay, (b) UFLS relay, (c) UVLS relay, and (d) LOS condition in generators in the presence of noise and missing PMU data

(a)

Models	1	2	3
Scenario 1	0.892	0.945	0.945
Scenario 2	0.900	0.935	0.938
Scenario 3	0.894	0.938	0.937
Scenario 4	0.882	0.924	0.917

(b)

Models	1	2	3
Scenario 1	0.990	0.990	0.991
Scenario 2	0.990	0.990	0.990
Scenario 3	0.990	0.990	0.990
Scenario 4	0.989	0.989	0.989

(c)

Models	1	2	3
Scenario 1	0.993	0.993	0.995
Scenario 2	0.993	0.990	0.992
Scenario 3	0.990	0.993	0.992
Scenario 4	0.993	0.987	0.990

(d)

Models	1	2	3
Scenario 1	0.937	0.951	0.958
Scenario 2	0.936	0.950	0.958
Scenario 3	0.936	0.950	0.957
Scenario 4	0.925	0.940	0.946

5.6.3 Case studies

To further illustrate the performances of the trained models, three different case studies are analyzed in the WECC system, and the trained models are used to predict any distance relay, UFLS relay, and UVLS relay operations, as well as LOS condition in generators. These case studies are among the most critical contingencies of the WECC system, which have system-wide effects and can lead the system toward instability. Therefore, the great performances of the trained models in these cases are essential for initiating proper remedial actions to avoid cascading outages and blackouts and can guarantee the reliability of the trained models. Note that, these case studies are only provided to show the performances of the trained models in three simulated examples of the online application of the proposed method, where out-of-sample contingencies occur. The values reported for the F1 scores (as well as the other metrics) in Tables 5.3, 5.5, and 5.6 are obtained from testing the trained models on the entire dataset (929 contingencies) using the K-fold cross-validation method.

5.6.3.1 Case study 1

In this case study, a bus fault occurs on bus 3 of the WECC system and is cleared after 4 cycles by removing three 500 kV transmission lines that comprise COI. As mentioned in previous chapters, the outage of these tie lines is a critical contingency for the WECC system as they transfer a significant amount of power. Therefore, the N-3 COI outage is considered in this case study. To show the performance of the proposed method under a new pre-fault operating condition, the pre-fault operation condition of the WECC system is modified, in this case study. In the new operating condition, a uniform increase of 2 percent in the large loads of the areas that import power through the COI (the loads above 100 MW) is considered. Moreover, to evaluate the performances of the trained models in the presence of measurement noises, different levels of measurement noises—including 0.03, 0.1, and 0.25 of the IEEE standard TVE—are added to the features of the models.

This contingency leads to 82 UFLS relay operations, 3 UVLS relay operations, and 9 distance relay operations. It also leads to LOS condition in 1412 generators. The models trained to predict UFLS and UVLS relay operations identified all the relay operation and no-operation cases (both classes 1 and 0), correctly, i.e., no false-negative or false-positive predictions, under all applied noise levels. This yields an F1score of 1, which is higher than the F1 score reported in Table 5.5 (b) and (c) for these models.

The performances of the models that predict the operations of distance relays and LOS conditions in generators, in terms of the number of *FN* and *FP* cases as well as the F1score, are provided in Table 5.7 (a) and (b), respectively. The F1 scores reported in Table 5.7 (a)

and (b) for case study 1 are higher than the F1 scores reported in Table 5.5 (a) and (d) for the same models, which shows the great performances of the models in this case study.

5.6.3.2 Case study 2

In this case study, the same contingency of case study 1 is analyzed. However, to evaluate the performances of the trained models in the case of a new pre-fault topology of the system, the pre-fault topology of the system is modified by taking two critical 500 kV transmission lines of the system out of service. Each of these transmission lines approximately carries 384 MW of power. Similar to case study 1, different levels of measurement noises are added to the features of the models.

This contingency leads to 1 UFLS relay operation in the system. All other UFLS and UVLS relays do not operate during this contingency. All the trained models under all the applied noise levels predict the operation of that 1 UFLS relay and no-operation of other UFLS and UVLS relays in the system. This yields an F1score of 1 for all the models trained to predict UFLS and UVLS relay operations. This F1 score is higher than the F1 scores reported in Table 5.5 (b)-(c) for these models.

The contingency also leads to 8 distance relay operations and LOS conditions in 1445 generators. The number of FN and FP cases as well as the values of the F1 scores of the models that predict the operations of distance relays and LOS conditions in generators are provided in Table 5.8 (a) and (b), respectively. As seen in Table 5.8, all the F1 scores obtained in case study 2 for the models that predict distance relay operations and LOS conditions in generators are higher than the F1 scores reported in Table 5.5 (a) and (d) for the same models.

Table 5.7 The performances of the models trained for predicting: (a) distance relay operation, (b) LOS condition in generators in the presence of different noise levels for case study 1

(a)

Models	metric	Noise level: 0.03 TVE	Noise level: 0.1 TVE	Noise level: 0.25 TVE
1	FN	0	0	1
	FP	0	0	0
	F1 score	1	1	0.941
2	FN	0	0	1
	FP	0	0	0
	F1 score	1	1	0.941
3	FN	0	0	0
	FP	0	0	0
	F1 score	1	1	1

(b)

Models	metric	Noise level: 0.03 TVE	Noise level: 0.1 TVE	Noise level: 0.25 TVE
1	FN	0	1	8
	FP	0	0	0
	F1 score	1	1	0.997
2	FN	0	0	0
	FP	0	0	0
	F1 score	1	1	1
3	FN	0	0	1
	FP	0	0	0
	F1 score	1	1	1

5.7.3.3 Case study 3

To evaluate the performances of the trained models in other types of contingencies, an N-3 generator outage contingency is considered in this case study. The selected three generators produce a total active power of around 1268 MW and are among the generators with the highest active power generation in the WECC system. Similar to case study 1, different levels of noise are added to the features of the models.

This contingency leads to 5 UFLS relay operations and 1 UVLS relay operation throughout the system. The models trained to predict UFLS and UVLS relay operations correctly identify all the relay operation and no-operation cases under all the applied noise levels. This contingency does not lead to any distance relay operation or LOS condition in the generators. The models trained to predict distance relay operations and LOS conditions in generators correctly identified no-operation of all the distance relays in the system and stable operation condition of all the generators. This yields an F1 score of 1 for all the trained models in this case study.

5.6.4 Analyzing the results

The case studies show that the trained models can reliably predict distance relay, UFLS relay, and UVLS relay operations, as well as LOS condition in generators in any type of contingency even under different pre-fault operating conditions and topologies of the system. To further shed light on how the proposed method provides valuable information about which areas of the system are affected by the disturbance and how the disturbance spreads throughout the system, a heat map is provided in Figure 5.8 for case study 1. The

heatmap shows parts of the WECC system where distance relay (shown by number 1), UFLS relay (shown by number 2), and UVLS relay (shown by number 3) operations, as

Table 5.8 The performances of the models trained for predicting: (a) distance relay operation, (b) LOS condition in generators in the presence of different noise levels for case study 2

(a)

Models	metric	Noise level: 0.03 TVE	Noise level: 0.1 TVE	Noise level: 0.25 TVE
1	FN	0	1	2
	FP	0	0	0
	F1 score	1	0.933	0.857
2	FN	0	0	0
	FP	0	0	0
	F1 score	1	1	1
3	FN	0	0	1
	FP	0	0	0
	F1 score	1	1	0.933

(b)

Models	metric	Noise level: 0.03 TVE	Noise level: 0.1 TVE	Noise level: 0.25 TVE
1	FN	1	41	108
	FP	0	0	0
	F1 score	1	0.986	0.961
2	FN	0	13	96
	FP	0	0	0
	F1 score	1	0.996	0.966
3	FN	0	7	100
	FP	0	0	0
	F1 score	1	0.998	0.964

well as LOS conditions in generators (shown by number 4) are predicted by the proposed method. Different shades of red colors in Figure 5.8 indicate different levels of trust in the predictions of the trained models. For each application of predicting UFLS, UVLS, and distance relay operation, as well as LOS conditions in generators, the lightest shade of red is for model 1 (the least reliability in the predictions); the darker shade is for model 2 (higher reliability in the predictions), and the darkest shade is for model 3 (the highest reliability in the predictions). The heatmap can serve as a visualizing tool that provides warnings of the impending problems in the system and helps in making effective decisions.

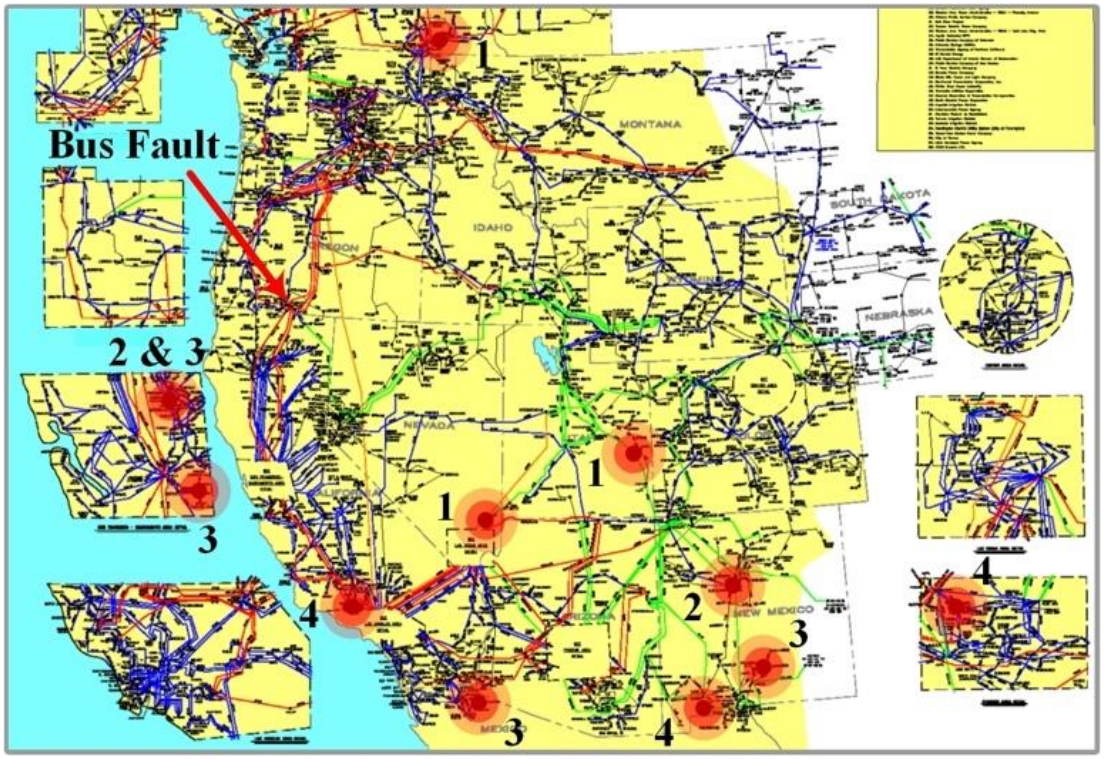

Figure 5.8 The heatmap of case study 1.

5.7 Summary

In this chapter, online dynamic security assessment and its necessity in modern power grids are thoroughly explained. It is discussed that how an online DSA system can improve

situational awareness and can prevent major outages and blackouts in the system. It is explained that how traditional methods of evaluating the dynamic security of the system are insufficient for online application and how the PMUs installed throughout modern power systems can provide online measurements of different parameters in the system, which can be used to develop ML-based online DSA methods. In Chapter 5.1.1, different research works on online DSA methods are reviewed. The research works in the literature review has developed ML-based algorithms to extract a pattern between a specific parameter, such as generator bus voltages, measured by PMUs and rotor angle, voltage, and small signal stability of the system. The shortcomings of the methods reviewed in the literature are also explained in Chapter 5.1.1.

Chapter 5.2 proposes an ML-based online DSA method that uses the voltage magnitudes/angles of the electrically closest buses to the relay/generator locations and predicts if any distance relay, UFLS relay, and UVLS relay will operate and if any generator in the system will experience LOS condition for several seconds later. The method uses the historical data and the results of offline transient stability studies performed on the WECC system to train different RF models to predict the relay operations, and LOS conditions in the generators. For each of the mentioned applications, 3 different RF models are trained. These models use different periods of voltage magnitude/angle measurement data obtained from PMUs installed on the 5 electrically closest high-voltage buses to the relay/generator locations as the input features. Different steps for creating a comprehensive dataset for training the RF models and tuning their hyperparameters to achieve the best performance are presented in Chapter 5.2 and 5.3. The

metrics used for evaluating the performances of the trained models and the test system are explained in Chapters 5.4 and 5.5, respectively.

In Chapter 5.6, the performances of the trained models are evaluated in the presence of noise and missing PMU data using the K-fold cross-validation method. The results show that the trained models are robust to standard noise levels of industrial PMUs (and higher) and missing PMU data. The results show that with the noise level of 0.03 and 0.1 of IEEE standard TVE, all the trained models have an F1 score of above 0.9 and for the noise level of 0.25 of IEEE standard TVE, which is considerably higher than the noise level of industrial PMUs, all the trained models still have F1 scores above 0.8. The F1 scores of all the trained models are higher than 0.88 in the four scenarios of missing PMU data with the noise level of 0.03 of IEEE standard TVE. The results show that all the RF models are fast enough to satisfy the requirement of an online DSA method.

The various RF models trained in this chapter that use different periods of measurement data can provide different levels of prediction speed and reliability in predictions. This creates an opportunity to compromise the speed and the reliability of the predictions. Therefore, the method can serve as a reliable and fast tool to increase situational awareness by providing valuable information about the impending distance relay, UFLS relay, and UVLS relay operations, as well as LOS conditions in generators throughout the system. The heatmap of a contingency is provided, which shows the areas of the system that are predicted to experience frequency/voltage drop and consequent distance relay, UFLS relay, and UVLS relay operations. It also visualizes the generators of which areas will experience LOS conditions during the disturbance. This can help for a better understanding of the

system condition and how the disturbance propagates in the system, which significantly helps in initiating more efficient remedial actions.

Chapter 6: Generator protection system modeling and impact assessment in transient stability analysis

Electric rotating machinery, including synchronous and induction generators, represent a very complex class of equipment that are subject to different types of failure. These failures can be categorized as follows [21], [90]:

1. Internal faults: within the generator protection zone
2. Abnormal operating or abnormal external system condition (such as an uncleared fault)

Power plants comprise almost 50 percent of the capital investment in power systems. Therefore, their outages due to faults, abnormal operating condition, or protective relay misoperation are very costly. Hence, a complete generator protection system which include different protection functions are designed to remove the faulted generator to preserve system integrity and minimize the damage to the generator [21], [91]. Some other generator protective functions, such as over-excitation limiter (OEL) and under-excitation limiter (UEL), can also send signals to generator excitation system to limit the generator field current and output reactive power in order to avoid prolonged abnormal operation condition of the generator.

As one of the most fundamental assets in power systems, generators play a significant role in defining the system behavior during different disturbances. Having the capability to trip the generator or impose limiting action on them, the response of different generator protective relays installed on the generators significantly impacts the behavior of the generators and the dynamic response of the system during disturbances. In this regard,

post-disturbance analysis of many of the major outages and blackouts reveal the significant role of generator protective relays in the chain of events leading to these major outages. More detailed explanation on the role of generator protective relays in some of the major outages is provided in Appendix B.

Considering the importance of modeling generator protective relays in transient stability studies, the crucial need for developing a framework for proper representation of generator protective relays in transient stability studies has long been identified by the industry. The proper modeling of generator protective relays in transient stability studies enables precise evaluation of the responses of these protective relays during different contingencies and their impact on the generator behavior and dynamic response of the system. This valuable information can be used in planning studies to have a better understanding of system dynamic response during different contingencies and devising proper preventive and remedial actions to avoid cascading outages and blackouts. It can also be used by protection engineers to study probable generator protective relay misoperations during different contingencies and implement proper changes in the design or settings of protection functions to avoid such misoperations.

Many research papers in the literature have tried to model different protective relays of generators in stability studies and evaluate the response of these protective relays during different types of contingencies. In this regard, the authors in [91] provided a detailed explanation of the capability curve of a generator and what factors limit the capability of a synchronous generator to provide active and reactive power. Then, the paper discusses the generator protective relays that are intended to prevent operating condition of a generator

from violating its capability curve. Finally, the paper includes simulation results of the real-world generation systems models to evaluate the generator and its loss-of-field (LOF) and LOS protection system behavior during different disturbances. References [92] and [93] provide explanations of LOF protection in generators and how this protection function is modeled. Then, these references evaluate the performance of the modeled LOF protective relay during various types of LOF events using real-time digital simulator (RTDS). An assessment of the different LOF detection techniques is also provided in [93]. The authors in [94] provided an explanation of reverse power condition (motoring) and how reverse power protection relays operate and how they are modeled. This reference also investigates the response of the reverse power protection relay and its impacts on the dynamic response of the generator during different case studies performed using MATLAB/Simulink. The function of different generator protective relays including phase backup protection, ground backup protection, LOF protection, over-excitation protection, abnormal frequency/voltage protection, and OOS protection and how various abnormal operating condition of a generator can affect the responses of these protective relays are elaborated upon in [95]. This reference also provides guidelines on the application and setting of the mentioned generator protective relays. The authors in [96] provided an overview of stability studies and evaluated the behavior of the impedance-based generator protective relays including LOF, LOS, and phase distance protection during various stability studies.

A comprehensive framework for modeling all the critical generator protective relays in stability studies should provide guidelines for proper modeling of all the critical generator protective relays in stability studies. This guideline should address the following questions:

1. How each of the generator protective relays (e.g., LOF protection, OEL and UEL protection functions, volt-per-hertz protection, OOS protection, to name but a few) can be properly modeled in stability studies?
2. What models in stability analysis software tool, such as PSLF, should be used to closely represent the dynamic behavior of the actual generator protective relays installed on the generators?
3. How the actual settings of the relays in the system can be mapped to different parameters of the models included in the dynamic file of the system for stability studies? In other words, how different parameters of the models included in stability studies should be tuned to closely represent the control block diagram of actual protective relays and their settings?

No previous work has developed such a comprehensive framework for modeling generator protective relays in stability studies. Furthermore, the previous works mostly considers a single generator to infinite bus system and solely study the response of the different generator protective relays to disturbances and their impact on generator dynamic response. However, the interaction of these protective relays with system dynamics and the impact of their operation on dynamic response of the system have not been analyzed in any prior work.

To fill this gap, a comprehensive framework for modeling generator protective relays is proposed in this chapter that addresses all the mentioned questions. The framework is utilized to model the protective relays of the generators in a specific area of the WECC system representing the 2028 planning case with their specific settings in the dynamic file

of the system that is used for transient stability studies. The generator protective relays modeled include under/over frequency protection relays, under/over voltage protection relays, volt-per-hertz protection relays, phase distance relays, OOS relays, LOF relays, stator overcurrent relays, reverse power protection relays. Furthermore, over-excitation limiter, and under-excitation limiter functions of the generators are modeled. Various types of contingencies in different regions of the system, including over 400 contingencies, are studied on the WECC system. The responses of the generator protective relays during these contingencies, as well as their impact on the dynamic response of the generator and the system are monitored. Note that in this work, we only considered generator protective relays that can be modeled in three-phase transient stability analysis software, such as PSLF. Therefore, generator protective relays such as ground protection relays, negative sequence relays, and differential protection relays are not considered in this work.

An explanation of the capability curve of generators, which limit the capability of the generator for operating in overexcitation and underexcitation condition is provided in the following section of this chapter. Various generator protective relays considered in this chapter along with the guidelines and the steps of the proposed framework for modeling them in transient stability studies are also provided. The results of the transient stability studies conducted on the WECC system as well as the evaluations of the responses of the generator protective relays and their impact on the dynamic response of the generator and the system are provided in the following sections of this chapter.

6.1 Generator capability curve

The ratings of synchronous generators are provided by the manufacturer in terms of the maximum MVA that the generator can deliver continuously at a specific voltage and power factor without overheating. There are many factors—such as stator (armature) current limit, rotor current limit (field current limit), stator end region heating limit, coolant pressure, and steady-state stability limit (SSSL)—that limit the capability of a generator to deliver active and reactive power. Generator capability curve, shown in Figure 6.1, is a curve in the P-Q plane that represents the machine thermal limits at the nominal voltage. This curve is provided by the manufacturer. In this section, different factors affecting the capability of a synchronous generator to deliver active and reactive power are explained in detail [91].

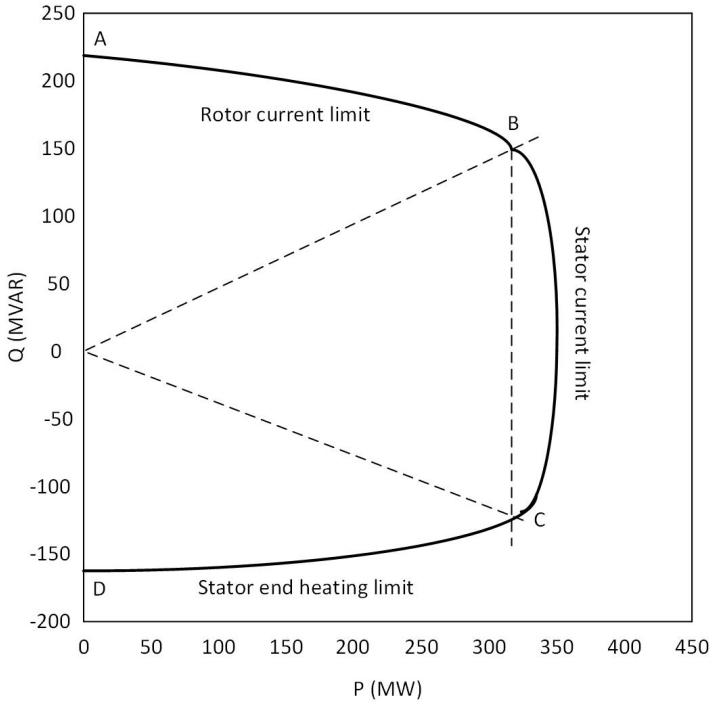

Figure 6.1 Generator capability curve

6.1.1 Stator current limit

With an increase stator current, which is accompanied by an increase in stator copper power losses, the temperature in the stator windings increases. Prolonged overheating condition can damage the stator winding. In this regard, there is a maximum current that a generator can deliver continuously without violating the thermal limit of the stator winding. This current limit, when mapped to the P-Q plane, shows a circle with center at the origin and a radius equal to the MVA rating of the generator (at rated voltage). This limit is shown by curve *BC* in Figure 6.1 [91].

6.1.2 Rotor current limit

Similar to the limit in stator current imposed by stator power losses, the rotor current (or field current) is limited due to rotor copper power losses. This current limit, when mapped to the P-Q plane, can be illustrated by a circle centered on the Q-axis and below the origin. This limit is shown by curve *AB* in Figure 6.1. Point B is the intersection of the stator and rotor current limits and represent the rated MVA and power factor of the generator [91].

Consider a simple power system diagram of Figure 6.2. In this diagram, the internal voltage and synchronous reactance of a generator are E_q and X_d, respectively (assuming constant filed current, neglecting the stator resistance, and assuming $X_d = X_q$). Also, the power system voltage and reactance (taking into account the reactance of the generator step-up transformer) are E_s and X_s, respectively. The center and the radius of the curve that represent the rotor current limit of the generator can be calculated using (6.1)-(6.2) [91].

$$Center(P, Q) = (0, -\frac{V_t^2}{X_d}) \quad (6.1)$$

$$Radius = \frac{E_q.V_t}{X_d} \quad (6.2)$$

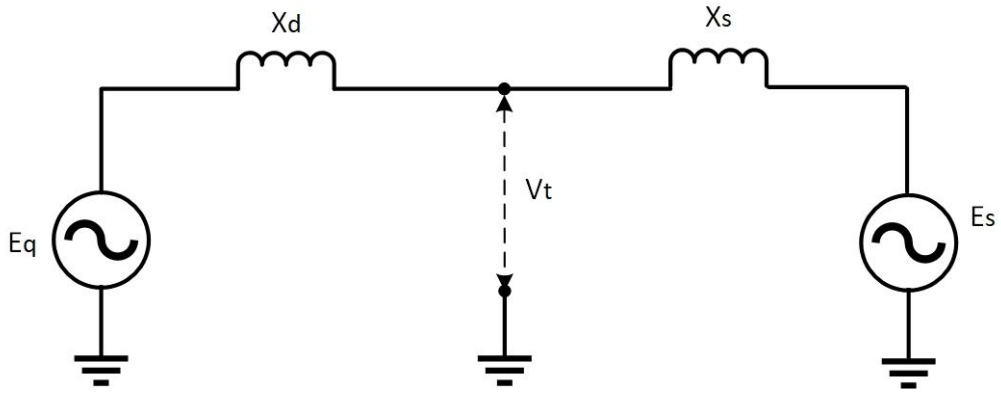

Figure 6.2 Simple power system diagram

6.1.3 Stator end region heating limit

The rotor magnetic flux passing through the stator is illustrated in Figure 6.3. As it is seen in this figure, the main rotor magnetic flux is a radial flux that is parallel to the stator laminations. The stator end ring flux, however, is an axial flux that is perpendicular to the stator lamination. This leakage flux creates eddy currents in the laminations leading to localized heating in the stator end region. This heating in the stator end region imposes another limit on the capability of generator to deliver active and reactive power in the underexcited region [91].

When a generator operates in the overexcitation region, the main magnetic flux is high. The high magnetic flux saturates the retaining ring, shown in Figure 6.3. When the retaining ring saturates, its reluctance increases, which means that there is a higher

magnetic resistance in the path of the leakage flux at the stator end region. Therefore, the leakage flux is low in this condition, and the overheating condition does not happen. On the other hand, when a generator operates in the underexcited region, the filed current and magnetic field is low, and the retaining ring is not saturated. Therefore, the reluctance of the retaining ring is low and the leakage current is high. Moreover, in the underexcited operating region, the magnetic flux produced by the stator adds to the magnetic flux produced by the rotor (field winding). Therefore, the end turn flux enhances the axial flux in the end region, which is responsible for creating overheating condition. Therefore, stator end region overheating is only the matter of concern when the generator operates in the underexcited region [91].

The stator end heating limit is depicted by curve *CD* in Figure 6.1. According to [97], the center and the radius of this circle is calculated using (6.3)-(6.6).

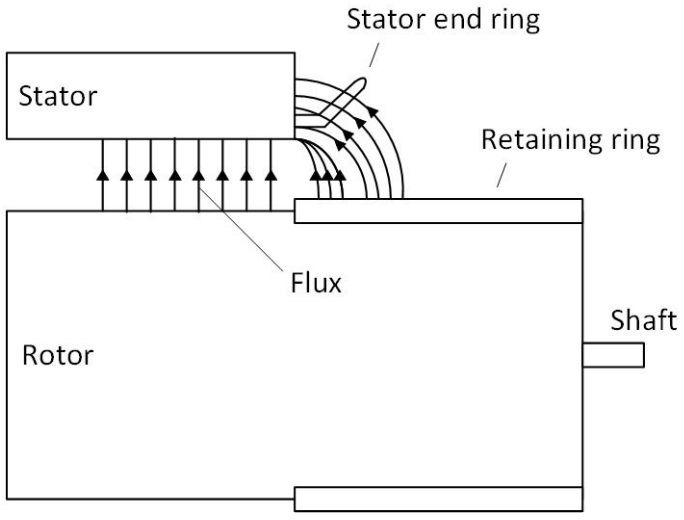

Figure 6.3 The main and leakage magnetic flux of a synchronous generator

$$Center(P,Q) = (0, K_1 \frac{V_t^2}{X_d}) \tag{6.3}$$

$$Radius = K_2 . \frac{V_t}{X_d} \tag{6.4}$$

$$K_1 = -\frac{N_a N_f - N_f^2}{N_a^2 + N_f^2 - 2N_a N_f} \tag{6.5}$$

$$K_2 = \sqrt{\frac{\Delta\theta}{K_t(N_a^2 + N_f^2 - 2N_a N_f)}} \tag{6.6}$$

Where, N_a and N_f are the number of turns of the stator (armature) and field windings, respectively. $\Delta\theta$ is the maximum tolerable temperature rise over the no-load temperature in the stator end region. Finally, K_t is a coefficient that relates the thermal energy to the square of the end region magnetic flux.

6.1.4 Steady-state stability limit

Another limit on the amount of active and reactive power that can be delivered by a generator is imposed by SSSL. Under normal operating conditions, there is a balance between the generated and consumed power and all the synchronous generators connected to the system operate at the same average speed. However, small changes in load and system configuration frequently occurs in power systems. The ability of the system to operate in the normal operating condition under these small changes in the system is referred to as steady-state stability [91].

If the simple power system diagram of Figure 6.2 is considered, the active power transfer capability is calculated using (6.7). In this equation, δ is the phase angle difference between E_q and E_s. Considering (6.7), the power-angle curve for different values of the internal generator voltage E_q ($E_{q0} > E_{q1} > E_{q2}$) is provided in Figure 6.4. At normal

operation condition, the generator operates at a point where $P_m = P_e$. The power-angle curve shows that for small load increases (increase in P_e), P_m increases to keep up with P_e till δ reaches 90°. Beyond 90°, the increase in P_e is accompanied by a decrease in P_m and the system loses synchronism.

$$P_e = \frac{E_q E_s}{X_d + X_s} sin\delta \tag{6.7}$$

Another condition for losing synchronism, can occur in the condition that for a fixed P_m, the operator decides to reduce the excitation of generator internal voltage E_q to absorb reactive power (for instance, the condition where there is an excess of reactive power in the system, and it is not completely compensated by switching off the shunt capacitors). As seen in Figure 6.4, by reducing E_q, the power angle δ increases, till it reaches 90°, where system reaches its SSSL. Any further decrease in E_q results in unstable operation condition. Note that, this analysis is valid for manual voltage regulator option. However, under automatic operation (AVR), the regulator promptly changes the field current to achieve a proper internal voltage for the operating condition, which changes the power angle to improve the SSSL [91].

For an ideal lossless system of Figure 6.2, the SSSL limit represents a curve on the P-Q plane whose center and radius is calculated using (6.8)-(6.9) [90]. Note that, when the power system is strong, X_s is low, and the SSSL locus is outside the generator capability curve. However, if the system is weak, X_s is high, and in this case, the SSSL locus might fall inside the generator capability curve and become more restrictive than the generator capability curve [91].

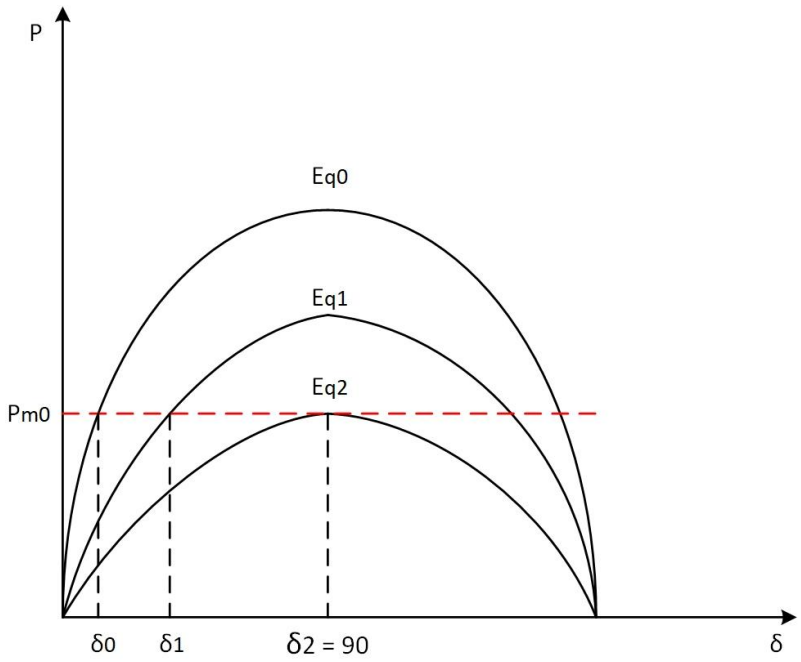

Figure 6.4 Power-angle curve for different generator internal voltages

$$Center\ (P,Q) = (0, \frac{V_t^2}{2}\left(\frac{1}{X_d} - \frac{1}{X_s}\right)) \tag{6.8}$$

$$Radius = \frac{V_t^2}{2}\left(\frac{1}{X_d} + \frac{1}{X_s}\right) \tag{6.9}$$

6.1.5 Effect of voltage and coolant pressure

Considering (6.1)-(6.9), it is clear that a generator capability curve is a function of its terminal voltage. The capability curve of a generator is typically provided at nominal voltage by the manufacturer. However, using (6.1)-(6.9), the generator capability curve can be easily plotted for other terminal voltages.

The effectiveness of a generator cooling system also plays a significant role in capability of the generator to deliver power. For instance, in a hydrogen-cooled generator, the capability curve is a function of hydrogen pressure [91]. In this regard, to show the

impact of the cooling system on the capability curve of a generator, the capability curve of an industrial 160 MW hydrogen-cooled steam turbine-driven generator is provided in Figure 6.5. Note that, in this figure, the dotted straight lines are the loci of constant power factor. Figure 6.5 shows that generator capability curves are in fact a group of curves with the coolant pressure as the parameter.

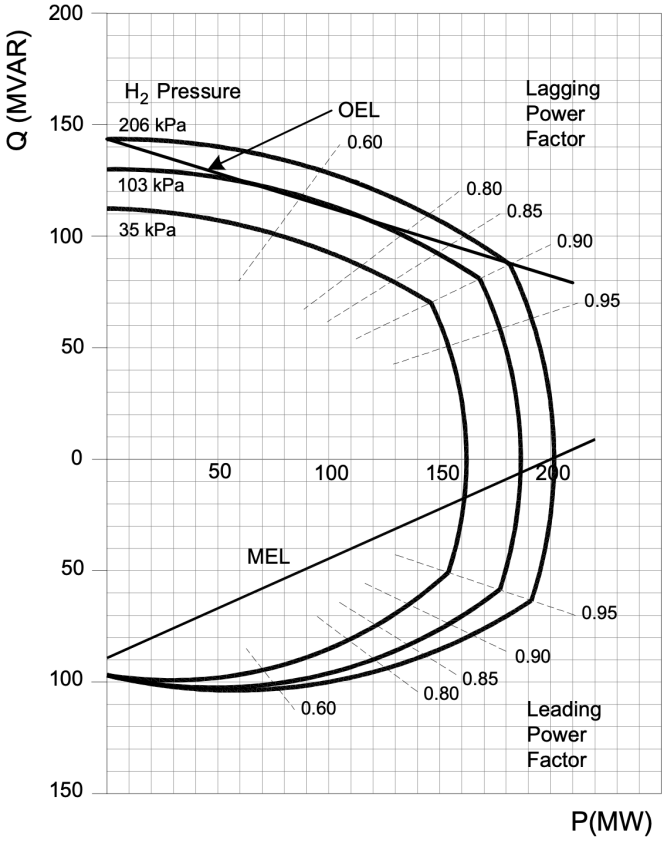

Figure 6.5 Capability curves of a 160 MW hydrogen-cooled steam-turbine generator [91]

6.2 Modeling generator overexcitation and underexcitation limiter

An introduction of generator OEL and UEL control functions along with their applications, as well as the PSLF model used to represent these relays in the dynamic file of the system used for performing transient stability studies are provided in this section. Also, the procedure for precisely representing the protection function of the actual OEL

and UEL functions implemented in industrial generators in transient stability studies is thoroughly explained.

6.2.1 Overexcitation and underexcitation limiter for generators

A generator excitation system energizes the magnetic field that keeps the generator in synchronism with the power system. Furthermore, the excitation system controls the amount of the reactive power that the generator can produce or absorb. Besides the manual control of excitation system, there are variety of automatic control functions that can be applied to excitation systems including automatic voltage regulation (AVR), constant power factor regulation, and constant reactive power regulation. All the automatic control modes are equipped with supplementary controls which ensure that the generator is always operating within its capability curve. These supplementary controls may even enhance the stability of a generator connected to a power system [95].

One of the most used generator excitation control modes, especially for large grid-connected generators, is the AVR mode. During small disturbances power or voltage oscillations are formed in the system, which are quickly damped. Turbine governor control or in some cases system load control maintain the frequency within acceptable limits. For major disturbances, however, the generator terminal voltage deviation is large enough to make the excitation system control to push the excitation system to work on full on (ceiling) or full off mode. In this condition, the supplementary control systems of the generator play a significant role in defining the behavior of the generator. For instance, during major disturbances caused by short circuits, the terminal voltages of generators dip. To compensate for this voltage dip, the excitation system controller increases the output

voltage to ceiling which leads to an increase in the generator field current. The supplementary control may operate to limit the field current to avoid overheating in the field winding. The supplementary control used in this case is usually OEL [95].

The OEL prevents the AVR from producing prolonged excessive field current that harms the generator due to overheating. The generator field winding is designed to continuously operate with the field current corresponding to the nominal load of the generator. Generator field winding can also withstand overload conditions for a limited amount of time (depending on the amount of overload). According to ANSI standard C50.13-1977, the permissible thermal overload of a round rotor generator can be represented by Figure 6.6. In this figure, curve A shows the field thermal capability and curve B shows the OEL curve [98].

Typically, the OEL function monitors the field winding current and if this current exceeds a preset pickup current for a specific time delay, the OEL acts through the AC regulator to ramp down the excitation to a preset value (which is typically considered 100% to 110% of the rated field current). If this regulating action fails to reduce the field current to an acceptable range, the OEL trips the AC regulator, transfers control to the DC regulator, and change the setpoint to a value corresponding to the rated value. If this action of OEL also fails to reduce the field current to an acceptable range, the limiter sends tripping signal to the exciter field breaker to trip the excitation system, and it also sends a tripping signal to the generator circuit breaker to trip the generator [98].

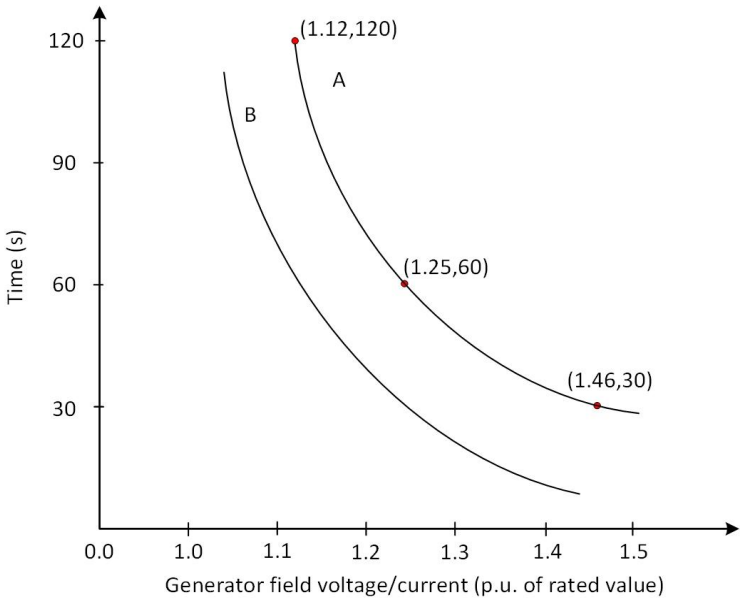

Figure 6.6 Coordination of OEL with field thermal capability

Two types of time delays are used for OEL [98]:

(a) Fixed-time time delay: OEL operates when the field current exceeds the pickup value for a fixed set time. In this case, the time delay is not proportional to the magnitude of the field current.

(b) Inverse-time time delay: OEL operates if the field current exceeds the pickup value for an amount of time that is proportional to the magnitude of the field current, and it matches the generator field thermal capability.

Note that, the generators with a very high exciter ceiling voltage may also be equipped with an instantaneous OEL, which acts instantaneously (without any time delay) through the AC regulator if the field current exceeds the pickup value and limit the field current to the field winding short time limit (which is typically considered 160% of the rated field current) [98].

OELs are also categorized in terms of their implementation into two categories [99]:

a) Summed type OEL: In this type, the OEL output signal is added to other signals at the summing junction of the AVR of the generator.

b) Takeover type OEL: In this type, which is also referred to as "hard" or "auctioneering" type, the OEL output signal bypasses the AVR of the generator and is directly fed into a low-value gate. The low-value gate gives the excitation control to the lower of the voltage regulator and OEL signal. When the OEL operates and sends its output signal to the low-value gate, the gate gives full control of the excitation system to the OEL until the limiter signal is below the pickup value [95].

Both types of these implementations are illustrated in Figure 6.7. This figure shows the block diagram of the "esdc4b" excitation system model in the PSLF model library [46] which represents IEEE (1992/2005) DC4B excitation system model.

As described in Section 6.1.4, during major disturbances in the system, it is also possible that there exists a surplus of produced reactive power in the system, which leads to prolonged overvoltage condition. In this case, if control actions such as switching reactive power sources, such as capacitor banks, fail to re-establish the balance between the produced and consumed reactive power, the excitation system controllers of the generators may reduce the excitation level and operate the generators in an underexcited condition to absorb the surplus power. However, as mentioned, there are limitations, including stator end region heating limit and steady-state stability limit, that restrict the capability of a generator to operate in an underexcited condition. In this condition, the supplementary control of UEL—also called minimum excitation limiter (MEL)—ensures

that the excitation system control does not reduce the field current to a level where the steady-state stability limit or stator end region heating limit are violated, or loss-of-field protection trips the generator [95].

The UEL of a generator takes a combination of the voltage and current or active and reactive power of the generator as its control signal. The UEL compare this control signal with a reference value and if it exceeds the value, the UEL imposes its limiting actions [95].

Similar to OELs, UELs are also categorized in terms of their implementation into two categories [99]:

a) Summed type UEL: In this type, the UEL output signal is added to other signals at the summing junction of the AVR of the generator (impact on the voltage error signal of the AVR)

b) Takeover type UEL: In this type, the UEL output signal bypasses the AVR of the generator and is directly fed into a high-value gate. The high-value gate gives the excitation control to the larger of the voltage regulator and UEL signal. When the UEL pickup value is reached, the high-value gate gives full control of the excitation system to the UEL until the limiter signal is below the pickup value [95].

Both types of these implementations are illustrated in Figure 6.7.

UEL Settings should be based on the needed protection including SSSL and stator end region heating limit (whichever is more restrictive). Furthermore, the limiter should be coordinated with the loss-of-field relay of the generator, so that the UEL operates before

the pickup value of LOF relay is reached. Figure 6.8 illustrates the UEL characteristic and its coordination with the calculated SSSL and LOF relay characteristics on the P-Q plane.

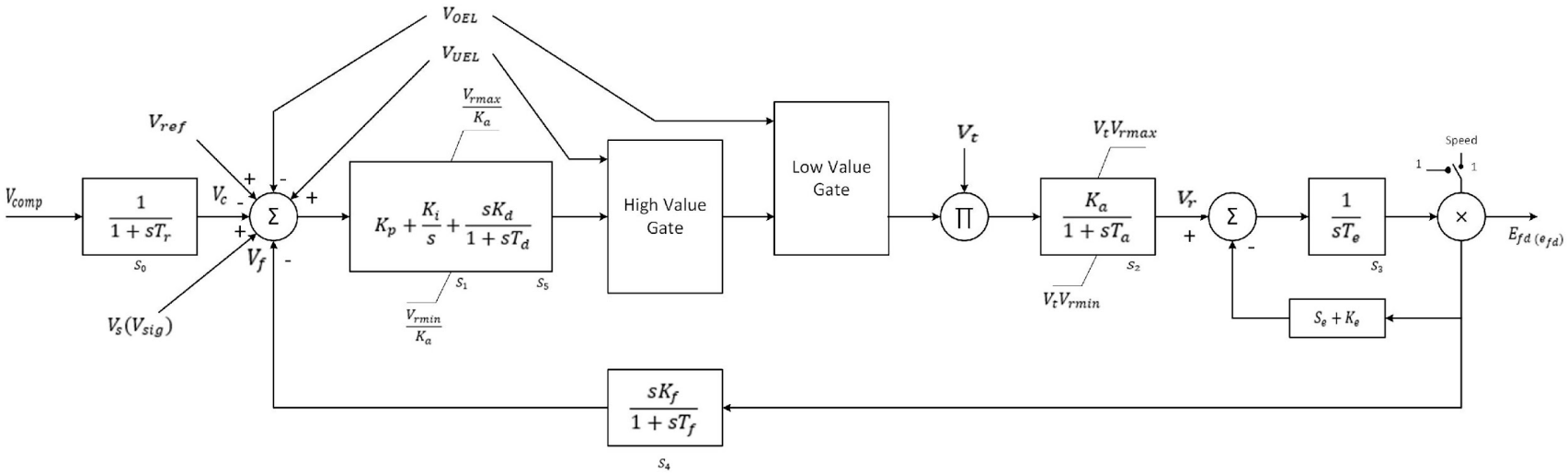

Figure 6.7 The block diagram of the *esdc4b* excitation system model [46]

Similarly, if the stator end region heating limit is more restrictive than the SSSL, the UEL can be used to protect against stator end region heating. In this case, the SSSL curve in Figure 6.8 is replaced by the stator end region heating limit curve [98].

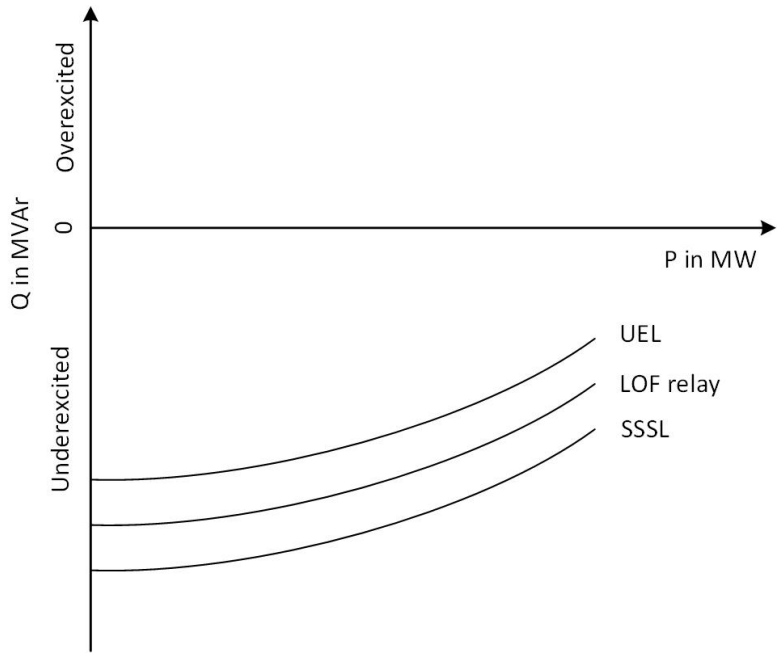

Figure 6.8 Coordination between UEL, LOF relay, and SSSL

6.2.2 The framework for modeling overexcitation limiters of generators

According to the industrial generator protective relay data, all the generators in the area under study are equipped with overexcitation limiters. 4 different type of relay settings are provided for these generators:

1. Some generators are equipped with the OELs that include two definite-time pickup levels, namely, high current level and medium current level. They also include a low current level for which the generator can operate continuously.

2. Some other generators are equipped with the OELs that only include one stage of hard limit operation. When the field current exceeds the pickup settings of these OELs, the OEL instantaneously imposes a hard limit on generator field current.
3. Some of the units are equipped with the OELs that only include an inverse-time OEL characteristic (similar to Figure 6.6.)
4. Some of the units are equipped with an inverse-time OEL characteristic along with a definite-time high field current limiter which acts when the field current exceeds approximately 140% of the field current full load (AFFL).

Two models of "oel1" and "gp3" in the PSLF model library [46] is used to model the OELs of the generators. The *oel1* is an OEL model for synchronous machine excitation systems. This model can provide instantaneous hard overexcitation limit and definite-time/inverse-time overexcitation characteristic. Therefore, it is a proper model to be used as the primary OEL function of the generators. The *gp3* is a generic generator protection system in PSLF library that can provide different protection functions (including one level of definite-time overexcitation protection) for generators. Therefore, it is used as the secondary (backup) OEL protection to provide some OEL characteristics that cannot be implemented by the *oel1* model, alone. More explanations on the *oel1* and *gp3* models can be found in Appendix C and D, respectively.

Note that to protect the proprietary data, random numbers are used to represent the assets of the system, such as buses and generators. Also, the actual settings of the protective relays of the generators are not provided for the same reason.

The procedure for properly modeling the OEL of the generators with any of the mentioned four types of settings using the *oel1* and *gp3* models are as follows.

1. Modeling the OEL of the generators with settings of type 1:

The OEL function of the generators with OEL settings of type 1 (two definite-time operation stages) are modeled with one *oel1* model and one *gp3* model. The *oel1* model can only provide one level of definite-time operation for its related generator, and only one *oel1* model can be included for a single generator in the dynamic file of the system used for performing transient stability studies. Therefore, both the definite-time stages of these OELs cannot be modeled with the *oel1* model.

The medium current levels of these OELs (which have lower pickup current values and are more likely to operate) are modeled with the *oel1* models. In this regard, the time-dependent element of the *oel1* model is used. The values of *Ifdset* and *Tpickup* parameters of the *oel1* are set as the medium current level of the OEL and its time delay, respectively. The *Ifcont* (which represent the maximum generator field current) parameter of the *oel1* model is set to be equal to the low current level of these OELs. Note that, the *Tpickup* parameter should be provided in negative value, since, according to PSLF user manual [46], negative value of *Tpickup* indicates the definite-time characteristic of the OEL.

To model the high current levels of the OELs (which have higher pickup current values and are less likely to operate) the *gp3* model is used in the alarm only mode. The overexcitation element of the *gp3* model does not provide an OEL function; rather, it provides overexcitation tripping function. Therefore, to avoid undue tripping of the generators, these models are only used in the monitor only mode. In any study, if

overexcitation trip alarm is observed for any generator, the high current level of that generator is modeled with the *oel1* model, and the simulation is performed, again (with disabling the *oel1* model related to the medium current level).

2. Modeling the OEL of the generators with settings of type 2:

The OEL functions of the generators with OEL settings of type 2 (only one stage of hard limit operation) are modeled with an *oel1* model. The instantaneous acting hard limiter of the oel1 model is used to represent the instantaneous hard limits of the OEL functions of these generators. The values of *Ifdmax* parameters of the *oel1* is set as the pickup value for the instantaneous hard limit of the OEL.

3. Modeling the OEL of the generators with settings of type 3:

The OEL functions of the generators with OEL settings of type 3 (an inverse-time characteristic) are modeled with the *oel1* model. The time-dependent element of the *oel1* model is used to represent the inverse-time characteristics of the OEL functions of these generators. The value of *Ifdset* parameters of the *oel1* model is set as the pickup current of the OEL. If the pickup current is not provided, it is assumed to be 110% of the AFFL of the related generator. In the case of representing an inverse-time characteristic, the time delay parameter of the oel1 model, i.e., *Tpickup*, should be positive and it should be equal to the time delay for the operation of the OEL for the field current that exceeds *Ifdset* by 1 p.u. Therefore, the related time delay for the field current of $Ifdset\ (p.u.) + 1$ should be obtained from the inverse-time OEL curve of the generator and used as *Tpickup*. The *Ifcont* parameter of the *oel1* (which represent the maximum generator field current) is set as the AFFL of each generator.

4. Modeling the OEL of the generators with settings of type 4:

The OEL functions of the generators with the OEL settings of type 4 (a definite-time and an inverse-time characteristic) are modeled with one *oel1* model and one *gp3* model. The reason is that the time-dependent element of the *oel1* model can provide either a definite-time or inverse-time characteristic (but not both). Therefore, one *oel1* model, alone, cannot completely represent the OEL functions of these generators. The *oel1* model is used to represent the inverse-time characteristics of the OEL function of these generators. The pickup field current for the inverse-time characteristic of these OELs is 110% of the AFFL. Therefore, the *Ifdset* parameter of the *oel1* is set to 110% of the AFFL. Similar to type 3, the *Tpickup* is set to the time delay for the field current that exceeds the AFFL by 1 p.u.

The definite-time characteristic of the OELs of these generators are modeled with the *gp3* model in alarm only mode. The pickup current for the definite-time characteristic of these OELs is 140% of the related AFFL. Therefore, the pickup field current of the *gp3* model is set to 140% of the AFFL. The related time delays for the definite-time characteristics of these OELs are used as the time delay of the overexcitation protection element of the *gp3* model. Note that, in any study, if overexcitation trip alarm is observed for any of these generators, the definite-time characteristic of that generator is modeled with the *oel1* model, and the simulation is performed, again (with disabling the *oel1* model related to the inverse-time characteristic).

Note that, according to the PSLF user manual [46], the pickup current and the maximum continuous field current settings of the *oel1* (*Ifdset*, *Ifdmax*, and *Ifdcont*) should

be provided in per unit based on the AFAG of the generator. The pickup and the maximum continuous field current in the setting data file are in Amps. Therefore, to properly convert these settings to per unit values, first, the AFAG of each generator should be obtained from its open circuit saturation curve. An example of a generator saturation curve and the related AFAG value is illustrated in Figure 6.9. After obtaining the AFAG of each generator, the pickup current (or the maximum continuous field current) can be converted to per unit using (6.10). Note that, if the pickup current is provided in the setting data file in per unit values but with a different per unit base than AFAG, it can be converted to per unit based on AFAG using (6.11).

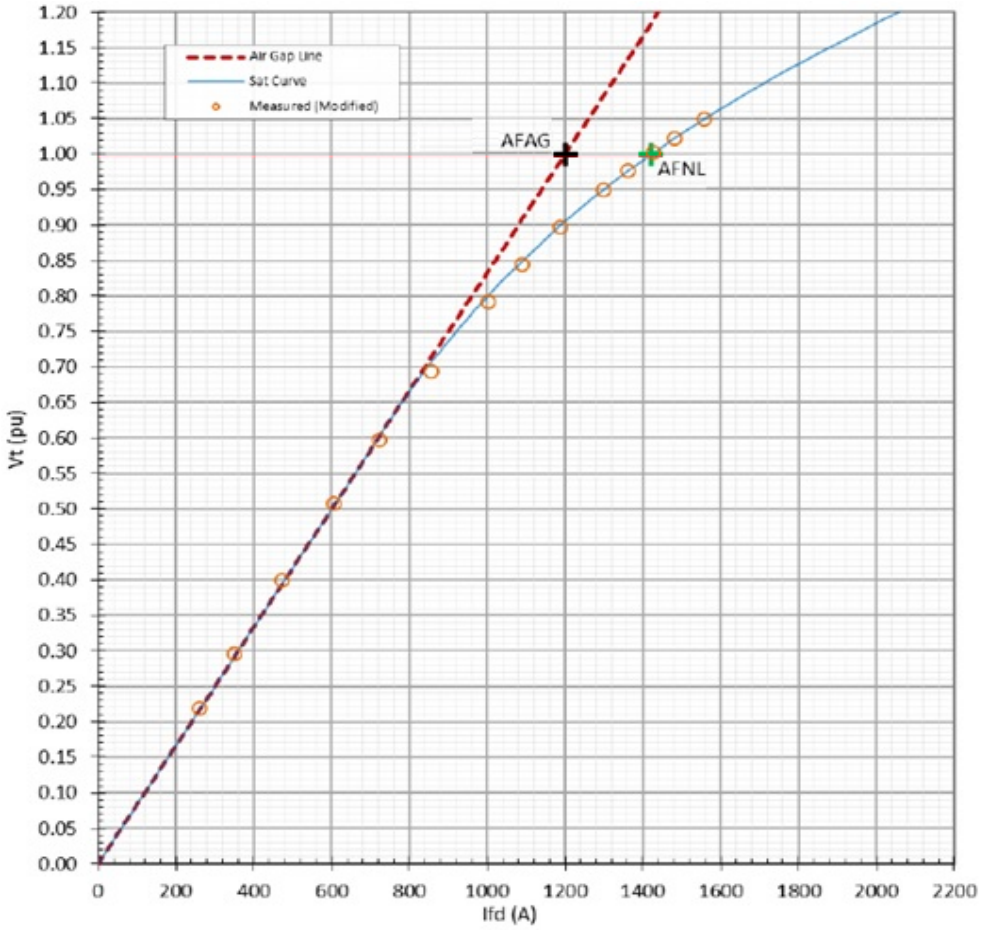

Figure 6.9 An open circuit saturation curve of a generator

$$If_{pickup}(p.u.) = \frac{If_{pickup}(amps)}{AFAG} \tag{6.10}$$

$$If_{pickup}(p.u.) = \frac{If_{pickup,old}(p.u.) \times If_{base,old}}{AFAG} \tag{6.11}$$

One of the parameters that has a big impact on the performance of the *oel1* model is the parameter used for adjusting voltage regulator reference, defined as *Runback* parameter. Different values of the *Runback* parameter define the various actions of the *oel1* model when the time-dependent element operates:

1. For positive values of *Runback*, the voltage regulator reference at the summing junction point shown in Figure 6.7 is biased by the output of the *oel1*. The output of *oel1* is not constant in this case; rather, it is ramped in the negative direction at the rate of $\frac{1}{Runback}$ per unit per second as long as field current/voltage remains above the *Ifcont* parameter. When the field current falls below *Ifcont*, the ramping of the output signal is stopped, and the value of the voltage regulator reference remains fixed at the biased value. This action of *oel1* is illustrated in Figure 6.10.

2. For negative values of *Runback*, the output signal of the *oel1* is a constant value and is equal to *Runback* per unit. The value of voltage regulator reference remains fixed at this biased value. This action of *oel1* is also shown in Figure 6.10.

3. For $Runback = 0$, the excitation system is forced to apply an immediate mandatory limit of *Ifcont* to the excitation system output voltage. This limit is permanent.

In this regard, if the setting data that shows how the output of the OEL function of each generator is added at the summing junction of AVR is provided, it can be used to tune the

Runback parameter. However, no such data was provided during this project. Therefore, we tried to tune the *Runback* parameter of the oel1 model of each generator to achieve a desirable performance. In this regard, positive values of *Runback* parameter are selected since for positive values the magnitude of the *oel1* output signal increase gradually and there is no sudden change in its magnitude, which gives smoother limiting actions (no sudden change in field current).

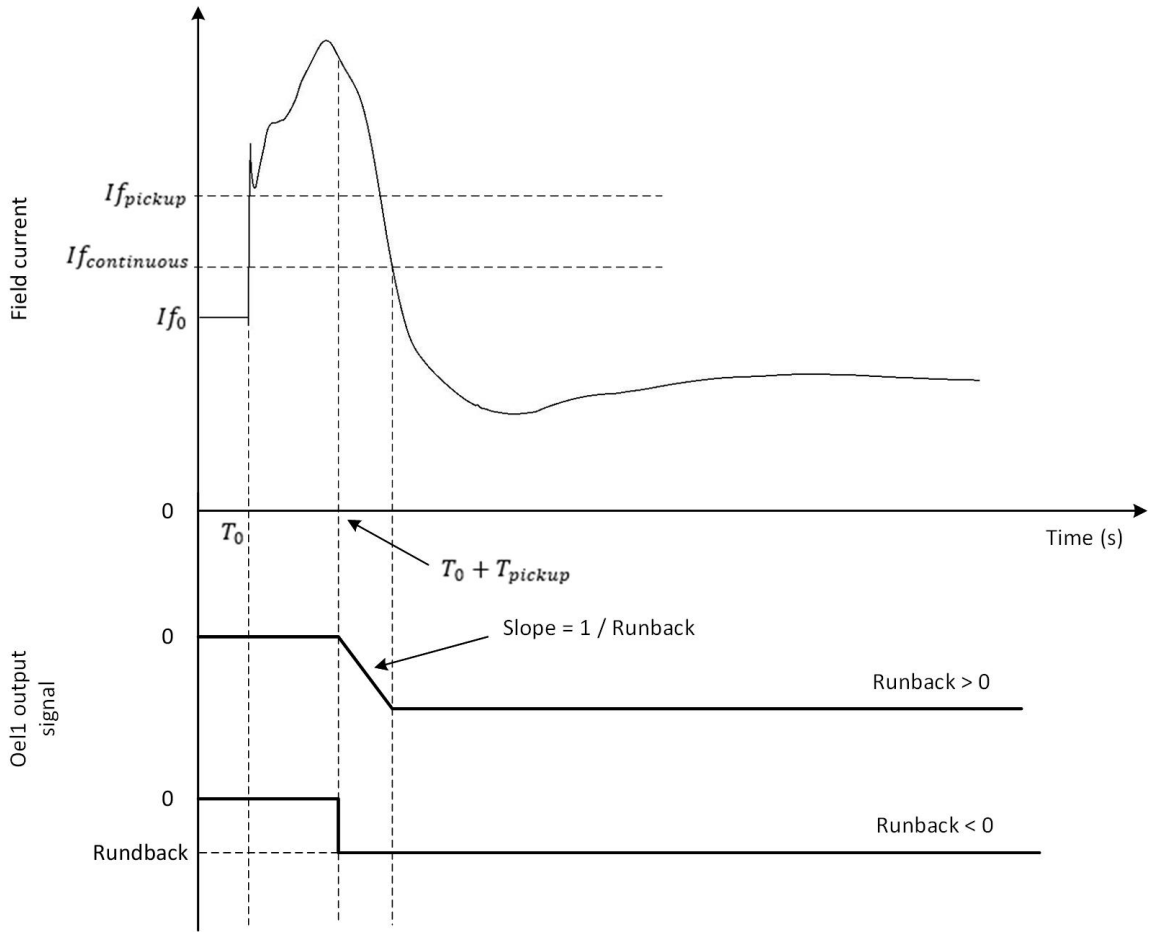

Figure 6.10 A sample field current and the *oel1* output signals for different values of *Runback*

To obtain a proper value for *Runback* (which defines the slope of the *oel1* output signal) a small test system is created. One of the generators of the small test system is replaced by each of the generators in the area under study (including any other associated models such as governor model, PSS model, and etc.). Then, an *oel1* model is included for the generator. Next, multiple transient stability studies of a fault that causes over-excitation condition in the generator (and the consequent oel1 operation of the generator) is performed by considering different *Runback* values of the *oel1*. The field current of the generator is monitored in these studies to find the *Runback* value that yields the best performance. Note that this procedure is performed for each generator, separately. The results shows that the *Runback* of 100 yields a good performance for all the generators. Therefore, this value is used for the *Runback* settings of all the *oel1* models.

6.2.3 The framework for modeling underexcitation limiters of generators

The UEL curve of the generators in the area under study are provided in the setting data file as piecewise linear curves in the P-Q plane. The lines in the curve connect a number of sampled points in the P-Q plane. Figure 6.11 shows a sample of these UEL curves. Note that the numbers on the P and Q axes are removed to keep the proprietary data.

For modeling the UEL function of the generators, the *uel2c* model is used in this project. The *uel2c* can provide a piece-wise linear UEL curve in the P-Q plane using up to 10 sample (p, q) points that are provided to this model as inputs. The UEL characteristic of the *uel2c* model is also illustrated in Figure 6.12. As seen in Figure 6.12, the UEL characteristic of the *uel2c* is similar to that of the industrial generators. Therefore, this

model can be used to represent the UEL functions of these generators. More details about the uel2c model can be found in Appendix E.

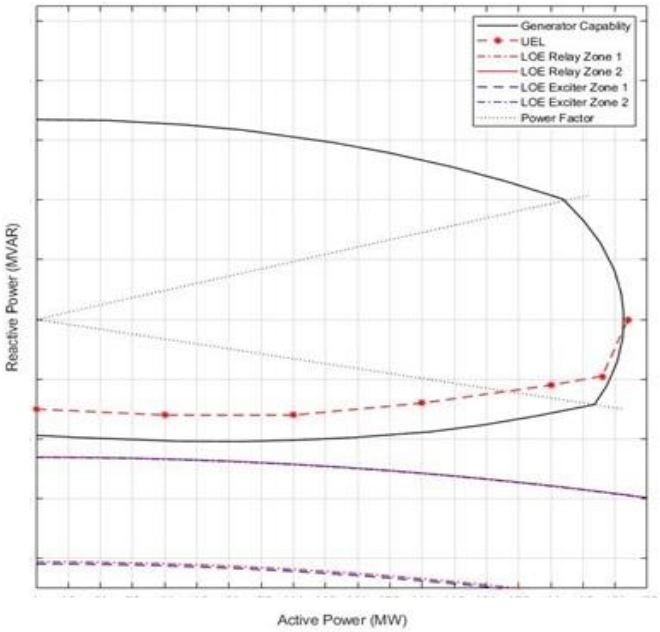

Figure 6.11 A sample of UEL characteristic of a generator

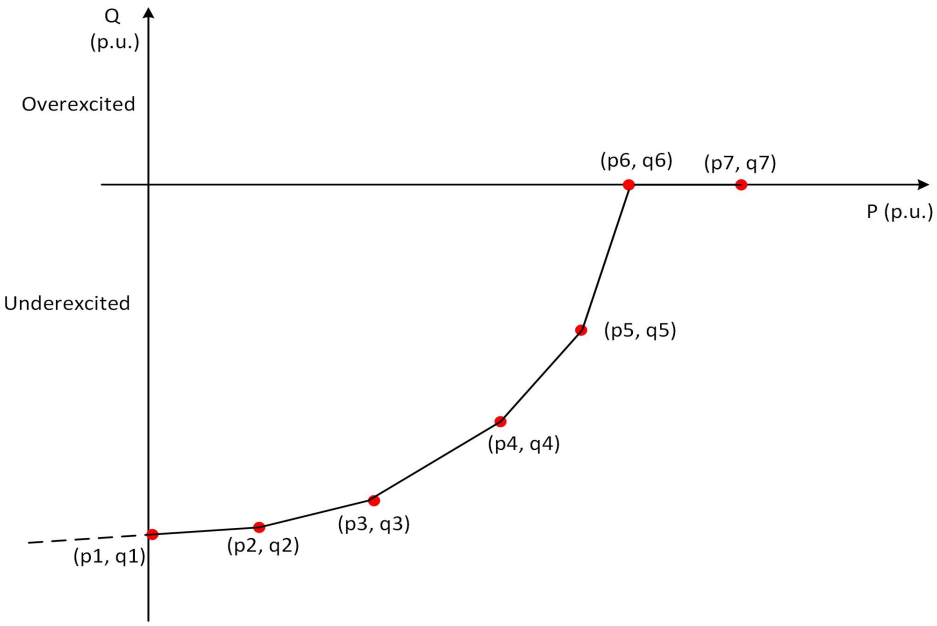

Figure 6.12 The UEL characteristic of the *uel2c* model

As seen in Figure 6.12, between two adjacent (p, q) points, the UEL characteristic of the *uel2c* is a straight line connecting the two points. Beyond each endpoint, the UEL characteristic is a straight line that is the continuation of the last segment of the line. To prevent *uel2c* from extending the last line segment of the UEL characteristic to overreach the first quadrant (positive reactive power) of the P-Q plane, the following procedure is taken to shape the last line segment of the UEL characteristics to fall on the P axis (Q = 0):

Assume that *n* samples of (p, q) points are provided in the setting data file, these *n* samples are fed into the *uel2c* to comprise the UEL characteristic of the *uel2c*. If the last sample, i.e., (p_n, q_n), has a zero reactive power ($q_n = 0$), the next (p, q) point of *uel2c*, i.e., (p_{n+1}, q_{n+1}), should be used to make the last line segment to fall on the P axis. Any point that satisfies $p_{n+1} > p_n$ and $q_{n+1} = 0$ conditions can be used for this purpose. However, if the last sample, i.e., (p_n, q_n), has a non-zero reactive power ($q_n < 0$), the next (p, q) point of the *uel2c*, i.e., (p_{n+1}, q_{n+1}), should be used to find the intersection of the last line segment, i.e., the line between points (p_{n-1}, q_{n-1}) and (p_n, q_n), with the P. The next (p, q) point, i.e., (p_{n+2}, q_{n+2}), should also be used to make the last line segment fall on the P axis. Any point that satisfies $p_{n+2} > p_{n+1}$ and $q_{n+2} = 0$ conditions can be used for this purpose.

If the number of sample points provided in the setting data file is more than the number of available (p, q) points of the *uel2c* model, some of the sample points in the data file should be removed. When removing extra sample points, the object is to select the points in a way that deleting these points results in the minimum change in the shape of the UEL characteristic. The approach for finding the most proper points to remove is as follows:

As seen in Figure 6.13, it is assumed that the point (p, q) between the two points of (p_1, q_1) and (p_2, q_2) is selected for removing. If this point is removed, and only (p_1, q_1) and (p_2, q_2) are fed into the *uel2c* as inputs, the resulting UEL characteristic will be a straight line between (p_1, q_1) and (p_2, q_2). This straight line passes from the point (p, q^*) (which has the same p as the removed point but a different q). where, q^* is calculated using (6.12). Thus, the error of removing (p, q) and approximating it with (p, q^*) (this approximation is done internally in the *uel2c* mode) can be calculated using (6.13).

$$q^* = q_1 + (\frac{q_2 - q_1}{p_2 - p_1})(p - p_1) \tag{6.12}$$

$$Error = |q^* - q| \tag{6.13}$$

Therefore, if *m* points need to be removed, the error of removing any sample point is calculated using (6.12) and (6.13), and the *m* point with the least error are selected for removing.

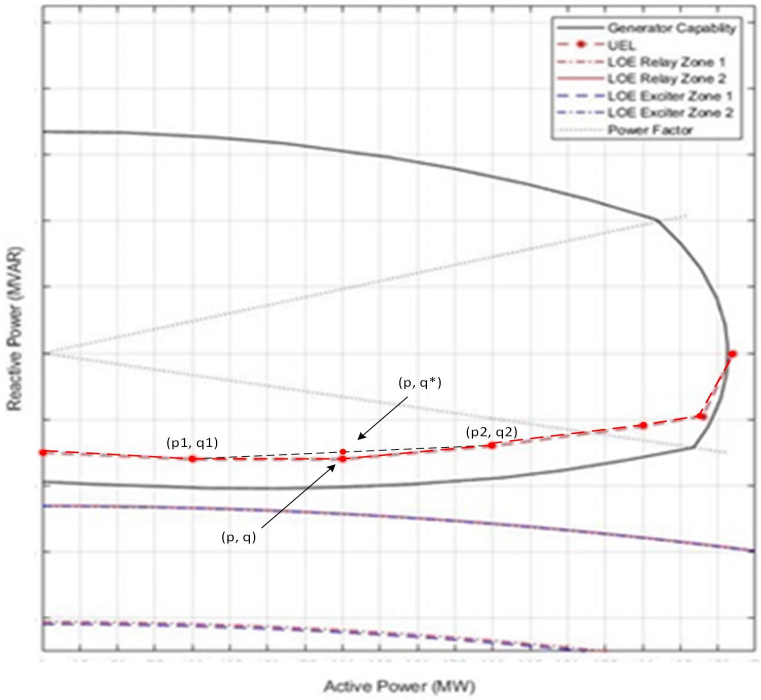

Figure 6.13 Selecting proper (p, q) samples to remove from the UEL curve

Note that, the sample points in the data file are provided in MW and MVAr. However, the *uel2c* model takes its input (p, q) points in per unit based on the machine nominal MVA. Therefore, the (p, q) samples should be converted to per unit based on the machine nominal MVA using (6.14) and (6.15). Note that, if these sample points are provided in per unit based on the system MVA, they can be converted to per unit based on the machine MVA using (6.16) and (6.17).

$$p(p.u.) = \frac{p(MW)}{S_{rated}} \tag{6.14}$$

$$q(p.u.) = \frac{q(MVAr)}{S_{rated}} \tag{6.15}$$

$$p(p.u.) = \frac{p_{old}(p.u.) \times S_{system}}{S_{rated}} \tag{6.16}$$

$$q(p.u.) = \frac{q_{old}(p.u.) \times S_{system}}{S_{rated}} \tag{6.17}$$

Where S_{rated} and S_{system} are the rated 3-phase MVA of the machine and the system, respectively; $p_{old}(p.u.)$ and $q_{old}(p.u.)$ are the p and q in the sample point (p, q) that are provided in per unit based on the system MVA.

The block diagram of the uel2c model is provided in Figure E. 2. As seen in this figure, many parameters (including different gains, coefficients, and time constants) can affect the performance of the uel2c model. Using the default value for these parameters yield a simplified block diagram of Figure 6.14. This block diagram can properly represent the UEL functions of the generators. Therefore, the default values for the parameters are used for modeling the uel2c.

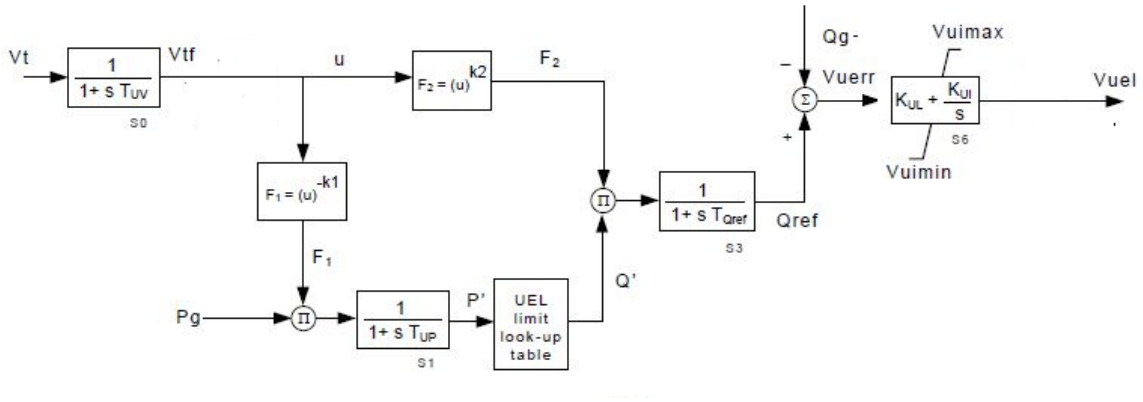

Figure 6.14 The simplified uel2c block diagram with using the default parameters [46]

6.3 Modeling generator loss-of-field protection

A brief introduction of LOF protection in generators along with its applications, as well as the PSLF dynamic models used to represent LOF relays in transient stability studies are provided in this section. Also, the procedure for precisely representing the actual LOF functions of the relays installed on the generators in transient stability studies is explained.

6.3.1 Loss-of-field protection for generators

LOF condition occurs when the DC source of the generator field winding is interrupted. The reasons for LOF condition include short circuit or open circuit conditions in the field circuit, accidental tripping of the field circuit breaker, voltage regulator system failure, as well as the loss of the main supply of the excitation system [93].

When the LOF condition occurs in generators, the rotor field gradually extinguishes. This leads to extinguishing of the magnetic coupling between rotor and stator magnetic field and consequently the machine loses its synchronism. In this condition the generator operates as an induction generator. To be able to produce the active power demanded by the system in the new condition, the generator (that is now operating as an induction

generator) should increase its rotor speed. Operating as an induction generator, the generator draws a significant amount of reactive power form the system, which causes high stator current (around two to four times of the rated current) and a decrease in the voltage. Also, slip-frequency eddy currents start to form in the rotor (which have a magnitude that is proportional to the generated rated power). These eddy currents cause overheating in the rotor. Furthermore, operating as an induction generator expose the generator to large pulsating torques and mechanical damages. The worst case (which causes more serious consequences) of LOF condition is when the generator loses excitation at full load (where slip may reach to range of 2% to 5%). Therefore, as described, operating in LOF condition can harm both the generator and the power system and proper protection should be in place to detect this condition and trip the generator to avoid such harms to generator and the power system [91] and [93].

There are no general guidelines indicating the maximum time that a generator can operate without field. It depends on the design of the generator and should be indicated by the manufacturer. As explained, power system also limits the permissible time a generator can operate without field. The high amount of reactive power drawn by the generator when operating without field may cause a voltage collapse in the system, especially if this occurs in a large generator connected to a weak system. Another possibility, as mentioned in Section 6.1.4, is the loss of steady-state stability of the system. When these problems occur, the system might lose voltage/steady-state stability in a few seconds. In this regard, voltage sag in the terminals of generators during LOF condition is a good indicator that the power system is not able to withstand the LOF condition [91].

The LOF protection of the generators should provide an early warning of LOF condition in generators to the operators before tripping the generator. This allows the operator to restore the field in the case of an accidental LOF condition due to tripping of the field circuit breaker. However, if no action is taken to restore the field or restoring the field is not possible, after the preset time delay passed, the LOF relay should trip the main generator breaker and the field breaker (to minimize the damage to the generator and probably the power system) and transfer unit auxiliaries [91].

The primary type of protection devices used against the LOF condition included undercurrent and undervoltage relays. These relays used field current and voltage, respectively, to detect LOF conditions. However, they were unable to detect all types of the LOF conditions. For instance, the undervoltage relays were unable to detect the LOF condition as a result of open circuit condition in the field. Furthermore, none of these relays were able to correctly distinguish LOF condition form system disturbances such as stable power swings or OOS conditions [93].

Nowadays, the mostly used scheme for LOF protection is impedance-based relays with negative offset R-X scheme, shown in Figure 6.15. The curves associated with SSSL, UEL, and generator capability curve (GCC) are also illustrated in this figure. Note that, in Figure 6.15, X_d and X'_d are the synchronous and transient reactance of the generator. An LOF condition is detected when the impedance trajectory enters any of the protection zones shown in Figure 6.15 and remains inside the zone for a preset period. Although this scheme is the most used scheme for LOF protection, it is vulnerable to misoperation due to stable

power swings and OOS conditions. In this regard, 13 misoperations of LOF relays reported during the North American blackout in 2003 [93], [100]-[101].

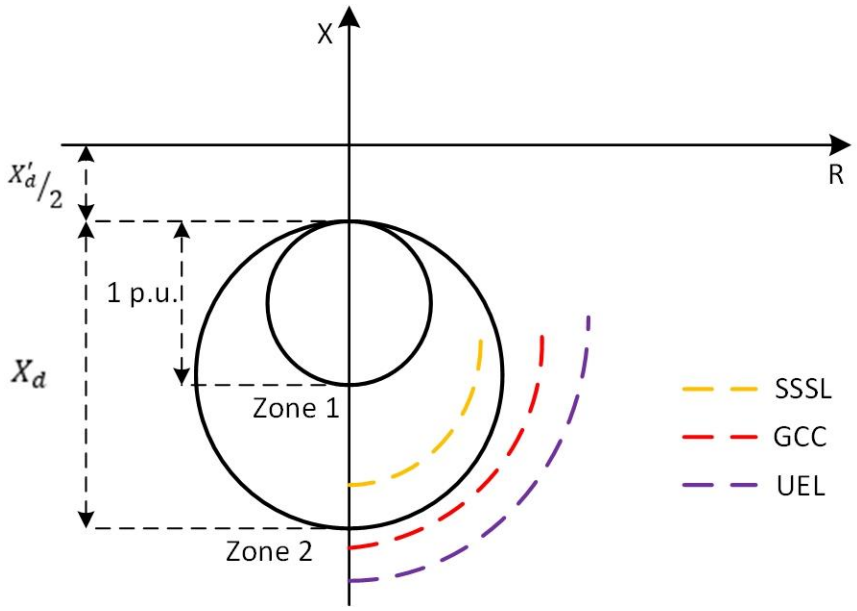

Figure 6.15 The negative offset impedance-based relay for LOF protection

Other types of LOF protection schemes are also utilized by the industry. One of these schemes is positive offset R-X scheme equipped with a directional element, which is shown in Figure 6.16 [102]. Note that in Figure 6.16, X_s is the system reactance. This scheme is faster than the negative offset scheme, and the directional element can improve its security against external short circuit faults [103]. This scheme, however, is also prone to misoperation. Moreover, both the negative and positive offset schemes need to be coordinated with generator capability curve, UEL curve, and SSSL in R-X plane, which can be challenging.

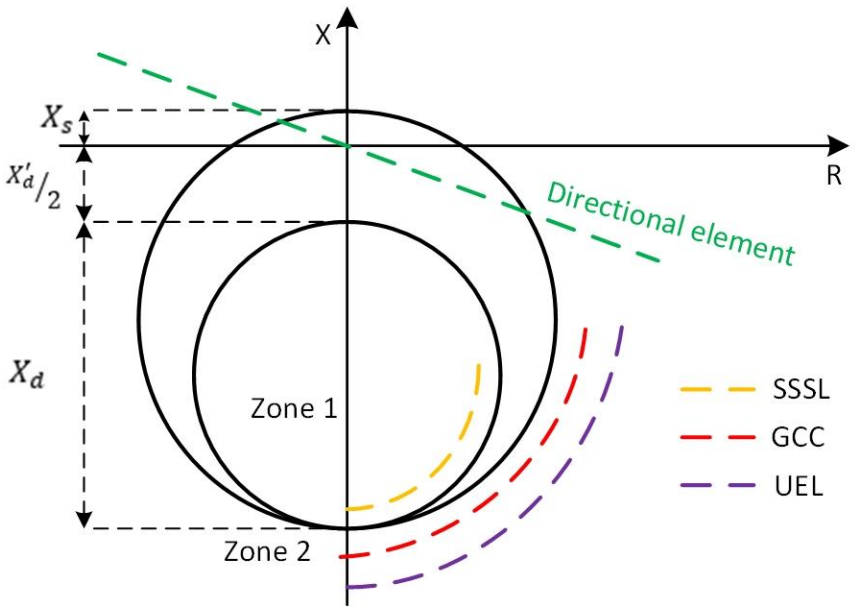

Figure 6.16 The positive offset impedance-based relay with directional element for LOF protection

Another scheme used by industry is admittance-based (G-B based) relay, which is depicted in Figure 6.17 [104]. The mentioned coordination challenges can be solved by using the admittance-based relays, if the UEL characteristic is available [105].

The time delays of zone 1 and 2 in each of the mentioned LOF schemes can be traditionally selected as 0.1 s and 0.5 s, respectively. However, different analysis, including analyzing the LOF relay performance in the presence of power swings, should be performed for more elaborate settings of the time delays [93].

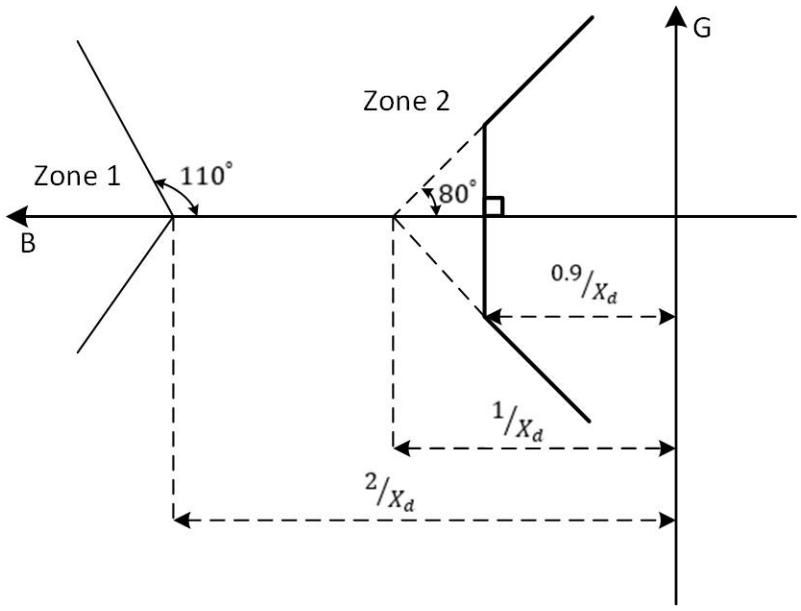

Figure 6.17 The admittance-based relay for LOF protection

6.3.2 The framework for modeling loss-of-field relays of generators

According to the generator protective relay setting data of the area under study, all the generators in the area are equipped with LOF relays with the negative offset impedance-based characteristic (the mostly used LOF characteristic in the industry). Therefore, these relays include two operation zones with negative offsets in the R-X plane and the corresponding time delays.

The "gp3" model in the PSLF model library [46] is used to model LOF protection function of the generators in transient stability studies. As described before, the *gp3* is a generic generator protection system in PSLF library that can provide different protection functions for generators. In terms of LOF protection, the *gp3* model is equipped with an impedance-based LOF protection element with two protection zones (with offset). Therefore, the *gp3* is a proper model to be used to model the LOF protection functions of

the industrial generators. The zone 1 and 2 reaches of the LOF relays used in the generators in the area under study are provided in ohms in the data file, whereas these settings of the *gp3* model should be provided in per unit based on the per unit base impedance calculated using (6.18). Also, note that, the current and voltage used by the relay is provided from CTs and VTs and the impedance settings of the relay is based on these converted currents and voltages, whereas the *gp3* observes the real impedance (without the effects of CTs and VTs). Therefore, proper VT ratio to CT ratio coefficient should be applied when calculating the p.u. values for the zone reach and zone offset. Equations (6.18) – (6.20) are used to convert the zone reach and zone offset parameters of the LOF relays to proper per unit values.

$$Z_{base}\ (ohms) = \frac{{V_{LL}}^2}{S_{rated}} \tag{6.18}$$

$$Z_{zone}(p.u.) = \frac{Z_{zone}\ (ohms)}{Z_{base}(ohms)} \times \frac{VT_{ratio}}{CT_{ratio}} \tag{6.19}$$

$$Z_{offset}(p.u.) = \frac{Z_{offset}\ (ohms)}{Z_{base}(ohms)} \times \frac{VT_{ratio}}{CT_{ratio}} \tag{6.20}$$

Note that in these equations, V_{LL} is the rated line-to-line terminal voltage of the generator. S_{rated} is the generator rated 3-phase MVA. Z_{zone} and Z_{offset} are the zone (1 or 2) reach and zone offset of the LOF relay. Therefore, using (6.18) – (6.20) the proper settings of the LOF function of the *gp3* model are calculated.

6.4 Modeling generator undervoltage and overvoltage protection

This section provides a brief introduction of undervoltage (UV) and overvoltage (OV) protective relays of generators and their applications, as well as the PSLF model used to represent these relays in the dynamic file of the system. The section also provides the

procedure for precisely representing the protection functionality of the actual UV and OV relays of the industrial generators in the area under study along with their precise setting in transient stability studies.

6.4.1 Undervoltage and overvoltage protection for generators

Voltage regulators are responsible for maintaining the terminal voltage of a generator within its rated operating voltage range by controlling the generator excitation level. Abnormal terminal voltages, i.e., voltages outside the rated operating voltage range, can cause damage to the generator or create an undesirable condition in the power system to which the generator is connected to [95].

Abnormal high voltage could cause a high stress on the dielectric of the generator or the insulation system of its step-up transformer, which can even lead to insulation failure. One type of overvoltage in generators is caused by transient surges due to lightning or switching actions. Surge protective devices are designed to protect power system assets from these transient surges. The other type of overvoltage in generators can occur when there is a disturbance in the system causing overvoltage condition in the generator, while the generator controls are defective or do not have adequate transient response [95] and [21]. For example, if the voltage control is performed manually, a sudden change in the load of the system can cause overvoltage condition on the remotely located generators. This is particularly true for remote large hydro units, as it might not be possible for their governor to close the wicket gates of these units fast enough to prevent overspeed condition in these units which is associated with overvoltage. This type of overvoltage is less likely to occur in a steam unit, as they have a tighter control against overspeed. In this regard,

steam turbines are not always equipped with overvoltage protection. However, overvoltage protection is often required for hydro units or combustion turbine units [21]. Overvoltage relays should have a pickup of about 110% of rated voltage along with a time delay. They also can be equipped with an instantaneous element with a pickup voltage of 130%-150% of rated voltage [21].

Undervoltage conditions usually do not harm the generators. Nevertheless, operating at a low voltage for an extended time can create overheating condition in the auxiliary motors for turbine generator sets and cause damages to these motors. Therefore, sometimes these auxiliary motors are monitored by undervoltage relays that can trip the generator offline to protect the motors. The undervoltage relays usually have a pickup of about 90% of rated voltage along with a time delay to avoid generator tripping during successful clearing of external faults [95]

6.4.2 The framework for modeling overvoltage and undervoltage relays of generators

According to the generator protective relay data, all the generators in the area under study are equipped with OV relays. Most of these relays include one pickup voltage along with the related time delay. Some of the generators, however, include two pickup voltages with different time delays. On the other hand, only some of the generators are equipped with UV relays and all of them have only one pickup voltage with a time delay.

The “gp3” model in the PSLF model library [46] is used to model the OV and UV relays of the generators. In terms of the over and undervoltage protection, the *gp3* model can provide one stage of OV and one stage of UV protection with related time delays. Therefore, this model can properly represent OV and UV relays of the industrial generators

in the area under study, as these generators mostly include one stage of OV and UV protection. For the units that include two stages of OV protection, a secondary *gp3* model is used. For these units the higher pickup voltage is used as the settings of the first *gp3* model (primary protection) and the lower pickup voltage, which have a longer time delay, is used as the settings of the second *gp3* model, which is in alarm only mode. For these units, in any study, if the second *gp3* model issues a tripping alarm, the study is performed again with considering the secondary *gp3* model as the primary gp3 and modifying its settings to trip the generator (rather than issuing alarms).

Note that in the *gp3* model, the pickup voltages of OV and UV protection functions should be provided in p.u. considering the nominal voltage of the generator as the per unit base. Therefore, if the actual settings of the OV and UV relays are provided in volts or in p.u. with another per unit base, they need to be converted to p.u. values based on the nominal voltage of the generator using (6.21) and (6.22). Note that the voltage fed to OV and UV relays are provided from VTs. Therefore, if the pickup voltages provided in the setting files are the voltages (in volts) observed at the secondary side of the VTs (relay side), the VT ratio should be multiplied to the pickup voltage.

$$V_{pickup}(p.u.) = \frac{V_{pickup}(v)}{V_{rated}} \tag{6.21}$$

$$V_{pickup}(p.u.) = \frac{V_{pickup,old}(p.u.) \times V_{base,old}}{V_{rated}} \tag{6.22}$$

In (6.21) and (6.22), $V_{pickup}(p.u.)$ is the pickup voltage in p.u. based on the nominal voltage of the generator. $V_{pickup,old}(p.u.)$ is the pickup voltage in p.u. based on any different base voltage ($V_{base,old}$) that is used to calculate the per unit values for OV relay pickup voltage in the setting file. Finally, V_{rated} is the nominal voltage of the generator.

Note that there are other generator OV and UV protection relays in the PSLF library, such as *lhvrt*, that can provide multiple stages of OV and UV protection for generators. However, as mentioned, the *gp3* model is a generic generator protection system which can provide several generator protection functions. Therefore, this model is used in this work to provide multiple protection functions for the generators. In this regard, considering that most of the generators only include one stage of OV and UV protection, to avoid including many different types of relay models for each generator, the *gp3* model is used in this work to provide generator OV and UV protection.

6.5 Modeling generator underfrequency and overfrequency protection

An introduction of underfrequency (UF) and overfrequency (OF) relays of generators and their applications, as well as the PSLF model used to represent these relays in the dynamic file of the system are provided in this section. Also, the procedure for precisely representing the protection function of the actual UF and OF relays of industrial generators in transient stability studies is thoroughly explained.

6.5.1 Underfrequency and overfrequency protection for generators

When a generator is in a stable operating condition at normal frequency, the total mechanical power input from the prime mover is equal to the total electrical power output of the generator (ignoring losses). Any significant change in the mechanical power input (such as prime mover failure) or in the electrical power output (such as sudden change in the load of the system) can disturb this balance and cause a change in frequency [95] and [98].

Operation of generators at low frequencies can decrease ventilation capability of the generator and lead to overheating condition. However, generally, turbines are more sensitive than generators and transformers to working at abnormal frequency. Specifically, the main concern for operating at abnormal frequencies is turbine blade fatigue, which can occur in steam turbines and combustion turbines over 200 MW [95]. The fatigue stress on turbine blades depends on their resonance frequencies, which itself is a function of the design and the length of the blades. There are multiple stages of different steam pressure in steam turbines. Each of these stages are composed of blades of different lengths. Therefore, there are multiple resonance frequencies in steam turbines. On the other hand, combustion turbines under 200 MW usually have limited number of blade sizes. Therefore, compared to steam turbines, combustion turbines have fewer resonance frequencies. Blade fatigue is cumulative and non-reversible. Furthermore, the capability of the auxiliary motor drives and shaft driven loads to operate in underfrequency condition is limited. If the frequency drops more than 2 Hz, power station auxiliary might trip out, leading to tripping of the entire unit. Generally, the boiler feed pumps, circulating water pumps, and condensate pumps are the auxiliary equipment that impose the tightest limits for underfrequency operation of steam generators. Therefore, proper protection should be in place to avoid generator operation at underfrequency condition.

In a 60-Hz system, the operation frequency between 59.5 and 60.5 Hz is considered allowable operation frequency, for which the generator can operate for unlimited time. Operation of generators in frequencies outside this range are not recommended [95]. The turbine underfrequency protection scheme should be applied to all steam and combustion

turbines and monitor the amount of time the generator operates at abnormal frequencies. In most North American power systems, severe underfrequency events are rare. Therefore, UF relays are usually called upon to restrain from tripping during normal frequency operation condition.

Overfrequency usually occurs when a sudden reduction in load or a large load rejection happens in the system and results in light-load or no-load operation of the generators. Usually, the governor runback or operator actions correct the turbine speed, and turbine OF relay is usually not required. Generator ventilation is improved during operating in overfrequency condition, and the flux density required to maintain a given terminal voltage is reduced. Therefore, if a generator operates within the allowable overfrequency limit of the turbine, it will not cause overheating in the generator while the generator operates within its rated apparent power and below 105% of its rated voltage [95].

6.5.2 The framework for modeling overfrequency and underfrequency relays of generators

According to the generator protective relay data, all the generators in the area under study are equipped with OF and UF relays. All the OF relays include one pickup frequency with a time delay. All the UF relays include at least one pickup frequency with a time delay, and most of them include at least 2 pickup frequencies with different time delays.

The “lhfrt” model in the PSLF model library [46] is used to model the OF and UF relays of the generators. The *lhfrt* is a low/high frequency ride through generator protection model in the PSLF library that can provide up to 10 stages of overfrequency and underfrequency protection. Therefore, this model is a proper choice for representing the OF and UF relays

of the industrial generators in the area under study. Note that in the *lhfrt* model each pickup frequency should be provided as an amount of deviation (in Hz or p.u.) from the nominal frequency (defined by *fref* parameter). For instance, if the *fref* parameter is selected as 60 Hz, and the first pickup frequency of the UF relay is 59.8 Hz, the parameter of the *lhfrt* model associated with the first pickup frequency (*dftrp1*) should be selected as -0.2. The *lhfrt* model monitors the deviation of the generator frequency from *fref*, using (6.23), and if it exceeds the first pickup frequency for a predefined amount of time, the relay trip the generator. Note that *dftrp* is the deviation of the generator frequency from the reference frequency (*fref*). More details about the *lhfrt* model are provided in Appendix F.

$$dftrp = |Monitored\ frequency\ in\ p.u.| \times fref - fref \tag{6.23}$$

6.6 Modeling generator reverse power protection

An introduction of reverse power relays (motoring protection) of generators as well as their principles and applications are provided in this section. Furthermore, the PSLF model used to represent these relays in the dynamic file of the system along with the procedure for precisely representing the protection function of the actual reverse power relays of industrial generators in transient stability studies is elaborated upon.

6.6.1 Reverse power protection for generators

Reverse power flow to a generator (motoring operation) occurs when the prime mover fails while the generator is online and excited. In this condition, rather than providing mechanical power to the generator, the prime mover acts as a mechanical load, and the generator operates as synchronous motor driving the prime mover. Operating in the motoring mode does not harm the generator, itself. However, it might damage the prime

mover. Moreover, the mechanical load that the prime mover impose to the generator might be high and appears as an active power loss for the power system [91].

Table 6.1 gives the detail of the potential problems that motoring operation could cause to different types of prime movers along with the percentage of the rated power of the machine that is required for operation in the motoring mode. Note that in Table 6.1, "motoring power" indicates the minimum active power required by the generator to run the prime mover at the rated rpm. This data is usually provided by the manufacturer [94].

As seen in Table 6.1, the reverse power can damage prime movers in different ways. Therefore, reverse power protection is necessary for all generators except hydro units designed to operate as synchronous condensers. The reverse power protection complements the built-in detection element of the generator control system. The most widely used reverse power protection relays includes a directional element to detect the reverse active power flow to the generator along with a related time-delay for the operation of the relay. The pickup reverse power is usually set to 20% to 50% of the motoring power mentioned in Table 6.1. The time delay, which is typically in the range of tens of seconds, is to avoid misoperation of relays during power swings caused by system disturbances or during synchronizing the machine to the system. The time delay should be less than allowable turbine motoring time (provided by the manufacturer). After the time delay, the relay generally trips the main generator breaker(s), trips the main field breaker(s), transfers the auxiliaries, and sends a trip signal to the prime mover [91] and [94].

Table 6.1 Motoring reverse power requirements and possible damages of motoring operation for different types of prime movers [106]

Prime mover	Motoring power (% of the rated power)	Possible damage
Steam turbine	0.5 – 6	Turbine blade damage, Explosion because of increased steam temperature, gearbox damage on geared sets
Gas turbine	10 – 15 for split shaft	Gear box damage
	> 50 for single shaft	
Hydro	0.2 – 2 for blades out of water	Blades and runner cavitation
	> 2 for blades in water	
Diesel engine	5 – 25	Fire or explosion due to unburnt fuel, mechanical damage to gearbox and shafts

The mechanism of reverse power protection relays is based on the fact that during reverse power flow to the generator, as shown in Figure 6.18, 180° phase shift occurs in the stator current (typically referred to as maximum torque angle). Therefore, if a directional relay with the maximum torque angle of 180° is used, it can detect the reverse power condition as the current phasor would shift 180° and enter the trip region of the relay [94]. Considering that the reverse power drawn by a generator during motoring operation is quite a small portion of its rated power, the reversed stator current is quite small, as well (compared to the forward current of the stator). Therefore, the directional relay used for reverse power protection should have a high degree of sensitivity. The installation of a reverse power protection system is illustrated in Figure 6.19.

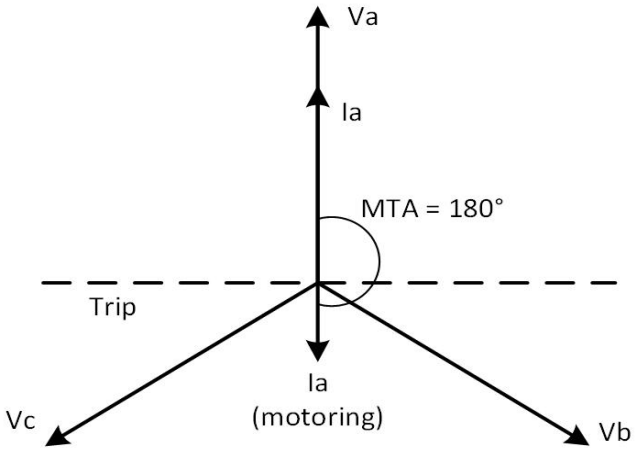

Figure 6.18 Phasor representation of generator voltage and current under reverse power flow

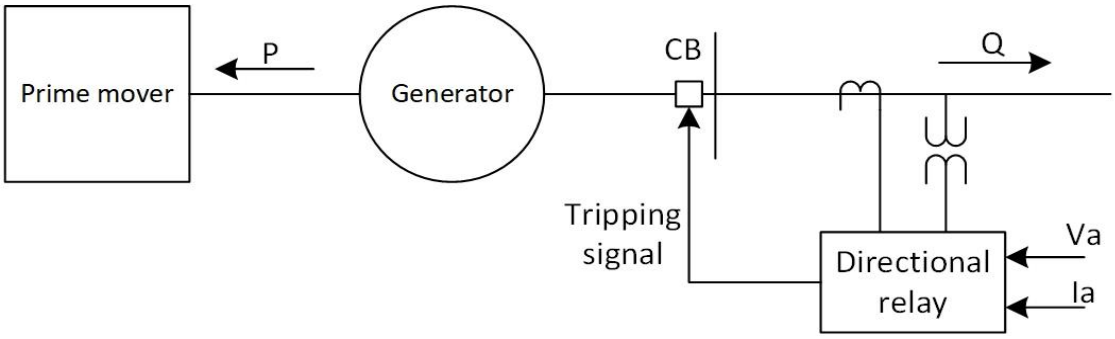

Figure 6.19 Reverse power protection relay installation

6.6.2 The framework for modeling reverse power protection relays of generators

According to the generator protective relay data, all the generators in the area under study are equipped with one stage of reverse power protection with a related time delay. The “gp3” model in the PSLF model library [46] can provide one stage of reverse power protection with a user-defined time delay. Therefore, this model is selected to represent the reverse power relays of the industrial generators in the area under study.

Note that in the *gp3* model, the pickup power for the reverse power protection should be provided in p.u. based on the rated MVA of the generator. Therefore, if the actual settings of the reverse power relays are provided in MW or in p.u. with another per unit base, they need to be converted to p.u. based on the rated MVA of the generator using (6.24) and (6.25).

$$P_{reverse,pickup}(p.u.) = \frac{P_{reverse,pickup}(MW)}{S_{rated}} \tag{6.24}$$

$$P_{reverse,pickup}(p.u.) = \frac{P_{reverse,pickup,old}(p.u.) \times S_{base,old}}{S_{rated}} \tag{6.25}$$

In (6.24) and (6.25), $P_{reverse,pickup}(p.u.)$ is the pickup reverse power in p.u. based on the rated MVA of the generator. $P_{reverse,pickup,old}(p.u.)$ is the pickup reverse power in p.u. based on any different base MVA ($S_{base,old}$), such as system base MVA, that is used to calculate the per unit values of the pickup reverse power in the setting file. S_{rated} is the rated MVA of the generator.

6.7 Modeling generator phase-fault backup protection

In generators, phase faults can occur in the winding end turns, where all three phase windings are close together, or in slots if two coils are placed in one slot. Phase faults usually change to ground faults. However, they should be detected in either condition, and proper protection should be implemented against them [21].

Three types of relays can provide backup protection for stator phase faults: voltage-controlled time-overcurrent relays, voltage-restraint time-overcurrent relays, and phase distance relays that are installed on the lines out of the plant. Voltage-restraint and voltage-

controlled time-overcurrent relays are generally used for small to medium sized generators, whereas phase distance protection is used for large generators [90].

The three types of phase-fault backup protection of generators will be explained in this section. Also, the PSLF models used to represent these relays in transient stability studies along with the procedure for precisely representing these relays of the industrial generators is explained in detail.

6.7.1 Voltage-controlled or voltage-restraint time-overcurrent backup protection for generators

The voltage-controlled or voltage-restraint overcurrent relays are nondirectional relays that are used to provide phase-fault backup protection for small to medium sized generators. The operations of these relays are independent of the angle between the voltage and current of the generator. Therefore, they operate at all power factors. As shown in Figure 6.20, these relays are connected to CTs at the terminal of the related generator (or at the neutral end). The voltage is fed to these relays through the generator VTs. This voltage is used to avoid the relay operation unless there exist a fault that decreases the voltage [90].

Generators normally operate close to the knee of their saturation curve. The synchronous reactance in this condition, $X_{d(sat)}$, is lower than the reactance of the machine for the faults that reduce the voltage of the generator, $X_{d(unsat)}$. Therefore, unless the voltage regulator increases the sustained reduced voltage (due to fault), the three-phase fault current is less than the maximum load current [90].

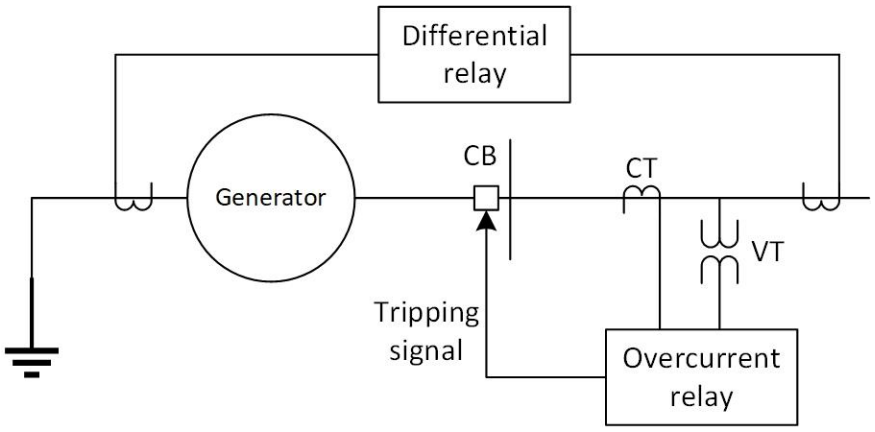

Figure 6.20 Overcurrent and differential protection relay installation

The voltage-controlled type time-overcurrent relays prevent the relay from operation until the fault reduces the voltage to a specific threshold (usually around 80% of the nominal voltage). On the other hand, the voltage-restraint type time-overcurrent relay decreases the pickup current of the relay as the terminal voltage decreases. Both schemes enable overcurrent relays to operate at currents that are less than the maximum load at the normal voltage. Therefore, the relay can detect the sustained three-phase fault current below the full load of the generator. Generally, the voltage-restraint type is less prone to misoperation due to starting current of motors or system power swings. Nevertheless, the short-time voltage depression due to these events does not probably lead to the operations of these relays [90].

In terms of the settings of these types of relays, the pickup current for the voltage-controlled type is usually set below generator nameplate current, whereas this pickup current is usually set above the generator nameplate for the voltage-restraint type relays. The reason for this setting of the pickup current is that as the voltage decreases, the voltage-restraint relays decrease the pickup current proportionally to values below the generator

nameplate current. In the voltage-controlled type, the control voltage setting should be selected below the lowest credible voltage at which the power system might operate. Otherwise, if this voltage setting is selected too high, the relay might misoperate during wide-area disturbances [95].

6.7.2 The framework for modeling voltage-restraint time-overcurrent backup protection for generators

According to the protective relay data, only some of the generators in the area under study are equipped with voltage-restraint type overcurrent (OC) relays. All the units with this type of OC relays include one pickup current along with an inverse-time element, the shape of which is defined by the model of the industrial relay used to provide the overcurrent protection, a parameter defining the shape of the inverse-time function, and the time dial coefficient. These OC relays also include a reset time function, the coefficient of which is defined by the time-dial coefficient.

The industrial models used to provide overcurrent protection include SEL-300G and GE-G60 models. Different inverse-time functions of the overcurrent protection of these relays—including U2, IEEE VI, and IEEE EI—are used with the related time-dial coefficients.

The *gp3* model in the PSLF library [46] is used to model the voltage-restraint inverse-time OC relays of the industrial generators in the area under study. The *gp3* can provide one stage of voltage-restraint inverse-time OC protection for the generators. The desired pickup current can be selected by setting the *ioc* parameter of the *gp3* model. Three

parameters of *koc*, *boc*, *poc*, and *troc* define the inverse-time and reset-time functions of the OC relay of the *gp3* model using (6.26) – (6.29).

$$T_{trip}(I_t) = \frac{koc}{(\frac{|I_t|}{I_{pickup}})^{poc-1}} + boc \tag{6.26}$$

$$T_{rest}(I_t) = \frac{troc}{(\frac{|I_t|}{I_{pickup}})^{2-1}} \tag{6.27}$$

$$T(I_t) = \begin{cases} T_{trip}(I_t) & if\ |I_t| > I_{pickup} \\ T_{rest}(I_t) & if\ |I_t| < I_{pickup} \\ -troc & if\ |I_t| = I_{pickup} \end{cases} \tag{6.28}$$

$$Trip = \int_0^t \frac{1}{T(I_t)} dt \tag{6.29}$$

The pickup current of the OC relay of the *gp3* model should be provided in p.u. based on the rated current of the generator. Therefore, if the pickup currents of generator OC relays are provided in Amps or in p.u. based on any other base current, the pickup currents should be converted to p.u. based on the generator rated current using (6.30) – (6.32). Note that as shown in Figure 6.20, the current fed to the OC relay is provided from the CTs. Therefore, if the pickup current of OC relay provided in the setting file is the current at the secondary side of the CTs, the CT ratio should be taken into account when setting the pickup current of the *gp3* model.

$$I_{pickup}\ (p.u.) = \frac{I_{pickup}\ (Amps)}{I_{rated}(Amps)} \tag{6.30}$$

$$I_{pickup}\ (p.u.) = \frac{I_{pickup,old}\ (p.u.) \times I_{base,old}(Amps)}{I_{rated}(Amps)} \tag{6.31}$$

$$I_{rated}\ (Amps) = \frac{S_{rated}}{\sqrt{3}.V_{LL}} \tag{6.32}$$

Where, I_{pickup} is the pickup current of the OC relay. I_{rated} is the rated terminal current of the generator. S_{rated} is the 3-phase rated MVA of the machine, and V_{LL} is the nominal line-to-line terminal voltage of the generator.

To precisely match the inverse-time and reset-time functions of the OC relays with the inverse-time and reverse-time functions of the *gp3* model, considering the industrial models of the OC relays used as well as the associated shape parameters and time-dial coefficients, the precise inverse-time and reset-time functions of the OC relays are obtained from the manual. Then, the *koc*, *boc*, *poc*, and *troc* parameters are tuned in a way that the resulting inverse-time and reset-time functions match the respected functions obtained from the manual. To further explain this process the following example is provided.

Assume that the actual OC relay of a generator is the SEL-300G model with the shape parameter of U2 and time dial coefficient of 4. According to the manual of SEL-300G [107], these parameters result in a trip time of $T_{trip}(I_t) = 4(\frac{5.95}{\left(\frac{|I_t|}{I_{pickup}}\right)^2 - 1} + 0.18)$ and the reset time of $T_{rest}(I_t) = 4(\frac{-5.95}{\left(\frac{|I_t|}{I_{pickup}}\right)^2 - 1})$. Comparing the obtained trip time and reset time with (6.26) and (6.27), the proper parameters that need to be included in the *gp3* model to yield a similar inverse-time and reset-time functions are obtained as follows:

$$koc = 5.95 \times 4 = 23.8, poc = 2, boc = 0.18 \times 4 = 0.72$$

$$troc = -4 \times 5.95 = -23.8$$

6.7.3 Phase distance backup protection for generators

As mentioned, for providing phase-fault backup protection for large generators, distance relays are utilized. The purpose of using distance relays is to protect the generator from supplying a sustained fault current to a fault on the power system. A common characteristic for this relay is a mho characteristic along with a related time delay. Generally, the faults in the transmission system should be cleared by system relays (such as the distance relays of the transmission lines). Therefore, the distance relay of the generator must be coordinated with the system protection to avoid operation before the system relay operation, and they should only operate if the system relay fails [96].

The current and voltage used by the generator distance relay are provided from CTs and VTs. The directional sensing is determined by the location of the CTs. However, the distance is measured from the location of VTs. Therefore, if CTs of distance relays are installed on the generator lead, depending on the connections, backup could be provided only for the system (distance relay looking into the system) or for the generator (distance relay looking into the generator) and not both. Unlike the case of protecting the system, in which a time delay is required for a proper coordination with the system relays, in the case of protecting the generator, no time delay is required.

6.7.4 The framework for modeling phase distance backup protection for generators

According to the protective relay data, most of the generators in the area under study are equipped with a phase distance backup protection relay with mho characteristic that has at least one protection zone. The mho characteristic of some of these relays include two protection zones. The settings provided include the reach of each zone (in ohms), the offset

impedance of each zone (in ohms), the impedance angle of each zone (in degrees), as well as the time delay associated with each zone.

The "oosmho" model in the PSLF library [46] is used to model the phase distance backup relays of the industrial generators in the area under study. The *oosmho* is an out-of-step mho relay with blinders. The mho characteristic of this relay only includes one protection zone. The relay is modeled on the branch that connect the generator to the power system—i.e., the step-up transformer of the generator—with its from bus being the generator terminal bus. For the generators that have the phase distance protections with two zones of protection, two *oosmho* is used, each of which representing one protection zone of the phase distance relay. More details about the *oosmho* model are provided in Appendix G.

For all per unit impedances, the per unit base utilized by the *oosmho* relay is obtained using the system MVA base and the rated voltage at the from bus. Therefore, the provided settings (zone reach and zone offset) that are in ohms need to be converted to p.u. based on per unit base of *oosmho*. Note that, the current and voltage used by the relay is provided from CTs and VTs and the impedance settings of the relay is based on these converted current and voltages, whereas the *oosmho* observes the real impedance of the line (without the effects of CTs and VTs). Therefore, proper VT ratio to CT ratio coefficient should be applied when calculating the p.u. values for the zone reach and zone offset. Equations (6.33) – (6.35) are used to convert the zone reach and zone offset parameters of the phase distance relays to per unit.

$$Z_{base}\ (ohms) = \frac{{V_{LL}}^2}{S_{syst}} \tag{6.33}$$

$$Z_{forward}(p.u.) = \frac{Z_{forward}\,(ohms)}{Z_{base}(ohms)} \times \frac{VT_{ratio}}{CT_{ratio}} \tag{6.34}$$

$$Z_{offset}(p.u.) = \frac{Z_{offset}\,(ohms)}{Z_{base}(ohms)} \times \frac{VT_{ratio}}{CT_{ratio}} \tag{6.35}$$

Note that in these equations, Z_{base} is the per unit base used by the *oosmho* relay. V_{LL} is the rated line-to-line voltage at the from bus of the branch (generator terminal bus). S_{syst} is the rated 3-phase MVA of the system. $Z_{forward}$ and Z_{offset} are the zone reach and zone offset of the relay. The parameter embedded in the *oosmho* for zone offset is *rr*, which represents the mho zone reverse reach in p.u. Positive values for *rr* represents behind the from bus (for providing reverse reach). Therefore, if the phase distance relay includes zone offset, the negative of the value calculated in (6.35) should be used for the *rr* parameter. Finally, to prevent blinders from interfering with *oosmho* relay operation (as there is no need for blinders in phase distance backup protection of generators) very high values are selected for the intercept of both blinders. Also, the intercept values for the blinders are selected very close to each other to minimize the chance of impedance trajectory falling between the two blinders. Moreover, the rotations of the blinders are set close to 90 degrees. In this case, the blinders are two close-to-vertical lines far from the origin of the R-X coordinate. Therefore, it is very unlikely that these blinders intersect with any probable impedance trajectory and cause any unwanted blinder interference.

6.8 Modeling generator out-of-step protection

An introduction of OOS condition in generators including how it occurs, what probable damages it can cause for generators, and how generators should be protected against it is provided in this section. Furthermore, the PSLF model used to represent OOS relays in

transient stability studies along with the procedure for precisely representing the protection function of the OOS relays of industrial generators is elaborated upon.

6.8.1 Out-of-step protection for generators

During OOS condition, the impedance trajectory observed from the generator terminal (looking into the system) varies as a function of the system and generator voltages and the angular separation between them [95]. If the two-machine equivalent of the system, shown in Figure 6.21, is considered (where E_G and E_H are constant magnitudes behind the transient impedances, Z_G and Z_H), the geometrical interpretation of the power equation for this two-machine system can be illustrated as Figure 6.22 [15]. Figure 6.22 shows an R-X diagram with the mho characteristic of the OOS relay installed on bus A. In this diagram, Z_G extends from the origin to point *G* at the third quadrant, Z_L extends from the origin to point *B* in the first quadrant, and Z_H extends from the tip of Z_L (point B) to point H in the first quadrant. *GH* is the total impedance across the system. If E_G and E_H are of equal magnitudes with δ degrees difference in phase angle (E_G leads E_H by δ degrees), the apparent impedance during a power swing falls on a straight line that is perpendicular to and bisecting the total system impedance (the dashed line). During the swing, as E_G further moves ahead of E_H in angles, the angle separation δ between E_G and E_H increases. On the R-X diagram, this angle separation is illustrated by the angle formed by the intersection of lines *PG* and *PH* at *P*. Point *P* is the apparent impedance observed at Bus A. When $\delta = 90^{\circ}$, the impedance is on the circle whose diameter is the total impedance of the system (line *GH*). This point is the point of maximum load transfer between *G* and *H*. When δ reaches 120 degrees and above, it is unlikely that the system recovers from the swing.

When the impedance locus intersects the total system impedance (line *GH*), the phase angle separation is 180 degrees ($\delta = 180^{\circ}$) and the systems are completely out of phase. This point which falls at the middle of the line *GH* (with the assumption that E_G and E_H are of equal magnitudes) is called the electrical center. The voltage at this point is zero, which is equivalent to a three-phase fault at the electrical center. As the impedance locus moves to the left of line *GH*, δ becomes bigger than 180° and finally the system will be in phase, again. If the system is not separated, the phase angle separation of E_G and E_H increases and the cycle repeats itself, and when the impedance locus reaches its starting point, one slip cycle has been completed. Note that, in Figure 6.22, if $|E_G| > |E_H|$, the electrical center of the system will be above the middle point of line *GH*, and if $|E_G| < |E_H|$, the electrical center of the system will be below the middle point of line *GH* [15] and [96].

When a generator lose synchronism, large cyclic variations in currents and voltages occur in the generator. Moreover, the generator operates in off-nominal frequency. This condition exposes the generator to threats such as high winding stress, high rotor iron currents, pulsating torques, and mechanical resonances. Also, it increases the risk of losing the auxiliaries of the affected unit and even, those of the nearby stable units. Therefore, to protect the generator from these damages, an OOS relay should be used to trip the generator during OOS condition (preferably, at the first slip cycle) [95] and [98]. OOS protection is required for relatively large generators that can go unstable for credible system contingencies and the power swing enters the generator or transformer zone. This information and the proper settings of the OOS relays to be used are identified in planning studies [95].

A simple mho relay at the high side terminals of the step-up transformer or loss-of-field relays can provide some level of OOS protection. However, it is desired that the generator only be tripped for unstable power swings that lead to OOS condition and unnecessary trippings for stable power swings are avoided. Moreover, it is desired that the tripping of

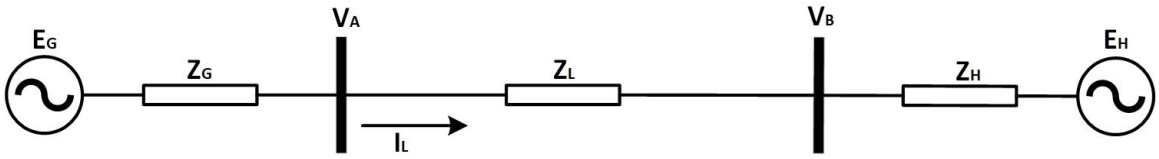

Figure 6.21 Two-machine equivalent of a power system

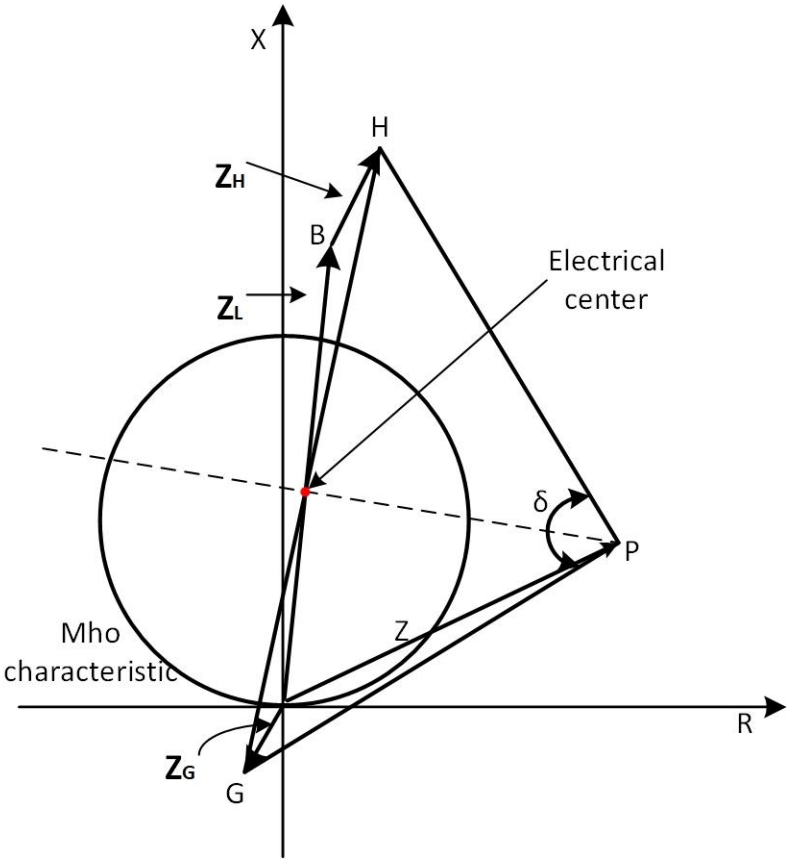

Figure 6.22 Geometrical interpretation of the power equation for the equivalent system

the generator be delayed until the phase separation decreases to a favorable value to minimize the stress on the breaker being tripped. To achieve these characteristics, a blinder characteristic supervised by a mho characteristic or a lens characteristic is usually used. The two basic scheme available for detecting out-of-step condition are as follows [98]:

(A) Mho element scheme:

The concept of this scheme is illustrated in Figure 6.23. In this scheme, an OOS relay is installed on the high voltage terminal of the step-up transformer (point H) and it monitors the apparent impedance seen at point H (looking into the network) and is set to reach into the local generator. The relay trips the generator if the impedance trajectory measured at point H enters the mho characteristic. The settings of the relay in term of the size of the mho circle should be tuned precisely to allow tripping for unstable power swings. As mentioned earlier, the maximum phase separation of the machine from the system, δ, for which the machine can maintain its synchronism with the system is 120°. Therefore, the size of the circle is set in a way that the angle δ_c at the point where swing impedance enters the mho circle be about 120°. If the size of the mho circle is selected too large, the relay may trip the generator even for stable swings. On the other hand, if a too small value selected for the mho circle, the relay may fail to trip for stable swings. Also, in this condition the tripping may occur when δ is close to 180°, which impose a high stress on the circuit breaker [98].

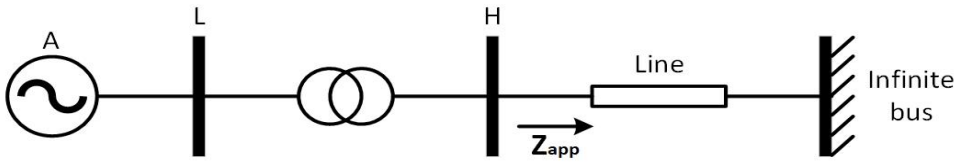

(a) System schematic

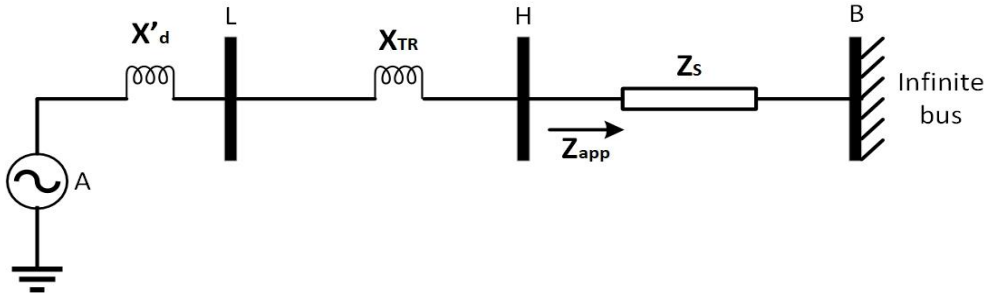

(b) System equivalent circuit

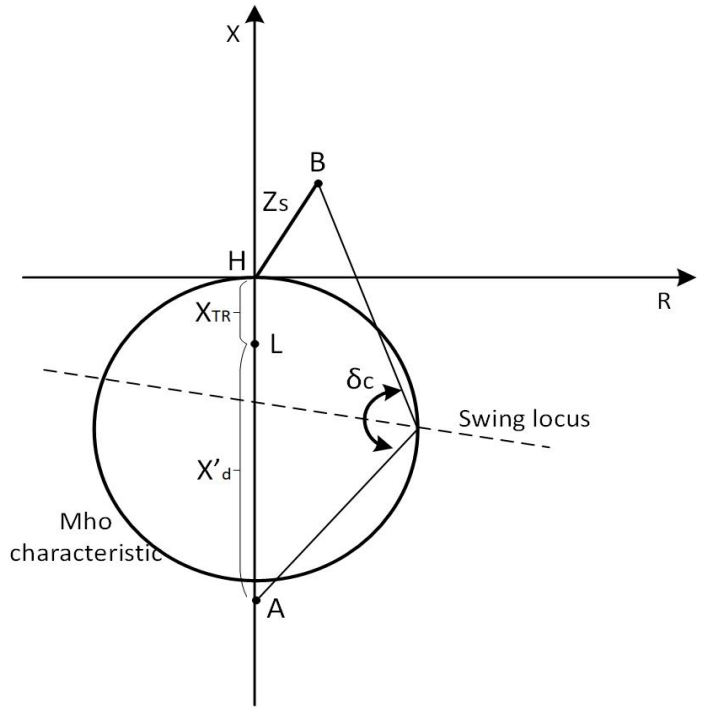

(c) Relay mho characteristics and swing locus (seen from point H)

Figure 6.23 Generator OOS protection using a mho element scheme

(B) Blinder scheme:

As shown in Figure 6.24, This scheme includes two impedance elements, namely, blinders, and a supervisory relay with an offset mho characteristic. Multiple ways of applying blinders are proposed so far. In one of these schemes, the generator is tripped if the impedance trajectory enters the mho circle and crosses both blinders, and the time that it takes for the swing to cross the blinder exceeds a particular value. This scheme offers advantages such as higher sensitivity, easier setting for preferred trip angle to avoid excessive stress on the breaker, and easier coordination with transmission line protection [98].

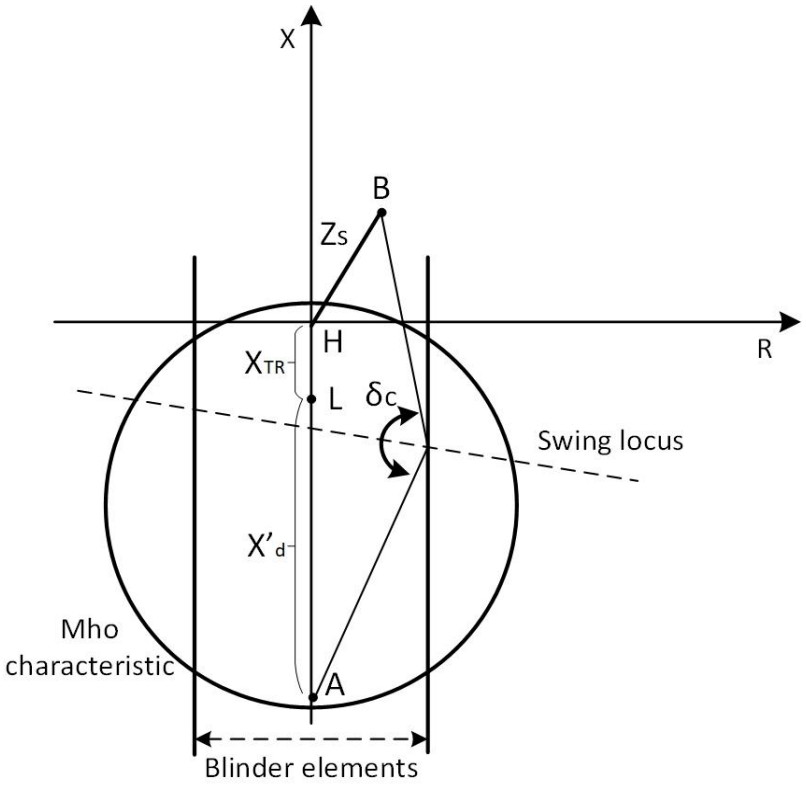

Figure 6.24 Generator OOS protection using a blinder scheme

6.8.2 The framework for modeling out-of-step protection for generators

According to the protective relay data, only one unit in the area under study(including multiple generators) is equipped with OOS protection relay with blinder scheme. The settings provided include mho circle diameter (in ohms), mho circle offset (in ohms), mho circle angle (in degrees), blinder impedances (in ohms), and a time delay for operation (in seconds) of the relay.

The *oosmho* model in the PSLF library [46] is used to model the OOS relays of the industrial generators in the area under study. According to [98], the relay is modeled on the high-voltage terminal of the step-up transformer of the generator. The settings provided for the units can be implemented in *oosmho* relay using the following parameters of this relay model: *ang* (mho circle angle in degrees), *rf* (mho zone forward reach in p.u.), *rr* (mho zone reverse reach in p.u. used with a negative sign to represent mho circle offset), *int1(2)* (blinders intercept in p.u.), *rot1(2)* (blinders rotation in degrees), *t1* (relay operating time in seconds).

For all per unit impedances, the per unit base utilized by the *oosmho* relay is obtained using the system MVA base and the rated voltage at the from bus (high voltage terminal of the generator step-up transformer). Therefore, the provided settings (mho circle diameter and offset as well as blinder impedances) that are in ohms need to be converted to p.u. based on per unit base of *oosmho*. Note that, proper VT ratio to CT ratio coefficient should be applied when calculating the p.u. values. Per unit base of *oosmho* for impedance is obtained by (6.33) considering V_{LL} as the line-to-line voltage of high-voltage terminal of the generator step-up transformer. Also, the forward reach (or mho circle diameter) and

mho circle offset are converted to p.u. using (6.34) – (6.35). Likewise, the blinder impedances are converted to p.u. using (6.36) – (6.37).

$$int_1(p.u.) = \frac{int_1\,(ohms)}{Z_{base}(ohms)} \times \frac{VT_{ratio}}{CT_{ratio}} \tag{6.36}$$

$$int_2(p.u.) = \frac{int_2\,(ohms)}{Z_{base}(ohms)} \times \frac{VT_{ratio}}{CT_{ratio}} \tag{6.37}$$

Note that in these equations, Z_{base} is the per unit base used by the *oosmho* relay. int_1 and int_2 are blinders 1 and 2 intercept in p.u, and $S_{3\varphi,\,system}$ is the system MVA base.

6.9 Modeling generator volt-per-hertz protection

An introduction of volt-per-hertz protection in generators including how it occurs, what probable damages it can cause for generators, and how generators should be protected against it is provided in this section. Furthermore, the PSLF model used to represent volt-per-hertz relays in transient stability studies along with the procedure for precisely representing the protection function of the volt-per-hertz relays of industrial generators in transient stability studies is elaborated upon.

6.9.1 volt-per-hertz protection for generators

The capability of generators and their transformers (step-up and auxiliary transformers) for continuous operation at high voltages and low frequencies is limited. This condition occurs as a result of severe system disturbances, especially the ones that lead to formation of uncontrolled islands in the system. If proper control actions are not taken to alleviate this condition, the high volt-per-hertz ratio leads to overexcitation conditions in generators and related transformers, which is turn leads to thermal damages to the cores due to excessive high magnetic flux. Excess magnetic flux causes saturation in core steel and as

the magnetic reluctance of the core increases due to saturation, the flux flows into the adjacent support structure, causing high eddy current losses in the core and its adjacent structure. Severe overexcitation can also lead to rapid damage and equipment failure. Therefore, volt-per-hertz relays are generally used in power plants to protect generators and transformers from excessive magnetic flux. These relays trip the generator when the volt-per-hertz ratio exceeds a predetermined threshold for a specified time. Typically, two levels of volt-per-hertz protection is used. One level provides protection for higher volt-per-hertz ratios with a shorter time delay, and the other level provides protection for lower volt-per-hertz ratios with a longer time delay. Figure 6.25 shows the shows typical volt-per-hertz versus time capability curves for generator and transformer. Note that, the volt-per-hertz protection is independent of the generator overvoltage control in the generator excitation system [95] and [98].

Table 6.2 Volt-per-hertz limitations of a generator and its step-up transformer [98].

V/Hz (p.u.)		1.25	1.2	1.15	1.1	1.05
Damage time (min)	Generator	0.2	1.0	6.0	20.0	∞
	Step-up transformer	1.0	5.0	20.0	∞	

Volt-per-hertz ratio is an easily measurable quantity that is proportional to magnetic flux. Typical volt-per-hertz limitations for a generator and step-up transformer are provided in Table 6.2 [98]. The low-voltage rating of the unit step-up transformer is typically 5% below the generator voltage rating. Hence, volt-per-hertz protection requirement is usually set by the transformer limitation. However, if the rating voltage of the generator and its

step-up transformer are the same, as shown in Table 6.2, the generator has a tighter limitation on the volt-per-hertz ratio.

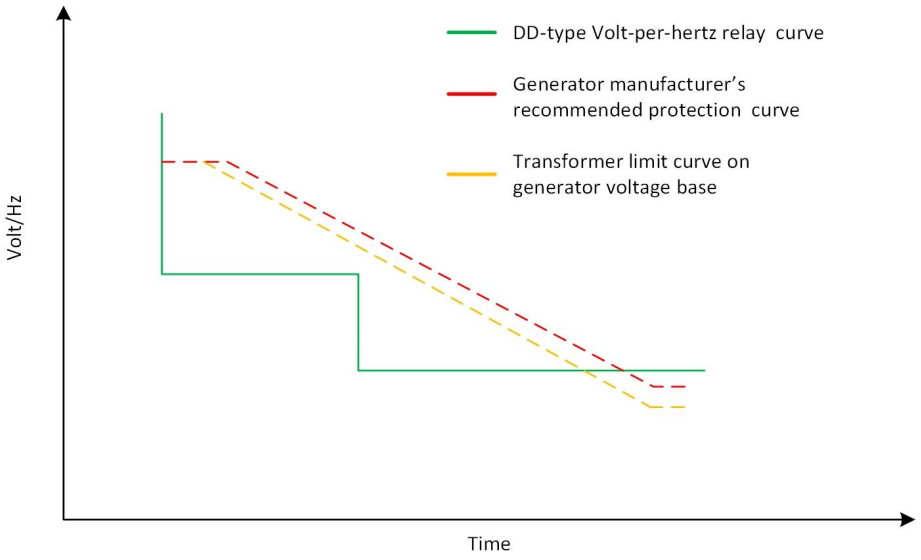

(a)

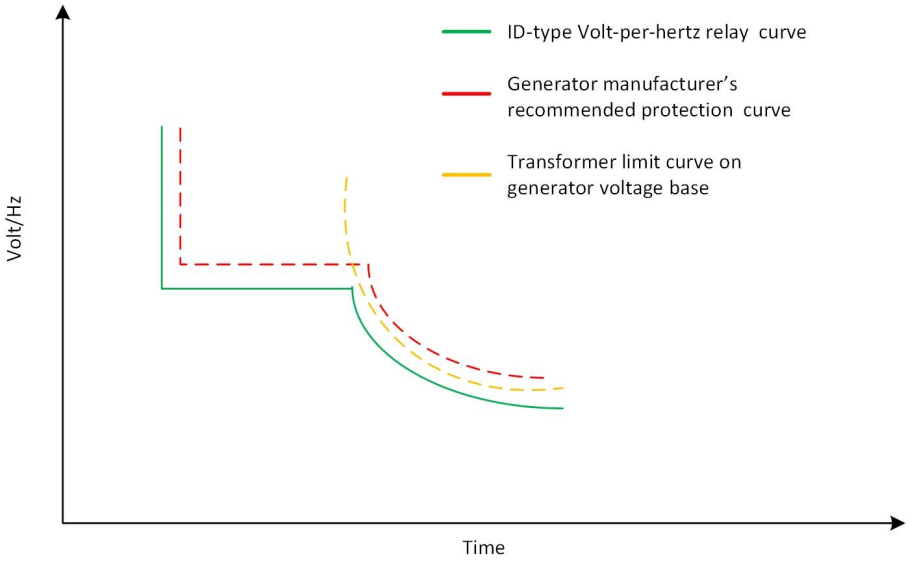

(b)

Figure 6.25 Typical relay characteristics for (a) dual definite-time (DD-type) and (b) combined inverse-time and definite-time (ID-type) volt-per-hertz protection

During disturbances, overexcitation due to a high volt-per-hertz ratio occurs as a result of overvoltage or underfrequency condition in the system. The overexcitation due to overvoltage condition occurs when a disturbance creates islands in the system, in which there is an excess of produced reactive power. In this condition, ideally, tripping of shunt capacitor banks in the islands reduces the system voltage to be in a tolerable range (continuous operation) for generator and transformers. Moreover, the automatic generator excitation control reduces the reactive power output to decrease the voltage within the island. Generators can even operate in underexcited condition and absorb reactive power. However, operating in underexcited condition, itself, is limited by generator underexciter capability. On the other hand, if the generator excitation control is in manual mode, no generator control action will take place and the output reactive power of the generator will not be reduced to decrease the voltage within the island. Therefore, if during severe disturbances, a large number of generators in the system are operating with their excitation voltage control in the manual mode, the high voltage problem in the island will significantly exacerbated. In this condition, if the voltage is not reduced to within the generator and transformer capabilities, volt-per-hertz protection trips the generator and the related transformers.

Overexcitation condition due to high volt-per-hertz ratio can occur due to sustained low system frequency. However, this is less likely than the case of sustained overvoltage, because in order for volt-per-hertz ratio to even be 1.05 at the rated voltage, the frequency needs to drop to 95% of nominal frequency and remains at this value (i.e., 57 Hz). System load shedding protection and generator underfrequency protection prevent sustained

operation of the system at such a low frequency. However, if this condition occurs, the volt-per-hertz relay trips the generator.

6.9.2 The framework for modeling volt-per-hertz protection for generators

According to the protective relay data, all the industrial generators in the area under study are equipped with a volt-per-hertz protection relay. These relays have three different types of volt-per-hertz versus time curve:

1. Two definite time characteristic (DD-type)
2. Inverse-time characteristic with inverse-time factor (I-type)
3. Inverse-definite characteristic with inverse-time factor (ID-type)

No PSLF volt-per-hertz relay model in PSLF library provides inverse time characteristics. Therefore, to avoid adding various types of protective relay models in the dynamic file of the system, the *gp3* model is used to provide volt-per-hertz protection for the generators. The *gp3* model can provide one stage of definite time volt-per-hertz protection. For properly representing each type of volt-per-hertz protection of the generators following procedure are taken:

1. Modeling DD-type characteristic:

For modeling volt-per-hertz relays of the generators with DD-type volt-per-hertz protection characteristics, two *gp3* models are used. The pickup volt-per-hertz ratio and the related time delay settings (*vhz* and *tvhz)* of the first *gp3* model are set to the higher pickup value and time delay of the generator volt-per-hertz relay, whereas the same settings of the second *gp3* model are set to the lower pickup value and time delay of the generator volt-

per-hertz relay. The second *gp3* model is used in alarm only mode (no tripping). However, in any study, if the second *gp3* model generates a tripping alarm, the study is performed again with enabling the tripping of the second *gp3* model.

2. Modeling I-type characteristic:

For modeling this type of volt-per-hertz protection characteristics of the generators with *gp3* models, that can only provide definite time characteristics, as accurately as possible, 10 gp3 models are used. The pickup volt-per-hertz ratio and the related time delay settings of the first *gp3* model are set to the inverse-time factor of the relay. Inverse-time factor of the relay is defined as the time delay for operation of the volt-per-hertz relay when volt-per-hertz ratio is equal to 2. This parameter is provided in the setting data file and is used to set the first *gp3* model. To capture the inverse-time behavior of the relay with the *gp3* models, the inverse-time function of the actual relays is extracted from the manual of the relay. Then, 9 different pickup volt-per-hertz ratio along with the related time delay are sampled from these inverse-time functions. Finally, each of these sample points is modeled with one *gp3* model. Except for the first *gp3* model, the other *gp3* models are used in alarm only mode. If in any study, these *gp3* models generates tripping alarms, the study is performed again with enabling the tripping of the related *gp3* model.

3. Modeling ID-type characteristic:

For modeling ID-type, similar process of modeling the I-type is performed. However, in this case, the pickup volt-per-hertz ratio and the related time delay settings of the first *gp3* model are set to the definite-time pickup volt-per-hertz ratio and the related time delay

of the relay. The other 9 *gp3* models are set based on the 9 sampled points from the inverse-time function of the related relays (extracted from the manual of the relay).

Note that the volt-per-hertz settings for the relays are provided in per unit based on the rated voltage of the generator and the nominal frequency of the system. The same per unit base is used by the *gp3* model. Therefore, no conversion is required. However, if the voltage and/or frequency is provided in per unit with other per unit bases, the proper base conversion can be done using (6.38).

$$V/Hz_{pickup}(p.u.) = \frac{V/Hz_{pickup,old}(p.u.) \times V_{base,old} \times f_{rated}}{V_{rated} \times f_{base,old}} \quad (6.38)$$

In (6.38), $V/Hz_{pickup}(p.u.)$ is the pickup volt-per-hertz ratio in p.u. based on the nominal voltage of the generator and nominal frequency of the system. $V_{pickup,old}(p.u.)$ is the pickup volt-per-hertz ratio in p.u. based on any different base voltage ($V_{base,old}$) and base frequency ($f_{base,old}$) that is used to calculate the per unit values for volt-per-hertz relay pickup in the setting file. V_{rated} is the nominal voltage of the generator, and f_{rated} is the nominal frequency of the system.

6.10 Test system and simulation results

Various generator protective relays introduced in this chapter is modeled on the generators in the area under study using the described procedures. The dynamic models of these protective relays are included in the dynamic file of the system that is used for performing transient stability studies. To analyze the performances of the generator protective relays modeled on the generators, different type of contingencies including line

faults and bus faults followed by the outage of one or more transmission lines, as well as generator outage contingencies are studied on the test system.

The WECC system data representing the 2028 planning case is considered as the test system. The system includes 25649 buses, 19728 transmission lines, and 4648 generators. The maximum generation capacity of the system is roughly 309 GW, and the load of the system is roughly 184.5 GW. Within the WECC system, a specific area including more than 750 buses, 720 transmission lines, and 100 generators is specifically considered for more detailed studies.

Overall, more than 400 contingencies are studied and the performance of the modeled protective relays along with their impacts on the behavior of the related generator, the other generators in the area, and the loads in the area are evaluated.

6.10.1 simulation results and case studies

Table 6.3 shows how many cases of different generator protective relay operations as well as the limiting actions of OEL and UEL were observed during performing transient stability studies on all the contingencies. Note that, except for the operations of OEL and UEL (which only imposes limit on the field current of the related generators), all other relay operations listed in Table 6.3 leads to tripping of the related generators. As can be seen in Table 6.3, generator protective relay operations occur frequently during different contingencies. Some of these generators that are tripped during the studied contingencies generate a large amount of active and reactive power and their outage have a significant impact on the behavior of the system (especially within the area under study). Therefore, modeling these protective relays are critical for having precise transient stability studies

and performing transient stability studies without modeling these protective relays might manifest incorrect behavior of the system.

Table 6.3 The number of generator protective relay operations during the studied contingencies

Relay	Number of the occurrences
Undervoltage and overvoltage protection	39
Underfrequency and overfrequency protection	19
Phase distance protection	37
Overcurrent protection	30
Overexcitation limiter	57
Underexcitation limiter	145

To further show how each protective relay operation can impact the behavior of its related generator, the other generators, and the system in overall, five case studies are selected among the studied contingencies for a more detailed analysis. Case studies 1 and 2 are provided to show the impact of UEL and OEL action on the dynamic behavior of the related generator. Note that, since these are limiting action and they do not result in tripping of the generator, the impacts on the system are negligible. Therefore, the impacts of these limiting actions on other generators and loads are not included in Case study 1 and 2. Case study 3 and 4 are provided to show how the phase distance and overcurrent relays of generators operate during a contingency and what is the impact of these operation on the dynamic response of the related generator and the system. Case study 5 provides an instance of a more severe contingency (including multiple generator protective relay operations as well as OEL and UEL actions) and evaluates the accumulated result of

modeling all these protective generators on the dynamic response of the related generators and the system. These case studies are provided in the remainder of this section. Note that, to keep the proprietary data, random numbers are used to refer to different power system assets.

6.10.1.1 Case study 1

In this case study, the impacts of the limiting action of the UEL of a 35 MVAr generator, called Gen1, on the dynamic response of the related generator are studied. The contingency studied in case study 1 is a 3-phase line fault on a 500 kV line, called Line 1, that is cleared 0.05 s later by opening the line. The UEL action of Gen1 starts at 4.7 s (3.7 s after the fault).

Figure 6.26 shows the output signal of the UEL, i.e., *vuel*. Note that, the magnitude of *vuel* depends on the magnitude of the error signal, *vuer*, which itself depends on the amount of the violation of the output reactive power of Gen1 from its reference value. The impact of the UEL action on the field current and the output reactive power of Gen 1 is illustrated in Figure 6.27 and 6.28, respectively. As can be seen in these figures, after the operation of the UEL at 4.7 s, the UEL action boosts the field current and consequenly, the reactive power in order to prevent the generator from operating in underexcited condition. With boosting of the field current by the UEL action, the magnetic flux produced by the field winding increases, which in turn leads to an increase in the induced EMF. As equation (6.39) indicates, the terminal voltage of a synchronous generator is proportional to the induced EMF. Therefore, the increase in the EMF leads to an increase in the terminal voltage of the generator, as well. This increase can be seen in Figure 6.29 that illustrated

the terminal voltage of Gen 1. Note that, in (6.39), I_A is the terminal current of the generator. R_A and X_A are the armature (stator) resistance and reactance, respectively.

$$V_A = E_A - I_A(R_A + jX_A) \tag{6.39}$$

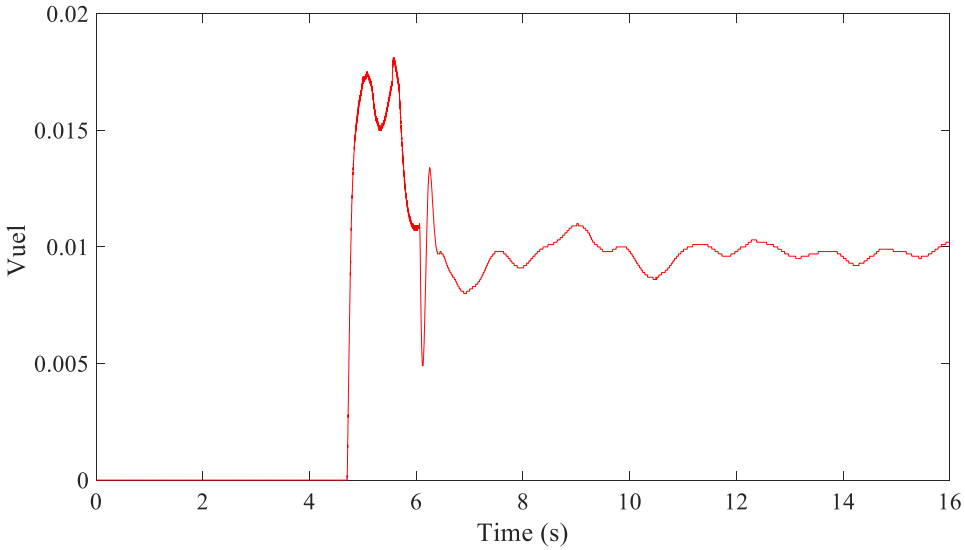

Figure 6.26 Output of the UEL of Gen1 (case study 1)

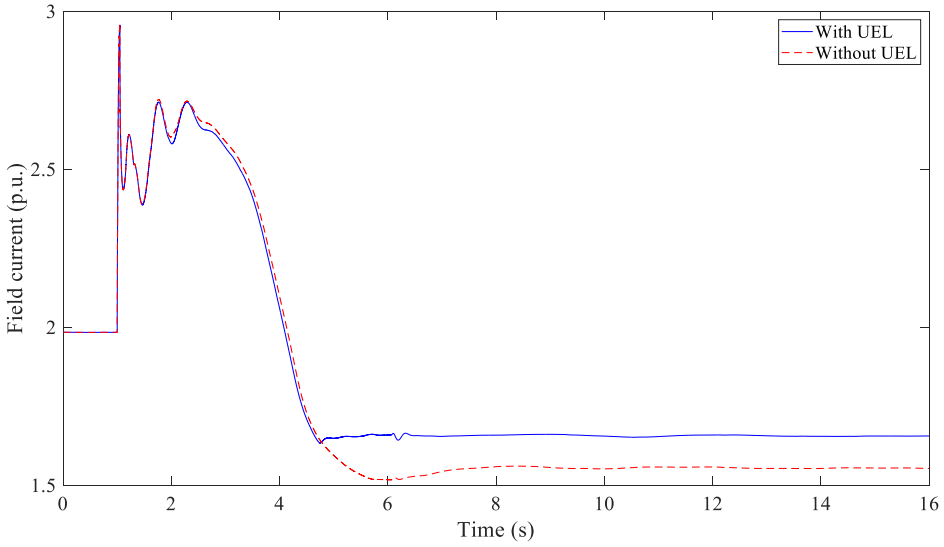

Figure 6.27 Field current of Gen 1 (case study 1)

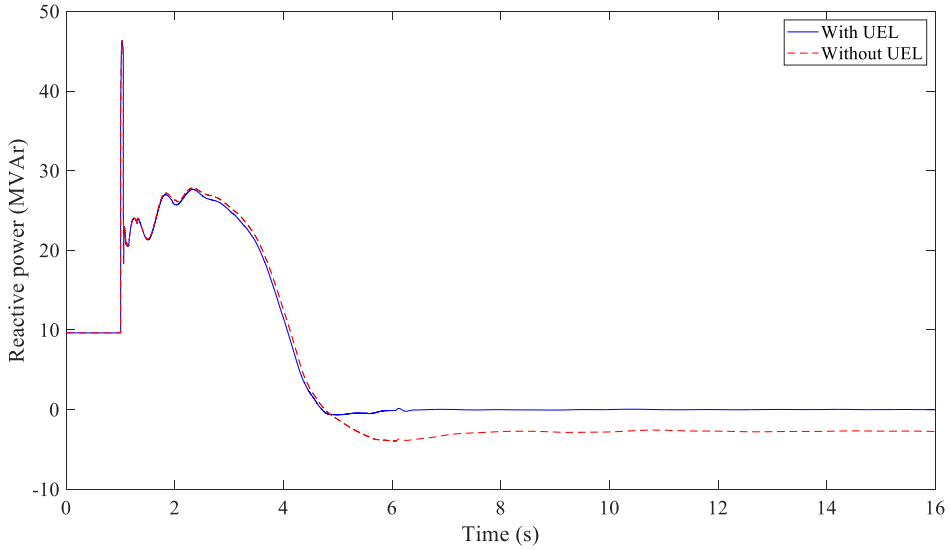

Figure 6.28 Reactive power of Gen 1 (case study 1)

6.10.1.2 Case study 2

The objective in this case study is to evaluate the impacts of the limiting action of the OEL of a 200 MVAr generator, called Gen 2, on the dynamic response of the generator. A 3-phase line fault on a 500 kV line, called line 2, that is cleared 0.05 s later by opening the

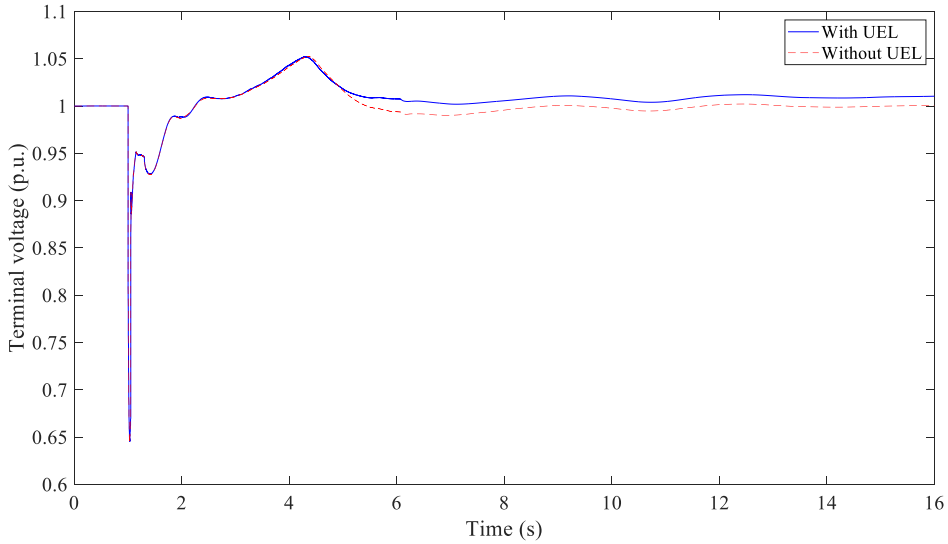

Figure 6.29 Terminal voltage of Gen1 (case study 1)

line is considered as the contingency to be analyzed in this case study. The OEL action of Gen 2 starts at 2.3 s (1.3 s after the fault).

The output signal of the OEL, i.e., *voel*, is illustrated in Figure 6.30. As seen in this figure, after the start of the OEL action at 2.3 s, *voel* starts to ramp in the negative direction with the slope of $1/Runback$. When the field current decreases to the maximum continuous field current level, defined by *Ifcont*, at 3.8 s, the ramping stops and the value of the *voel* remains constant. Figures 6.31 and 6.32 depict the impact of the OEL action on the field current and the output reactive power of Gen 2, respectively. As seen in these figures, with the start of the OEL action at 3.8 s, the OEL decreases the field current and consequently the reactive power of Gen 2 to prevent the generator from operating in overexcited condition. In this condition, the decrease in the field current leads to a decrease in the magnetic flux produced by the field winding, which in turn leads to a decrease in the induced EMF. According to (6.39), this decrease in the EMF leads to a decrease in the terminal voltage of the generator. This decrease in the terminal voltage with modeling OEL function of Gen 2 is illustrated in Figure 6.33.

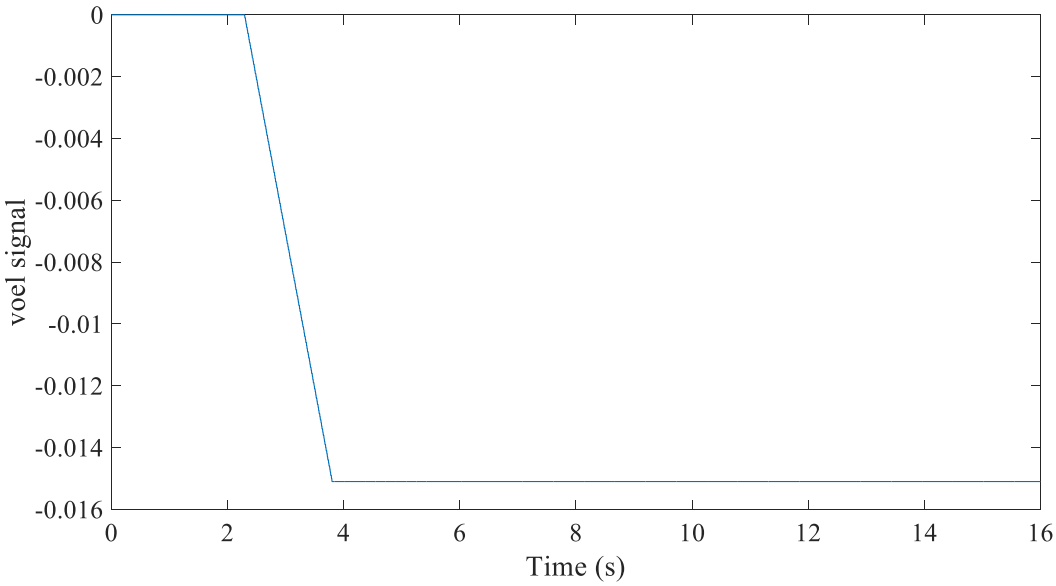

Figure 6.30 Output of the OEL of Gen 2 (case study 2)

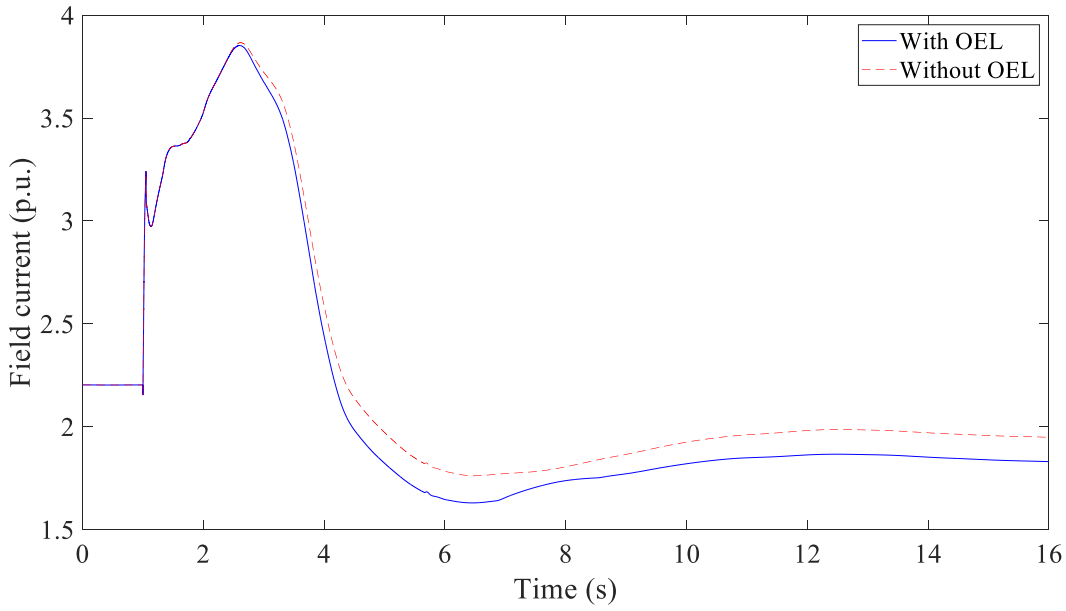

Figure 6.31 Field current of Gen 2 (case study 2)

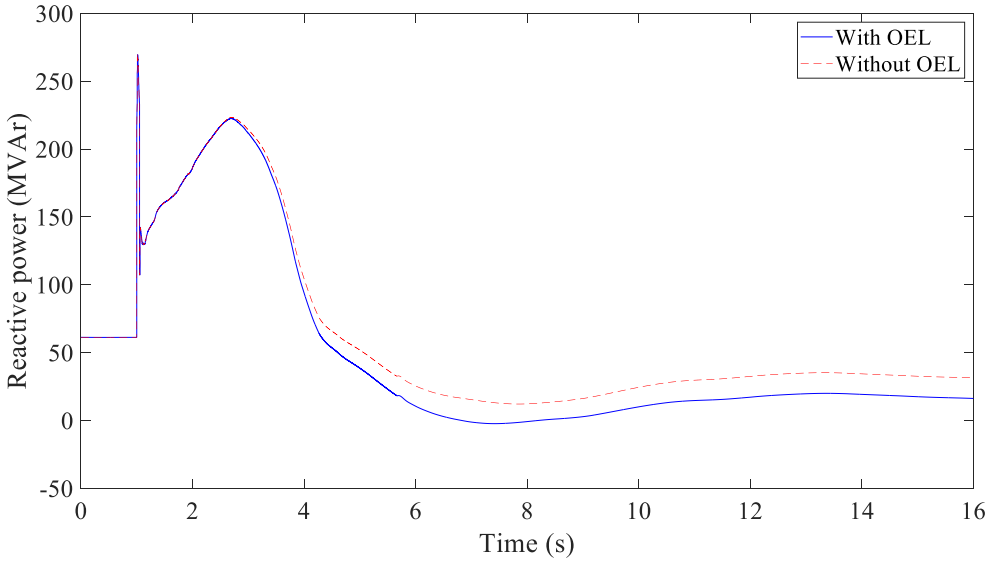

Figure 6.32 Reactive power of Gen 2 (case study 2)

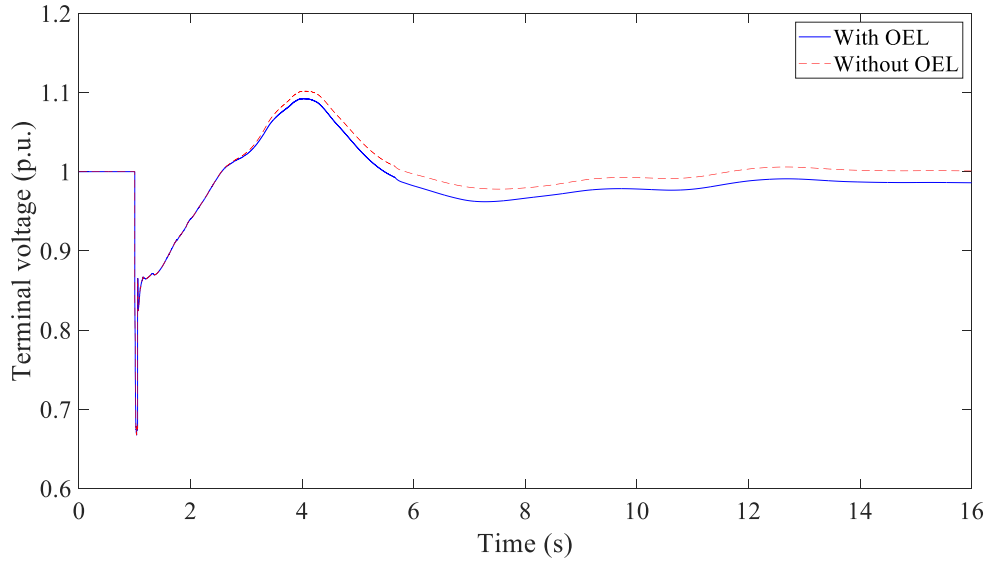

Figure 6.33 Terminal voltage of Gen 2 (case study 2)

6.10.1.3 Case study 3

In this case study, the impacts of generator phase distance relay operations (which leads to tripping of the generators) on the behavior of the related generators, other generators in the area, and the loads in the area are investigated. The contingency analyzed in this case

study is a bus fault on a 500 kV bus, called Bus 1, which is cleared by tripping two generators, called Gen 3 and 4, along with their step-up transformers at 1.2 s (0.2 s after the fault). The rated MVA of the tripped generators are 205 and 319 MVAr, and they are connected to the faulted bus through their step-up transformers. The contingency leads to the phase distance relay operations of three 205 MVAr generators—called Gen 5, 6, and 7—and one 319 MVAr generator, called Gen 8. All the mentioned phase distance relays operate at 1.25 s (0.25 s after the fault). With operation of the phase distance relays, the step-up transformers of Gen 5-8 are taken out of the service, which leads to islanding of these generators. Due to the islanding, Gen 5-8 start to lose synchronism and eventually, the overfrequency protection of these generators trip Gen 8 at 1.53 second and Gen 5-7 at 1.66 second.

Figure 6.34 shows the impedance trajectory observed by the phase distance relay of Gen 5 at steady-state condition and during the disturbance. During the disturbance, the impedance trajectory traverse into both zone 1 and 2 of the mho characteristic of the relay. The impedance trajectory remains inside the zone 1 for a period equal to the zone 1time delay of the relay. Hence, the relay operates and trips the generator. Similar figures can also be obtained for the phase distance relays of Gen 6, 7, and 8. However, for brevity, only the impedance trajectory and the phase distance relay characteristics of Gen 5 are provided.

Figure 6.35 and 6.36 shows the terminal voltages and currents of Gen 5-8. As seen in these figures, after operation of phase distance relays of Gen 5-8 at 1.25 s the terminal currents of these generators drop to zero. Also, as mentioned, with operation of phase

distance relays, the generators are isolated from the grid and considering that the generators are also tripped by the operations of their overfrequency relays, there is no voltage support for the terminal voltages of Gen 5-8. Therefore, as seen in Figure 6.36, the terminal voltage drops significantly in this contingency.

To evaluate the impact of these phase distance relay operations and the outage of Gen 5-8 on other generators in the area under study, the field current, and the terminal voltages of a set of generators in the area are provided in Figures 6.37, and 6.38, respectively. Note that for clarity, Figures 6.37 and 6.38 are provided in the zoomed in mode.

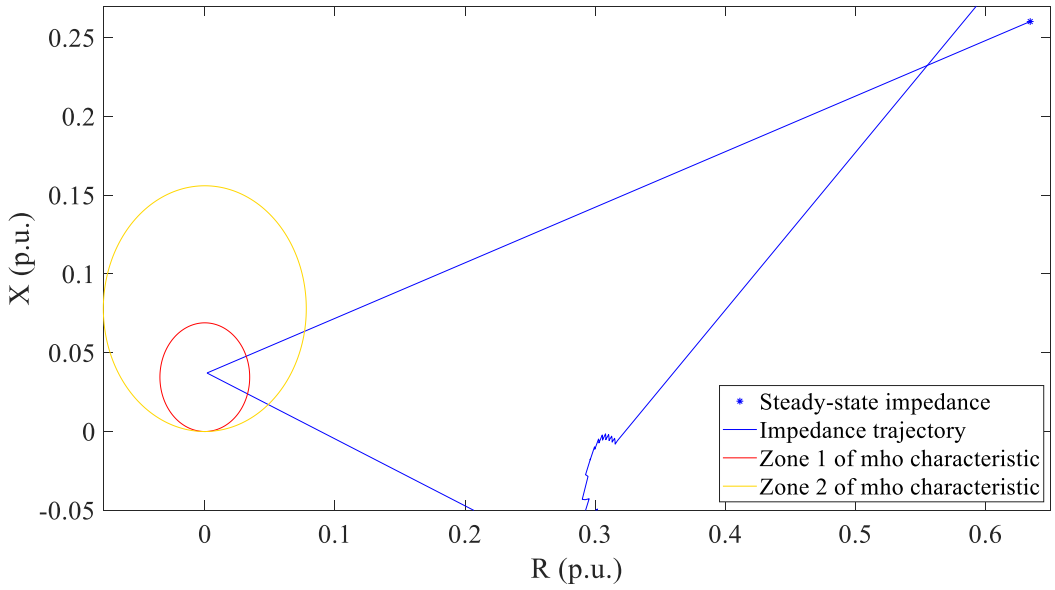

Figure 6.34 Impedance trajectory observed by the phase distance relay of Gen 5 and its mho characteristics (case study 3)

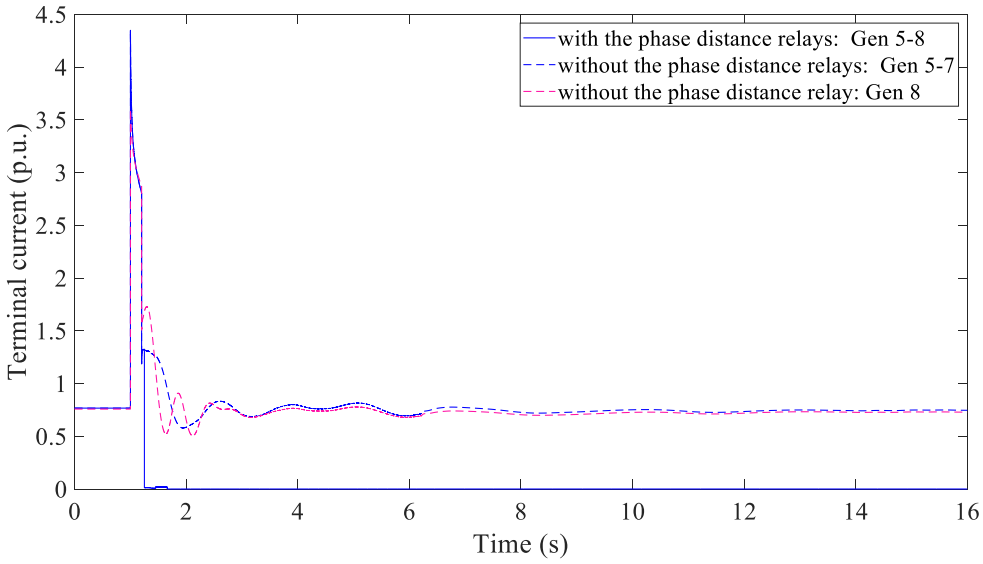

Figure 6.35 Terminal currents of Gen 5-8 (case study 3)

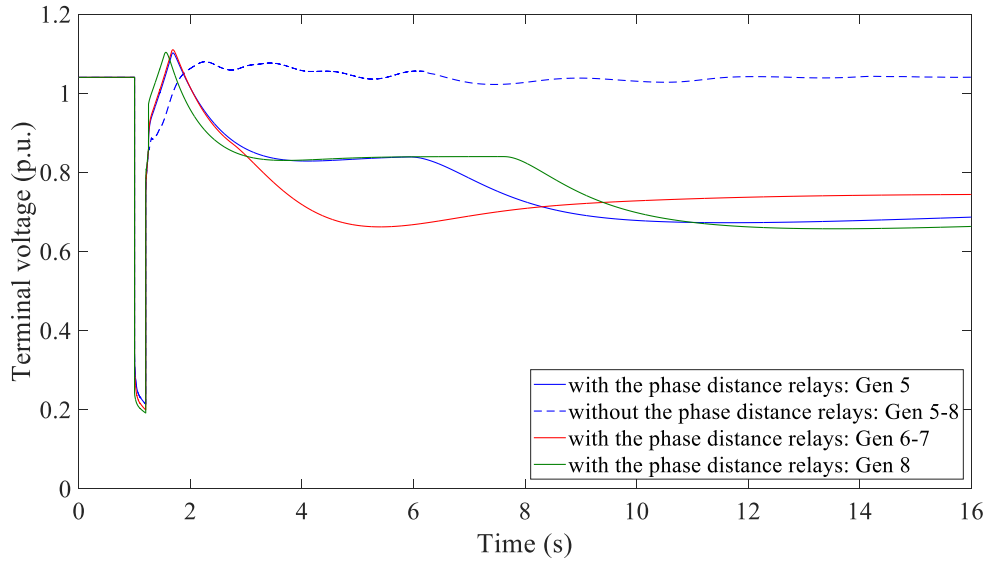

Figure 6.36 Terminal voltage of Gen 5-8 (case study 3)

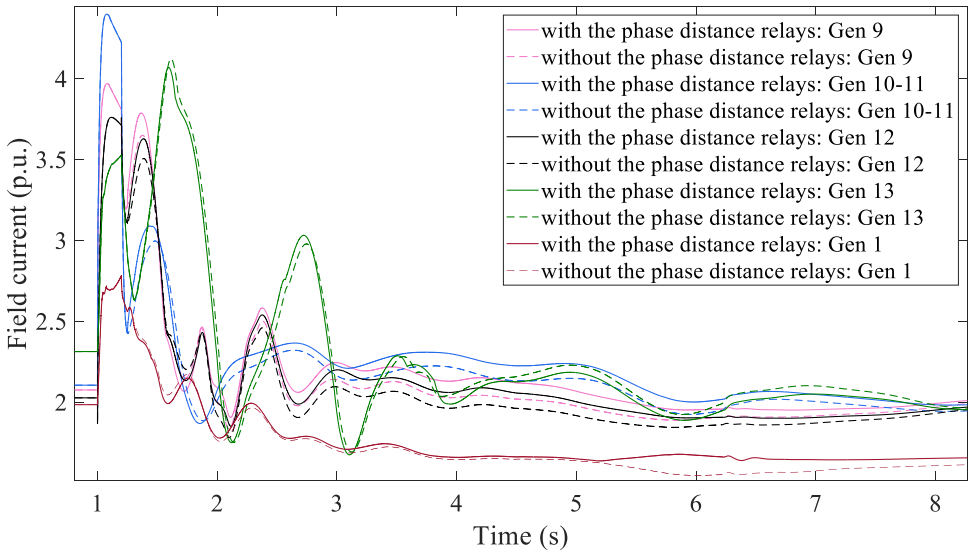

Figure 6.37 Field currents of a set of generators (case study 3)

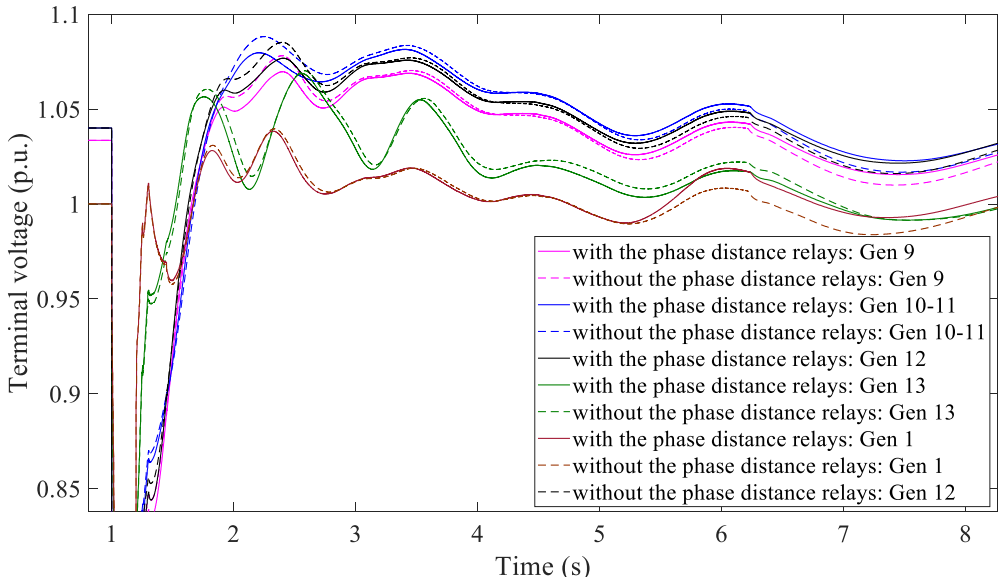

Figure 6.38 Terminal voltages of a set of generators (case study 3)

As seen in Figures 6.37 and 6.38, as a result of the phase distance relay operations of Gen 5-8, the field current and the terminal voltage of other generators in the area under study, especially Gen 1, are impacted. This shows the importance of modeling generator protective relays in having a more precise assessment of system behavior.

The impacts of the phase distance relay operations of Gen 5-8 on the loads in the area under study in terms of the voltage of the load buses is illustrated for a set of the loads in the area in Figure 6.39.

As seen in Figure 6.39 the operation of phase distance relays impacts the voltages of the load buses. Thus, the voltages of the load buses are not similar in both cases of modeling and not modeling generator protective relays. In terms of the active and reactive power of the loads, these phase distance relay operations specifically lead to a change in the active powers of Load 2 and reactive powers of Load 3 and 4. These changes in the active power of Load 2 and reactive power of Loads 3 and 4 are illustrated in Figures 6.40 and 6.41.

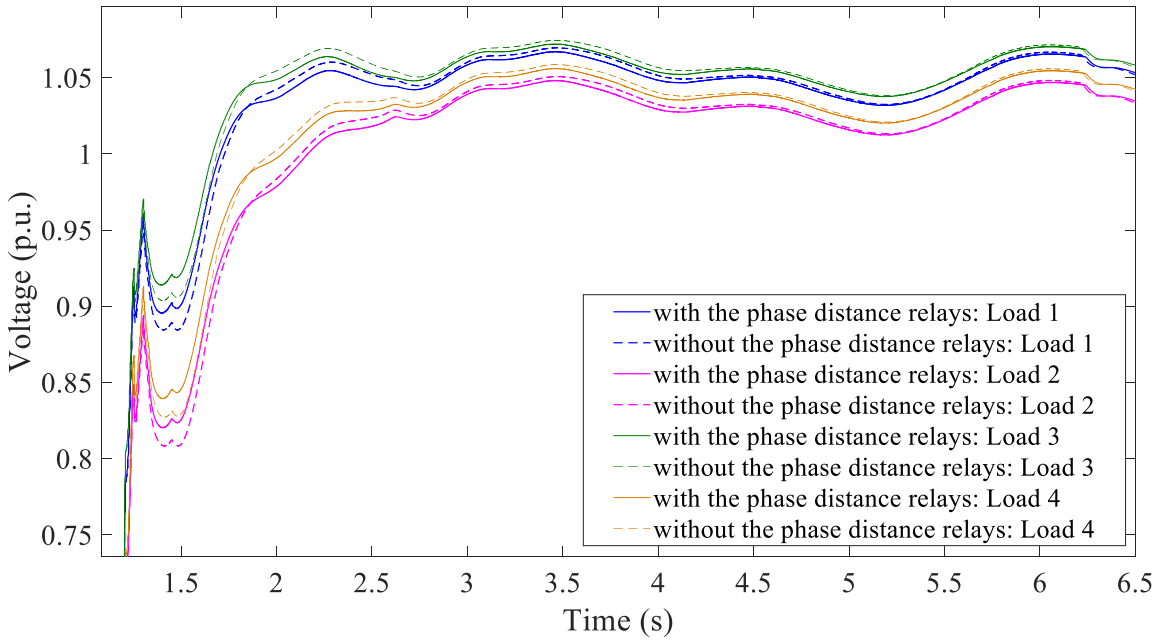

Figure 6.39 Load voltage of a set of loads (case study 3)

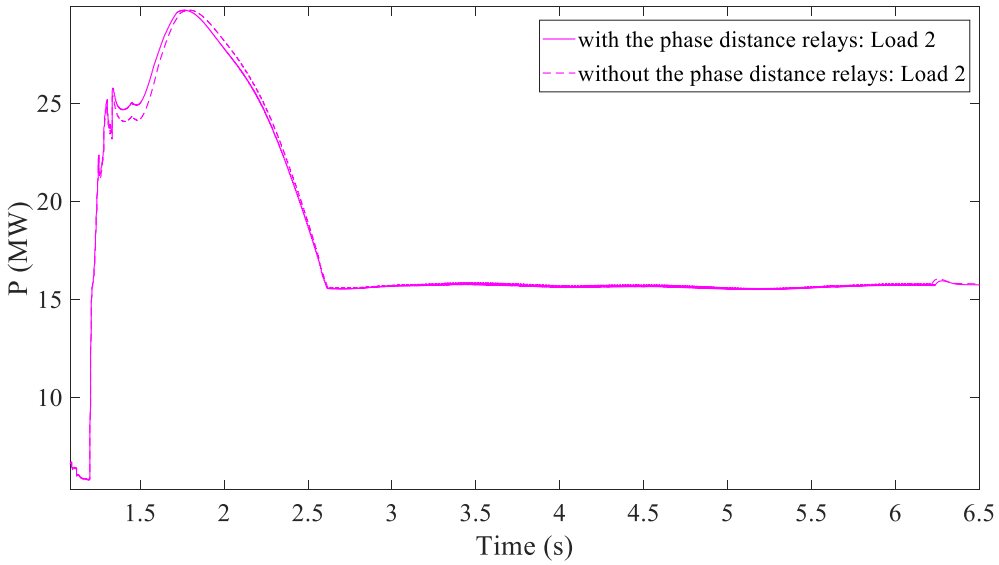

Figure 6.40 Active power of Load 2 (case study 3)

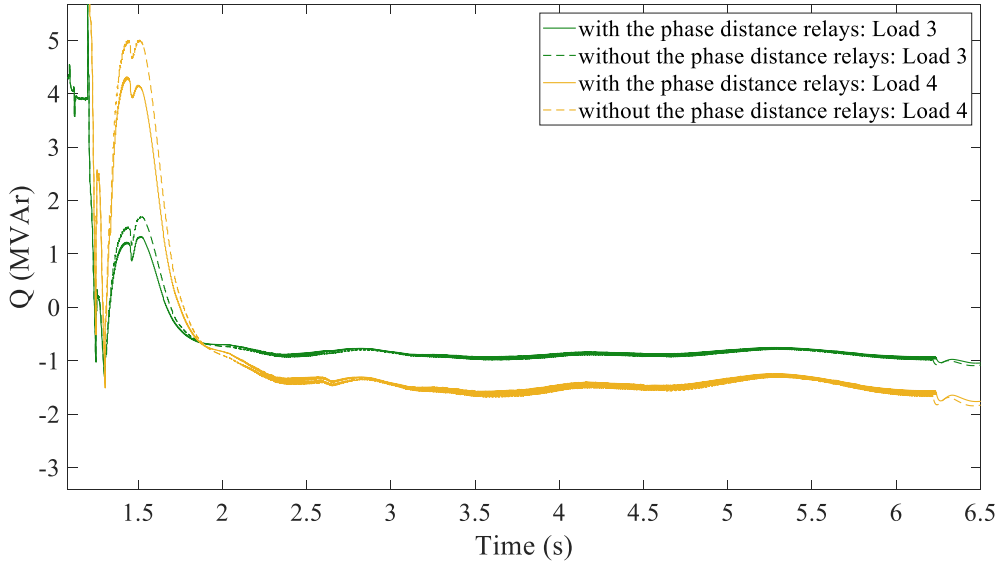

Figure 6.41 Reactive power of Load 3 and 4 (case study 3)

6.10.1.4 Case study 4

In this case study, the impacts of generator overcurrent relay operations (which leads to tripping of the generators) on the behavior of the related generators, other generators in the area, and the loads in the area are investigated. For this case study, a line fault contingency on a 500 kV line, called Line 3, is studied. The fault is cleared 0.05 s later by

opening the faulted line. During this contingency, the voltage-restraint time overcurrent relay of a 192 MVAr generator, called Gen 14, operated at 5.14 s (4.14 s after the fault) and tripped the generator. To show the impact of the relay operation on Gen 14 the terminal current and voltage of this generator is provided in Figure 6.42 and 6.43. As seen in Figure 6.42, the terminal current remains above the pickup current of the OC relay of Gen 14 (the red dashed line) long enough to cause the relay to operate and trip the generator. As seen, with tripping of Gen 14 at 5.14 s, the terminal current drops to zero, and the system experience the outage of this 192 MVAr generator. This outage cannot be seen without modeling the OC relay of Gen 14. Also, in the case of modeling the OC relay of Gen 14, the terminal voltage significantly drops, as a result of the tripping of Gen 14.

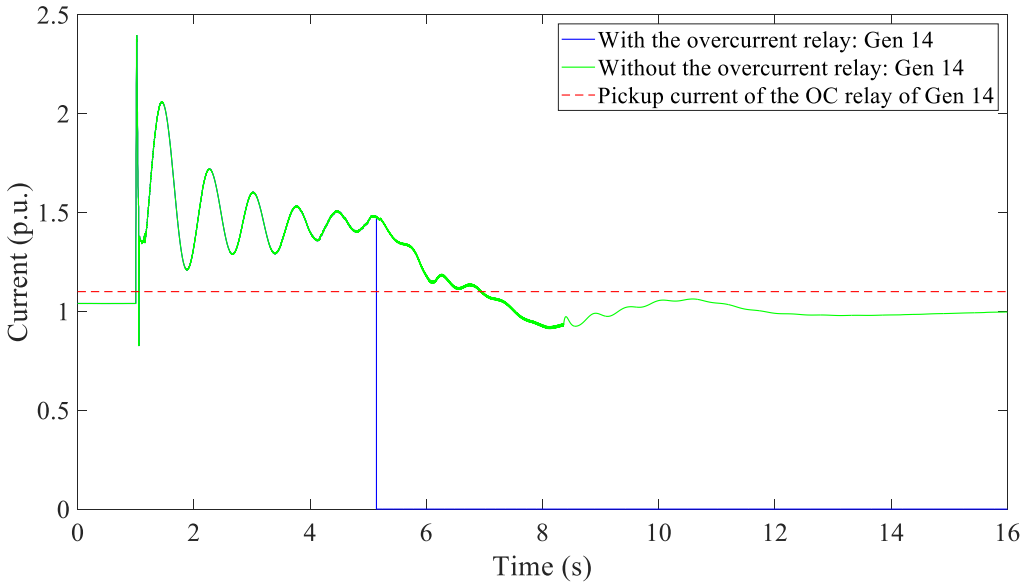

Figure 6.42 Terminal current of Gen 14 (case study 4)

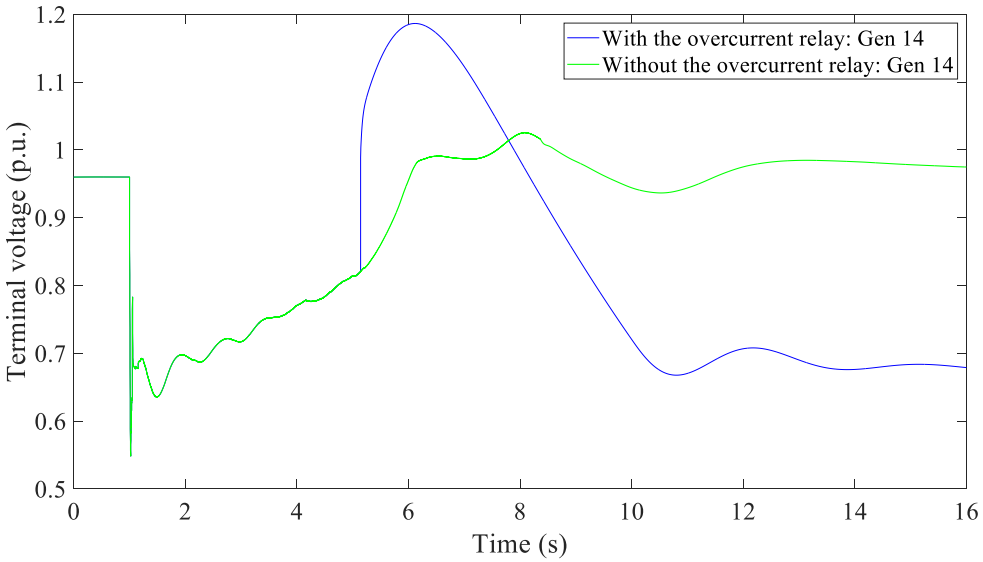

Figure 6.43 Terminal voltage of Gen 14 (case study 4)

To show the impact of the OC relay operation of Gen 14 on other generators in the area under study, the field currents and the terminal voltages of a set of generators in the area are illustrated in Figure 6.44 and 6.45. Note that, for clarity, the terminal voltages of the generators are shown in the zoomed mode in Figure 6.45.

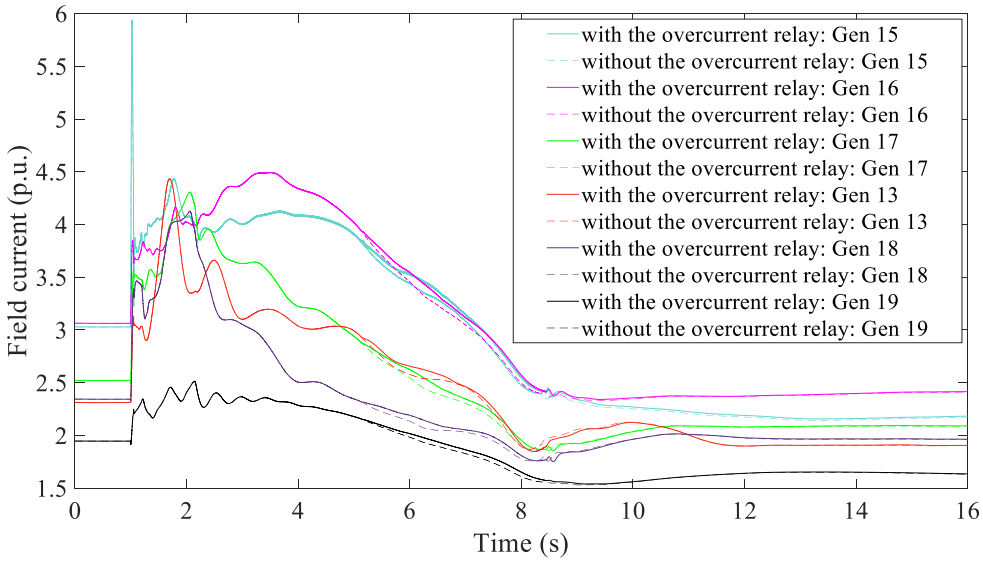

Figure 6.44 Field current of a set of generators (case study 4)

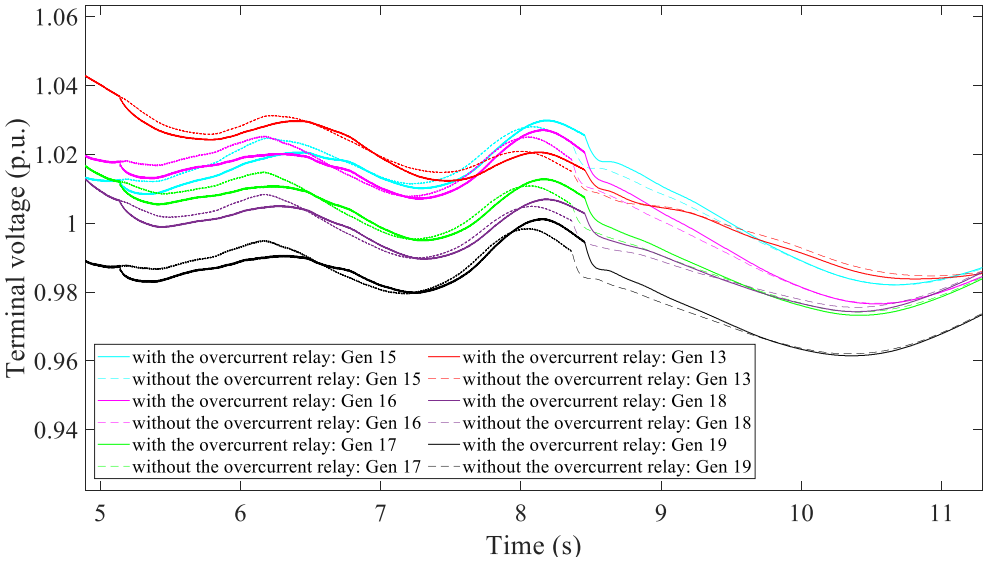

Figure 6.45 Terminal voltages of a set of generators (case study 4)

As seen in Figure 6.44 in the case of modeling the OC relay of Gen 14, the field current of the generators in the area under study are slightly more than the case of not modeling the relay. The reason is that in the case of modeling the OC relay of Gen 14, the operation of the relay leads to tripping of Gen 14. Therefore, the active and reactive power produced by Gen 14 should be picked up by the other generators, which lead to slight increase in the field current of these generators. As shown in Figure 6.45, this increase in the field current, in turns, leads to increase in the terminal voltages of these generators, as well.

To show the impact of the OC relay operation of Gen 14 on the loads in the area under study, the voltages of a set of the load buses in the area are provided in Figures 6.46. As seen in this figure, with modeling the OC relay of Gen 14, the voltages at load buses are significantly reduced due to the outage of Gen 14 at 5.14 s. This depressed voltage condition last for approximately 3 seconds. The sudden voltage drop in these load buses may lead to operation of any automatic under voltage load shedding relays that might be

installed on the load buses, and lead to undesired load shedding. Therefore, modeling this protective relay of Gen 14 is necessary for having a precise assessment of the response of the generator, itself, and the system.

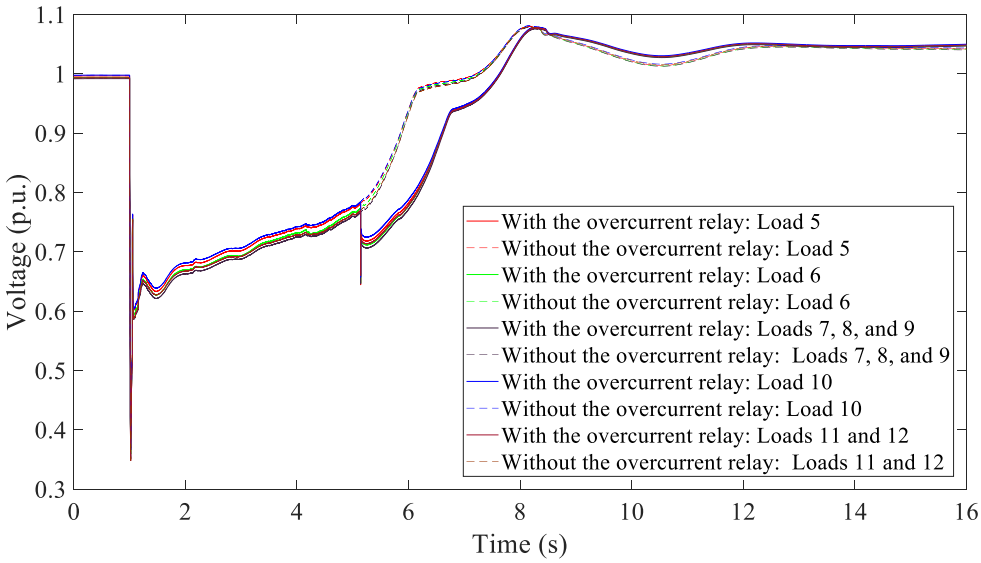

Figure 6.46 Load voltage of a set of loads (case study 4)

The active and reactive power of the set of loads are also provided in Figure 6.47 and 6.48. Note that, for clarity the set of loads is divided to two subset (Set 1 and 2) and the active and reactive power of each subset is shown in different figures in the zoomed mode.

As seen in Figure 6.47 and 6.48, the active and reactive power of the loads are also significantly impacted by the operation of OC relay of Gen 14, which further highlights the importance of modeling generator protective relays in transient stability studies.

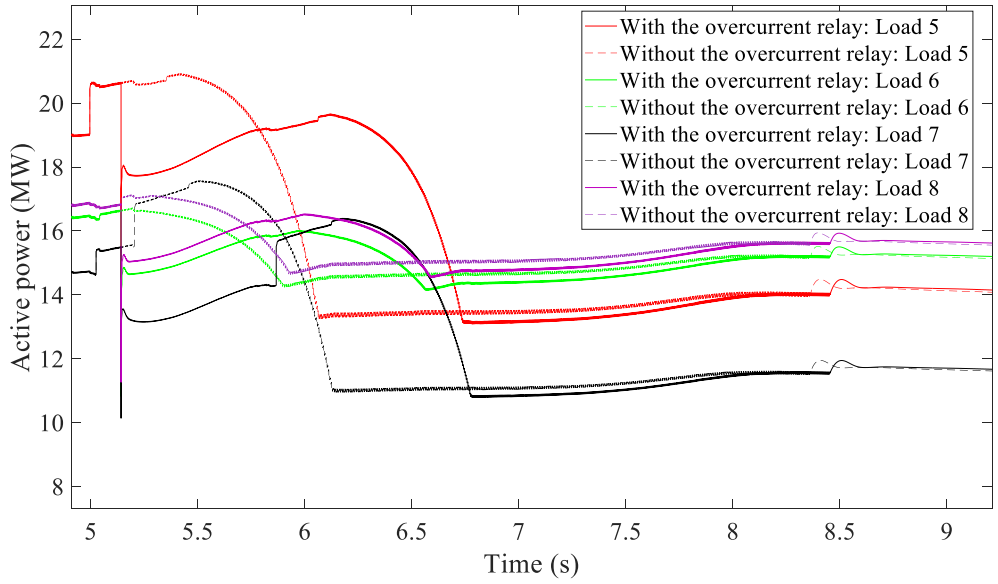

(a)

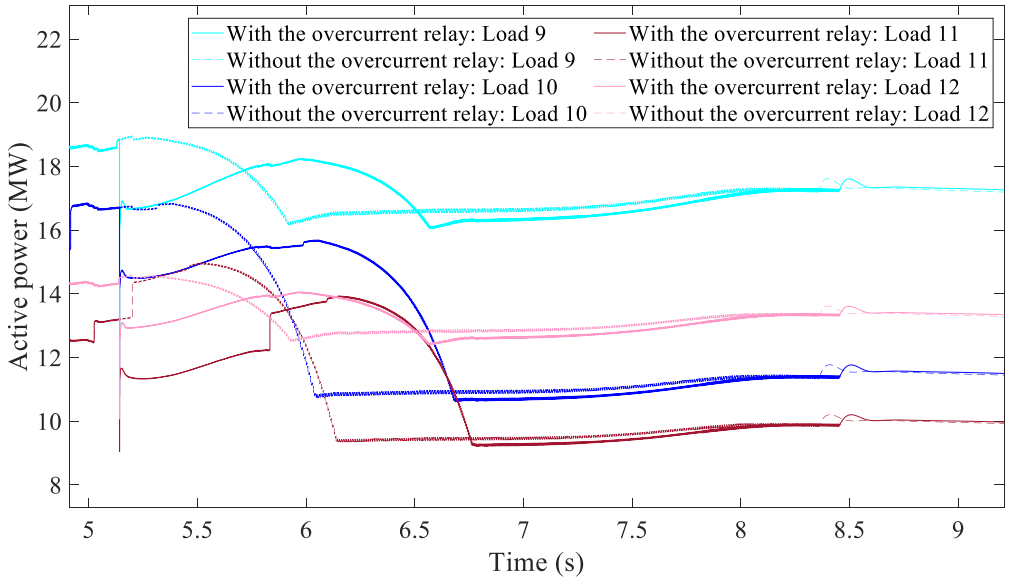

(b)

Figure 6.47 Active power of a set of loads (case study 4)

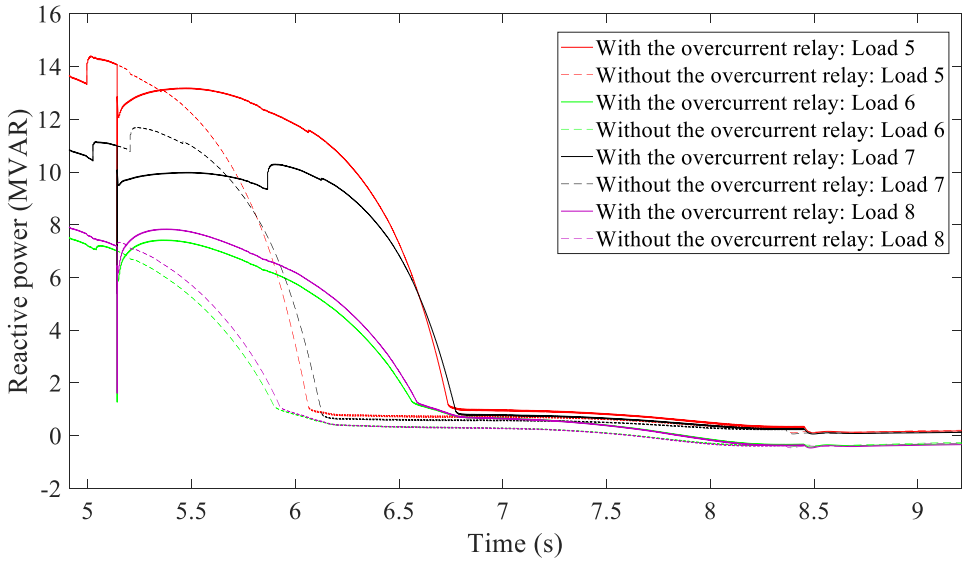

(a)

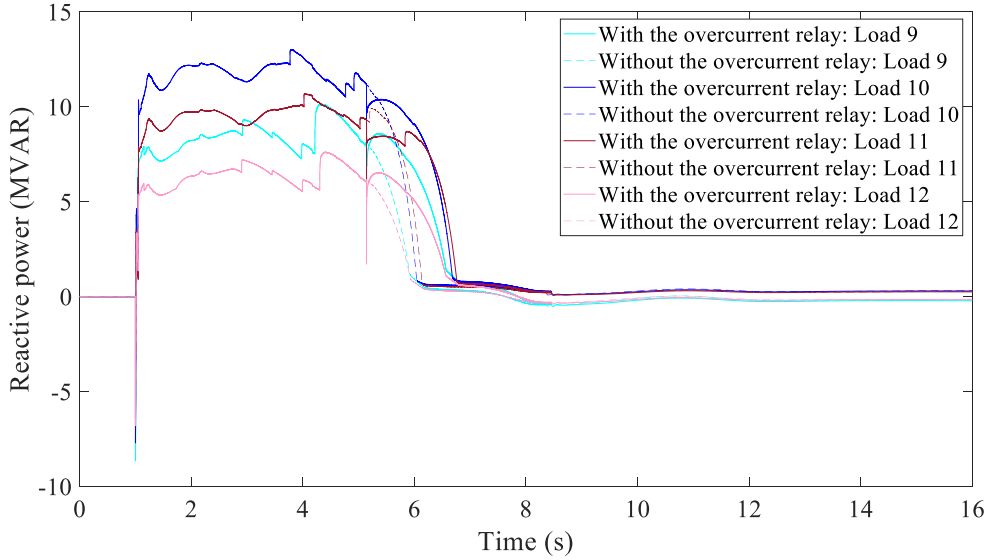

(b)

Figure 6.48 Reactive power of a set of loads (case study 4)

6.10.1.5 Case study 5

In this case study, the goal is to study the cumulative impacts of modeling all the described protective relays as well as OEL and UEL functions of the generators in the area under study on the response of the generators and the system during a severe contingency.

The results are compared with the case of not including any of the generator protective relays in transient stability study of the contingency. The contingency considered in this case study is a simulation of a real-world disturbance which occurred due to a wildfire. The contingency is simulated by applying a 3-phase line fault on 40% of Line 2 along with a bus fault on a 500 kV bus, called Bus 2. The fault is cleared after 4 cycles by tripping Line 2 and Line 3 (which is connected to Bus 2).

The list of the generator protective relay operations in the area under study as well as the OEL and UEL actions of these generators during the contingency along with their operation time are provided in Table 6.4. One interesting observation during this contingency is both the OEL and UEL actions for Gen 2. This severe contingency leads to a sudden overshoot in the field current of Gen 2 and consequent OEL action of Gen 2 at 2.54 s. Then, the field current decreases to a level that leads to UEL action at 7.14 s. The impacts of OEL action of Gen 2 are illustrated in Figure 6.49 and 6.50 by comparing the field current and terminal voltage of Gen 2 in two cases of modeling the OEL and not modeling the OEL function of Gen 2. Likewise, the impacts of the subsequent UEL action of Gen 2 on the field current and terminal voltage of this unit are depicted in Figure 6.51 and 6.52.

Table 6.4 List of protective relay operations and OEL/UEL actions in case study 5

Generator	Protection function	Operation time (s)
Gen 14	Overcurrent	4.99
Gen 20	Overcurrent	3.56
Gen 2	OEL	2.54
Gen 17	OEL	4.08
Gen 2	UEL	7.14
Gen 1	UEL	6.56

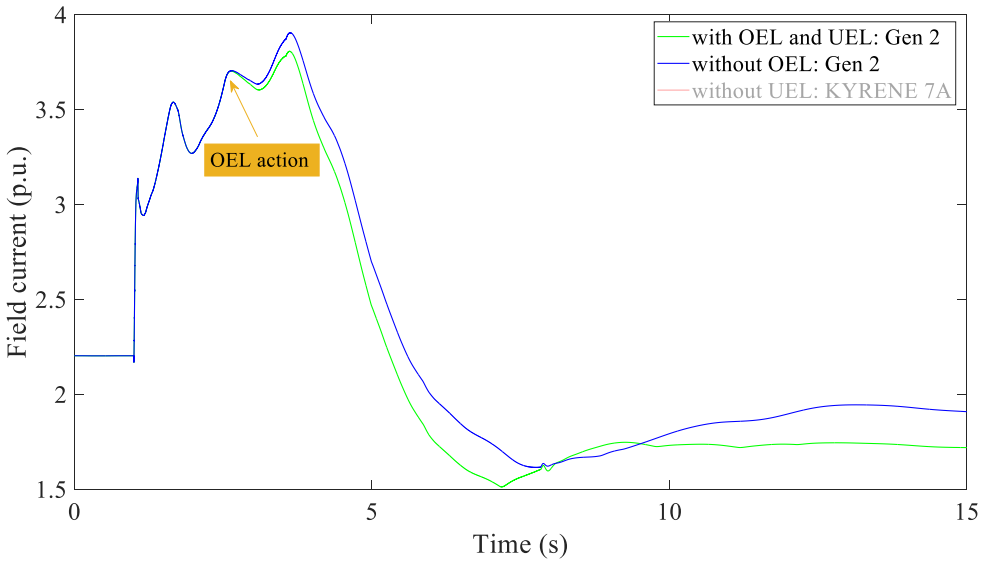

Figure 6.49 Field current of Gen 2 with and without modeling OEL function

(Case study 5)

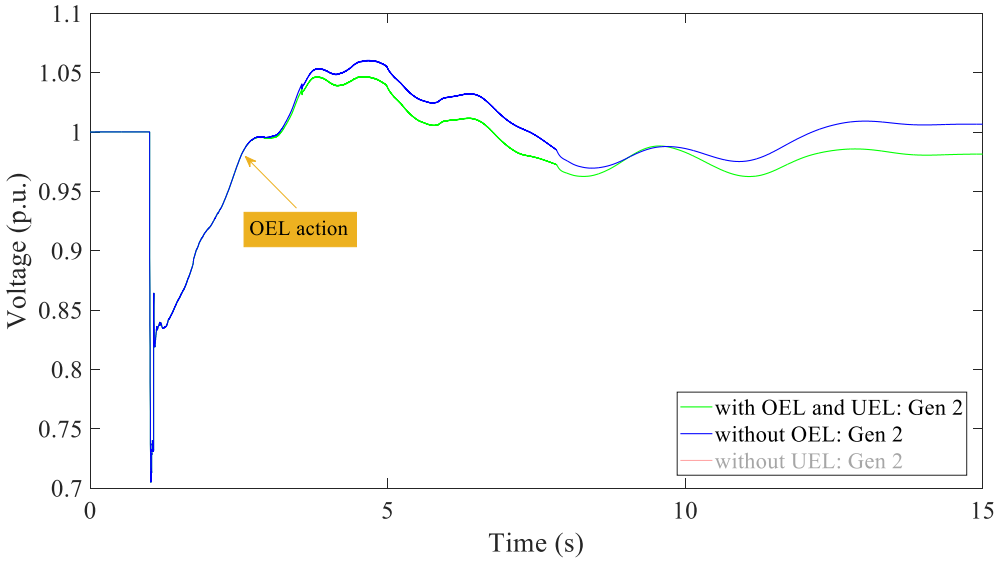

Figure 6.50 Terminal voltage of Gen 2 with and without modeling OEL function

(Case study 5)

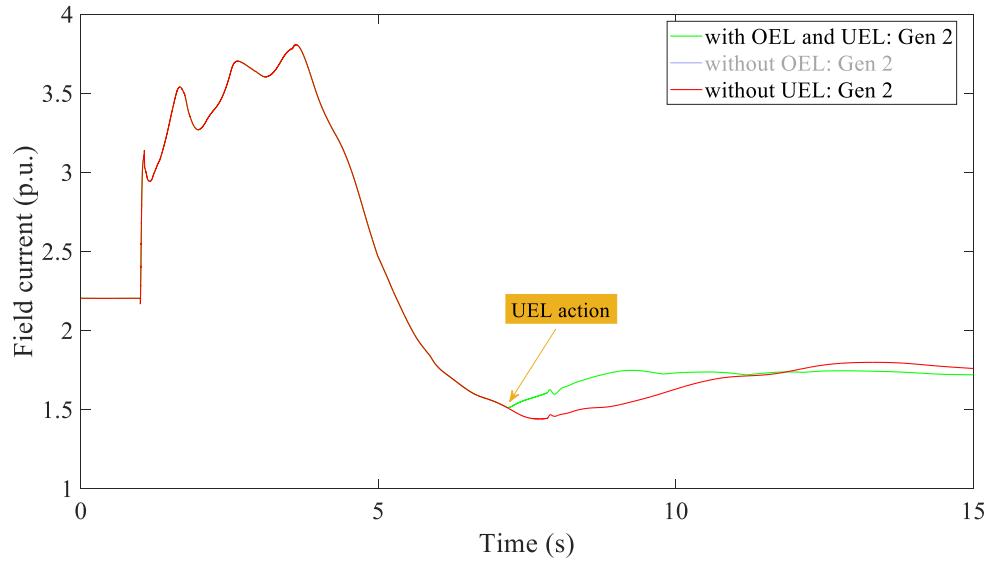

Figure 6.51 Field current of Gen 2 with and without modeling UEL function

(Case study 5)

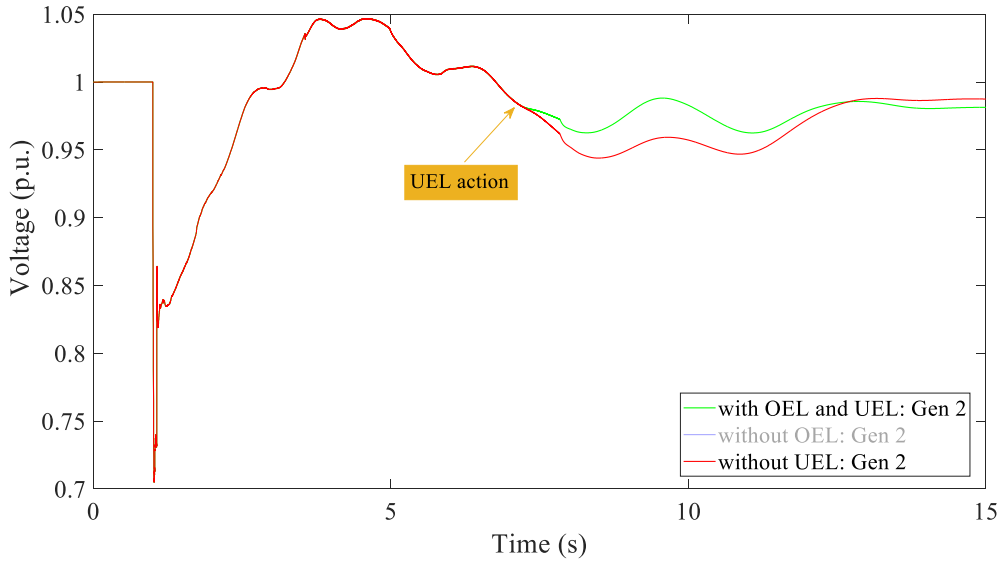

Figure 6.52 Terminal voltage of Gen 2 with and without modeling UEL function (Case study 5)

As seen in Figure 6.49, with the OEL action of Gen 2 at 2.54 s, the field current of Gen 2 decreases to prevent the generator from operating in the overexcited condition. This is the reason that the green curve (the field current with modeling OEL and UEL functions) remains below the blue curve (the field current without modeling OEL function). As explained earlier in this chapter, the decrease in the field current with modeling OEL function of Gen 2 leads to a decrease in the terminal voltage of this generator, as well. This decrease in terminal voltage of Gen 2 can be seen in Figure 6.50. As shown in Figure 6.51, after the UEL action of Gen 2 at 7.14 s, the green curve (the field current with modeling OEL and UEL functions) remains above the orange curve (the field current without modeling UEL function). This shows that at 7.14 s the field current is boosted by the UEL action to prevent the generator from operating in an underexcited condition. This increase

in the field current with modeling the UEL function leads to an increase in the terminal voltage of Gen 2. This increase in the terminal voltage is illustrated in Figure 6.52.

As seen in Table 6.4, the overcurrent relays of Gen 14 and 20 operate during this contingency and trip the generators. Furthermore, OEL actions of Gen 2 and 17 as well as UEL actions of Gen 1 and 2 are observed during this contingency. The impact of these overcurrent relay operations as well as the mentioned OEL and UEL actions on the dynamic response of other generators and loads in the area under study are evaluated.

Figure 6.53 shows the field current of a set of the generators in the area under study during the contingency. After tripping of Gen 20 at 3.56 s, the active and reactive power mismatch occurred due to the outage of Gen 20 should be compensated by other generators. This leads to an increase in the field current of all the generators, except Gen 2. This increase in the field current of the generators is observable in Figure 6.53, where the field currents with modeling generator protective relays are higher than the case of not modeling generator protective relays (the case in which the tripping of Gen 20 does not occur). The reason for the exceptional behavior of Gen 2 (having a lower field current with modeling generator protective relays) is the OEL action of Gen 2 that occurs at 2.54 s and prevent the field current of this generator from increasing like that of the other generators.

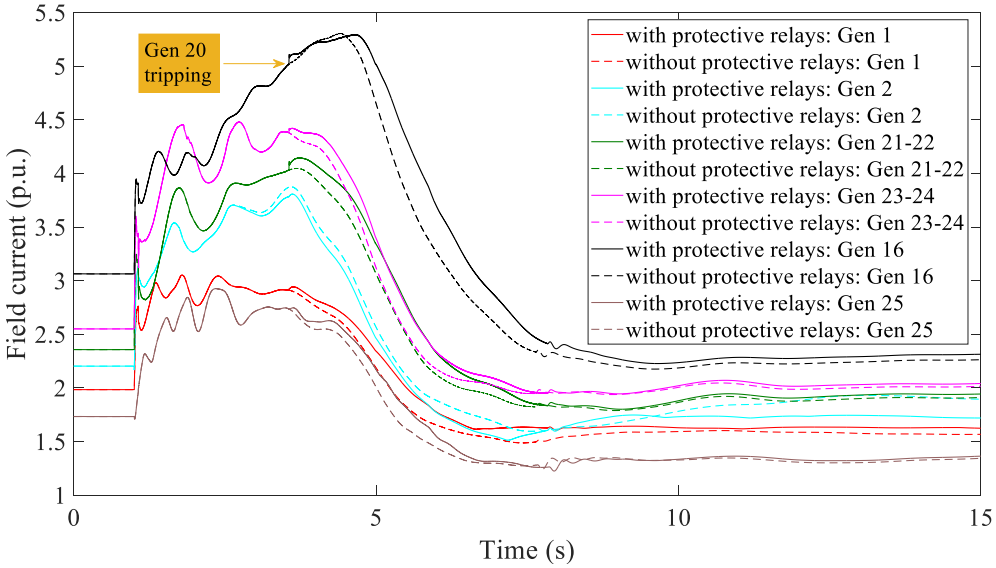

Figure 6.53 Field current of a set of generators (case study 5)

The terminal voltages of the set of generators are provided in Figure 6.54. As seen in this figure, after tripping of Gen 20, the terminal voltages of other generators in the area are also impacted. In this regard, a depressed terminal voltage condition is observed in the terminal voltages of all the generators due to outage of Gen 20. Figure 6.53 and 6.54 highlights the importance of modeling generator protective relays in performing a precise assessment of the dynamic behavior of the generators in the system.

To assess the impacts of modeling generator protective relays on the system loads, the voltages of a set of load buses are provided in Figures 6.55. As seen in this figure, the set of loads can be divided into two subsets, called Set 1 and 2. Set 1 includes Loads 13-15, and Set 2 includes Loads 6, 7, and 16. As seen in Figure 6.55, the impact of the outage of Gen 20 is more significant on the loads in Set 1, whereas the impact of outage of Gen 14 is more significant on the loads in Set 2 (although the loads in Set 1 are also impacted by the outage of Gen 14). The sudden significant voltage drop observed in the loads in Set 2 (which last about 3 seconds) has a potential to trigger any under voltage load shedding

relays that might exist in those load buses and lead to partial or complete loss of load. To show this impact on the active and reactive power of these loads in a clearer manner, the active power of the loads in Set 1 and 2 are illustrated in Figure 6.56 (a) and (b), respectively. Likewise, the reactive power of the loads in Set 1 and 2 are shown in Figure 6.57 (a) and (b), respectively.

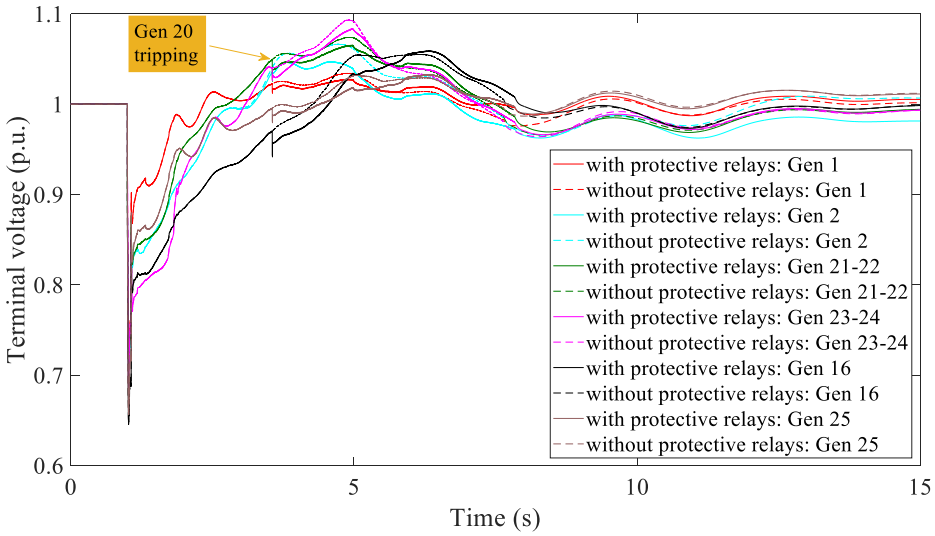

Figure 6.54 Terminal voltages of a set of generators (case study 5)

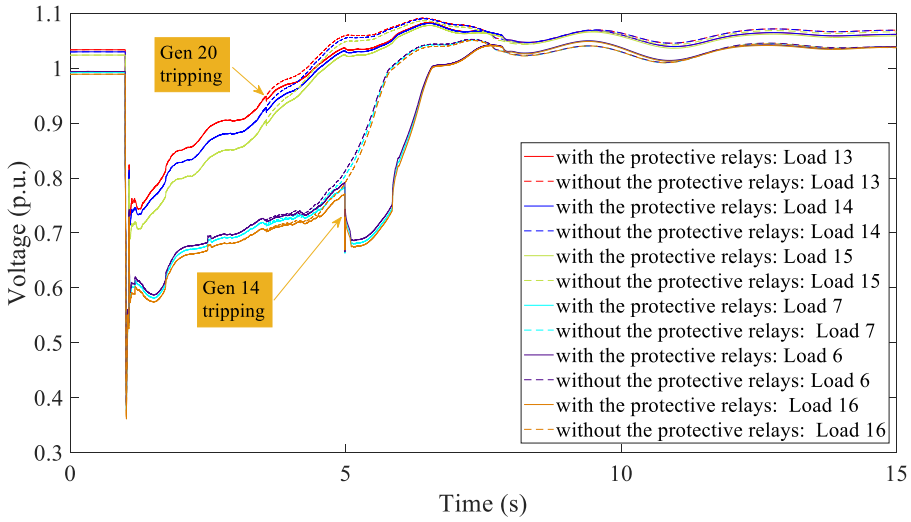

Figure 6.55 Load voltage of a set of loads (case study 5)

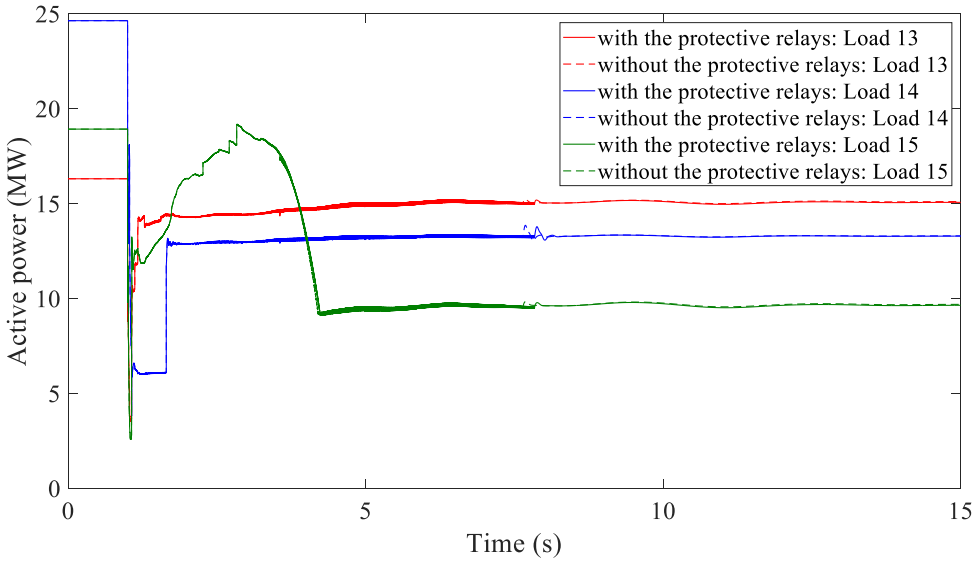

(a)

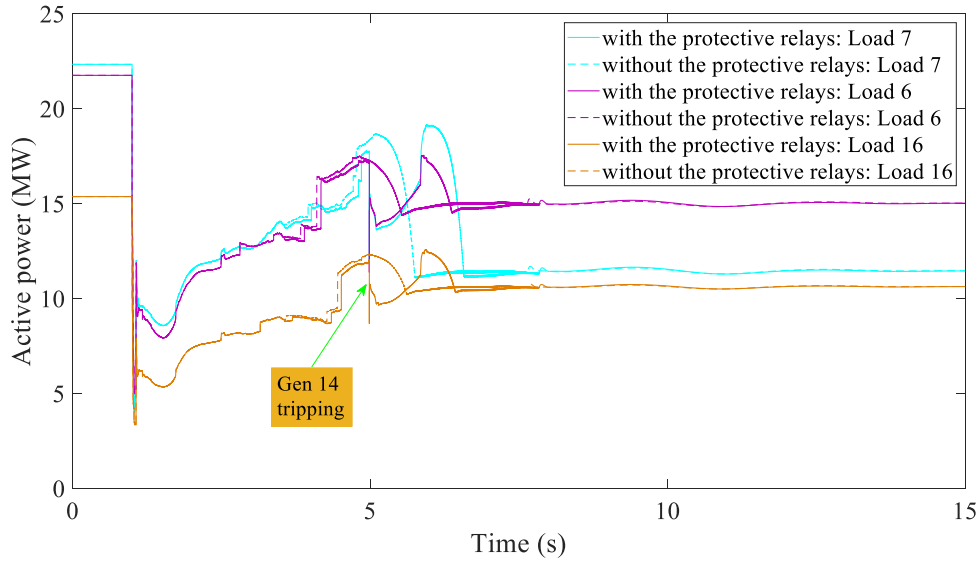

(b)

Figure 6.56 Active power of a set of loads (case study 5)

As seen in Figure 6.56 (a), the active power of the loads in Set 1 are not significantly impacted by the outage of Gen 20 and the active power of these loads are approximately the same in two cases of modeling and not modeling the generator protective relays. However, as seen in Figure 6.56 (b), the active power of the loads in Set 2 are completely

different in two cases of modeling and not modeling the generator protective relays, which shows the significant impact of the outage of Gen 14 on the behavior of these loads. The Same behavior can also be observed in Figure 6. 57 (a) and (b) for the reactive power of the loads in Set 1 and 2.

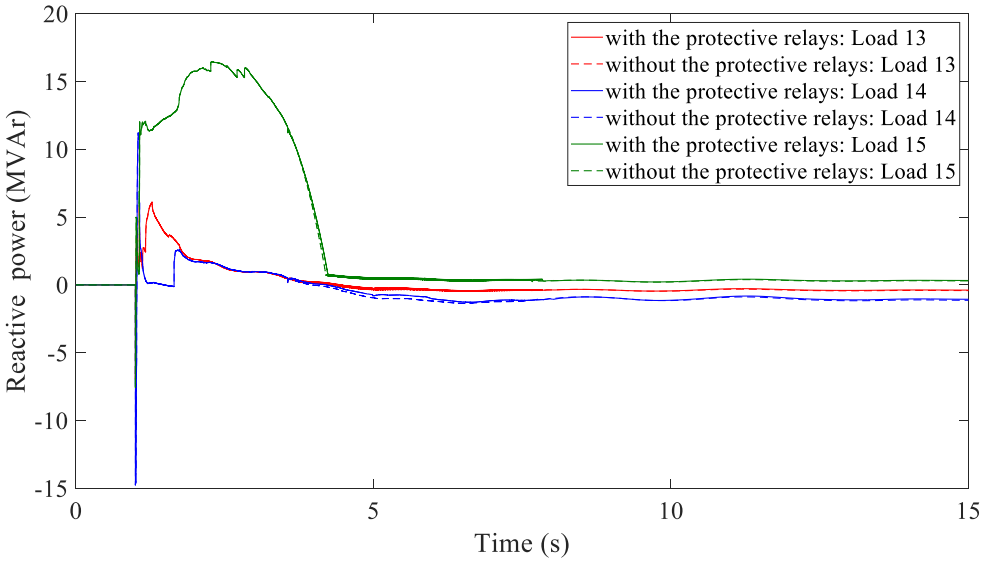

(a)

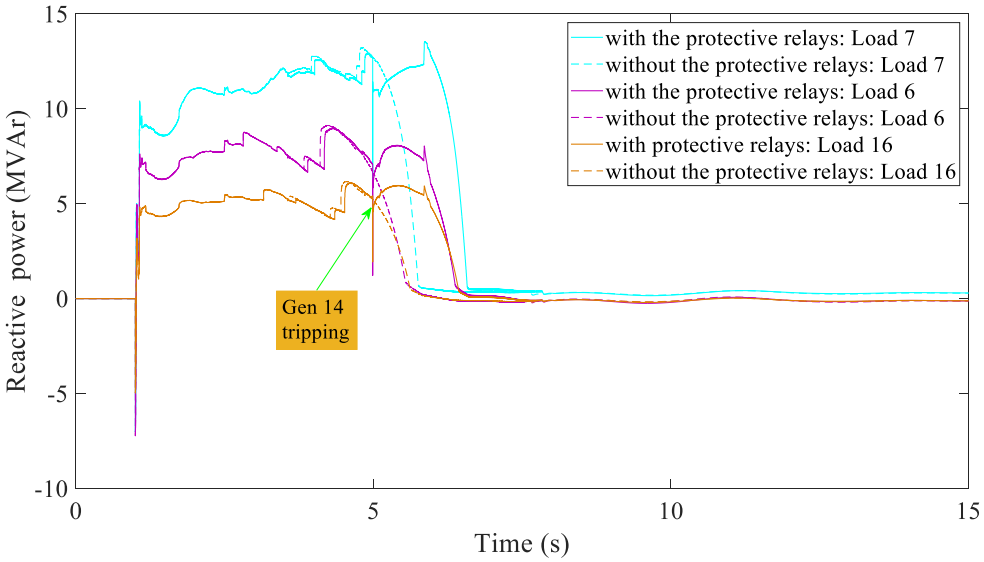

(b)

Figure 6.57 Reactive power of a set of loads (case study 5)

These case studies show that how modeling generator protective relays can significantly impact the behavior of the generators and the system. They also show that the results of transient stability studies performed without modeling generator protective relays might not precisely capture the behavior of the generator and the system. Therefore, modeling these protective relays as accurate as possible is vital for having precise transient stability studies.

6.11 Summary

In this chapter, the importance of modeling generator protective relays in performing precise transient stability studies is thoroughly explained. The capability curve of generators that imposes limitations on the capability of the generator for operating in overexcitation and underexcitation condition is also explained. Brief introductions of different generator protective relays as well as the OEL and UEL functions that are used in industrial generators along with their application and mechanism are also provided in this chapter. The proposed framework for precisely modeling generator protective relays as well as their OEL and UEL functions in transient stability studies is introduced and elaborated upon. Finally, 5 different case studies are performed on the WECC system data representing the 2028 planning case to study the impacts of modeling generator protective relays as well as their OEL and UEL functions on the results of the transient stability studies. It is observed that the operation of the generator protective relays and the limiting actions of OEL and UEL functions can have a significant impact on the generator dynamic response and on the dynamic response of other generators and loads in the system.

Therefore, modeling these protective relays as well as OEL and UEL functions is necessary for performing precise transient stability studies.

Chapter 7: Conclusions and Future Work

7.1 Conclusions

Conducting accurate and precise transient stability studies is essential for obtaining a proper assessment of system behavior. Analyzing how the system responds to different contingencies and what control actions are required to maintain reliable and secure operation of the system is not possible without performing precise stability studies. Dynamic characteristics of the fundamental assets in the system, such as generators and loads, along with the protection system behavior direct the response of the system following a disturbance. Therefore, proper representation of dynamic models of different system assets as well as protection systems is essential for performing precise stability studies.

The importance of modeling protection systems in stability studies is thoroughly studied in the literature review and it is illustrated that without proper modeling of the protection systems, stability studies might not represent the actual behavior of the system. However, due to various technical and practical challenges, there are limitations in representing automated protection schemes in the stability studies. One of the most important protective relays which are currently not represented in stability studies is distance relays. Distance relays play a crucial role in defining the behavior of a system and need to be modeled in the system for performing precise stability studies. Nevertheless, the current trend in stability studies does not include distance relay models due to two reasons: first, the current limitation of stability software, such as PSLF, does not allow adding thousands of distance relay models required for modeling distance relays on all the lines of

a bulk power system such as the WECC system. Second, keeping the setting data of thousands of distance relays updated in the dynamic data file of the system is a challenging task. Therefore, there always has been a gap between transient stability studies and modeling the behavior of the distance relays. The first part of this work aims at filling this gap by proposing two methods that address the mentioned challenges and limitations and make modeling distance relays in transient stability studies possible.

The proposed methods identify the critical distance relays which are required to be modeled in the transient stability studies to accurately capture the behavior of the system. The first method is an iterative algorithm which is based on iteratively using two techniques to identify the critical lines. The first technique is evaluating the apparent impedance observed from both ends of each transmission line and the second one is applying minimum voltage evaluation technique along each transmission line for each time interval of the transient stability study. Since its required data can be easily obtained from the normal practice of transient stability study, the algorithm can easily be used in power system planning studies for identifying the critical lines which are prone to experience distance relay operation during different contingencies.

The second method proposed for identifying the critical distance relays for each contingency is a machine learning-based method. The method is based on learning the latent pattern between the impedance trajectories observed by distance relays during the early stages of a contingency and the operations of these relays for several seconds later. The RF classifier is used as the machine learning algorithm in this dissertation. For creating the dataset required for training the RF model, extensive offline transient stability studies

are performed. A two-stage grid search method is used to tune the hyperparameters of the RF model in order to achieve the best performance in terms of the Recall value. The K-fold cross-validation method is also used to evaluate the performances of the RF models trained at each iteration of the grid search method. After being trained using the created dataset, the RF model can predict the operation of distance relays during any contingency using the results of early-terminated transient stability studies. If the trained model predicts the operation of any distance relay, the method identifies that relay as critical and model it in the transient stability study. The SHAP feature importance method is also used to evaluate the importance of each feature in defining the prediction of the trained RF model, which will significantly enhance the interpretability of the model.

The WECC system representing the 2018 summer peak load case has been used as the test case for both the proposed methods. First, the shortcoming of the widely used representation of the buses in a system, that is the bus-branch representation, in analyzing bus faults was studied. It was shown that when a bus fault is simulated using the bus-branch model, all the distance relays connected to the bus operate which is not usually the case in real-world systems where the buses are modeled with the node-breaker model and the bus fault is usually cleared by removing one line. Then, to show that how performing transient stability studies using outdated relay settings can lead to an inaccurate assessment of system behavior, a case study is performed on the WECC system, and it is shown that the behavior of the system is completely different when some of the relay settings are outdated.

To show the importance of modeling distance relays in performing precise stability studies and for evaluating the performance of the proposed methods in identifying the

critical distance relays, different contingencies are studied considering different topologies and operating points of the WECC system. The contingencies are among the severe contingencies of the WECC system which have wide-spread impact throughout the system and have the potential to lead the system toward instability. In each contingency, three different cases of not modeling any distance relay, only modeling critical distance relays identified by the proposed methods, and modeling distance relays on all the lines with the voltage level of 345 kV and above (the reference case) are considered, and the results of transient stability studies in each case are compared.

The results reveal that the transient stability studies carried out without modeling distance relays might be completely different from the actual behavior of the system. Furthermore, it can be seen from the results that both the proposed methods yield exactly the same results as the reference case, and they can precisely identify the critical distance relays required for studying each contingency. Compared to the reference case, the proposed methods add a far smaller number of distance relays to the dynamic data file of the system used for performing transient stability studies. Therefore, in bulk power systems where modeling distance relays on all the lines exceeds the current limitation of the software, the methods can help operators in conducting planning studies with only modeling critical distance relays which are likely to operate. Since the settings of distance relays are modified in the system for various purposes, keeping track of all these changes and applying them in the dynamic data file of the system is a challenging task. However, the proposed methods alleviate this task by considerably reducing the number of distance relays required to be modeled in the dynamic data file of the system for performing stability

studies. Therefore, the operator just needs to keep track of the changes in the settings of a small number of distance relays. Finally, having a considerably smaller number of relays modeled in transient stability studies reduces the computational burden of the system and enables the operators to include more dynamic models which they think are essential for their transient stability studies.

The advent of PMUs and their application in power grids provide a wide range of applications such as situational awareness for operational decision making by providing synchronous measurement data. The reliable and synchronous online measurements provided by PMUs have paved the way for the advent of online DSA which is one of the key requirements in modern power systems with ever-growing uncertainties. Online DSA methods analyze the system stability at the current operation condition and trigger automatic control actions or inform the operator if the situation is predicted to be insecure. Therefore, they are valuable tools for utilities providing them with early warnings of the pending troubles in the system and gives them enough time to initiate remedial actions, which can play a significant role in preventing major outages in the system. The hurdles and limitations associated with the conventional methods on one hand and the availability of overwhelming amount of online data owing to the advancements made in power system monitoring, on the other hand, have increased the interest in the machine learning-based online DSA methods. These methods have proven to be effective and fast tools for real-time analysis of the modern power system stability.

The second part of this dissertation proposes an ML-based online DSA method that uses the voltages of the electrically closest HV buses to the relay/generator locations and

predicts if any distance relay, UFLS relay, and UVLS relay will operate and if any generator in the system will experience LOS condition for several seconds later. The method uses the results of offline transient stability studies performed on the WECC system to train different RF models to predict the relay operations, and LOS conditions in the generators. For each of the mentioned applications, 3 different RF models are trained. These models use different periods of measurement data as the input features. The performances of the trained models are evaluated in the presence of noise and missing PMU data using the K-fold cross-validation method.

The results show that the trained models are robust to standard noise levels of industrial PMUs (and higher) and missing PMU data. The results show that with the noise level of 0.03 and 0.1 of IEEE standard TVE, all the trained models have an F1 score of above 0.9 and for the noise level of 0.25 of IEEE standard TVE, which is considerably higher than the noise level of industrial PMUs, all the trained models still have F1 scores above 0.8. Almost all the trained models keep an F1 score higher than 0.88 for all the four cases of missing PMU data. The results show that all the RF models are fast enough to satisfy the requirement of an online DSA method. Also, the various RF models that use different periods of measurement data can provide different levels of prediction speed and reliability, which enables compromising the earliness and the reliability of the predictions.

The method can serve as a reliable and fast tool to increase situational awareness by providing early predictions of impending distance relay, UFLS and UVLS relay operations, as well as LOS conditions in generators throughout the system. The heatmap of a contingency is provided, which shows the areas of the system that are predicted to

experience frequency/voltage drop and consequent distance relay and/or UFLS/UVLS relay operations. It also visualizes that the generators of which areas will experience LOS conditions. This can significantly help in understanding the system condition and how the disturbance propagate in the system, which provides an opportunity to initiate more efficient remedial actions.

Generators are one of the most critical assets in power systems. Their behavior during severe disturbances significantly impacts the response of the system to the disturbance. In this regard, precisely capturing the behavior of the generators during disturbances is crucial to have a precise assessment of system behavior. As generators are very important and expensive assets in power systems, they are usually equipped with multiple protective relays with different protection functionalities. Under/over voltage protection, under/over frequency protection, loss-of-field protection, volt-per-hertz protection, phase distance protection, overcurrent protection, out-of-step protection, and reverse power protection are among the common protective relays that are used to protect generators. The responses of these protective relays direct the behavior of the generators during disturbances, and in turn, impacts the response of the system to the disturbances. In this regard, the post-disturbance analysis of prior major outages and blackouts reveal the important role of the generator protective relays in the chain of events leading to these outages and blackouts. Therefore, modeling these protective relays in transient stability studies significantly enhances the accuracy of these studies. In this regard the need for developing a framework for modeling generator protective relays in transient stability studies has long been identified by the industry.

In the final part this dissertation, an introduction on different types of generator protective relays used in industrial generators along with their application and mechanism is provided. Furthermore, a comprehensive framework for modeling different generator protective relays in transient stability studies is developed. The developed framework provided following guidelines for modeling generator protective relays in transient stability studies:

1. Selecting proper dynamic models to represent different protection functions of generators
2. How to map different parameters and settings of the protective relays to the associated parameter in the dynamic model in order to have a block diagram and settings that represent the actual protective relay in transient stability studies as precise as possible
3. What considerations should be taken into account when modeling the generator protective relays in transient stability studies.

Therefore, the proposed framework can greatly assist the engineers in modeling different generator protective relays in transient stability studies in order to increase the accuracy of these studies. Modeling the generator protective relays with the help of the developed framework provides the opportunity to analyze the behavior of protective relays, their interactions with the transients of the system, as well as their impact on the dynamic response of the generator and the system during different contingencies. These analyses not only provide insight into the dynamic response of the generator and the system during different contingencies (which is crucial for devising proper preventive and remedial

actions), but it also identifies any probable generator protective relay misoperation or miscoordination with other protective relays. Thus, it can also help protection engineers to make proper modifications in the related protection schemes and settings to avoid such misoperations and miscoordinations.

The WECC system data representing the 2028 planning case is used as the test system. A specific area within the WECC system is especially selected for modeling generator protective relays and performing transient stability studies of different contingencies. To see how different generator protective relays as well as OEL and UEL functions operate during contingencies, 403 contingencies are performed on the test system and the operation of generator protective relays and the activation of OEL and UEL functions are monitored during these contingencies. To show in more details that how modeling generator protective relays as well as the OEL and UEL functions can impact the dynamic response of the related generator, other generators in the system, as well as the system, 5 contingencies are selected for a more detailed analysis. To compare the dynamic response of the system with and without modeling the generator protective relays, for each contingency, two cases of modeling and not modeling generator protective relays are considered.

The results show that during the 403 contingencies studied, 137 cases of generator relay operations, which leads to tripping of the generator, are observed. Furthermore, 202 OEL and UEL actions are observed during these contingencies. These relay operations and limiting actions cannot be captured without modeling generator protective relays and OEL/UEL functions. The results also show that the dynamic response of the generators—

in terms of the field current, active and reactive power, terminal voltages—and the dynamic response of the system—in terms of the voltages of load buses and their active and reactive power—are different in the two cases of modeling and not modeling generator protective relays. This highlights the importance of modeling generator protective relays in performing precise transient stability studies.

7.2 Future work

The ever-increasing penetration level of renewable resources in modern power systems has created new challenges for predicting the responses of various protective relays during different contingencies and properly coordinating these protective relays. The intermittent characteristics of the renewable resources increase the uncertainty level in the operation condition of the modern power system. The level of uncertainty in the active and reactive power flow of the lines as well as the apparent impedance observed at line terminals increases with increase in the penetration level of renewable resources. This high level of uncertainty makes it a challenging task to properly tune the settings of protective relays and coordinate them with together. Furthermore, the inverters that are usually used for connecting the renewable resources to power systems can introduce new dynamics to power systems and they might interfere with the normal operations of different protective relays in the system.

Therefore, one proper continuation for this work can be modeling distance relays and generator protective relays using the methods proposed in this dissertation for power systems with high penetration level of renewable resources and evaluating the behavior of these protective relays during different type of contingencies. Such studies can shed light

on the impact of high penetration level of renewable resources on the performances of the protective relays in the system. They can also help in devising proper modifications in the protection schemes, settings, and coordination of these relays to ensure correct operations even under a high penetration level of renewable resources.

REFERENCES

[1] L. G. Perez, A. J. Flechsig, and V. Venkatasubramanian, "Modeling the protective system for power system dynamic analysis," *IEEE Transactions on Power Systems*, vol. 9, no. 4, pp. 1963–1973, Nov. 1994.

[2] D. C. Elizondo, J. D. L. Ree, A. G. Phadke, and S. Horowitz, "Hidden failures in protection systems and their impact on wide-area disturbances," *IEEE Power Engineering Society Winter Meeting*, pp. 710–714, Columbus, OH, USA, 2001.

[3] Final report on the August 14, 2003 blackout in the United States and Canada: Causes and Recommendations, U.S.–Canada Power System Outage Task Force, 2004.

[4] N. Samaan et al., "Modeling of protection in dynamic simulation using generic relay models and settings," *in IEEE Power and Energy Society General Meeting (PESGM)*, pp. 1-5, Boston, MA, USA, 2016.

[5] M. Abdi-Khorsand and V. Vittal, "Identification of critical protection functions for transient stability studies," *IEEE Transactions Power Systems*, vol. 33, no. 3, pp. 2940-2948, May 2018.

[6] D. P. Nedic, "Simulation of large system disturbances," Ph.D. dissertation, Department of Electrical Engineering and Electronics, The University of Manchester Institute of Science and Technology, Manchester, U.K., 2003.

[7] V. Venkatasubramanian and Y. Li, "Analysis of 1996 western American electric blackouts," *Proceeding Bulk Power System Phenomena-Stability and Control*, Cortina d'Ampezzo, Italy, 2004.

[8] G. Andersson, et. al., "Causes of the 2003 major grid blackouts in North America and Europe, and recommended means to improve system dynamic performance," *IEEE Transactions on Power Systems*, vol. 20, no. 4, pp. 1922–1928, Nov. 2005.

[9] P. Pourbeik, P. S. Kundur, and C. W. Taylor, "The Anatomy of a Power Grid Blackout," *IEEE PES Magazine*, September 2006.

[10] FERC, "Arizona-Southern California outages on September 8, 2011, causes and recommendations," *FERC and NERC report*, Apr. 2012.

[11] P. Chatterjee, M. Khorsand, and K. W. Hedman, "Enhanced assessment of power system behavior during multiple contingencies," *in North American Power Symposium (NAPS)*, pp. 1-6, Fargo, ND, 2018.

[12] J. S. Thorp, A. G. Phadke, S. H. Horowitz, and S. Tamronglak, "Anatomy of power system disturbances: importance sampling," *International Journal of Electrical Power and Energy Systems*, vol. 20, pp. 147-152, February 1998.

[13] M. K. Hedman, "Analytical approaches for identification and representation of critical protection systems in transient stability studies," Ph.D. Dissertation, Arizona State University, April 2017.

[14] M. Li, A. Pal, A. G. Phadke, J. S. Thorp, "Transient Stability Prediction based on Apparent Impedance Trajectory Recorded by PMUs," *International Journal of Electrical Power & Energy Systems*, vol. 54, pp. 498-504, January 2014.

[15] NERC, *Protection System Response to Power Swings*, System Protection and Control Subcommittee, NERC, August 2013, Available: https://www.nerc.com/comm/PC/System%20Protection%20and%20Control%20Subcommittee%20SPCS%2020/SPCS%20Power%20Swing%20Report_Final_20131015.pdf

[16] J. Berdy, "Application of Out-Of-Step Blocking and Tripping Relays," *in General Electric Power Management*, Ontario, Canada, Available: http://store.gedigitalenergy.com/faq/Documents/Alps/GER-3180.pdf.

[17] IEEE, *Power Swing and Out-of-Step Considerations of Transmission Line*, A report to the Power System Relaying Committee of the IEEE Power Engineering Society, IEEE PSRC WG D6, July 2005.

[18] A. R. Van and C. Warrington, *Protective Relays Their Theory and Practice*, vol. 1, 2nd Edition, Chapman and Hall, 1968.

[19] N. Fischer, G. Benmouyal, Da. Hou, D. Tziouvaras, J. Byrne-Finley, and B. Smyth, "Tutorial on Power System Blocking and Out-Of-Step Tripping," *Proceedings of the 39th Annual Western Protective Relay Conference*, Spokane, WA, October 2012.

[20] W. A. Elmore, "System Stability and Out-Of-Step Relaying," *Applied Protective Relaying*, Westinghouse Electric Corporation, 1982.

[21] P. M. Anderson, *Power System Protection*. Piscataway: Wiley-IEEE Press, 1998.

[22] C. J. Mozina, "Advanced Application of Multifunction Digital Generator Protection," Beckwith Electric Company, Available: https://www.beckwithelectric.com/docs/tech-papers/genprot01.pdf.

[23] J. Holbach, "New Blocking Algorithm for Detecting Fast Power Swing Frequencies," *Proceedings of the 30th Annual Western Protective Relay Conference*, Spokane, WA, October 2003.

[24] C. W. Taylor, J. M. Haner, L. A. Hill, W. A. Mittelstadt, and R. L. Cresap, "A New Out-Of-Step Relay with Rate of Change of Apparent Resistance Augmentation," *IEEE Transaction on Power Apparatus and Systems*, vol. 102, no. 3, pp. 631-639, March 1983.

[25] J. M. Haner, T. D. Laughlin, and C. W. Taylor, "Experience with R-Rdot Out-Of-Step Relay," *IEEE Transactions on Power Delivery*, vol. 1, no. 2, pp. 35-39, April 1989.

[26] G. Benmouyal, D. Hou, and D. Tziouvaras, "Zero-setting Power Swing Blocking Protection," *Proceeding of the 31st Annual Western Protective Relay Conference*, Spokane, WA, October 2004.

[27] A. Guzman, V. Mynam, and G. Zweigle, "Backup Transmission line Protection for Ground Faults and Power Swing Detection using Synchrophasors," *Proceeding of the 34th Annual Western Protective Relay Conference*, Spokane, WA, October 2007.

[28] S. M. Rovnyak, C. W. Taylor, and Y. Sheng, "Decision Tree using Apparent Resistance to Detect Impending Loss of Synchronism," *IEEE Transactions on Power Delivery*, vol. 15, no. 4, pp. 1083-1093, October 2000.

[29] T. Amraee and S. Ranjbar, "Transient Instability Prediction using Decision Tree Technique," *IEEE Transactions on Power Systems*, vol. 28, no. 3, pp. 3028-3037, August 2013.

[30] K. H. So, J. Y. Heo, C. H. Kim, R. K. Aggarwal, and K. B. Song, "Out-Of-Step Detection Algorithm using Frequency Deviation of Voltage," *IET Generation, Transmission, and Distribution*, vol. 1, no. 1, pp. 119-126, January 2007.

[31] R. Jafari, N. Moaddabi, M. Eskandari-Nasab, G. B. Gharehpetian, and M. S. Naderi, "A Novel Power Swing Detection Scheme Independent of the Rate of Change of Power System Parameters," *IEEE Transactions on Power Delivery*, vol. 29, no. 3, pp. 1192-1202, June 2014.

[32] M. Abdi-Khorsand and V. Vittal, "Modeling Protection Systems in Time-Domain Simulations: A New Method to Detect Mis-Operating Relays for Unstable Power Swings," *IEEE Transactions on Power Systems*, vol. 32, no. 4, pp. 2790-2798, July 2017.

[33] A. Gopalakrishnan, SG Aquiles-Perez, DM Macgregor, DB Coleman, PF Mcguire, KW. Jones, J. Senthil, JW. Feltes, G. Pietrow, and A. Bose "Simulating the Smart

Electric Power Grid of the 21st Century - Bridging the Gap between Protection and Planning" *Georgia Tech Protective Relaying Conference,* 2014, Atlanta, Georgia.

[34] V. Vittal, S.Lotfifard, A. Bose, M. Khorsand, I. Kiaei, "Evaluation of Protective Relay Dynamic Response Via a Co-simulation Platform," *Final PSERC Project Report*, September 2017, available at: https://pserc.wisc.edu/publications/reports/2017_reports/S-66_Final_Report.pdf

[35] Y. Liu, S. Hadley, J. Gracia, T. Smith, and I. Snyder, "Development of Dynamic Models & Tools for Interconnection-wide Simulations," Oak Ridge National Laboratory, the US Department of Energy, June 17, 2014. Available: https://www.energy.gov/sites/prod/files/2014/07/f17/3-2014-AGM-Review-Liu_3.pdf

[36] D. S. Kirschen and D. P. Nedic, "Consideration of hidden failures in security analysis," *14th Power Systems Computation Conference*, pp. 24–28, Seville, Spain, 2002.

[37] S. Tamronglak, "Analysis of power system disturbances due to relay hidden failures," Ph.D. Dissertation, Department of Electrical Engineering, Virginia Tech, Blacksburg, VA, USA, 1994.

[38] J. Holbach, "New out of step blocking algorithm for detecting fast power swing frequencies," *Power System Conference: Advanced Metering, Protection, Control, Communication, Distributed Resources*, pp. 182–199, Clemson, SC, 2006.

[39] B. Shrestha, R. Gokaraju, and M. Sachdev, "Out-of-step protection using state-plane trajectories analysis," *IEEE Transactions on Power Delivery*, vol. 28, no. 2, pp. 1083–1093, Apr. 2013.

[40] Y. R. Alsyoufi, A. A. Hajjar, "A high-speed algorithm to discriminate between power swing and faults in distance relays based on a fast wavelet," *Electrical Power System Research*, vol. 172, pp. 269-276, July 2019.

[41] S. Slehimehr, B. Taheri, F. Razavi, M. Parpaei, M. Faghihlou, "A new power swing detection method based on chaos theory," *Electrical Engineering*, vol.102, pp. 663-681, June 2020.

[42] "ISO New England operating procedure No. 24 - protection outages, settings and coordination," ISO New England, Feb. 2019 [Online]. Available: https://www.iso-ne.com/static-assets/documents/2019/02/op24_rto_final.pdf.

[43] H. Wang, J. S. Thorp, "Optimal locations for protection system enhancement: a simulation of cascading outages," *IEEE Transactions on Power Delivery*, vol. 16, issue. 4, October 2001, pp. 528-533.

[44] H. Wu and X. Wang, "Design-oriented transient stability analysis of PLL-synchronized voltage-source converters," *IEEE Transactions on Power Electronics*, vol. 35, no. 4, pp. 3573–3589, Apr. 2020.

[45] H. Wu and X. Wang, "Design-oriented transient stability analysis of grid-connected converters with power synchronization control," *IEEE Transactions on Industrial Electronics*, vol. 66, no. 8, pp. 6473-6482, Aug. 2019.

[46] PSLF User's Manual, PSLF Version 18.1-01, General Electric.

[47] H. Wayne Beaty, *Handbook of electric power calculations*, Third Edition, McGraw-Hill Education, 2000, 1997, 1984, pp. 16.13-18.

[48] A. F. Abidin, A. Mohamed, H. Shareef, "Intelligent detection of unstable power swing for correct distance relay operation using S-transform and neural network," *Expert Systems with Applications*, Elsevier, vol. 38, issue 12, pp. 14969-14975, Nov. 2011.

[49] P. Gawande and S. Dambhare, "Secure third zone operation of distance relay using impedance prediction approach," *2016 National power system conference (NPSC)*, pp. 1-6, Bhubaneswar, India, Dec. 2016.

[50] T. Yiu, "Understanding random forest: how the algorithm works and why it is so effective," toward data science, Jun. 12, 2019, URL: https://towardsdatascience.com/understanding-random-forest-58381e0602d2.

[51] G. Biau, E. Scornet, "A random forest guided tour", Springer, vol. 25, Issue. 2, pp. 197-227, Jun. 2016.

[52] R. Vakili, M. Khorsand, "Machine-learning-based advanced dynamic security assessment: prediction of loss of synchronism in generators," *in 52nd North American Power Symposium (NAPS)*, Tempe, AZ, 2020.

[53] D. Olsun and D. Delen, Advanced data mining techniques, Springer, p.138, 2008.

[54] "Hyperparameter optimization," Wikipedia, May. 9, 2021, URL: https://en.wikipedia.org/wiki/Hyperparameter_optimization.

[55] "A practical guide to support vector classification," Technical Report, National Taiwan University, May. 2016. URL: https://www.csie.ntu.edu.tw/~cjlin/papers/guide/guide.pdf.

[56] D. Chicco, "Ten quick tips for machine learning in computational biology", BioData Mining. 10 (35): 35, Dec. 2017.

[57] J. Bergstra, Y. Bengio, "Random search for hyper-parameter optimization," *Journal of Machine Learning Research*, vol. 13, pp. 281-305, Feb. 2012.

[58] T. Fushiki, "Estimation of prediction error by using k-fold cross-validation," *Statistics and Computing*, vol. 21, pp. 137-146, Oct. 2009.

[59] M. Sanjay, "Why and how to cross validate a model?," towards data science, Nov. 12, 2018, URL: https://towardsdatascience.com/why-and-how-to-cross-validate-a-model-d6424b45261f.

[60] S. M. Lundberg, and SI. Lee, "A unified approach to interpreting model predictions," *31st International Conference on Neural Information Processing Systems (NIPS)*, Dec. 2017.

[61] Ch. Molnar, Interpretable machine learning: A guide for making black box models explainable, 2021.

[62] Random forest classifier, scikit learn, scikit learn developers, URL: https://scikit-learn.org/stable/modules/generated/sklearn.ensemble.RandomForestClassifier.html.

[63] Y. Xu, Z. Y. Dong, K. Meng, R. Zhang, and K. P. Wong, "Real-Time Transient Stability Assessment Model Using Extreme Learning Machine," *IET Generation, Transmission & Distribution*, vol. 5, no. 3, p. 314-322, 2011.

[64] K. Morison, L. Wang, and P. Kundur, "Power System Security Assessment," *IEEE Power Energy Magazine*, vol. 2, no. 5, pp. 30–39, 2004.

[65] A. Muir and J. Lopatto, "Final Report on the August 14, 2003 Blackout in the United States and Canada: Causes and Recommendations," Canada, Apr. 2004.

[66] K. Sun, S. Likhate, V. Vittal, V. S. Kolluri, and S. Mandal, "An Online Dynamic Security Assessment Scheme Using Phasor Measurements and Decision Trees," *IEEE Transactions on Power Systems*, vol. 22, no. 4, pp. 1935–1943, Nov. 2007.

[67] C. Liu et al., "A Systematic Approach for Dynamic Security Assessment and the Corresponding Preventive Control Scheme Based on Decision Trees," *IEEE Transactions on Power Systems*, vol. 29, no. 2, pp. 717–730, 2014.

[68] J. L. Cremer, I. Konstantelos, and G. Strbac, "From Optimization-Based Machine Learning to Interpretable Security Rules for Operation," *IEEE Transaction on Power Systems*, vol. 34, no. 5, pp. 3826–3836, Sep. 2019.

[69] C. Ren and Y. Xu, "A Fully Data-Driven Method Based on Generative Adversarial Networks for Power System Dynamic Security Assessment with Missing Data," *IEEE Transaction on Power Systems*, vol. 34, no. 6, pp. 5044–5052, Nov. 2019.

[70] L. S. Moulin, A. P. A. da Silva, M. A. El-Sharkawi, and R. J. Marks, "Support Vector and Multilayer Perceptron Neural Networks Applied to Power Systems Transient Stability Analysis with Input Dimensionality Reduction," *in IEEE Power Engineering Society Summer Meeting*, Chicago, IL, USA, 2002, pp. 1308–1313.

[71] F. R. Gomez, A. D. Rajapakse, U. D. Annakkage, and I. T. Fernando, "Support Vector Machine-Based Algorithm for Post-Fault Transient Stability Status Prediction Using Synchronized Measurements," *IEEE Transaction on Power Systems*, vol. 26, no. 3, pp. 1474–1483, Aug. 2011.

[72] L. S. Moulin, A. P. A. daSilva, M. A. El-Sharkawi, and R. J. MarksII, "Support Vector Machines for Transient Stability Analysis of Large-Scale Power Systems," *IEEE Transaction on Power Systems*, vol. 19, no. 2, pp. 818–825, May 2004.

[73] B. Wang, B. Fang, Y. Wang, H. Liu, and Y. Liu, "Power System Transient Stability Assessment Based on Big Data and the Core Vector Machine," *IEEE Transactions on Smart Grid*, vol. 7, no. 5, pp. 2561–2570, 2016.

[74] Q. A. Al-Gubri, M. A. M. Ariff, and I. S. Saeh, "Performance Analysis of Machine Learning Algorithms for Power System Dynamic Security Assessment*," in 4th IET Clean Energy and Technology Conference (CEAT 2016)*, Kuala Lumpur, Malaysia, 2016, p. 37 (6)-37 (6).

[75] C. Ren, Y. Xu, Y. Zhang, and C. Hu, "A Multiple Randomized Learning based Ensemble Model for Power System Dynamic Security Assessment," *in 2018 IEEE Power & Energy Society General Meeting (PESGM)*, Portland, OR., Aug. 2018, pp. 1–5.

[76] R. Diao, V. Vittal, and N. Logic, "Design of a Real-Time Security Assessment Tool for Situational Awareness Enhancement in Modern Power Systems," *IEEE Transaction on Power Systems*, vol. 25, no. 2, pp. 957–965, May 2010.

[77] R. Diao et al., "Decision Tree-Based Online Voltage Security Assessment Using PMU Measurements," *IEEE Transaction on Power Systems*, vol. 24, no. 2, pp. 832–839, May 2009.

[78] J. M. Gimenez Alvarez, "Critical Contingencies Ranking for Dynamic Security Assessment Using Neural Networks," *in 2009 15th International Conference on Intelligent System Applications to Power Systems*, Brazil, Nov. 2009, pp. 1–6.

[79] J. Shang, J. Zhang, W. Zhoa, and J. Liu, "ANN Based Dynamic Voltage Security Assessment for a Practical Power System," *in 2007 International Power Engineering Conference (IPEC)*, pp. 794–798.

[80] L. Zhu, C. Lu, Z. Y. Dong, and C. Hong, "Imbalance Learning Machine-Based Power System Short-Term Voltage Stability Assessment," *IEEE Transactions on Industrial Informatics*, vol. 13, no. 5, pp. 2533–2543, Oct. 2017.

[81] I. C. Gunadin, M. Abdillah, A. Soeprijanto, and O. Penangsang, "Steady-State Stability Assessment Using Neural Network Based on Network Equivalent," *TELKOMNIKA*, vol. 9, pp. 411–422, Dec. 2011.

[82] I. C. Gunadin, M. Abdillah, A. Soeprijanto, and O. Penangsang, "Determination of Steady State Stability Margin Using Extreme Learning Machine," *WSEAS Transactions on Power Systems*, vol. 7, no. 3, Jul. 2012.

[83] A. Y. Abdelaziz, M. R. Irving, A. M. El-Arabaty, and M. M. Mansour, "Out-of-Step Prediction Based on Artificial Neural Networks," *Electrical Power System Research*, vol. 34, no. 2, pp. 135–142, Aug. 1995.

[84] A. N. AL-Masri, M. Z. A. Ab Kadir, H. Hizam, and N. Mariun, "A Novel Implementation for Generator Rotor Angle Stability Prediction Using an Adaptive Artificial Neural Network Application for Dynamic Security Assessment*," IEEE Transactions on Power Systems*, vol. 28, no. 3, pp. 2516–2525, Aug. 2013.

[85] "IEEE Standard for Synchrophasor Measurements for Power Systems," *in IEEE Std C37.118.1-2011*, pp.1-61, Dec. 2011.

[86] D. Ritzmann, P. S. Wright, W. Holderbaum, and B. Potter, "A Method for Accurate Transmission Line Impedance Parameter Estimation," *IEEE Transactions on Instrumentation and Measurement*, vol. 65, no. 10, pp. 2204–2213, Oct. 2016.

[87] "Model 1133a power sentinel," Arbiter Systems, 2021. https://www.arbiter.com/catalog/product/model-1133a-power-sentinel.php

[88] "MicroPMU datasheet, PSL power standard lab," PSL power standard lab. https://pdf.directindustry.com/pdf/power-standards-lab/micropmu/207207-856169.html

[89] M. He, V. Vittal, and J. Zhang, "Online Dynamic Security Assessment with Missing PMU Measurements: A data Mining Approach," *IEEE Transactions on Power Systems*, vol. 28, no. 2, pp. 1969–1977, May 2013.

[90] J. L. Blackburn, *Protective Relaying: Principles and Applications*, second edition. New York: Marcel Dekker, 1998.

[91] R. Sandoval, A. Guzman, and H. J. Altuve, "Dynamic Simulations Help Improve Generator Protection," *in 2007 Power Systems Conference: Advanced Metering, Protection, Control, Communication, and Distributed Resources*, Clemson, USA, 2007, pp. 16-38.

[92] A. Hasani, F. Haghjoo, F. F. da Silva, and C. L. Bak, "Loss of Field Protection of Synchronous Generator in a Realistic Framework Using RTDS," *in 2018 IEEE International Conference on Environment and Electrical Engineering and 2018 IEEE Industrial and Commercial Power Systems Europe (EEEIC / I&CPS Europe)*, Palermo, Italy, 2018, pp. 1-5.

[93] A. Hasani, F. Haghjoo, F. F. da Silva, and C. Leth Bak, "Synchronous Generator Loss of Field Protection: A Real-Time Realistic Framework and Assessment of Some Recently Proposed Methods," *IEEE Transactions on Power Delivery*, vol. 34, no. 3, pp. 971-979, June 2019.

[94] M. M. Aman, Ghauth Bin Jasmon, Qadeer Ahmed Khan, A. Halim Bin Abu Bakar, and Jasrul Jamani Jamian, "Modeling and Simulation of Reverse Power Relay for Generator Protection," *in 2012 IEEE International Power Engineering and Optimization Conference*, Melaka, Malaysia, 2012, pp. 317-322.

[95] S. Patel et al., "Performance of Generator Protection During Major System Disturbances," *IEEE Transactions on Power Delivery*, vol. 19, no. 4, pp. 1650-1662, Oct. 2004.

[96] P. Kumar, D. Fredickson, and K. Chanda, "Stability Studies for System Dependent Generator Protection Functions," *in Western Protective Relay Conference*, 2011.

[97] S. S. Choy and X. M. Xia, "Under Excitation Limiter and its Role in Preventing Excessive Synchronous Generator Stator End-Core Heating," *IEEE Transactions on Power System*, vol. 15, no. 1, pp. 95-101, Feb. 2000.

[98] P. Kundur, *Power System Stability and Control*. New York: McGraw-Hill, 1994.

[99] G. Anagnostou and B. C. Pal, "Impact of Overexcitation Limiters on the Power System Stability Margin Under Stressed Conditions," *IEEE Transactions on Power Systems*, vol. 31, no. 3, pp. 2327-2337, May 2016.

[100] D. Reimert, *Protective Relaying for Power Generation Systems*, 3rd ed. New York, NY, USA: Taylor & Francis, 2006.

[101] “Power Plant and Transmission System Protection Coordination,” NERC System Protection and Control Subcommittee, Rev. 1, Jul. 2010

[102] Generator Protection REG670 2.0 ANSI, *Application Manual*, ABB, Zurich, Switzerland, 2014, pp. 264–270

[103] IEEE Guide for AC Generator Protection, IEEE Standard C37, pp. 102–2006, Nov. 2006.

[104] Multifunctional Machine Protection, *Technical Manual*, Siemens Siprotec, Munich, Germany, pp. 131–145, 2010.

[105] H. J. Hermann and D. Gao, “Under-Excitation Protection Based on Admittance Measurement Excellent Adaptation on Capability Curves,” *in Proceedings 1st International Conference on Hydropower Technology & Key Equipment*, Beijing, China, 2006.

[106] P. Rush, “Network Protection & Automation Guide”, *ALSTOMT&D Energy Automation & Information (2002)*, ASIN: B00480IKQO.

[107] SEL-300G manual, available at: http://www.tasker.us/source/sel/300g_im_07_06_manual.pdf.

[108] Wikipedia the free encyclopedia 2018, Decision Tree, https://en.wikepedia.org/wiki/Decision_tree

[109] P. Gupta, Decision trees in machine learning, Toward data science, May 17, 2017, https://towardsdatascience.com/decision-trees-in-machine-learning-641b9c4e8052

[110] L. Davidson, The most common machine learning terms, explained, Springboard Blog, April 30, 2019, https://wwww.springboard.com/blog/machine-learning-terminology

[111] S. Rawale, Understanding decision tree, algorithm, drawbacks, and advantages, May 30, 2018, https://medium.com/@sagar.rewale3/understanding-decision-tree-algorithm-drawbacks-and-advantages-4486efa6b8c3

[112] North American Electric Reliability Council Web Site, Disturbance Report Database Reliability Assessment. Available at: www.nerc.com/dawg/database.html

[113] G. C. Bullock, “Cascading voltage collapse in West Tennessee—August 22, 1990,” *in Proceeding Georgia Tech Protective Relaying Conference*, Atlanta, GA, May 2, 1990.

APPENDIX A

DECISION TREES IN MACHINE LEARNING

The decision tree is a decision support tool which utilizes a tree-like model of decisions and their possible consequences [108]. Besides being commonly used in operations research, the decision tree is one of the most popular algorithms that has been implemented for solving wide areas of classification and regression problems in machine learning. A decision tree can be used to visualize decisions and decision makings, and as the name shows, it has a tree-like structure starting from the root at the top and goes down to the leaf [66] and [109].

A decision tree is composed of a root, internal nodes, branches, leaves, and classification rules [66]. Each internal node is an attribute on a feature (e.g. whether the voltage of a particular bus is higher than a particular number or not). Each branch shows the outcome of a test. Each leaf represents a class label (in classification problems), and each classification rule is the path from the root to leaf.

In a simple way, a decision tree starts from its root and works by repeating some questions and building an "if-then" framework which leads to a precise classification by narrowing the pool of possibilities over time [110]. Figure A.1 illustrates a simple example of a decision tree for deciding if a person is fit or not using his or her BMI.

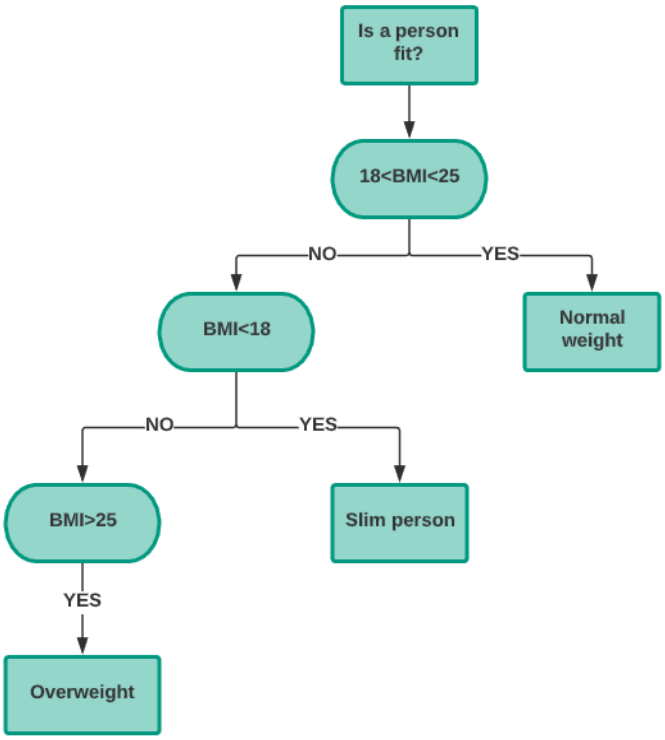

Figure A.1 A simple example of a decision tree

Decision tree algorithm has some advantages and disadvantages, the most important of which is provided in the following [111]:

Advantages:

1. Easier data preparation during pre-processing.
2. No need for normalization and scaling of data.
3. The process of building a decision tree is not sensitive to missing values in the data
4. Easy to interpret and visualize

Disadvantage:

1. Decision trees are unstable, meaning that a small change in the data can cause a large change in their structure.
2. Calculations can be more complex than other algorithms in some cases.
3. Training decision trees is often costly and requires a lot of time.
4. Decision trees are prone to overfit the training set and perform poorly on the new out-of-sample cases

APPENDIX B

HISTORICAL RECORDS OF THE ROLE OF GENERATOR PROTECTIVE RELAYS DURING DISTURBANCES

In this appendix, a brief overview of the role that generator protective relays played during some well-known disturbances is provided [95].

B.1 August 10, 1996, WSCC disturbance

On August 10, 1996, the Western Systems Coordinating Council (WSCC) system was separated into four islands due to s major disturbance. This islanding led to the interruption of service of 7.5 million customers for period ranging from several minutes up to 9 hours. Post-analysis of this disturbance revealed the significant role of generator protective system during this disturbance [95] and [112]:

1) Sustained low voltage: sustained low voltage during the disturbance created undesirable conditions in some generators—such as low drum level, low pressure, to name but a few—which eventually led to tripping of these units. In this regard, prolonged low voltage condition was the reason for 16.3% of the tripped units. Prolonged low voltage condition also caused the undervoltage relay of many auxiliary support systems of the generators to either trip the auxiliary system or transfer to backup. However, in some cases this transfer was unsuccessful.

2) Load rejection: post-analysis revealed that the reason behind tripping of 18.5% of the units was load rejection. During load rejection, the voltages of the hydro units were boosted to the ceiling (overvoltage condition). Duration of this overvoltage condition (which was above the relay settings) depended on the type of the excitation system of the related units and their control functions. Furthermore, the speed of some of the hydro units increased even up to 2 times of their normal speed (leading to operating frequency of 120 Hz). The response times of the units to this

overspeed condition were different and depended mainly on the governor response time and the water head level. For non-fault load rejections, the units should not be tripped. However, during this load rejection condition, some generator protective relays—including third-harmonic neutral undervoltage relay, fundamental neutral undervoltage relay, overvoltage relay, and overfrequency relay—tripped their related generators. Some of these relay operations were due to errors in relay coordination. However, the most of them were merely the anticipated protective relay performance during high frequency operation.

3) Backup overcurrent relays: Power swings and prolonged low voltage condition also led to the operation of the voltage restrained overcurrent relays or directional overcurrent relays and consequent tripping of several units including two large units in the WSCC system.

4) Underfrequency relays: underfrequency tripping schemes should be coordinated with the turbine manufacturers' recommendations on the capability of the turbine to operate in low-frequency condition. Some utilities had installed underfrequency relays on their generators. These relays lacked undervoltage supervision and some of them tripped during this disturbance.

5) Exciter/field problems: this major disturbance also created undesired conditions in the excitation system of several units—including loss of field and overexcitation conditions—and led to tripping of these units. Volt-per-hertz relay was involved in many of these trips. The miscoordination between volt-per-hertz relays, overvoltage relays, and overexcitation limiters as well as the miscoordination

between loss-of-field relays underexcitation limiters were the cause for several trips.

6) Overvoltage: overvoltage condition in some parts of the system also led to several loss-of-field relay operation and the consequent tripping of the generators.

B.2 February 21, 1995, PECO Disturbance

This disturbance which occurred on February 21, 1995, started by the failure of a 230-kV lightning arrester on the line from Whitpain substation to North Wales substation. The fault was cleared in five cycles by actions of the relays and tripping of the breakers at the line terminals. Furthermore, due to various reasons, six other transmission lines were incorrectly tripped. Approximately 1 s later, one of the lines at North Wales substation automatically reclosed into the fault. Meanwhile, the North Wales relays failed to clear the fault, leaving it to linger for 114 cycles before being cleared by the action of relays and breakers at remote stations. This second fault also led to tripping of 4 more transmission lines. The generator ground overcurrent relays of the Limerick 1 and 2 units (which were connecter to the related step-up transformers) also tripped these two units during the second fault [95].

B.3 August 22, 1987, Tennessee Disturbance

The Tennessee disturbance, which occurred on August 22, 1987, started by phase-to-phase flashing of a 115-kV switch while the operator was trying to isolate a damaged air blast breaker. Because of the lack of bus differential protection, the fault remained on the bus for more than 1 second and was finally cleared by the backup relays at remote locations. The long fault duration, led to stalling of motor loads in Memphis and the surrounding

TVA area. The stalled motors started to draw large amounts of reactive power even after clearing the fault, which led to a depressed voltage condition on both 161- and 50-kV systems in Southwestern Tennessee that continued for 10 to 15 seconds. During this time, zone 3 of distance relays operated at several remote substation. Furthermore, the voltage controlled/restrained overcurrent relays and distance relays of some of the generator also operated and tripped the related generators. This led to cascading trips that eventually tripped all the source lines into TVA's South Jackson, Milan, and Covington substations [95] and [113].

B.4 June 5, 1967, PJM Disturbance

This disturbance which occurred on June 5, 1967, left the eastern portion of the Pennsylvania–New Jersey–Maryland (PJM) interconnection completely without power. Before the event, the area was experiencing a heavy load and power transfer condition. Then, at 10:16 A.M. a 230-kV line between Nottingham and Plymouth Meeting in the Philadelphia area sagged due to the heavy load and flashed over when it contacted a 4-kV circuit. Due to this event, the line loading increased in the upcoming minutes and voltage sagged at various locations in PJM area. To support system voltage, the reactive power output of the generator increased. Then, about 30 seconds after the initial event, the loss-of-field relay of the unit 2 at the Brunner Island plant near Harrisburg, PA tripped the related generator, which deteriorated the system condition even more. The isolation of eastern PJM occurred about 2 min into the event, which was followed by the collapse of the island that occurred about 5 min later. During this disturbance, about 26 generators

were automatically tripped: 12 by loss-of-field relaying, 6 due to abnormal current or voltage, 4 by turbine protection, and 4 by other protective devices [95].

APPENDIX C

THE OEL1 MODEL

The *oel1* is an OEL model for synchronous machine excitation systems that takes generator field current as its input and can provide different OEL functions for the generator. This OEL model is developed to represent the generic behavior of different types of excitation limiters. It is not meant to represent the exact model any specific type or model of OEL; rather, it can represent the effect of many different types of OELs [46].

Oel1 includes three separate elements:

1. One time-dependent element which has either a definite-time or inverse-time characteristic. The timer of this element starts counting when the field current or field voltage (defined by parameter *Vdflag*) reaches the related pickup value (defined by parameter *Ifdset*).

2. One instantaneous hard limiter element which operates without any time delay when generator field current reaches the related pickup value (defined by *Ifdmax*). When this element operates it sends a signal to the excitation system to be used as an overriding limit on field voltage. Note that, the instantaneous hard limiter always senses the field current, but acts by limiting the field voltage. Depending on whether the *Ifdmax* parameter is positive or negative, the limiter imposes different types of hard limits on the field voltage. If *Ifdmax* is positive, the field voltage is limited to *Ifdmax*. If *Ifdmax* is negative, the field voltage is reduced and limited to the maximum continuous field current of the generator (defined by *Ifcont* parameter). Note that, if this action of the *oel1* is activated, no OEL signal will be sent to the

summing junction of AVR (i.e., limiting action 1 is stopped when the instantaneous limiting action of *oel1* is activated).

3. A two-stage tripping element which has one higher pickup current level of *Ifdmax* with the related time delay of *Tmax* and one lower pickup current level of *Ifdset* with the related time delay of *Tset*. When this element operates, it trips the generator off.

The time delay associated with the time-dependent element is defined by *Tpickup* parameter. If *Tpickup* is set as a positive value, the OEL will have an inverse-time characteristic. In this condition, *Tpickup* is the operation time of the OEL for a constant field current that exceeds *Ifdset* by 1 p.u. On the other hand, if *Tpickup* is set as a negative value, the OEL will have a definite-time characteristic. In this condition, *Tpickup* is the minimum period that the field current should remain above *Ifdset* for the OEL to operate. In both cases, the timer immediately reset if the field current falls belove the *Ifdset* before the timer has timed out.

When the time-dependent element operates, the limiter can implement three different types of limiting actions, which is defined by the *Runback* parameter:

4. For positive values of *Runback*, the voltage regulator reference (at the summing junction point shown in Figure 6.7) is biased by the output of the *oel1*. The output of *oel1* is not constant in this case; rather, it is ramped in the negative direction at the rate of $\frac{1}{Runback}$ per unit per second as long as field current/voltage remains above the *Ifcont* parameter. When the field current falls below *Ifcont*, the ramping

of the output signal is stopped, and the value of the voltage regulator reference remains fixed at the biased value.

5. For negative values of *Runback*, the output signal of the *oel1* is a constant value and is equal to *Runback* per unit. The value of voltage regulator reference remains fixed at this biased value.

6. For $Runback = 0$, the excitation system is forced to apply an immediate mandatory limit of *Ifcont* to the excitation system output voltage. This limit is permanent.

The implementation of limiting actions 1 and 2 of the oel1 is independent of the type of the excitation system and is implemented in the same way for all the excitation system models. Whereas the implementation of action 3 of the oel1 model is dependent on the type of the excitation system, and not all the excitation system models respond to this action of the oel1.

Note that, the *oel1* model considers the field current required to give 1 p.u. stator voltage on open circuit in the absence of saturation (AFAG) as the per unit base for all the field current settings.

APPENDIX D

THE GP3 MODEL

The *gp3* model is a generic generator protection system which takes generator field current, terminal voltage and current, mechanical and electrical power of the generator as its input and provides the following generator protection functions [46]:

- One stage of volt-per-hertz protection with a pickup value defined by *vhz* (in p.u.) and a time delay defined by *tvhz* (in seconds).
- One stage of undervoltage protection with a pickup value defined by *vuv* (in p.u.) and a time delay defined by *tvuv* (in seconds).
- One stage of overvoltage protection with a pickup value defined by *vov* (in p.u.) and a time delay defined by *tvov* (in seconds).
- One stage of reverse power protection with a pickup value defined by *pmtr* (in p.u.) and a time delay defined by *tmptr* (in seconds).
- One stage of overfrequency protection with a pickup value defined by *fof* (in p.u.) and a time delay defined by *tof* (in seconds).
- One stage of underfrequency protection with a pickup value defined by *fuf* (in p.u.) and a time delay defined by *tuf* (in seconds).
- A two-zone loss-of-field protection with impedance offset: The zone 1 and 2 pickup impedances are defined by *xz1* and *xz2*, respectively (in p.u.). The zone 1 and 2 time settings are defined by *tz1* and *tz2*, respectively (in seconds). The relay impedance offset is defined by *xoff* (in p.u.).

- One stage of delta power imbalance for power/load unbalance relay ($P_{mech} - P_{elec}$) with a pickup value defined by *delp* (in p.u.) and a time delay defined by *tdelp* (in seconds).

- A stator overcurrent relay: The pickup value is defined by *ioc* (in p.u.). The time factor, time coefficient, inverse-time exponent, and reset time are defined by *koc*, *boc*, *poc*, and *troc*, respectively (in seconds).

- One stage of over-excitation protection with a pickup value defined by *ifoc* (in p.u.) and a time delay defined by *tfoc* (in seconds).

This model can monitor a single generator to which it is applied, or monitor all the generators within an area, zone, or the entire system depending on the value of flag2.

For the under/overfrequency protection, the generator speed in p.u. is used by the model as the frequency of the generator. If the terminal voltage of the generator drops below 0.7 p.u., the OF and UF relay is disabled till the voltage is recovered back above 0.75 p.u.

For voltage-restraint time stator overcurrent protection the following logic holds for tripping the generator by the *gp3* model:

$$T_{trip}(I_t) = \frac{koc}{(\frac{|I_t|}{I_{pickup}})^{poc-1}} + boc \tag{D.1}$$

$$T_{rest}(I_t) = \frac{troc}{(\frac{|I_t|}{I_{pickup}})^{2-1}} \tag{D.2}$$

$$T(I_t) = \begin{cases} T_{trip}(I_t) & if\ |I_t| > I_{pickup} \\ T_{rest}(I_t) & if\ |I_t| < I_{pickup} \\ -troc & if\ |I_t| = I_{pickup} \end{cases} \quad \text{(D.3)}$$

$$Trip = \int_0^t \frac{1}{T(I_t)} dt \quad \text{(D.4)}$$

Also, the voltage-restraint function for inverse-time stator overcurrent relay is provided in Figure D. 1.

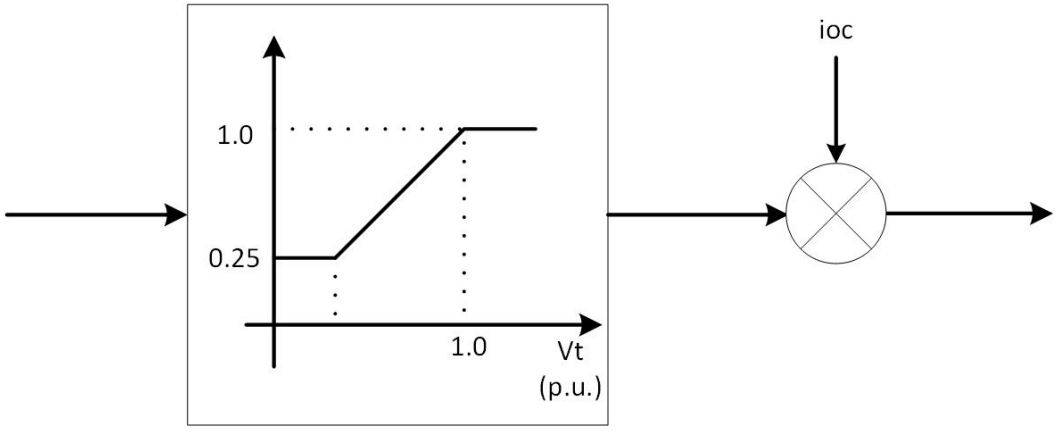

Figure D.1 Voltage restraint function in inverse-time over-current relay

For loss-of-field protection function, the relay operates in zone 1 if (D.5) holds for *tz1* seconds. Likewise, the relay operates in zone 2 if (D.6) holds for *tz2* seconds. If the generator stays inside zone 1 or 2 for less than *tz1* or *tz2* seconds, the relay timer is reset. The R-X diagram for the offset-mho relay characteristics of the loss-of-field protection is provided in Figure D. 2.

$$R_{gen}^2 + (X_{gen} - X_{off} + \frac{X_{z1}}{2})^2 < (\frac{X_{z1}}{2})^2 \quad \text{(D.5)}$$

$$R_{gen}^2 + (X_{gen} - X_{off} + \frac{X_{z2}}{2})^2 < (\frac{X_{z2}}{2})^2 \quad \text{(D.6)}$$

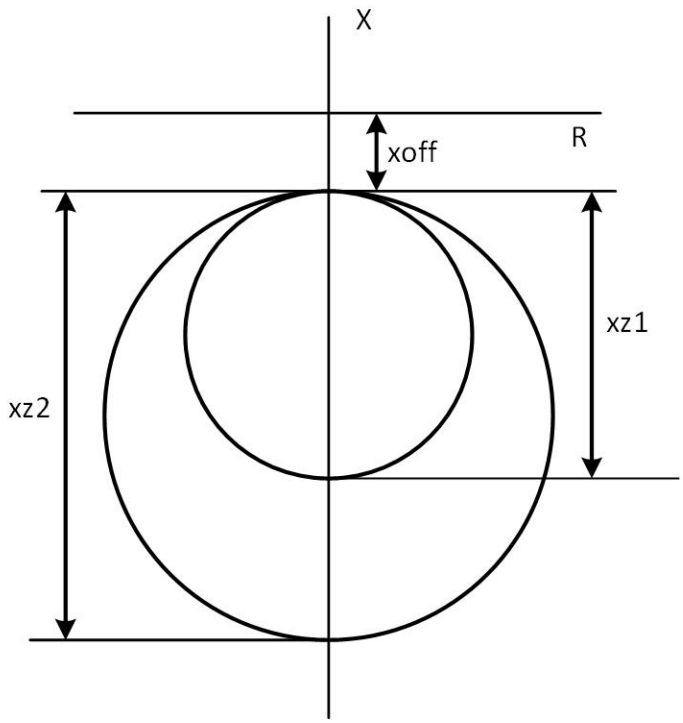

Figure D.2 R-X diagram for offset-mho relay characteristics of loss-of-field protection

APPENDIX E

THE UEL2C MODEL

The *uel2c* is an IEEE UEL2C underexcitation limiter model in the PSLF model library that can provide a piece-wise linear UEL characteristic in the P-Q plane using up to 10 (p,q) points [46]. The UEL characteristic of the *uel2c* model is shown in Figure E.1.

The (p,q) points are provided to the *uel2c* model as the input parameters that comprise the UEL look-up table. This look-up table must contain at least two points, namely, (p1,q1) and (p2,q2), and it must be defined in the fourth quadrant of the P-Q plane. As seen in Figure E.1, between two adjacent (p,q) points, the characteristic of the UEL is a straight line connecting the two points. Beyond each endpoint, the UEL characteristic is a straight line that is the continuation of the last segment of the line. Note that, if just two (p,q) points are provided the UEL characteristic is just a straight line. The block diagram of the uel2c model is provided in Figure E.2.

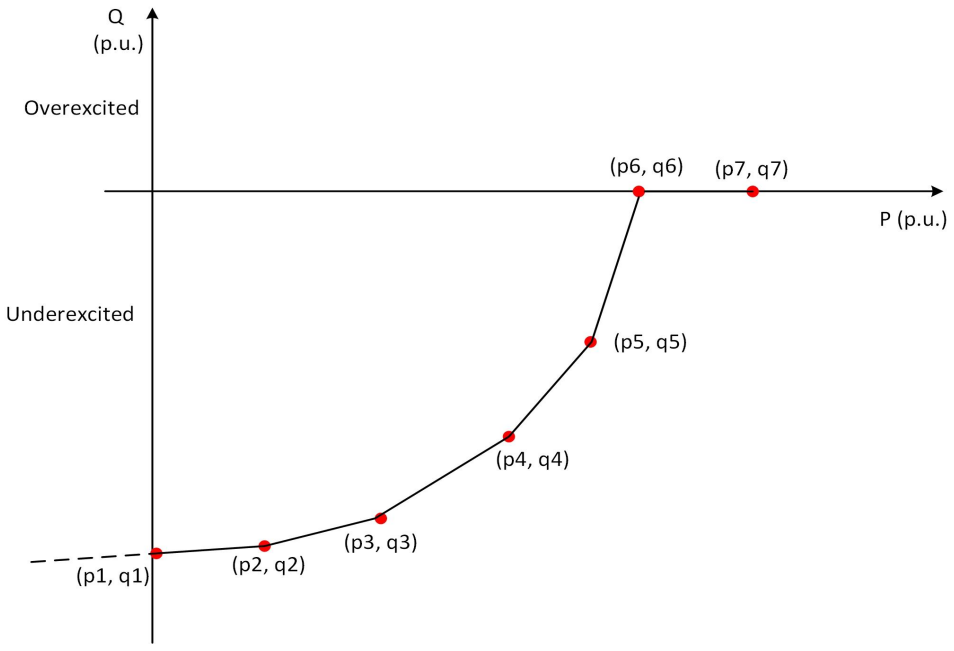

Figure E.1 A UEL characteristic

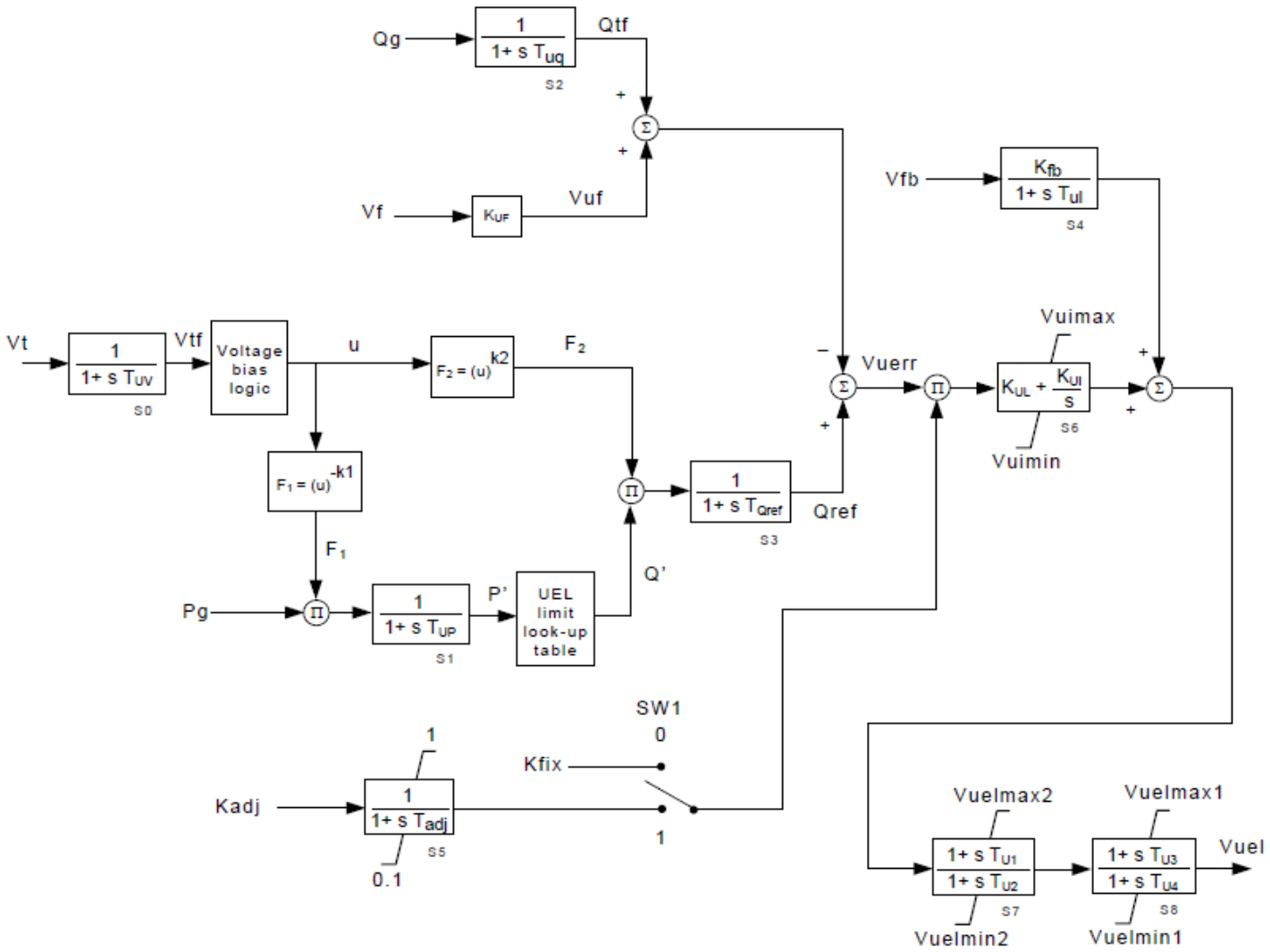

Figure E.2 Block diagram of the *uel2c* model [46]

As seen in Figure E.2, many parameters can affect the performance of the uel2c model. The logic of the voltage bias can be described as follows [46]:

$if\ V_{tf} > 1.0\ p.u.$

$\quad u = V_{tf}$

$else$

$\quad if\ V_{tf} > V_{bias}$

$\quad\quad u = 1$

$\quad else$

$\quad\quad u = V_{tf}/V_{bias}$

$\quad end\ if$

$end\ if$

APPENDIX F

THE LHFRT MODEL

The *lhfrt* model is a low/high frequency ride through generator protection system in the PSLF model library [46]. This model can provide up to 10 stages of over/underfrequency protection (pickup frequency deviations defined by *dftrp1* to *dftrp10* in Hz or p.u.) along with the related time delays (defined by *dttrp1* to *dttrp10* in seconds). The relay calculates the deviation of the generator terminal bus frequency from the reference frequency (*dftrp*) using (F.1). If *dftrp* remains higher than any of the pickup frequency deviations (*dftrp1* to *dftrp10*) for longer than the related time delay, the relay trip the generator.

$$dftrp = |Monitored\ frequency\ in\ p.u.| \times fref - fref \tag{F.1}$$

Note that the reference frequency for this model (*fref*) is 60 Hz by default. However, this parameter can be modified by user. The *lhfrt* relay, by default, monitors the frequency of the generator terminal bus. However, if desired, the settings of the relay can be modified to monitor a remote bus frequency.

APPENDIX G

THE OOSMHO RELAY

The *oosmho* model is an out-of-step mho relay with blinders in the PSLF model library [46]. The model takes the voltage and total current (including the current flowing into the charging capacitors or any line-connected shunts) at the from end of a branch (can be a transmission line, transformer, or series capacitance) and calculate the apparent impedance seen looking into the branch at its from end. The relay sends tripping signal to the circuit breaker of the branch if the impedance trajectory stays inside the mho circle for at least *T1* (the parameter defining the relay operation time) seconds. If at any time before *T1*, the impedance trajectory leaves the mho circle, the timer of the model resets. Also, if at any time, the impedance trajectory falls between the two blinders, the timer resets.

The mho zone of the *oosmho* relay is defined by three parameters of *ang* (mho zone angle in degrees), *rf* (mho zone forward impedance reach in p.u.), and *rr* (mho zone reverse impedance reach in p.u.). This mho zone is illustrated in Figure E.1. The location and the angles of the blinders are defined by *int1* and *int2*—representing blinders 1 and 2 intercept (on the R axes) in p.u., respectively—as well as *rot1* and *rot2*—representing blinders 1 and 2 rotations in degrees. Finally, the time delay of the circuit breaker—i.e., the time it takes for the circuit breaker (upon receiving the tripping signal from its *oosmho* rely) to open the line—is defined by *tcb*.

For all p.u. impedances, the per unit base, Z_{base}, is obtained using the system MVA base and the rated voltage at the from bus.

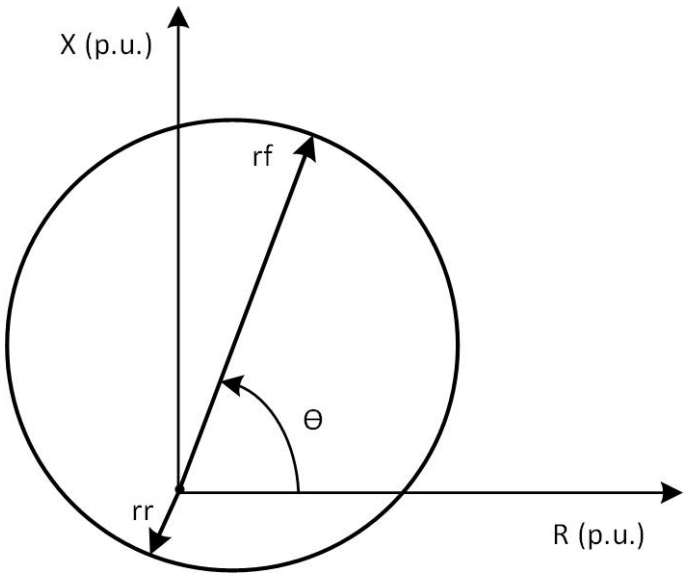

Figure G.1 Mho characteristic of the *oosmho* relay